Acceleration and Optical Interferometry

A thesis submitted in partial fulfilment
of the requirements for the Degree of
Doctor of Philosophy in Physics
at the University of Canterbury

Richard Neutze

University of Canterbury
1995

Abstract

The influence of acceleration on a number of physical systems is examined. We present a full relativistic treatment of a simple harmonic oscillator with relativistic velocities. The line element for Schwarzschild geometry is expanded in a set of Cartesian coordinates and is shown to be locally equivalent (neglecting curvature) to the line element of a linearly accelerating frame of reference. We consider the rate of a linearly accelerating quantum mechanical clock and the measurement of frequency by non-inertial observers, requiring this measurement to be of finite duration. These analyses demonstrate the standard measurement hypothesis for accelerating observers only approximates the physical behaviour of these systems.

We derive the output of an optical ring interferometer in a variety of experimental contexts. A full relativistic reanalysis of the modified Laub drag experiment of Sanders and Ezekiel is performed, correcting a number of errors in their work and giving an overall discrepancy between experiment and theory of 1300 ppm. We examine the behaviour of a ring interferometer containing an accelerating glass sample. Our analysis predicts sideband structure will arise when a glass sample is oscillated along one arm of a Mach-Zehnder interferometer and the resulting output Fourier analysed. We also predict a resonant cavity containing a linearly accelerating glass sample will display optical ringing. A rigorous analysis of a ring interferometer with angular acceleration is presented. This predicts a resonant cavity with angular acceleration will also display optical ringing and demonstrates the beat frequency in a ring laser with angular acceleration is the instantaneous Sagnac beat frequency. Finally, we analyse the optical output of a rotating ring laser with one mirror oscillating, predicting sideband structure in spectra obtained from Fourier analysis of the beat between the opposite beams, and the beat between adjacent modes when the laser has multimode operation.

Acknowledgements

I am indebted to both of my supervisors, Dr. William Moreau and Professor Geoffrey Stedman, for the advice and encouragement they have given me throughout the course of this work. The enthusiasm for my work displayed by Bill during the formulative stages of this research played a large part in my decision to undertake doctoral studies at this stage of my life. When Bill accepted sabbatical leave in 1994, Geoff was only too happy to become co-supervisor of my thesis. I am very grateful to Geoff for his guidance throughout this period as I looked beyond my doctorate and aimed to develop my expertise in directions which would lead to a career in science.

I have enjoyed the environment of this department and the company of other graduate students. Hughan, Richard, Kumar, Steve, Tom, Siva and Wang have all provoked lively discussions from time to time, thus helping to make the years pass quickly. I am particularly indebted to Hughan who proved a valuable foil for many of my more speculative ideas.

I wish thank my parents and my family for the love and support they have given me throughout my life, especially for providing a stimulating environment for an inquisitive young mind as I grew up in rural New Zealand.

Over the last four years Kate has prevented me from allowing obsession with my thesis to become the bane of my life. My most treasured memories from these years arise from our journeys together around New Zealand. For this, and for the continuous support which Kate has provided, I will always be grateful.

I am thankful to the New Zealand Vice Chancellors Committee and the William Georgetti trust for their financial support throughout the course of this work.

Contents

Chapter 1

Introduction

1.1 Relativity and optics: an informal overview

Special relativity grew out of Einstein's dissatisfaction with the state of the theory of electrodynamics at the turn of this century. Lorentz [82] was able to explain the phenomenon of angular aberration and the light drag experiment of Fizeau [45] by postulating a static ether which was not dragged along by the motion of material media. For Einstein, the special status this ether theory gave to the inertial frame in which it was stationary was entirely unsatisfactory. Lorentz's electrodynamics, as a preferred frame theory, was even more stringent than Galilean relativity for which, kinematically, no inertial frame was preferred. Furthermore, the form of Maxwell's equations within an ether theory were greatly complicated when electromagnetic phenomena were viewed from an inertial frame moving relative to the ether.

A key example which led Einstein to reject the electrodynamics of Lorentz was an apparent asymmetry which arose when considering the behaviour of a conductor moving relative to a magnetic field. Within Lorentz's ether theory the description, based upon Maxwell's equations, of the behaviour of the conductor was substantially different for the two cases: i) the conductor stationary with respect to the ether and the magnetic field moving; and ii) the reverse. Einstein rejected this asymmetry and introduced the *principle of relativity* [37] in which it was postulated that the laws of nature take the same form in any inertial frame of reference. Combined with an additional postulate that all observers agree on the value of the speed of light in vacuum, this principle led directly to the special theory of relativity. Within the special theory Einstein demonstrated that Maxwell's equations take the same form in any inertial frame of reference, which immediately removed the asymmetries of the Lorentz's ether theory. In his *Autobiographical Notes*, written forty years after publication of the special theory, Einstein stated 'The special theory of relativity owes its origin to Maxwell's equations of the electromagnetic field.

Inversely the latter can be grasped formally in a satisfactory fashion only by way of the special theory of relativity' [62].

Aside from his conviction of the requirement for symmetry in any physical theory, Einstein, as were Lorentz, FitzGerald and Poincare before him, was strongly influenced by the observation of angular aberration [19] and the results of the light drag experiment of Fizeau [45]. Although not critical in Einstein's development of the special theory of relativity, the null result of the experiment of Michelson and Morley [99], which was designed to detect a phase shift at second order in velocity due to the motion of the Earth relative to the ether, provided compelling experimental evidence in support of special relativity. Historically this experiment has been (incorrectly) credited as one of the founding pillars upon which relativity was based. While this claim was repeatedly denied by Einstein [62], the experiment of Michelson and Morley, more than any other experiment of nineteenth century, compelled Einstein's peers to accept the special theory of relativity as the most legitimate description of electromagnetic phenomena.

Despite the successes of special relativity, Einstein was uncomfortable with the elevated status it gave inertial observers. Within two years of Einstein's publication of the special theory two highly significant discoveries were made which were to pave the way to the general theory. The first was Minkowski's realisation that, within the special theory of relativity, space and time could be described geometrically [100]. Within this framework Minkowski showed that spatial separations and time like intervals should be treated on an equal footing, a remarkable philosophical break from the Newtonian concepts of absolute space and absolute time. A second breakthrough which occurred in the same year was Einstein's discovery of the principle of equivalence [38], which exploited the empirical coincidence of inertial and gravitational mass. Generalising the principle of relativity to hold under arbitrary coordinate transformations Einstein was led to the requirement of general covariance which, combined with the geometric description of flat space-time and the equivalence principle, led to the general theory of relativity [39], a geometric description of gravitation.

In the decades following the publication of general relativity several optical experiments were performed which verified a number of important predictions of the general theory. Dyson, Eddington and Davidson [36] observed the bending of light as it passed near the sun in the solar eclipse of May 29, 1919. This early verification of a novel prediction of the general theory marks a milestone

in the acceptance of general relativity by Einstein's contemporaries. Considerably more accurate measurements of the bending of electromagnetic radiation by a massive body were provided by Fomalont and Sramek in 1976 [46]. In their experiment Fomalont and Sramek successfully recorded the deviation of the path taken by radio waves emitted from a quasar as it was eclipsed by the sun, achieving experimental confirmation of general relativity to an accuracy of $\sim 1\%$. Closely related was the experiment, in 1979, of Reasenberg et al. [120] who tracked the path taken by a spacecraft which continuously emitted an electromagnetic signal. From the measured delay in propagation time from the satellite to the Earth based laboratory Reasenberg et al. were able to confirm the predictions of Schwarzschild geometry to 0.2%.

One of the most significant laboratory based experiments to confirm a central prediction of any gravitational theory which incorporates the equivalence principle, of which the general theory of relativity is one, was that of Pound and Rebka [119] who located a Fe^{57} Mössbauer source and receiver at different heights in their laboratory, enabling them to measure the gravitational redshift induced by the Earth's gravitational field. Closely related was the experiment of Hay et al. [58] who mounted a Mössbauer source and receiver upon a rotating disk and detected the second order transverse Döppler shift. Colella, Overhauser and Werner [29] also measured a gravitationally induced phase shift in de Broglie waves using neutrons. In their experiment a ring neutron interferometer was inclined at a variety of angles relative to the surface of the earth. A phase shift arising from gravitational redshift in the de Broglie waves was detected through measuring the intensity of the recombined neutron beams as a function of the inclination of the interferometer.

A ring interferometer has proved a valuable experimental tool for studying a variety of non-reciprocal phenomena arising within relativity theory. The classic light drag experiment of Fizeau [45], improved upon by Michelson and Morley [98] and Zeeman [156], employed a passive ring optical interferometer with water moving along along two arms. More recently several high precision light drag experiments have been performed, using a ring laser and moving glass samples, by Bilger and Zavodny [16], Bilger and Stowell [15] and Kowalski et al. [76]. Sanders and Ezekiel [128], in a closely related experiment, used a passive ring resonator technique to measure Fresnel drag. In these experiments a non-reciprocal phase shift was converted into a beat frequency between the opposite beams of the active cavity, enabling an improvement of several orders of magnitude in the resolution achieved. A phase shift in de

Broglie waves arising from the motion of media has also been detected using a ring neutron interferometer. Klein et al. [68] and Bonse and Rumpf [17] observed a phase shift when their sample's boundaries were moving relative to the laboratory, whereas Arif et al. [8] detected a null phase shift result when the boundary of the moving media was stationary with respect to the interferometer. This null phase shift was predicted by Horne et al. [63] and arises from the neutron-nucleus potential being independent of the velocity of the media when the neutron's energy is removed from a nuclear resonance. Arif et al. [6, 7] performed a similar experiment, this time using a sample with a nuclear resonance at thermal energies. As such the neutron-nucleus potential became velocity dependent, inducing a phase shift directly analogous to the historical experiment of Fizeau.

As early as 1913 Sagnac, using a passive ring optical interferometer, reported an observation of the phase shift induced by rotation [125]. Since this first observation the Sagnac effect has become a topic of wide experimental and theoretical interest [118, 60, 5]. With the invention of the ring laser the sensitivity of optical devices to rotation was dramatically improved. The most precise of these is that possessed by the Canterbury Ring Laser Group, which has measured the Sagnac beat frequency induced by the rotation of the Earth with a precision of three parts in 10^{22} [139]. A rotationally induced phase shift has also been observed for super-conducting Cooper pairs [159], in neutron interferometry [153], in atom interferometry with ^{40}Ca beams [121] and in interferometry with bare electrons [56].

A ring interferometer and ring laser are also sensitive to a variety of post Newtonian gravitational effects [133, 130]. In particular, it has been suggested that the influence of Lense-Thirring frame dragging by a rotating massive body is detectable, in principle, by a ring laser. A comprehensive review of the various classical and quantum gravitational effects to which ring interferometers and ring lasers are sensitive has been given by Stedman [136].

These experiments, along with numerous others, set Einstein's theory of gravitation on a firm empirical basis and have led to its almost universal acceptance within the scientific community. While our discussion above has not attempted to fully review the labyrinth of interconnections which characterise the discipline of relativistic optics, this summary does highlight the strong links which exist between theoretical and experimental studies of the theory of relativity and the theory of optics. From this perspective it is valuable to search for further optical experiments which will test the mathematical for-

malism of general relativity. This quest provides the underlying goal of the work performed throughout this thesis.

Our primary interest in optical interferometry is in connection with the Canterbury Ring Laser Group. With this motivation we are led to consider experimental proposals for which a ring interferometer or ring laser is ideally suited. Given our desire to search for novel observable consequences of the formalism of standard relativity using optical interferometry it is most natural to seek generalisations of previous successful experiments. Obvious extensions include consideration of the effects of acceleration in the laboratory based experiments of Sagnac [125] and Sanders and Ezekiel [128], or to introduce time dependent boundary conditions in optical experiments performed in a rotating frame of reference. In this thesis we present a full analysis of precisely these generalisations. Chapters 6, 7 and 8 respectively present, within the context of optical interferometry, a relativistic treatment of light drag within a linearly accelerating dielectric sample, an analysis of the optical behaviour of a ring interferometer and ring laser with angular acceleration and we determine the optical response of a rotating ring laser with one mirror oscillating.

However, along the path to mastering the dual formalisms of general relativity and optical interferometry, required for the analyses presented in chapters 6, 7 and 8, several other problems of physical interest have arisen and been solved. Within this thesis we present the results of the most successful of these 'detours', all of which provide insight into the physical consequences of the theory of relativity. This thesis has the title *Acceleration and optical interferometry.* It is the influence of acceleration and relativistic effects in optical interferometry which provide the threads which sew together the apparently self contained and independent blocks of work presented in each chapter. All work reported within this thesis belongs to either of these two categories in relativistic physics and the final three chapters combine these parallel interests, leading to a series of novel experimental predictions which either fall within, or just outside, the technological sphere accessible to todays experimentalist.

1.2 Structure of this thesis

Throughout this thesis we are primarily concerned with the manner in which acceleration affects the behaviour of physical systems. Our analyses, by their very nature, are intrinsically relativistic and this thesis should be regarded as the application of the theory of relativity to a number of problems, predom-

inantly optical systems, of physical interest. Each chapter presents original material in its own right and is self contained.

In chapter 2 we give an unorthodox derivation of hyperbolic motion, which describes the worldline of a uniformly accelerating particle. This approach is chosen as the formalism, when applied to the classical problem of a mass being acted upon by an idealised spring obeying Hooke's law, provides a natural extension of simple harmonic motion into the relativistic realm. Having motivated the physical model, we present a full relativistic solution for the motion of a massive particle when attached to a centre of attraction by an idealised spring.

In chapter 3 we expand the Schwarzschild line element and define a local Cartesian coordinate system with its origin a finite distance from the centre of the non-rotating, spherically symmetric gravitating body. This expansion enables a simple comparison to be drawn between the line element of an, appropriately chosen, linearly accelerating frame of reference. This comparison provides a clear illustration, using a well known solution of Einstein's field equations, of how the equivalence principle is incorporated into the general theory of relativity.

Chapter 4 represents our first discussion of optical phenomena, which remains the focus for the remainder of the thesis. Within this chapter we derive the Döppler effect for two non-inertial observers, the first linearly accelerating and the second stationary in Schwarzschild geometry, when the source is inertial. Unlike the geometric formalism of general relativity we find the Döppler shift relations are dependent upon the duration of the measurement. Before calculating these frequency transformation formula we discuss the rate at which a linearly accelerating clock runs, demonstrating that the rate of a quantum mechanical clock is affected by its acceleration. We also briefly review the literature concerned with helicity-rotation coupling.

From chapter 5 on our attention turns solely to relativistic problems in optical interferometry. In this chapter we present a full reanalysis of the light drag experiment of Sanders and Ezekiel. This reanalysis is motivated by a number of questions of principle which arise because of the especially complicated geometry used in this experiment, and the unsatisfactory treatment, or total neglect, of these features in the analysis of Sanders. Our analysis demonstrates an overall discrepancy between experimental results and theoretical predictions of 1300 ppm. This discrepancy is 4.7 times larger than Sanders

and Ezekiel's stated experimental uncertainty and is significantly worse than their claim of an overall agreement between experiment and theory to 60 ppm.

We unify our interest in non-inertial systems and optical interferometry in the final three chapters of this thesis. In the first of these, chapter 6, we perform an analysis of light drag in an accelerating dielectric using the covariant formulation of Maxwell's equations. As predicted by Tanaka [146], we find light which propagates through accelerating media suffers a shift in frequency. When the dielectric is accelerated along one arm of a ring interferometer this frequency shift leads to potentially observable experimental effects, causing the response profile of a resonant cavity to become asymmetric and induces a beat between the opposite arms of a passive ring cavity. If the sample is oscillated then Fourier analysis of the recorded beat between the opposite arms would produce sideband structure in the final spectra. We also consider an analogous case of a dielectric freely falling along an arm of a resonant cavity stationary in a gravitational field.

Chapter 7 presents an analysis of the optical behaviour of a ring interferometer with angular acceleration. When the mirrors are separated by vacuum we utilise a transit time technique to calculate the observable phase shifts. When material media separates the mirrors we apply the covariant form of Maxwell's equations and formulate and solve the wave equation for this system. Both approaches yield identical predictions in the appropriate limits. Our results predict an asymmetric response profile for a resonant cavity with angular acceleration. We also show the beat frequency for a ring laser with angular acceleration is precisely that given by the Sagnac effect for an instantaneously co-rotating ring laser.

In chapter 8 we derive the effect of oscillating a mirror within a rotating ring laser. To approach this problem we develop a novel formalism through which we may calculate optical phase shifts in non-Minkowskian frames of reference with time dependent boundary conditions. Our analysis predicts sideband structure will be observed when the beat between the counter-rotating beams, and the beat between adjacent modes of the ring laser, are recorded and Fourier transformed. This discussion is highly relevant to the current experimental interests of the Canterbury Ring Laser Group.

1.3 Notation and conventions

Throughout this thesis we employ the Minkowski metric in Cartesian coordinates with $\eta_{\mu\nu} = \text{diag}(-1, 1, 1, 1)$. We adopt the convention that inertial frames of reference are labelled I and non-inertial frames of reference S. Cartesian coordinates of an inertial frame of reference are labelled with uppercase (T, X, Y, Z) and lowercase (t, x, y, z) are used to represent the Cartesian coordinates of a non-inertial frame of reference. Apart from the Schwarzschild line element, which is introduced by reference to a well known text [101], all other non-inertial coordinate systems used within this thesis are defined by a coordinate transformation from Minkowski space-time. We use SI units throughout, keeping all factors of c, G and h. Angular frequency is denoted ω whereas natural frequency is denoted $\nu \equiv \omega/2\pi$.

Chapter 2

Hyperbolic Motion and the Relativistic Spring

In this chapter we derive hyperbolic motion from the basic classical model of a uniformly accelerating particle. When moving from the classical domain into the relativistic realm we must replace the particle's classical momentum with its relativistic counterpart. We also apply this prescription to the problem of a massive particle which is acted upon by an idealised spring. This leads to a natural relativistic generalisation of simple harmonic motion. We present a full relativistic solution for the motion of this massive particle.

2.1 Classical motivation

A particle undergoing constant acceleration and the simple harmonic oscillator are two elementary topics in classical mechanics that are thoroughly discussed in all of the standard expositions of the subject [49]. But while the relativistic generalisation of constant acceleration, defined with respect to instantaneously comoving inertial frames, has received a complete treatment in the literature [3, 49, 101, 103], the relativistic extension of simple harmonic motion, by comparison, has received considerably less attention. This omission is surprising as the simple harmonic oscillator is one of the most important problems in classical mechanics and is thoroughly discussed in all of the standard expositions of the subject [49]. Furthermore, since the simple harmonic oscillator is a central idea in physics, from normal modes of vibration in molecules and solids to those in relativistic quantum fields, it is worthwhile considering a complete and rigorous relativistic treatment of the basic classical model.

Synge [141] has given an exact expression for the period of a relativistic oscillator in terms of an integral which Goldstein [49] has identified as being expressible in terms of standard elliptical integrals. Skinner [135] covers the topic in a problem. All three of these authors give the relativistic correction to the period to leading order, but they have not calculated the world line

nor analysed the motion in any detail. The question "What happens to a simple harmonic oscillator when the energy is such that the velocities become relativistic?" is a natural one to ask. Moreau, Easther and Neutze [105] were the first to provided a detailed and rigorous solution. In brief, the effect of time dilation along the world line is to cause simple harmonic motion at low energy to become anharmonic at high energy.

In this chapter we derive and solve the equations of motion for a relativistic particle attached to a centre of attraction by an idealised spring. We approach this problem from a somewhat different perspective to that previously reported [105]. We begin, in section 2.2, by considering the motion of a relativistic particle which is acted upon by a constant force. We apply the prescription of Moller [103] and replace the particle's classical momentum with its relativistic momentum when making the transition from Newtonian mechanics to relativistic mechanics. The resulting solution is well known and the particle follows hyperbolic motion. This approach to hyperbolic motion, which is now regarded as somewhat 'old fashioned', is chosen as it highlights the physical assumptions made in deriving the relativistic corrections to the classical motion. Furthermore, in section 2.3 we are able to apply the same formalism to derive a very natural relativistic generalisation of the motion of a simple harmonic oscillator. In developing the relativistic oscillator by analogy with a well known problem in relativistic mechanics, the physical basis for this generalisation is made transparent. Having established the equations of motion for our relativistic oscillator we present a full solution in section 2.3.2.

2.2 Hyperbolic Motion

Hyperbolic motion is one of the standard examples of relativistic motion and is discussed in virtually all texts on general relativity. Its importance is twofold: it provides an intuitive example from which one can appreciate the distinction between rest mass and relativistic mass in relativistic mechanics; and, through the equivalence principle, accelerated motion provides a useful tool through which one can grasp many of the important features of gravitation without first mastering the full mathematical structure of general relativity.

First consider, within the framework of Newtonian mechanics, a particle which is moving along the X axis of an inertial frame I and is acted upon by a force F applied parallel to the X axis which is independent of the particle's

position and velocity. Newton's equation of motion for this system is

$$\frac{d\,P^1}{dT} = F \ , \tag{2.1}$$

where

$$P^1 = m\frac{dX}{dT} \tag{2.2}$$

is the particle's classical momentum along the X axis of I, and m is the inertial mass of the particle. In Newtonian mechanics the inertial mass of a particle is identical to its rest mass m_0 and is independent of the particle's velocity. In classical mechanics the solution to Eq. (2.1) predicts that this particle will follow parabolic motion.

We now follow the prescription given by Moller [103, pp.65-68] and make the transition from Newtonian mechanics to relativistic mechanics by: (a) identifying the variable T in Eq. (2.1) as parameterising the coordinate time of the inertial frame I; and (b) the inertial mass m of the particle in Eq. (2.2), which denotes the particle's resistance to acceleration, becomes the 'relativistic mass' $m \equiv m_0\,\gamma$, where $\gamma \equiv 1/\sqrt{1-(dX/dT)^2/c^2} = dT/d\tau$ and τ is the proper time along the worldline of the particle. Applying this prescription to Eq. (2.2) we find the particle's momentum becomes

$$P^1 = m\frac{dX}{dT} \equiv m_0\,\gamma\frac{dX}{dT} = m_0\frac{dX}{d\tau} \ , \tag{2.3}$$

which is the relativistic momentum of the particle.

We again consider the motion of a particle, restricted to move along the X axis, which experiences a force F applied parallel to the X axis which is independent of the particle's position and velocity [103, p.73-74]. The relativistic expression for Newton's equation of motion, Eq. (2.1), is therefore

$$\frac{dP^1}{dT} = m_0\frac{d}{dT}\frac{dX}{d\tau} = m_0\frac{d^2X}{d\tau^2}\frac{d\tau}{dT} = F \ , \tag{2.4}$$

where we have simply replaced the classical momentum with its relativistic counterpart, defined by Eq. (2.3). If we assume our particle is stationary at $X = 0$ when $T = 0$ then Eq. (2.4) has the solution

$$T = \frac{c}{a}\sinh(\frac{a\,\tau}{c}) \ , \tag{2.5}$$

$$X = \frac{c^2}{a}\cosh(\frac{a\,\tau}{c}) - \frac{c^2}{a} \ , \tag{2.6}$$

where we have defined the acceleration constant $a \equiv F/m_0$. This demonstrates that our accelerating particle will follow hyperbolic motion in I and is in agreement with the Newtonian case in the limit of $a\,\tau/c \ll 1$.

From the above formulation of this problem it would appear that we have chosen a special frame of reference from which to view this motion, namely the inertial frame I in which we have defined the force F acting on our particle. However, it is easily demonstrated that our particle will follow the same characteristic motion when viewed from any inertial frame of reference. If we make a Lorentz boost to another frame I' moving with velocity $c\tanh\Theta$ relative to I, then the worldline of the particle in I' is described by

$$T' = \frac{c}{a}\left\{\sinh(\frac{a\tau}{c} - \Theta) + \sinh\Theta\right\} , \tag{2.7}$$

$$X' = \frac{c^2}{a}\left\{\cosh(\frac{a\tau}{c} - \Theta) - \cosh\Theta\right\} . \tag{2.8}$$

Thus, apart from a difference in the choice of the origin for primed and unprimed coordinates, the motion of the accelerating particle appears identical in any inertial frame. When $\tau = c\Theta/a$ the particle is instantaneously stationary in I'. Eqs. (2.7) and (2.8) give, at this moment, $d\tau = dT'$ and $d^2X'/d\tau^2 = d^2X'/dT'^2 = a$. Thus a particle following hyperbolic motion always has an acceleration a with respect to the inertial frame with which is is instantaneously comoving.

It is convenient to express the equation of motion, Eq (2.4) in in terms of the covariant form of Newton's second law

$$\frac{dP^\mu}{d\tau} = F^\mu , \tag{2.9}$$

where F^μ is the Minkowski force acting on the particle and $P^\mu \equiv m_0 dX^\mu/d\tau$ are the 4-vector components of the relativistic momentum. In the inertial frame of reference instantaneously comoving with the particle, Eqs. (2.7) and (2.8) with $\Theta = a\tau/c$ give $d^2T'/d\tau^2 = 0$ and $d^2X'/d\tau^2 = a$ such that the magnitude of the Minkowski force,

$$F_\mu F^\mu = m_0^2 a^2 , \tag{2.10}$$

is constant. In a modern formulation of the problem of a uniformly accelerating observer one commonly uses this equation as a convenient starting point [101]. Thus, the prescription of replacing the particle's classical momentum with its relativistic momentum is consistent with a modern formulation of the problem of a uniformly accelerating observer.

2.3 Relativistic Spring

In classical mechanics a particle which is attached by a perfect spring to a fixed point in an inertial frame I will follow simple harmonic motion. This problem has become one of the central ideas in physics, finding application in spectroscopy, the theory of solids, quantum field theory, and numerous other areas of current research. It is therefore of interest to derive and solve the equations of motion arising from a relativistic treatment of the basic classical model.

2.3.1 Relativistic equations of motion

As in section (2.2), we begin our relativistic treatment of a simple harmonic oscillator by first considering the classical formulation of the problem. Hooke's law in Newtonian mechanics states that the force acting on a particle connected by an idealised spring to the origin of an inertial frame I is proportional to the negative of the particle's displacement in I. Without loss of generality we assume that our particle is constrained to move along the X axis. Classically, Newton's equation of motion for the system is

$$\frac{dP^1}{dT} = -kX \ , \tag{2.11}$$

where k is the spring constant. In classical mechanics the solution to Eq. (2.11) predicts that our particle will display simple harmonic motion.

We now apply the same formalism which we used in section 2.2 and make the transition from classical mechanics to relativistic mechanics by identifying T as the coordinate time of I and replacing the classical momentum of the particle in Eq. (2.11) with its relativistic counterpart, Eq. (2.3). The relativistic equation of motion for a particle attached to an idealised spring is therefore

$$\frac{dP^1}{dT} = m_0 \frac{d}{dT}\frac{dX}{d\tau} = m_0 \frac{d^2X}{d\tau^2}\frac{d\tau}{dT} = -kX \ ,$$

such that

$$\frac{d^2X}{d\tau^2} + \omega^2 X \frac{dT}{d\tau} = 0 \ , \tag{2.12}$$

where we have defined $\omega \equiv \sqrt{k/m_0}$ and is the angular frequency with which a classical harmonic oscillator would oscillate. It should be appreciated that Eq. (2.12) has been derived in a manner directly analogous to the derivation of Eq. (2.4) in section 2.2, which predicted that a particle acted upon by

a force of constant magnitude and direction would follow hyperbolic motion. The physical assumptions made in the derivation of this equation of motion for a relativistic oscillator are transparent and this formalism has provided a very natural generalisation of a classical oscillator into the relativistic realm. This approach is physically equivalent to those taken in all of the literature known to the author concerned with a relativistic generalisation of the classical harmonic oscillator [49, 105, 135, 141].

From the invariance of the magnitude of the four velocity we have

$$\left(\frac{dT}{d\tau}\right)^2 - \frac{1}{c^2}\left(\frac{dX}{d\tau}\right)^2 = 1 \ . \tag{2.13}$$

Differentiating with respect to τ produces

$$\frac{d^2T}{d\tau^2}\frac{dT}{d\tau} - \frac{1}{c^2}\frac{d^2X}{d\tau^2}\frac{dX}{d\tau} = 0 \ .$$

Using this expression to substitute for the $d^2X/d\tau^2$, Eq. (2.12) becomes

$$\frac{d^2T}{d\tau^2} + \frac{\omega^2 X}{c^2}\frac{dX}{d\tau} = 0 \ , \tag{2.14}$$

and integrating with respect to τ we obtain

$$\frac{dT}{d\tau} + \frac{\omega^2 X^2}{2\,c^2} = C_1 \ . \tag{2.15}$$

The integration constant C_1 is evaluated by choosing the initial conditions $X = 0$ and $dX/dT = v_0$ at $T = \tau = 0$. From Eqs. (2.12) and (2.13)

$$C_1 = \left(\frac{dT}{d\tau}\right)_{T=\tau=0} = \left(1 - \frac{v_0^2}{c^2}\right)^{-1/2} \equiv \gamma_0 \ .$$

Physically γ_0 is the total energy of the particle expressed in units of its rest mass. This can be seen from the relativistic expression for energy when the particle is at the origin of I. At this point the potential energy is zero such that $E = m_0 c^2 \sqrt{1 + v_0^2\,\gamma_0^2} = m_0 c^2\,\gamma_0$, where we have used $P^1 = m_0\,\gamma_0\,v_0$ at the origin.

Substituting Eq. (2.15) into Eq. (2.12) we obtain the equation of motion, with respect to the proper time variable τ, for a relativistic particle attached to an idealised spring with the centre of attraction the origin of I,

$$\frac{d^2X}{d\tau^2} + \omega^2 X\left(\gamma_0 - \frac{\omega^2\,X^2}{2\,c^2}\right) = 0 \ . \tag{2.16}$$

This equation of motion may also be obtained from a Lagrangian formalism in which a relativistic particle is considered to move in the one dimensional harmonic oscillator potential $\frac{1}{2}\,k\,X^2$, as was demonstrated by Moreau et al. [105].

As in section 2.2, it is intuitive to recast these equations of motion in terms of the covariant form of Newton's second law, Eq. (2.9). This also serves to to illustrate the analogy between the classical description of an idealised spring and its relativistic generalisation. From Eq. (2.16), the X component of the Minkowski force is

$$F^1 = -m_0\,\omega^2 X\left(\gamma_0 - \frac{\omega^2 X^2}{2\,c^2}\right) \ .$$

Combining Eqs. (2.13), (2.14) and, from Eq. (2.15),

$$\frac{dT}{d\tau} = \gamma_0 - \frac{\omega^2 X^2}{2\,c} \ , \tag{2.17}$$

we obtain

$$F^0 = -m_0\,\omega^2\,X\sqrt{\left(\gamma_0 - \frac{\omega^2\,X^2}{2\,c^2}\right)^2 - 1} \ ,$$

such that

$$F_\mu F^\mu = \{-m_0\,\omega\,X\}^2 \ . \tag{2.18}$$

Written in this form the analogy between the classical idealised spring and its relativistic counterpart is striking. The magnitude of the Minkowski force exerted on the particle by the idealised spring is proportional to the negative of its displacement from the centre of attraction evaluated in the rest frame of the centre of attraction. This corresponds intuitively to the classical formulation of Hooke's law. Of course Eq. (2.18) is not form invariant under a Lorentz boost. Throughout this chapter we work entirely within a special frame of reference, namely that in which the centre of attraction is stationary.

2.3.2 Solution to the equations of motion

The solution of Eq. (2.16) determines the motion of our particle in terms of proper time for a given total relativistic energy $m_0\,c^2\,\gamma_0$. Because of the transcendental nature of the equation, we can only obtain the solution in the form $\tau(X)$. Then Eq. (2.15) determines the world line in the form $T[X, \tau(X)]$. But before solving these equations it is conceptually useful to discuss qualitatively the effect of the cubic terms in Eq. (2.16) and to obtain the nonrelativistic limit of this equation.

It is instructive to consider Eq. (2.16) in the form,

$$\frac{d^2X}{d\tau^2} + \omega^2 \left[1 + \frac{K(X)}{m_0 c^2}\right] X = 0 \ , \tag{2.19}$$

where we have defined the kinetic energy of the particle at X by

$$K(X) \equiv E - m_0 c^2 - \frac{1}{2} k X^2 = m_0 c^2 \left\{\gamma_0 - 1 - \frac{\omega^2}{2\,c^2}\right\} \ .$$

Interpreting the instantaneous angular frequency of the relativistic oscillator as the coefficient of X, we find the angular frequency $\omega(X) = \omega\sqrt{1 + K(X)/m_0c^2}$ varies with the kinetic energy $K(X)$, from a maximum value of $\omega\sqrt{\gamma_0}$ at the origin to a minimum value of ω at the turning points. Thus the effect of time dilation is to cause the relativistic oscillator to become anharmonic, with a range of angular frequencies along its world line. The strength of the anharmonicity increases with increasing total relativistic energy, and in the nonrelativistic limit the oscillator becomes harmonic. In this limit $K(X)/m_0c^2 = v^2/2c^2 \ll 1$, and Eq. (2.19) becomes

$$\frac{d^2X}{d\tau^2} + \omega^2 X + O\left(v^2/c^2\right) = 0 \ , \tag{2.20}$$

with the proper time equivalent to the coordinate time at this order. This recovers Eq. (2.11) in the non-relativistic limit, which was the classical starting point for this analysis.

To derive the relativistic solution we first multiply Eq. (2.16) by $dX/d\tau$ and integrate to obtain

$$\left(\frac{dX}{d\tau}\right)^2 + \omega^2 X^2 \left(\gamma_0 - \frac{\omega^2 X^2}{4\,c^2}\right) = c^2\left(\gamma_0^2 - 1\right) \ ,$$

where we have used $dX/d\tau = v_0\,\gamma_0$ at $X = 0$ to evaluate the constant of integration. Rearranging we can express this in the form,

$$d\tau = \pm \frac{2dX}{\sqrt{\left(A_+^2 - \omega^2 X^2\right)\left(A_-^2 - \omega^2 X^2\right)}}, \tag{2.21}$$

where $A_\pm = c\sqrt{2\left(\gamma_0 \pm 1\right)}$, and the + sign is to be chosen for $dX > 0$ and the − sign for $dX < 0$ so that $d\tau$ is always positive. Physically A_-/ω is the maximum amplitude of the oscillation. This can be seen as follows: when the particle is at its maximum amplitude, X_0, the particle has no kinetic energy such that all of its energy $E = m_0c^2\gamma_0$ will comprise of the particle's potential energy plus its rest mass. Therefore $E = m_0c^2 + \frac{1}{2}kX_0^2 = m_0c^2\,\gamma_0$ and hence

$$X_0 = \frac{c}{\omega}\sqrt{2\left(\gamma_0 - 1\right)} = \frac{A_-}{\omega} \ . \tag{2.22}$$

By a change of variable, $X = (A_-/\omega)\sin\alpha$, Eq. (2.21) can be expressed in the standard form of an elliptic integral of the first kind [50],

$$\tau(X) = \frac{2c}{A_+\omega}\int_0^{\phi}\frac{d\alpha}{\sqrt{1-\kappa^2\sin^2\alpha}} \equiv \frac{2c}{A_+\omega}F(\phi,\kappa) \quad , \tag{2.23}$$

where $\kappa \equiv A_-/A_+$ and $\phi \equiv \sin^{-1}(\omega X/A_-)$.

The world line $T(X)$ can now be obtained from Eq. (2.17),

$$dT = \left(\gamma_0 - \frac{\omega^2 X^2}{2c^2}\right)d\tau \quad .$$

If we substitute Eq. (2.21) for $d\tau$ and again make the change of variable $X = (A_-/\omega)\sin\alpha$, the integration produces

$$T = \gamma_0\tau - \frac{\kappa A_-}{c\omega}\int_0^{\phi}\frac{\sin^2\alpha\, d\alpha}{\sqrt{1-\kappa^2\sin^2\alpha}} \quad . \tag{2.24}$$

The integral in Eq. (2.24) can be expressed as $[F(\phi,\kappa) - E(\phi,\kappa)]/\kappa^2$, where

$$E(\phi,\kappa) \equiv \int_0^{\phi}\sqrt{1-\kappa^2\sin^2\alpha}\, d\alpha \quad ,$$

is an elliptic integral of the second kind [50]. Making this substitution and substituting Eq. (2.23) for τ, we find that

$$T(X) = \frac{1}{\omega}\left\{\sqrt{2(\gamma_0+1)}E(\phi,\kappa) - \sqrt{\frac{2}{\gamma_0+1}}F(\phi,\kappa)\right\} \quad , \tag{2.25}$$

where $X = (c/\omega)\sqrt{2(\gamma_0-1)}\sin\phi$ and $\kappa = \sqrt{(\gamma_0-1)/(\gamma_0+1)}$.

In figure 2.1 we show plots of the normalised displacement, $(\omega X)/A_-$, versus ωT for $\beta_0 = v_0/c = 0.20$, 0.90, and 0.99 for one complete cycle. The amplitudes for these three world lines are respectively 0.20, 1.61, and 3.49 to three figure accuracy. The three world lines show that, unlike simple harmonic motion, the period of the anharmonic relativistic motion is not independent of the amplitude. For $\beta_0 = 0.20$ the world line is very close to the sine wave form of nonrelativistic simple harmonic motion. At $\beta_0 = 0.90$ the curvature is becoming more concentrated at the turning points. At $\beta_0 = 0.99$ the world line has become markedly anharmonic, being nearly straight between the turning points. Only in the vicinity of the turning points, where the magnitude of the Hooke's law force is maximum and the velocity is becoming nonrelativistic, is the force effective in changing the velocity.

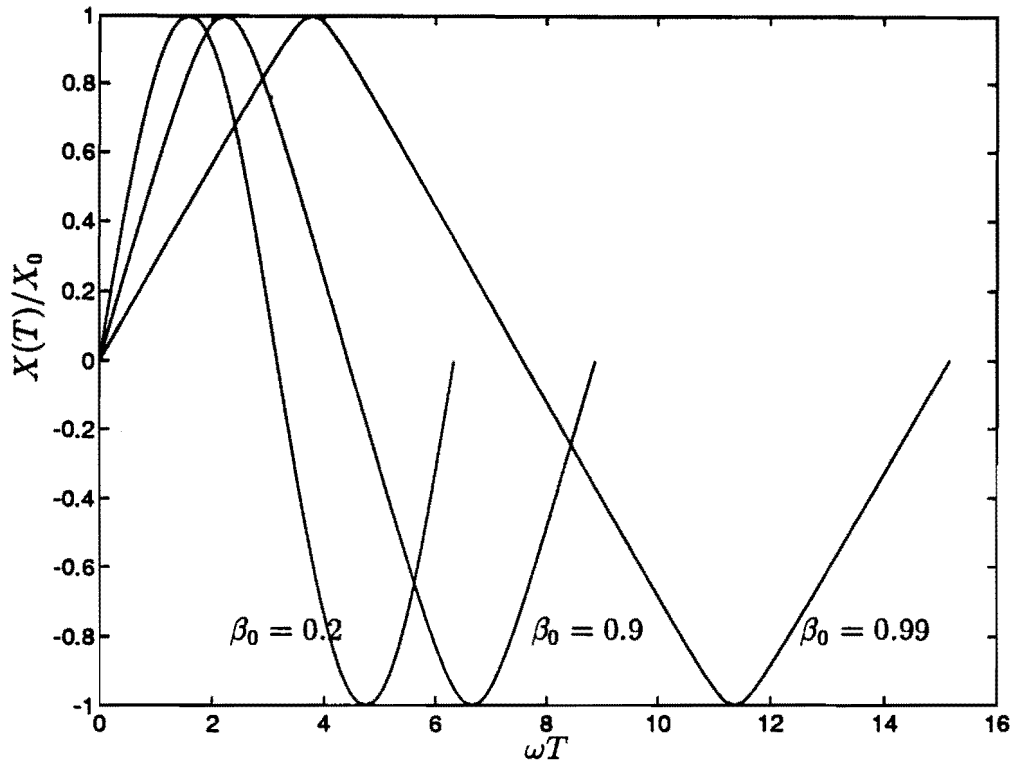

Figure 2.1: The normalised displacement $X(T)/X_0$ as a function of the normalised coordinate time, ωT, for one complete cycle with $\beta_0 = 0.20$, 0.90, and 0.99. The corresponding amplitudes are 0.20, 1.61, and 3.49 to three figure accuracy. The world lines become more anharmonic with increasing energy. At $\beta_0 = 0.99$ the world line is nearly straight between the turning points, indicating that only in these regions where the velocity is becoming non-relativistic is the force effective in changing the velocity. Unlike simple harmonic motion, the period of the relativistic motion is not independent of the amplitude.

It is interesting to examine the motion in the ultra-relativistic region where $\gamma_0 \gg 1$. In this case $\kappa \to 1$ and $A_+ \to A_- \to c\sqrt{2\gamma_0}$. Then Eq. (2.25) becomes

$$\tau = \frac{1}{\omega}\sqrt{\frac{2}{\gamma_0}}\int_0^\phi \sec\alpha d\alpha = \frac{1}{\omega\sqrt{2\gamma_0}}\ln\left(\frac{1+\sin\phi}{1-\sin\phi}\right) = \frac{1}{\omega\sqrt{2\gamma_0}}\ln\left(\frac{\sqrt{2\gamma_0}+X}{\sqrt{2\gamma_0}-X}\right) , \tag{2.26}$$

and Eq. (2.24) becomes

$$T = \gamma_0\tau - \frac{\sqrt{2\gamma_0}}{\omega}\int_0^\phi \tan\alpha\sin\alpha d\alpha \ . \tag{2.27}$$

Substituting Eq. (2.26) for Θ in Eq. (2.27) and integrating by parts, after a cancellation we obtain the simple result,

$$T = \frac{\sqrt{2\gamma_0}}{\omega}\sin\phi = \frac{X}{c} \ . \tag{2.28}$$

In the ultra-relativistic region the world line approaches that of a photon, $X = cT$, as the effect of the central force is negligible. Also, from Eq. (2.22),

the amplitude becomes very large: $X_{max} \approx c\sqrt{2\gamma_0}/\omega \gg c/\omega$. In the limiting case where $\gamma_0 \to \infty$, the amplitude $X_{max} \to \infty$, and the motion ceases to be periodic. Of course a massive particle can never reach this limit.

Starting from a natural extension of the classical model of a simple harmonic oscillator we have derived the equations of motion for a relativistic particle attached to an idealised spring. In our approach the key physical assumption, that the classical momentum should be replaced by the relativistic momentum, entered in a natural and transparent manner. This approach complements our earlier derivation of the equations of motion starting from a suitably defined Lagrangian [105]. Our solution has shown that as the energy of an oscillator is increased its worldline changes from the sine wave of simple harmonic motion to an anharmonic periodic wave with the curvature concentrated more and more at the turning points and the period increasing with amplitude. This anharmonicity is a relativistic effect due to time dilation along the world line.

Chapter 3

Local equivalence of Schwarzschild geometry with an accelerating frame

In this chapter we draw a comparison between the line element of Schwarzschild geometry, expressed in local Cartesian coordinates, with an appropriately chosen linearly accelerating frame of reference. This comparison provides a clear illustration of how the equivalence principle is incorporated into general relativity.

3.1 The principle of equivalence

In the last months of 1907 Einstein made the discovery which was to lead him to a geometric theory of gravitation. Within a review article on his special theory of relativity [38], published two years earlier, Einstein discussed the problem of how to generalise this theory to include the measurements of non-inertial observers. He was convinced that the key to this extension lay in the empirical coincidence of the equality of inertial and gravitational mass. To interpret and exploit this coincidence, Einstein introduced a new physical principle, later to be called the principle of equivalence. This principle extended the observed equality between inertial and gravitational mass by stating that all observations performed in either a hypothetical homogeneous gravitational field or a uniformly accelerating frame of reference will be identical. Thus these two systems are indistinguishable and therefore physically equivalent, with the laws of physics taking the same form within both systems of reference. From this perspective the metric theory of Minkowski [100], which described the observations of inertial observers in flat spacetime, if generalised to include metrics with non-vanishing curvature would describe the spacetime structure of a gravitational field. It was this conceptual leap, unanticipated by his contemporaries, which led Einstein to a geometric description of gravitation.

Experimental support for the equivalence principle is provided by several

high precision experiments which have been performed which set limits on the difference between the accelerations, a_A and a_B, of objects A and B of different composition, when falling within the gravitational field of the Earth or Sun. The empirical independence of the acceleration of a body in a gravitational field from its internal structure is the origin of the so called 'weak equivalence principle' [155]. If we define the parameter

$$\eta \equiv \frac{a_A - a_B}{1/2(a_A + a_B)} \ ,$$

then the pendulum experiments performed by Newton [111] set a limit of $|\eta| < 10^{-3}$ and the torsion balance experiments of Eötvös [42] found $|\eta| < 10^{-9}$. Using a triangular torsion balance, with two masses of aluminium and one of gold at the vertices, Roll, Krotkov and Dicke [122] searched for a twenty four hour variation in the torque exerted on their balance by the gravitational field of the sun. A temporal variation would arise if the gravitational acceleration of aluminium and silver differed, due to the changing orientation of the sun relative to the Earth based laboratory. With this experiment they were able to demonstrate that the acceleration of macroscopic amounts of gold an aluminium were equal to within $|\eta| < 10^{-11}$. Braginski and Panov, using a similar experimental arrangement, improved on this sensitivity by an order of magnitude when comparing the acceleration of aluminium to that of platinum [20]. Experiments to test the validity of the weak equivalence principle for individual atoms and elementary particles have been inaccurate with the exception of neutrons, where Koester [69] set a lower limit of $\eta < 10^{-4}$. Adelberger [2] has discussed the motivation for a rekindling of interest in experimental tests of the universality of free fall. Because general relativity has proved an accurate theory for gravitational phenomena this interest is primarily concerned with the search for short range 'feeble' interactions which may lie hidden beneath gravitation. To date, however, no such interactions have been uncovered.

Since the development of the general theory of relativity much has been written about the equivalence principle (see, for example, Norton [112] and references therein). Despite this large amount of literature and the wide variety of perspectives taken, Moreau, Neutze and Ross [106] were the first to provide a concrete example, taken from a specific solution of the field equations, of how the equivalence principle is incorporated into general relativity. Earlier failures [32] to draw an explicit comparison between an accelerating frame and a gravitational field stem from the fact that there does not exist a physical realisation of a homogeneous gravitational field in general relativity. Through

an appropriate choice of coordinate system for a linearly accelerating frame of reference, Moreau et al. demonstrated the first order equivalence of a local coordinate system stationary in Schwarzschild geometry with an accelerating frame of reference. Disparity between the two coordinate systems was shown to arise directly from the curvature of the Schwarzschild spacetime manifold.

In this chapter we present this demonstration of the local equivalence of Schwarzschild geometry with an accelerating frame of reference. We do not attempt, however, to provide a comprehensive review of the extensive literature on the equivalence principle. Instead, in section 3.5 we touch briefly on some of the diverging interpretations which exist within the literature. From a pragmatic perspective, one is free to choose whichever philosophical interpretation of this principle one pleases, but the local equivalence of Schwarzschild geometry with a linearly accelerating frame of reference is irrefutable.

The equivalence principle pertains to the equivalence of a uniformly accelerated frame in flat spacetime and the local effects of a gravitational field in curved spacetime. In the context of Schwarzschild geometry, this equivalence would apply between a local, stationary frame whose origin is fixed at some radial distance R from the center of the spherically symmetric, non-rotating, gravitating body and an accelerated frame in flat spacetime with a suitable value of acceleration. Thus we are motivated to transform the Schwarzschild line element to a set of displaced rectangular coordinates. The resulting expression for the Schwarzschild line element in a small region in the neighbourhood of the displaced origin consists of terms of two distinct types: (1) those that correspond to a line element in a uniformly accelerated reference frame in flat spacetime; and (2) those that correspond to curvature and are related to geodesic deviation. Only the second set of terms contribute to nonzero Riemann tensor elements. This dissection of the Schwarzschild line element into acceleration and tidal effects provides a specific example of the equivalence principle at work in general relativity.

In chapter 6 we utilise this close relationship between Schwarzschild geometry and an accelerating frame of reference when we consider three optical experiments with linearly accelerating, and freely falling, dielectric samples. The local equivalence of Schwarzschild geometry with a linearly accelerating frame of reference enables us to discuss the propagation of light through an accelerating dielectric, and in a gravitational field, within the one unified framework.

3.2 Schwarzschild solution in local Cartesian coordinates

In the first months of 1916 Karl Schwarzschild [132] published the solution of the spacetime manifold surrounding a non-rotating, spherically symmetric mass distribution. Interestingly Karl Schwarzschild arrived at this solution shortly before Einstein's publication of his generally covariant theory of gravitation [39] and Schwarzschild's solution was based on the restricted field equations of the 1913 paper of Einstein and Grossmann [41], which are valid for vacuum. Also in 1916 Johaness Droste [35] independently published a much simpler derivation of the Schwarzschild solution. The Schwarzschild line element in the coordinates of Droste is [101],

$$ds^2 = -(1 - \frac{2m}{r})c^2\,dt^2 + (1 - \frac{2m}{r})^{-1}dr^2 + r^2(d\theta^2 + \sin^2\theta d\phi^2), \qquad (3.1)$$

where $m \equiv GM/c^2$ is the geometric mass of a non-rotating, spherically- symmetric body.

In general relativity the fundamental concept is that of the spacetime manifold. The intrinsic, observer independent properties of the spacetime manifold are described by the metric tensor and its derivatives. A coordinate system is a one-to-one onto map from a subset of the manifold M to an open subset of $\mathbb{R}^n$ [152]. A change from one coordinate system to another merely relabels the events on the spacetime manifold. Thus a coordinate transformation does not result in any change to the motion of physical objects on the spacetime manifold, but merely represents an alternative choice for the description of this motion.

As motivated above, we are interested in a local coordinate system using rectangular coordinates whose origin is fixed at coordinate distance R from the center of the spherically symmetric, non-rotating, gravitating body. The coordinate transformation to this set of displaced rectangular coordinates with the z axis pointing directly from the centre of attraction is given by

$$x = r\sin\theta\cos\phi \;\; ; \quad y = r\sin\theta\sin\phi \;\; ; \quad z = r\cos\theta - R \;\; . \qquad (3.2)$$

Solving Eqs. (3.2) for r, we have

$$r = R\sqrt{1 + \frac{2z}{R} + \frac{x^2 + y^2 + z^2}{R^2}} \qquad (3.3)$$

Taking the differential of Eq. (3.3) and squaring,

$$dr^2 \;\; = \;\; \left[1 + \frac{2z}{R} + \frac{x^2 + y^2 + z^2}{R^2}\right]^{-1} \left[\frac{x^2}{R^2}dx^2 + \frac{y^2}{R^2}dy^2 + \left(1 + \frac{z}{R}\right)^2 dz^2\right.$$

$$+\frac{2xy}{R^2}dxdy+\frac{2x}{R}\left(1+\frac{z}{R}\right)dxdz+\frac{2y}{R}\left(1+\frac{z}{R}\right)dydz\Bigg]. \tag{3.4}$$

We can also write

$$r^2(d\theta^2+\sin^2\theta d\phi^2)=dx^2+dy^2+dz^2-dr^2, \tag{3.5}$$

with the final term given by Eq. (3.4).

Substitution of Eqs. (3.3), (3.4), and (3.5) into Eq. (3.1) gives the Schwarzschild line element expressed in the displaced rectangular coordinates.

$$\begin{aligned} ds^2 &= -\left[1-\frac{2m/R}{\sqrt{1+\frac{2z}{R}+\frac{x^2+y^2+z^2}{R^2}}}\right]c^2dt^2+dx^2+dy^2+dz^2 \\ &\quad -\left[1+\frac{2z}{R}+\frac{x^2+y^2+z^2}{R^2}\right]^{-1}\left\{1-\left[1-\frac{2m/R}{\sqrt{1+\frac{2z}{R}+\frac{x^2+y^2+z^2}{R^2}}}\right]^{-1}\right\} \\ &\quad \times\left[\frac{x^2}{R^2}dx^2+\frac{y^2}{R^2}dy^2+\left(1+\frac{z}{R}\right)^2dz^2\right. \\ &\quad \left.+\frac{2xy}{R^2}dxdy+\frac{2x}{R}\left(1+\frac{z}{R}\right)dxdz+\frac{2y}{R}\left(1+\frac{z}{R}\right)dydz\right] \end{aligned} \tag{3.6}$$

Equation (3.6) is exact for all values of $R>0$.

We are interested in a small region about the origin $x=y=z=0$ and assume $|x/R|$, $|y/R|$, and $|z/R|\ll 1$. We do not assume $m/R\ll 1$, and so do not make a weak field approximation. Neglecting second order terms in $|x/R|$, $|y/R|$, and $|z/R|$ in all factors in Eq. (3.6), we write a first-order expression for the line element as

$$\begin{aligned} ds^2 &= -\left(1-\frac{2m}{R}+\frac{2mz}{R^2}\right)c^2dt^2+dx^2+dy^2+\left(1-\frac{2m}{R}+\frac{2mz}{R^2}\right)^{-1}dz^2 \\ &\quad +\frac{4m}{R}\left(1-\frac{2m}{R}+\frac{2mz}{R^2}\right)^{-1}\left(\frac{x}{R}dxdz+\frac{y}{R}dydz\right), \end{aligned} \tag{3.7}$$

for small displacements about the origin with no restriction on the magnitude of $2m/R$.

3.3 Linearly accelerating coordinate systems

For the purposes of comparison with the first order Schwarzschild line element, Eq. (3.7), and the interpretation of its diagonal terms, we consider the line element of an accelerating frame of reference in flat spacetime. As discussed in the previous section, a coordinate system is merely a choice for the labelling

of spacetime points on the spacetime manifold. A change from one coordinate system to another does not alter the spacetime manifold itself. We therefore search for a convenient coordinate transformation from an inertial frame of reference, I, in flat spacetime which represents an accelerating frame of reference suitable to our purposes.

An inertial frame I in flat spacetime using Cartesian coordinates which span the entire manifold is described by the Minkowski line element,

$$ds^2 = -c^2\,dT^2 + dX^2 + dY^2 + dZ^2 \ . \tag{3.8}$$

As discussed in section 2.2, an observer O with constant linear acceleration relative to the inertial frame with which O is instantaneously comoving will follow hyperbolic motion in I. Without loss of generality we restrict the motion of this observer to lie along the Z axis of I and assume O defines the origin of an accelerating frame of reference, S. A Lorentz boost from I to an inertial frame of reference moving parallel to the Z axis leaves the X and Y coordinates unchanged. It is therefore natural to define the spatial coordinates perpendicular to the acceleration of S by $x = X$ and $y = Y$, where we have adopted the convention, used throughout this thesis, that uppercase $\{T, X, Y, Z\}$ represent inertial time and spatial coordinates, and lowercase $\{t, x, y, z\}$ represent non-inertial coordinates. If we require that both Z and z are zero when $T = t = 0$, combined with the requirement that O, who defines the origin of S, follows hyperbolic motion, we are led to a set of coordinate transformations from I to S which are given by [3]

$$\begin{aligned} T &= \frac{c}{a} f(z) \sinh\left(\frac{a\,t}{c}\right) \ , \\ X &= x \ , \\ Y &= y \ , \\ Z &= \frac{c^2}{a} f(z) \cosh\left(\frac{a\,t}{c}\right) - \frac{c^2}{a} f(0) \ , \end{aligned} \tag{3.9}$$

where, in complete generality, $f(z)$ may be an arbitrary function. It should be noted that if all $\{x, y, z\}$ are fixed then every point in S follows hyperbolic motion in I, which demonstrates that this relabelling of the spacetime manifold has defined a set of linearly accelerating coordinate systems.

It is very natural to define a coordinate system for which $z = Z$ when S is instantaneously comoving with I, which occurs when at $t = T = 0$. This system is unique and is given by

$$f(z) = 1 + \frac{a\,z}{c^2} \ , \tag{3.10}$$

which is defined for $z > -c^2/a$. The line-element for this accelerating coordinate system is given by the substitution of Eqs. (3.9) and (3.10) into Eq. (3.8), which yields

$$ds^2 = -\left(1 + \frac{a\,z}{c^2}\right)^2 c^2\,dt^2 + dx^2 + dy^2 + dz^2 \ . \tag{3.11}$$

This choice for an accelerating frame of reference has the nice feature that the spatial components of the metric are Euclidean. Furthermore, by making a Lorentz boost of Eqs. (3.9) to a frame I' moving with velocity $c\tanh\theta$ relative to I, it is easily demonstrated that the spatial coordinates of S are identical to those of the inertial frame with which the origin of S is instantaneously comoving. This provides an intuitive interpretation of this coordinate system as we recognise that coordinate displacements represent proper distances in S. It is for this reason that this coordinate system is commonly referred to as a rigid accelerating frame of reference [3, 32, 101, 103, 104]. An alternative derivation of this coordinate system is given by Misner et al. [101]. They consider a a uniformly accelerating observer who is Fermi-Walker transporting an orthonormal tetrad of basis vectors, one of which, e_0, is parallel to the the observer's 4-velocity. Because the orthogonal spatial coordinates of this tetrad are defined to measure proper spatial distances, the coordinate system above is recovered. For reasons of priority this coordinate system has become commonly known as a uniformly accelerating frame in Fermi coordinates and we adopt this convention.

General relativity predicts that a free particle will follow a geodesic of the spacetime through which it is moving, described by the geodesic equation [152, Eq. 3.3.3]

$$\frac{d^2X^\mu}{d\tau^2} = -\Gamma^\mu{}_{\alpha\beta}\frac{dX^\alpha}{d\tau}\frac{dX^\beta}{d\tau} \ , \tag{3.12}$$

where τ is the proper time along the worldline of the particle, and we have adopted the Einstein summation convention. The Christoffel symbols $\Gamma^\mu{}_{\alpha\beta}$ are given by [152, Eq. 3.1.30]

$$\Gamma^\mu{}_{\alpha\beta} = \frac{1}{2}\,g^{\mu\rho}\left\{\frac{\partial g_{\alpha\rho}}{\partial x^\beta} + \frac{\partial g_{\beta\rho}}{\partial x^\alpha} - \frac{\partial g_{\alpha\beta}}{\partial x^\rho}\right\} \ .$$

Calculating the equation of motion for a particle freely falling along the z axis of an accelerating frame in Fermi coordinates we find

$$\frac{d^2z}{d\tau^2} = -a\,\gamma^2\left(1 + \frac{a\,z}{c^2}\right) \ , \tag{3.13}$$

where $\gamma \equiv dt/d\tau = 1/\sqrt{1-(dz/dt)^2/c^2}$. Thus the acceleration of a free particle is dependent on both its velocity and position in S. The geodesic equation for a particle freely falling in Schwarzschild geometry is given by the substitution of the metric components of the line element Eq. (3.7) into the geodesic equation. For purely radial motion we obtain, at $r = R$, the equation of motion for a particle freely falling in Schwarzschild geometry [101, Eq. 25.28],

$$\frac{d^2r}{d\tau^2} = -\frac{G\,M}{R^2} \ , \tag{3.14}$$

which is independent of the velocity of the particle. Because this equation of motion is independent of the particle's velocity at R, whereas Eq. (3.13) is not, it follows that Fermi coordinates do not provide an appropriate choice with which to make a comparison with our first order Schwarzschild line element, Eq. (3.7). We therefore return to Eq. (3.9) and search for an alternative accelerating coordinate system for which the geodesic equation for a particle restricted to move along the z axis is independent of the velocity of the particle.

We proceed by substituting the Eq. (3.9) into Eq. (3.8), which yields the line element for an arbitrary linearly accelerating frame of reference,

$$ds^2 = -[f(z)]^2\,c^2\,dt^2 + dx^2 + dy^2 + [f'(z)\,c^2/a]^2\,dz^2 \ , \tag{3.15}$$

where $f'(z) \equiv df(z)/dz$. From Eq. (3.12) and the line element above we obtain the equation of motion for a particle freely falling along the z axis of this arbitrary frame of reference,

$$\frac{d^2r}{d\tau^2} = -\frac{a^2}{c^2[f(z)\,f'(z)]} + \left[\frac{f'(z)}{f(z)} + \frac{f''(z)}{f'(z)}\right]\left(\frac{dz}{d\tau}\right)^2 \ . \tag{3.16}$$

Requiring Eq. (3.14) gives us two conditions which much be satisfied,

$$f'(z) = \frac{a^2\,R^2}{G\,M\,c^2\,f(z)} \ ,$$

$$\frac{f'(z)}{f(z)} + \frac{f''(z)}{f'(z)} = 0 \ ,$$

which have the solution

$$f(z) = \sqrt{\kappa + \frac{2\,a\,z}{c^2}} \ , \tag{3.17}$$

where $a = G\,M/R^2$, κ is a constant of integration, and $f(z)$ is defined on the region $z > -\kappa\,c^2/2a$.

From Eq. (3.15) this accelerating coordinate system has the line element

$$ds^2 = -\left(\kappa + \frac{2\,a\,z}{c^2}\right)c^2\,dt^2 + dx^2 + dy^2 + \left(\kappa + \frac{2\,a\,z}{c^2}\right)^{-1} dz^2 \ . \tag{3.18}$$

This line element, with $\kappa = 1$, was previously obtained by French [47], who suggested that, because of its apparent similarity with the Schwarzschild line element, it would enable a pedagogical introduction to gravitation to be provided for students familiar to special relativity but unfamiliar with the general theory. Broucke [22] also discussed this line element, suggesting that it provided the most natural description of a linearly accelerating frame of reference as it could be derived from a linearisation of the Schwarzschild line element. While the article of Broucke appeared a few years earlier than that of French, it has become commonplace to refer to this coordinate system as a uniformly accelerating frame using French's coordinates. We also adopt this convention throughout this thesis.

Because of obvious differences between this line element, Eq. (3.18), and the line element for Fermi coordinates, Eq. (3.11), one should appreciate that the variable z in French's coordinates does not represent proper distance in S but is related to distances measured by standard measuring rods aligned along the z-axis by $\sigma(z') = \int_{z'_i}^{z'_f} (\kappa + 2\,a\,z/c)^{-1/2}\,dz$. In a small spatial interval surrounding $\kappa - 2\,a\,z/c = 1$ the spatial coordinates of French are equal to the spatial coordinates of a Fermi frame and therefore represent proper spatial intervals.

3.4 Comparison of the first-order Schwarzschild and accelerating frame line elements

If we compare the first-order Schwarzschild line element, Eq. (3.7), with the line element for an accelerating frame of reference using French's coordinates, Eq. (3.18), we see that, with $a = MG/R^2$ and $\kappa = 1 - 2m/R$, the two are identical except for the off diagonal terms in the former. These extra terms correspond to curvature that is still present in the small region about the origin in which $|x/R|$, $|y/R|$, and $|z/R| \ll 1$. In fact *only* the off-diagonal terms in Eq. (3.7) contribute to the elements of the Riemann tensor while the diagonal terms correspond *exactly* to accelerated motion in flat spacetime. This may be seen by multiplying the off-diagonal components of the metric tensor by a factor Q, $g_{13} \to g_{13}Q$ and $g_{23} \to g_{23}Q$ in Eq. (3.7). Calculation of the components of the Riemann tensor using this modified line element demonstrates all nonzero components of the Riemann tensor vanish as $Q \to 0$.

For example, to first order we obtain

$$R^0_{101} = -\frac{4m^2Q}{R^4}\left[1 - \frac{2m}{R} + \frac{2mz}{R^2}\right], \tag{3.19}$$

which becomes zero as $Q \to 0$. The persistence of curvature in the region of small displacements about the origin confirms the result of Ohanian [113].

In deriving Eq. (3.17) we have required that the equation of motion of a free particle moving parallel to the z axis of our accelerating frame is identical to the equation of motion of a particle falling radially in Schwarzschild geometry. Thus the off diagonal terms in the first order Schwarzschild line element which correspond to curvature do not affect the worldline of a radially falling particle at first order. As discussed in section 3.3, the z coordinate does not measure proper distance in the z direction in the accelerating frame. For the same reason z (and r) do not measure proper distance in Schwarzschild geometry. The key point, however, is that for geodesic motion along the z axis ($dx = dy = 0$), in both the Schwarzschild manifold and the flat spacetime manifold the z coordinate is related to proper distance in the same way to first order, and worldlines $z(t)$ of test particles will be the same to this order.

It is interesting to compare where coordinate time t is kept in the two spacetimes as it demonstrates the effect of time dilation in each of them. From Eq. (3.18), with $a = MG/R^2$ and $\kappa = 1 - 2m/R$, we see that coordinate time in the accelerated frame is kept by a clock fixed at $z = R$. Equation (3.1) indicates that the Schwarzschild coordinate time is kept by a clock at spatial infinity. A clock fixed at $r_1 = R$ in Schwarzschild geometry will run at the same rate as a clock fixed at the origin of the accelerating frame. In comparison, a clock located at $z_2 = \Delta z$ in the accelerating frame will run at a different rate to a clock located at $r_2 = r_1 + \Delta z$ in Schwarzschild geometry. The rates of these second clocks compared to the first clocks is

$$d\tau_1 = (1 - \Delta\phi)d\tau_2, \tag{3.20}$$

where $\Delta\phi = m\,\Delta z_2/R^2$ in the accelerated frame in flat spacetime and $\Delta\phi = m/R - m/(R + \Delta z_2)$ in the Schwarzschild spacetime. Thus $z_2 = R$ in the accelerated frame corresponds to $z_2 \to \infty$ in the Schwarzschild geometry. The linearly rising potential in the accelerated frame in flat spacetime takes only a finite distance R to generate the same time dilation as the $-m/r$ potential in the Schwarzschild geometry in an infinite distance. Thus both cases exhibit time dilation and coordinate times will coincide to first order in the vicinity of

the origin if coordinate time is kept by a clock fixed at $z = R$ in the accelerated frame in flat spacetime and a clock fixed at infinity in the Schwarzschild spacetime.

3.5 What is the significance of the principle of equivalence?

In this chapter we have drawn a comparison between a specific solution to Einstein's field equations and an accelerating frame of reference in flat spacetime. Throughout we have avoided any weak field approximation. This demonstrates, in a pedagogical manner, how the equivalence principle is incorporated into general relativity. The resulting expressions show the gravitational field surrounding a non-rotating spherically symmetric gravitating body can, in a local region, be separated into two distinct components: that which corresponds to an accelerating reference frame in flat spacetime and that which corresponds to curvature. It is worthwhile to briefly reflect on how this example relates to the wider literature concerned with the equivalence principle.

A modern definition of a 'true' gravitational field is that it is a spacetime manifold for which the curvature is non-zero. This is closely related to the fact that the presence of any gravitational source, that is energy or momentum, will cause the spacetime to become curved. Without the presence of gravitational sources the spacetime will remain flat. From this perspective inertial or 'fictitious' forces which arise from accelerated motion do not induce 'true' gravitational fields. It would therefore appear that a traditional statement of the equivalence principle, such as that given by Pauli [117, p.145], is flawed. Pauli's statement of the equivalence principle reads:

> *For every infinitely small world region (ie a world region which is so small that space- and time-variation of gravity can be neglected in it) there always exists a coordinate system $K_0(X_1, X_2, X_3, X_4)$ in which gravitation has no influence either on the motion of particles or any other physical processes.*

Eminent relativists such as Synge [142, p. ix] have argued strongly against this and other formulations of the equivalence principle which claim the local effects of gravitation can be transformed away:

> I have never been able to understand this Principle. .... Does

> it mean that the effects of a gravitational field are indistinguishable from the effects of an observers acceleration? If so it is false. In Einstein's theory, either there is a gravitational field or there is none, according as the Riemann tensor does not or does vanish. This is an absolute property, it has nothing to do with any observer's worldline.

Furthermore, Ohanian [113] has shown that the effects of curvature, manifest as tidal distortions to microscopic idealised liquid droplets, remain even as the dimensions of the laboratory become arbitrarily small. It is therefore possible, in principle, for any observer to determine whether they are embedded within a 'true' gravitational field, that arising from curvature of the spacetime manifold, or if their apparent gravitational field arises from 'fictitious' inertial forces.

However, in adhering to the definition that a gravitational field is curvature alone one is throwing away the predominant effect of a gravitational field on the motion of bodies within it, which is identical to the effect of acceleration, as demonstrated in this chapter for Schwarzschild geometry. Furthermore, and more importantly, one is also resurrecting precisely the distinction whose breakdown was crucial for Einstein's discovery of the general theory of relativity. It is significant that throughout his career Einstein was unwaivering in his presentation of the equivalence principle as the physical equivalence of a hypothetical homogeneous gravitational field with an accelerating frame of reference. For Einstein a linearly accelerating frame *is physically equivalent* to a homogeneous gravitational field, hence special relativity, a theory of flat spacetime, is a theory of a special type of gravitational field. It was this discovery which led Einstein to generalise Minkowski's metric description of flat spacetime to include metrics of non-vanishing curvature and thus provided the genesis of the general theory of relativity. This perspective was succinctly stated by Einstein in 1918 [40]:

> Inertia and gravity are *wesensgleich* (identical in essence). From this and from the results of the special theory of relativity it necessarily follows that the symmetrical "fundamental tensor" ($g_{\mu\nu}$) determines the metrical properties of space, the inertial behaviour of bodies in it, as well as gravitational action.

This interpretation of the equivalence principle, which implies that non-inertial frames of reference in flat spacetime provide a legitimate representation

of the predominant effects of gravitation, is clearly that adhered to by the numerous authors who have appealed to the equivalence principle to relate their measurements or predictions for accelerated systems to those which would be observed in a 'true' gravitational field. Throughout this thesis we also take this perspective. A very good review of the debate concerning the equivalence principle, and the most convincing presentation of the interpretation favoured above that this author has read, was given by Norton [112].

Chapter 4

Measurement of Frequency by non-inertial observers

In this chapter we are concerned with the measurement of frequency by non-inertial observers. We derive the Döppler shift transformations for both a linearly accelerating observer and an observer stationary in Schwarzschild geometry when the radiation source is inertial. Unlike the geometric formalism of general relativity we find the Döppler shift relations depend explicitly on the duration of the measurement. Before calculating these frequency transformation formula we show a simple quantum mechanical clock will violate the accelerating clock principle, and the minimum magnitude of this violation is dependent on the mass of the clock. We also briefly review a related discussion on the coupling of the helicity of light to rotation.

4.1 General covariance and the hypothesis of locality

In his introduction to his celebrated paper of 1916, *'The foundation of the general theory of relativity'* [39], Einstein discussed at length the physical basis of the theory of measurement within a classical context. From these reflections Einstein concluded that all measurements consisted merely of the detection of point like spacetime coincidences. As the occasion of a spacetime coincidence is entirely independent of the motion of any observer who notes this coincidence, we find that any coordinate system carried by any observer provides a perfectly legitimate description of these spacetime events. Thus the coordinate system used to describe any measurement is immaterial and one is left with no alternative but to regard all imaginable systems of coordinates as equally valid. This leads immediately to the requirement of general covariance [39]:

> *The general laws of nature are to be expressed by equations which hold good for all systems of coordinates, that is, are covariant with respect to any substitution whatsoever (generally co-variant).*

This principle, applied to the special case of inertially moving observers, combined with the assumption of the constancy of the velocity of light in vacuum, led directly to the special theory of relativity. Upon Einstein's discovery of the principle of equivalence [38] (see chapter 3), based upon the empirical coincidence of inertial and gravitational mass, his conviction in the principle of general covariance led ultimately to the general theory of relativity, a geometric description of gravitation.

Based upon the principle of general covariance the general theory of relativity contains an unambiguous prescription for predicting the results of any measurement performed by any observer with arbitrary motion. In answering the question, how are the measurements of non-inertial observers related to those of inertial observers, general relativity responds: *the results of measurements performed by an accelerated observer at any point in spacetime are identical with those of the hypothetical inertial observer at the same event with the same velocity* [88]. While this prescription has been elegantly incorporated into the mathematical formalism of general relativity, it should be recognised that its status is that of a central assumption upon which the theory of relativity is founded, and therefore deserving of scrutiny. This assumption is referred to as the *hypothesis of locality*, or the standard measurement hypothesis, and can be regarded as a natural consequence of the classical concept that all measurements simply consist of the recording of spacetime coincidences.

With the advent of quantum mechanics, however, it has become apparent that this classical notion of measurement needs refinement. In particular, the simultaneous determination of conjugate physical quantities is intrinsically restricted by Heisenberg's uncertainty principle. Many attempts have been made to develop a quantum theory of gravitation. Several physicists have argued that the reconciliation of the principle of general covariance with a quantum description of measurement poses grave difficulties [154, 86]. Mashhoon, one of the strongest proponents of the need for physics to move beyond the assumption of locality, has suggested that if the acceleration length and time scales of the observer, $\mathcal{L}$ and $\mathcal{L}/c$ respectively, are of a similar magnitude to the phenomena under observation then the locality hypothesis will be violated [91].

In this chapter we are primarily concerned with the measurement of the frequency of light by non-inertial observers. If we were to accept, unconditionally, the prescription of general relativity then this problem would simply require a straightforward application of the mathematical formalism of geometric optics

and little physical insight would be gained. However, as is well known, the measurement of frequency cannot be resolved instantaneously but is fundamentally limited by the Heisenberg energy-time uncertainty relation [30]. Even classical arguments based upon Fourier analysis show that if a frequency resolution $\Delta\nu$ is desired then the characteristic duration of the measurement must be at least $\Delta\tau \sim 1/\Delta\nu$. If an instantaneous measurement of frequency were attempted then $\Delta\tau = 0$ such that $\Delta\nu = \infty$ and no information at all is revealed. The desire to avoid the assumption that the measurement of frequency is merely an instantaneous point like event, implicit in the formalism of general relativity, has motivated the work of Mashhoon [86, 87, 89, 90, 91, 92, 95], Moreau [104] and Neutze and Moreau [108, 109]. All of this work accepts general relativity as providing an accurate description of electromagnetic wave propagation in non-inertial spacetimes, but applies the additional physical constraint that the time interval characteristic of the measurement of frequency is non-zero. These analyses have shown the Döppler shift relations predicted by the formalism of general relativity, which assumes the validity of the locality hypothesis, are only approximate when the ratio $c\Delta\tau/\mathcal{L}$ is not negligible within the desired accuracy of the measurement, where $\mathcal{L}$ is the length scale characteristic of the acceleration of the observer. While these analyses have all been classical in nature, their conclusions may be regarded as indicating the nature of corrections which would arise from a fully quantum mechanical treatment of the problem.

In order for an observer O to accurately measure the frequency of a light signal O must carry along her world line a sufficiently accurate clock. We therefore initially discuss the measurement of time by accelerating clocks and provide, to our knowledge, the first treatment of a simple model of a quantum mechanical clock with linear acceleration. In section 4.3 we briefly review previous discussions of the measurement of frequency by rotating observers. This problem is closely related to our primary interest in the influence of acceleration on the measurement frequency. This literature has revealed that the frequency of light when measured by a rotating observer will differ from that predicted by general relativity because of coupling between the helicity of light and rotation. Sections 4.4 and 4.5 represent our most significant contribution to the debate concerning the measurement of frequency by non-inertial observers. In these sections we calculate, respectively, an analytic expression for the Döppler shift for an accelerating observer and for an observer stationary in Schwarzschild geometry when the light source is moving inertially. These transformation formulae demonstrate that the Döppler shift relations derived

using the geometric formalism of general relativity are only approximate when the effects of acceleration are not negligible over the time scale characteristic of the measurement.

4.2 Measurement of time by accelerating clocks

If we accept the hypothesis of locality it follows immediately that *the rate at which a clock with arbitrary motion records the passage of time is identical to that of a hypothetical instantaneously comoving inertial clock.* This consequence of the standard measurement hypothesis is itself referred to as the *standard clock hypothesis.* The most significant experimental evidence in support of this clock hypothesis has been provided by Hafele and Keating [53]. Transporting atomic clocks in jet aeroplanes both eastward and westward around the earth, Hafele and Keating continuously compared the rate of these moving clocks with a reference clock based on the Earth's surface. From their experimental data they were able to verify the validity of the clock hypothesis under moderate accelerations.

Nevertheless, the standard clock hypothesis has received some scrutiny. Most notable objections are those of Khan [66, 67] and Kowalski [71]. In this work both authors have suggested that both the acceleration and the instantaneous velocity of a clock affects its rate.

Khan introduced a *principle of reciprocity* so as to motivate the rejection of the accelerating clock hypothesis. Khan's reciprocity principle required that two observers in relative motion make identical assessments of one another's motion through the use of their own measuring devices. When applied to the case of a linearly accelerated observer, Khan's principle of reciprocity leads to the conclusion that there would be no twin paradox. The existence of the twin paradox has been well established, with experimental support provided by the experiment of Hafele and Keating [53]. Therefore, Khan's violation of the twin paradox is sufficient to reject his theory as it was originally formulated.

Kowalski has also suggested an alternative to the accelerating clock principle. Kowalski considered the example of two identical clocks which are both synchronised and stationary in an inertial frame I and separated by a proper distance L. Kowalski then accelerated these clocks and eventually brought them to rest in a second inertial frame I', again requiring them to be separated by a proper distance L. The physical assumption which forms the basis

of Kowalski's alternative to the accelerating clock principle is Kowalski's demand that these two clocks also be synchronised in the second inertial frame I'. Within the geometric formalism of general relativity, however, two accelerating clocks which maintain their spatial separation do not remain synchronised with respect to their instantaneously comoving frame of reference. This asynchronisation effect can be interpreted as the origin of the phenomenon of gravitational redshift within an accelerating frame. Thus Kowalski's theory goes beyond the accelerating clock hypothesis.

Mainwaring and Stedman included both of these authors' discussions of the accelerating clock hypothesis within one generalised framework [85]. In presenting alternatives to the standard clock hypothesis Mainwaring and Stedman expressed the rate of an accelerating clock as a power series of the proper acceleration a, such that

$$\frac{d\tau_a}{d\tau_i} = 1 - \lambda \sum_{n=1}^{\infty} g_n a^n \ , \tag{4.1}$$

where τ_a represents the time interval recorded by an accelerating clock, τ_i is the time interval recorded by interval of the hypothetical instantaneously comoving inertial clock and g_n a coefficient with dimensions $L^{-n}T^{2n}$. Terms of first order in Eq. (4.1) were sufficient to describe the alternative theories of Khan and Kowalski. Within their framework, Mainwaring and Stedman clearly demonstrated the alternative theories of Khan and Kowalski were preferred frame theories. As such the transverse Döppler shift experiments of Hay et al. [58] and Turner and Hill [148], who mounted an Fe^{57} Mössbauer source and receiver on a rapidly rotating disk and measured the absorption as a function of angular velocity, are able to place stringent limits on the parameter λ. Drawing this comparison Mainwaring and Stedman concluded $\lambda \ll 1$ for both alternative clock principle theories, which is significantly less than the magnitude of the accelerating clock principle violations suggested Khan and Kowalski, whose theories both assumed λ was the order of unity.

Another significant discussion of the role of clocks in a non-inertial context is that of Salecker and Wigner [126], who proposed to measure spacetime separations using quantum clocks and light signals. This analysis aimed to determine the fundamental limitation which quantum mechanics places on the measurement of spacetime distances in a gravitational context. Their work was motivated by the underlying principle of general relativity that coordinates have no meaning independent of their observation [154]. Salecker and Wigner showed the accuracy of a quantum mechanical clock is inevitably limited by

its mass. Assuming the uncertainty in the location of the clock is not so large as to cause further significant uncertainty in recording time intervals by a macroscopic detector, they showed the measurement of a spatial distance using a clock of mass m intrinsically contained an uncertainty of the order $\Delta Z \sim c\Delta T \sim \sqrt{\hbar T/m}$.

Salecker and Wigner's model for a microscopic quantum clock which could measure spacetime distances consisted of two mirrors separated by an unknown spatial distance d, with the time interval for a minimum uncertainty light wavepacket to propagate back and forth between the mirrors being recorded by a quantum clock of mass m. From the measurement of this time interval the separation of the mirrors can be inferred. In the work below we reconsider the arguments of Salecker and Wigner but assume the spatial distance d between each mirror is known and treat this apparatus as a clock in its own right. Such a clock, assumed to be moving along a geodesic, has been described by Misner et al, [101, pp. 397-399] as a useful model for a clock in a gravitational context. The recording of a time interval using such a clock consists of the counting the number of times the wavepacket intercepts one of the mirrors in an interval of duration T.

First consider such a clock which is stationary in an inertial frame I and aligned so that the wavepacket propagates along the Z-axis. Each detection of the wavepacket at the first mirror would correspond to a time interval $2d/c$ so the rate at which this clock runs is $c/2d$ counts per second. For each count to be resolvable the spread of the wavepacket must be less than the dimensions of the clock, $c\Delta T \leq d$, where ΔT is the temporal spread of the wavepacket and, as such, also corresponds to the fundamental temporal resolution achievable with our clock. Upon each reflection off the mirrors of the clock this wavepacket imparts an indeterminate momentum $\sim \hbar/c\Delta T$ to the clock, which follows from the Heisenberg position/momentum uncertainty relation. This uncertainty is at least the order of magnitude of the uncertainty in the momentum of the clock itself, which is assumed to have an uncertainty in its position $\Delta Z \leq d$. Because of this indeterminant momentum our clock has a minimum uncertainty in its velocity given by $\Delta v \sim \hbar/mc\Delta T$ where m is the mass of the clock. Therefore, at a later time T the clock may be a distance $T\Delta v \sim T\hbar/mc\Delta T$ from where it would have been located in classical mechanics. A macroscopic observer O records the time interval measured by our microscopic clock by receiving light signals from the clock itself. In order to maintain the accuracy of our clock we demand the uncertainty in the location of the clock does not,

itself, lead to an uncertainty contribution greater than ΔT in the recording of time by our macroscopic detector. Therefore $T\Delta v \sim \hbar T/mc\Delta T < c\Delta T$ from which it follows that $\Delta T > \sqrt{\hbar T/mc^2}$, which recovers the result of Salecker and Wigner [126]. Thus the mass of our clock, which is accurate to ΔT over a time interval T, is required to be

$$m > \frac{\hbar T}{(c\Delta T)^2} \ . \tag{4.2}$$

We now assume our clock is stationary in a rigid accelerating frame of reference, which has the spacetime metric given by Eq. (3.11). We locate the two mirrors at $z = z_0$ and $z = z_0 + d$ and the light propagates parallel or antiparallel to the z-axis. The coordinate time for the centre of our wavepacket to complete a round trip from a mirror at $z = 0$ to a second mirror at $z = d$ and back is found by calculating the null geodesics of the accelerating frame. Substituting $ds = dx = dy = 0$ into Eq. (3.11) and integrating we find

$$\begin{aligned}
\Delta t|_{z_0 \to z_0+d} &= \int_{z_0}^{z_0+d} \frac{dz}{c\,(1 + a\,z/c^2)} = \frac{c}{a} \ln\left\{1 + \frac{a(z_0+d)}{c^2}\right\} - \ln\left\{1 + \frac{az_0}{c^2}\right\} \\
&\approx \frac{d}{c}\left(1 - \frac{a(z_0 + d/2}{c^2})\right) \ , \\
\Delta t|_{z_0+d \to z_0} &= \int_{z_0+d}^{z_0} -\frac{dz}{c\,(1 + a\,z/c^2)} \approx \frac{d}{c}\left(1 - \frac{a(z_0+d/2)}{c^2}\right) \ .
\end{aligned}$$

Therefore the coordinate time interval for the light pulse to make a round trip of the clock is

$$\Delta t = \left\{1 - \frac{a(z_0 + d/2)}{c^2}\right\} \frac{2d}{c} \ . \tag{4.3}$$

In an inertial context the arrival of the wave-crests at the mirror corresponds to a proper time interval $2d/c$. If O were to assume her clock was unaffected by acceleration and therefore accredited successive arrivals of the wavepacket as representing a proper time interval $\Delta\tau = 2d/c$, such that we can replace $2d/c$ by $\Delta\tau$ in Eq (4.3), O would register a relation between the rate of her clock and the rate of coordinate time

$$dt = \left(1 - \frac{a(z_0 + d/2)}{c^2}\right) d\tau \ ,$$

which, at first order in $a(z_0 + d/2)/c^2$, corresponds exactly to the relationship between proper time and coordinate time for an observer located at $z = z_0 + d/2$ using the formalism of general relativity, which assumes the standard clock

hypothesis. If we adopt the notation of Mainwaring and Stedman, Eq. (4.1), we find

$$\frac{d\tau_a}{d\tau_i} = 1 \pm \frac{a\,d}{2c^2} \ ,$$

where the positive (negative) sign applies to an observer who counts the wavepacket detections at the lower (upper) mirror and, as previously stated, τ_a represents the time interval recorded by our accelerating clock and τ_i represents that of a hypothetical instantaneously comoving inertial clock. Thus, for our simple model, one finds the accelerating clock principle is violated by a factor $\pm d/2\mathcal{L}$, where $\mathcal{L}$ is the length scale characteristic of the acceleration. For example if our clock had $d \sim 10$ cm and $a \sim 100$ m.s^{-2} then this discrepancy is of the order of 5 parts in 10^{17}.

One could, of course, decrease the separation of the mirrors until a satisfactory agreement between our clock and the accelerating clock principle is achieved. However, decreasing d comes at a cost. As was previously discussed for the case of an inertial clock, for our clock to operate at all we require the resolution $c\Delta T < d$. If we decrease the dimensions of the clock to the level of an infinitesimal separation between the mirrors then, as given by Eq. (4.2), the mass of our clock would have to become infinite for our clock to be functional. From Eq. (4.2), a functional clock of mass m which is accurate to ΔT over a time interval T is required to have $d > c\Delta T > \sqrt{\hbar T/m}$. Therefore we find, based upon a simple model of a quantum mechanical clock, *a violation of the accelerating clock hypothesis is predicted* with

$$\left|\frac{d\tau_a}{d\tau_i} - 1\right| \geq \frac{a}{2c^2}\sqrt{\frac{\hbar T}{m}} \ . \tag{4.4}$$

The author believes this novel prediction, or a similar version of it, would also be reached if one were to consider the behaviour of a more sophisticated model of a quantum mechanical clock when accelerating. We note, however, that we have maximised this violation in our derivation by requiring the light to propagate parallel or antiparallel to the direction of acceleration. In order to gauge the significance of this minimum violation of the accelerating clock principle we consider a clock with a mass ~ 1 amu (for example a single Cs atom) and acceleration 100 m.s^{-1} which we require to have maximal accuracy for 1000 years, then the RHS of Eq. (4.4) is only ~ 2 parts in 10^{15}.

Despite the above conclusions, we will accept the standard clock hypothesis as a valid description for the behaviour of clocks when accelerating throughout the remainder of this thesis. This discrepancy may be overcome by increasing

the mass of the clock until agreement with the accelerating clock principle is achieved to the desired accuracy, or simply correcting the rate of the clock to take into account the influence of acceleration. We do, however, wish to draw the readers attention to the physical basis of this conclusion. In this case the length scale characteristic of the measurement is the dimension of the clock, d, and the acceleration length scale for the clock is $\mathcal{L} = c^2/a$. As we find throughout this chapter, and as discussed in detail by Mashhoon [86], the violation of the hypothesis of locality for the measurement of time is proportional to $d/\mathcal{L}$, the constant of proportionality being $\frac{1}{2}$ in this instance.

4.3 Helicity-rotation coupling

Experimental and theoretical studies of the influence of rotation in optical interferometry are now entering their second century [5]. Through the observation of the Sagnac effect [125], and the experimental verification of the second order Döppler effect using a Mössbauer source and receiver mounted on a rapidly rotating disk [58], the influence of rotation has played an important role in modern physics through providing verification of the theory of relativity in an accelerated context. It is therefore aesthetically appealing that, through experimental study of the effects of rotation on optical and neutron interferometry, it may be possible to search for spin-rotation coupling induced violations of the theory of relativity [88, 95, 61, 134].

In this chapter we are primarily concerned with the measurement of the frequency of light by non-inertial observers. When considering the measurement of the frequency of circularly polarised light by rotating observers the concept of helicity-rotation coupling arises naturally. From this perspective, spin-rotation coupling is closely related to our primary interest. We therefore briefly review the physical basis for the discussions reported within the literature concerned with helicity-rotation and spin-rotation coupling.

The hypothesis of locality provides a correct and consistent description of systems involving classical point particles and electromagnetic rays whose interactions, by definition, do not involve any extension in space and time. Mashhoon has suggested a natural prescription for the extension of this hypothesis to include the measurement of wave phenomena. This prescription reads [90]: 'the hypothesis of locality can be employed to define the electromagnetic field quantities as measured by the accelerating observer. The (nonlocal) Fourier analysis of the field is then used to define the frequency

and propagation vector of radiation in a covariant manner'. By the use of the term nonlocal, Mashhoon is alluding to the fact that Fourier analysis cannot instantaneously resolve frequency, but rather is an integral over the time history of the radiation. If the observation has a characteristic duration $\Delta\tau$ then a resolution in frequency $\Delta\nu \sim 1/\Delta\tau$ may be obtained.

We now apply this prescription, as did Mashhoon, to the problem of the frequency of circularly polarised light measured by an observer O' with angular velocity Ω. From general relativity, which incorporates the locality hypothesis, the components of the electromagnetic tensor $\mathcal{F}_{\alpha\beta}$ in a non-inertial frame S are

$$\mathcal{F}_{\alpha\beta}(\tau) = F_{\mu\nu}\,\frac{\partial X^{\mu}}{\partial x^{\alpha}}\frac{\partial X^{\nu}}{\partial x^{\beta}}\ , \tag{4.5}$$

where $F_{\mu\nu}$ specify the components of the Faraday tensor in an inertial frame I, and x^{α} denote the non-inertial coordinates of S. Let S be rotating with angular velocity $\boldsymbol{\Omega}$ parallel to the Z-axis of I. The natural coordinate transformation from I to S is

$$\begin{aligned} t &= T\ , \\ x &= X\cos(\Omega t) + Y\sin(\Omega t)\ , \\ y &= Y\cos(\Omega t) - X\sin(\Omega t)\ , \\ z &= Z\ . \end{aligned}$$

Consider right (left) circularly polarised light propagating in vacuum parallel to the Z-axis of I with frequency ω in I. This is described by the vector potential

$$\boldsymbol{A} = \mathcal{R}\left\{A_0(\hat{\boldsymbol{X}} \pm i\hat{\boldsymbol{Y}})\,\exp -i\omega(T - Z/c)\right\}\ ,$$

such that, according to an observer O' stationary in S, the vector potential is

$$\boldsymbol{A}' = \mathcal{R}\left\{A_0(\hat{\boldsymbol{x}} \pm i\hat{\boldsymbol{y}})\,\exp i(\omega Z/c - [\omega \mp \Omega]t)\right\}\ . \tag{4.6}$$

Applying the prescription of Mashhoon and defining the frequency of light observed by O' as the Fourier transformation of Eq. (4.6) with respect to the proper time along the worldline of O', we find the frequency of this light measured by O' is $\omega' = \gamma(\omega \mp \Omega)$, where $\gamma = 1/\sqrt{1 - (x^2 + y^2)\Omega^2/c^2}$ when O' is located at $(x, y, 0)$. If the duration of the measurement $\Delta\tau$ is sufficiently long that a frequency resolution less than Ω is achievable, $\Delta\tau > 1/\Omega$, then we may expect to observe a frequency splitting between radiation of opposite helicity. The Döppler shift transformations of general relativity predict, in this context, that $\omega' = \gamma\omega$ for both right and left circularly polarised light. It is the vector

nature of the electromagnetic radiation, combined with Mashhoon's non-local prescription for defining frequency, which leads to the discrepancy between this result and the result of general relativity which is based upon the invariance of the phase. Thus the difference in frequency between general relativity and the prediction of Mashhoon, $\mp\gamma\Omega$, is a consequence of the coupling of the helicity of the light with rotation.

In general the Frequency transformations which include the effect of helicity-rotation coupling are given by [90],

$$\omega' = \gamma\left\{\omega - \boldsymbol{v}\cdot\boldsymbol{k} - \hat{\boldsymbol{H}}\cdot\boldsymbol{\Omega}\right\} \tag{4.7}$$

where $\hat{\boldsymbol{H}} = \pm c\boldsymbol{k}/\omega$ is the helicity of the photon, the positive (negative) sign chosen for right (left) circularly polarised light and $\boldsymbol{v} = \boldsymbol{\Omega}\times\boldsymbol{r}$ is the velocity of O' in I. Again this expression differs from the standard Döppler shift, given by $\omega' = \gamma\{\omega - \boldsymbol{v}\cdot\boldsymbol{k}\}$, because of helicity/rotation coupling. If we attempted to resolve this discrepancy we would require a measurement with a characteristic duration $\Delta\tau > 1/(\gamma\hat{\boldsymbol{H}}\cdot\boldsymbol{\Omega})$. From this perspective Mashhoon's application of a non-local definition of frequency, which led to the prediction of helicity-rotation coupling, and the requirement that the measurement be of finite duration in order to resolve this violation of the standard Döppler shift formula, is closely related to other material presented within this chapter. In sections 4.4 and 4.5 we also predict a discrepancy between the geometric formalism of general relativity and the Döppler shift transformation formulae for non-inertial observers. This difference arises from the fundamental requirement that any measurement of frequency must be of finite duration. Unlike the prediction of helicity/rotation coupling our predictions do not depend upon the vector nature of light.

An interesting consequence of Eq. (4.6) is that, with right circularly polarised light and $\Omega = \omega$, the radiation field loses its temporal variation when viewed by O'. One should appreciate that Eq. (4.6) is a direct result of the formalism of general relativity, and is independent of Mashhoon's extension of the hypothesis of locality. This loss of temporal variation is in contrast with an important feature of special relativity, that a time dependent electromagnetic field is time dependent when viewed by any inertial observer. Mashhoon [94] has motivated a non-local theory of electrodynamics on the basis of this feature of special relativity, postulating that an electromagnetic field which is time dependent when viewed by an inertial observer also appears time dependent with respect to arbitrary observers. To achieve this Mashhoon suggested that the

Faraday tensor for an accelerating observer be given by

$$\mathcal{F}_{\alpha\beta} = F'_{\alpha\beta} + \int_{\tau_0}^{\tau} K_{\alpha\beta}{}^{\gamma\delta}(\tau,\tau') F'_{\gamma\delta}(\tau')\, d\tau' \quad , \tag{4.8}$$

where τ_0 is the time O begins to accelerate and the kernel $K_{\alpha\beta}{}^{\gamma\delta}(\tau,\tau')$ is anti-symmetric in its first and second pair of indices and depends on the acceleration of O. To recover a Lorentz invariant theory Mashhoon required that the kernel vanishes when there is no acceleration and the nonlocal part of Eq. (4.8) be proportional to $\lambda/\mathcal{L}$, vanishing in the eikonal limit. Developing a theory within this framework on the basis that *no observer can remain at rest with an electromagnetic wave*, Mashhoon concluded that the field as measured by the rotating observer would be

$$\mathcal{F} = \frac{\gamma\omega}{\omega'}\left[1 \mp \frac{\Omega}{\omega} e^{i\omega'\tau}\right] F' \quad ,$$

such that, with $\Omega = \omega$, the field varies linearly with proper-time and the amplitude is larger (smaller) for positive (negative) helicity radiation. It was suggested that the difference in amplitude between right and left circularly polarised light could be searched for as experimental justification for this non-local theory. However, without empirical evidence to suggest the general theory of relativity should be modified to include terms of the the form of Eq. (4.8), this suggestion of Mashhoon will remain an imaginative extension of general relativity without compelling physical basis.

While outside of our current interest in the measurement of the frequency of light by accelerating observers, it is appropriate that we pause, briefly, to review some closely related experimental proposals reported in the literature. It has been suggested by a number of authors [88, 95, 61, 134] that it may be possible to experimentally detect the coupling of the intrinsic spin of fermions to rotation. The analogue of Eq. (4.7) for fermions is

$$\omega' = \gamma\{\omega - \boldsymbol{v}\cdot\boldsymbol{k} - \boldsymbol{\sigma}\cdot\boldsymbol{\Omega}/\hbar\} \quad , \tag{4.9}$$

which has been derived from natural assumptions for the evolution of spin in a rotating frame in reference [95]. Spin-rotation coupling has also been predicted by Hehl and Ni [61], who used the covariant framework of general relativity to transform the Dirac equation into a rotating frame of reference.

Mashhoon [95] has recently argued that indirect experimental verification of this phenomenon has already been reported, claiming that Venema et al. [151], who searched for exotic spin interactions using the nuclear magnetic precession

of atomic mercury, recorded the coupling of spin to the rotation of the Earth as a bias in their results. In the presence of of a magnetic field $\sim 10^{-3}$ G, the nuclear spin precession frequencies of two ground state mercury isotopes, ^{199}Hg (I= $\frac{1}{2}$) and ^{201}Hg (I= $\frac{3}{2}$), contained in the same vapour cell were measured. Two magnetic field configurations were considered, parallel and anti-parallel to the rotation of the Earth. The influence of the rotation of the earth, ~ 11.6 μHz, was systematically subtracted out and the resolution obtained after several runs was a factor of 20 below this frequency. Furthermore, because of the random alignments of the atoms in the gas, it was considered that the orbital contributions would cancel and would not simulate the effect of spin-rotation coupling.

Silverman [134] has proposed that the degenerate hydrogen states 1S(F=1; $m_F = \pm 1$) could also be split by the rotation of the Earth. The equivalence of this proposal with the claim that the intrinsic spin of an elementary particle will coupling to the Earth's rotation follows from the converse of Larmor's theorem whereby the dynamics of particles in a rotating frame of reference manifest a formal equivalence (at first order) to the dynamics of particles in a constant magnetic field. As Zeeman splitting occurs when Hydrogen atoms are exposed to a magnetic field, their degenerate magnetic substrates should also be split by rotation. Silverman suggested a direct search for hyperfine splitting induced by the rotation of the Earth could prove successful if current experimental uncertainty can be reduced by a further two orders of magnitude.

A polarised neutron interferometer may also provide a convenient instrument with which to search for spin-rotation effects. As proposed by Mashhoon and Werner [88], the polarisation of neutrons could be flipped in one arm of the interferometer and then allowed to propagate a distance Δl before being realigned and combined with the opposite beam at the detector. In such an experiment a spin-rotation induced phase shift of the order $\Omega \Delta l / v_n$ should be observable, where v_n is the speed of the neutrons. As this phase shift is significantly less than the usual Sagnac phase shift it was suggested that a figure of eight interferometer be used to remove the dominant Sagnac bias. Audretsch and Lämmerzahl [9] have analysed a similar experimental proposal using atomic beam interferometry. An improvement of several orders of magnitude is expected for the atomic case as atoms can be slowed, using laser cooling techniques, to very low velocity.

While these experimental proposals fall outside of the primary interest of our work reported within this chapter, concerned with the Döppler shift rela-

tions for light propagating in vacuum when measured by non-inertial observers, they do illustrate the need for physics to move beyond the locality hypothesis is receiving serious consideration from the scientific community. Furthermore, several of the predictions arising from a natural extension of the locality hypothesis would appear to be within, or just beyond, the current technological sphere. It is therefore highly desirable to further examine the experimental consequences of relaxing the locality hypothesis. In the following section we continue this examination and consider the measurement of frequency by a linearly accelerating observer and an observer stationary in Schwarzschild geometry when the source is inertial.

4.4 Frequency measurement by a linearly accelerating observer

We now turn our attention to the measurement of frequency by linearly accelerating observers. Interest in this problem [87, 104, 108] again stems from the fundamental restriction that frequency cannot be measured instantaneously. From our previous discussion we would expect the Döppler shift relations derived assuming the hypothesis of locality to be only approximate when $c\Delta\tau/\mathcal{L} = a\,\Delta\tau/c$ is not negligible, $\Delta\tau$ representing the time characteristic of the measurement of frequency and a is the linear acceleration of the our observer O. This proves to be the case, with the Döppler shifted frequency differing by an amount $\nu\, a\,\Delta\tau/c$ from the prediction of standard relativity.

Using his prescription for extending the locality hypothesis based upon Fourier analysis, Mashhoon [87] calculated the frequency components of the electromagnetic field when measured by a linearly accelerating observer. Considering a Gaussian light wavepacket with a temporal variation $\exp(-i\omega_0 T - \frac{1}{2}T^2/\Delta\tau^2)$ in an inertial frame I, Mashhoon showed the frequency profile of this radiation when recorded by an accelerating observer became asymmetric. The degree of asymmetry could be parameterised by the ratio $a\,\Delta\tau/c$, becoming highly asymmetric when this was the order of unity. Thus the hypothesis of locality, which would predict that the frequency distribution of the light would remain a Gaussian independent of the acceleration of the observer, proves to be approximate when $c\Delta\tau/\mathcal{L}$ is not negligible. Physically this asymmetry stems from the measurement of frequency using Fourier analysis being non-instantaneous, with $\Delta\tau$ characterising the duration of the wavepacket in this example.

In this and in the following section we build upon the analysis of Mashhoon and derive analytic expressions for the Döppler shift for both a linearly accelerating observer and an observer stationary in Schwarzschild geometry. The model we use is inherently classical and is not based on Fourier analysis. Instead we assume an inertial harmonic source emits a pulse of radiation of finite duration, $\Delta\tau$. The frequency of this radiation is measured by a non-inertial observer O. From the measured duration of the pulse and the invariance of the number of wavecrests O determines the frequency of the pulse with an associated uncertainty. In this classical model the uncertainty arises from the uncertainty of the phase at either end of the pulse as the signal may be between peaks at the end points. Classically this introduces an uncertainty in O's counting of the peaks $\Delta N = \pm 1$. Thus the minimum uncertainty in the frequency for N peaks is given by [30]

$$\Delta\nu \sim 1/\Delta\tau \ .$$

By enabling an analytic expression for the frequency for non-inertial observers to be calculated, this model explicitly illustrates the manner in which the non-instantaneous nature of frequency measurement affects the Döppler shift formula. Our expressions for the respective Döppler shifts contain a dependence on the duration of the measurement when the observer is non-inertial. This dependence is not predicted by the frequency transformations derived using the standard geometric formalism of general relativity.

One of the aims of this work is to illustrate the likely consequences for the Döppler effect which a full quantum mechanical treatment of this problem would unveil. While our model illustrates the effect of frequency measurement being of finite duration, thus containing an important feature of a quantum mechanical theory of measurement, the model itself is inherently classical. In order for phase to be well defined we require a large photon number for the quantum state of the electromagnetic field [83]. Therefore, this model should not be regarded as a prescription for measuring the frequency of a single photon. The reader should also appreciate that we accept the validity of the standard clock hypothesis throughout, assuming the clocks of our non-inertial observers run at the rate predicted by standard relativity. Furthermore, we do not diverge from general relativity when describing the propagation of an electromagnetic pulse in vacuum. *Our only physical assumption which goes beyond the theory of relativity is our requirement that the measurement of frequency cannot be performed instantaneously.* This physical basis is entirely consistent with the central argument used by Mashhoon when extending the

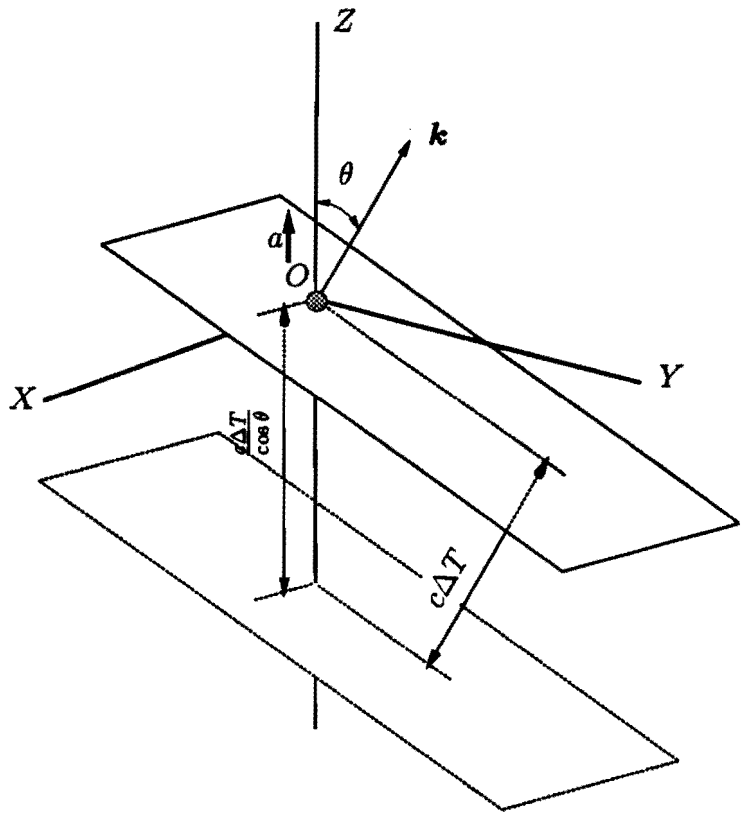

Figure 4.1: The first and final (dotted) planes of constant phase of the wavepacket which intersect the accelerating observer O at $\tau = 0$ and at τ respectively. This illustration is viewed from the inertial frame I

locality hypothesis to apply to the measurement of wavelike phenomena [86, 87, 89, 90, 91, 92, 95].

4.4.1 Calculation of the Döppler effect

Consider a monochromatic source of electromagnetic radiation, Σ, which is moving inertially in Minkowski spacetime and has mass m. Σ emits a plane wave pulse of finite duration ΔT containing N wave peaks, which propagates in vacuum until it intercepts the worldline of an observer, O, who is following hyperbolic motion. We assume the effect of radiation back reaction on the worldline of Σ and the effect of Σ on spacetime curvature are negligible. This requires $h\nu \ll mc^2$ and is itself small. As discussed in section 4.2, we also assume the clock carried by O is sufficiently massive that we may neglect its uncertainty in measuring proper time intervals [126], yet not so massive that its effect on spacetime curvature is significant.

Let τ denote the proper time along the worldline of O. At $\tau = 0$, O detects

the arrival of the electromagnetic radiation. Define I as the inertial frame in which O is stationary at this instant. Choose the axes of I such that O passes through the origin of I at time $T = \tau = 0$ and continues along the Z axis. Eq. (2.5) gives the worldline of O in I as $X = Y = 0$ and

$$T = \frac{c}{a}\sinh(\frac{a\tau}{c}) \ , \tag{4.10}$$

$$Z = \frac{c^2}{a}\cosh(\frac{a\tau}{c}) - \frac{c^2}{a} \ . \tag{4.11}$$

When measured in I this radiation pulse has frequency ν, wave vector $\boldsymbol{k}$ and duration ΔT, as illustrated in figure 4.1. The angle between the Z axis of I and $\boldsymbol{k}$ is θ. The worldlines of the points where each end of the electromagnetic pulse cuts the Z axis are given respectively by

$$\begin{aligned} Z\cos\theta &= cT \ , \\ Z\cos\theta &= c(T - \Delta T) \ . \end{aligned} \tag{4.12}$$

We wish to evaluate the proper time interval between the detection of each end of the wave-train by O. From our construction, the beginning of the pulse intercepted the worldline of O at $\tau = 0$. The time at which O detected the end of the pulse is found by substituting (4.10) and (4.11) into (4.12) and solving for τ. Noting the identities

$$A\sinh\alpha + B\cosh\alpha = \sqrt{A^2 - B^2}\,\sinh\left(\alpha + \frac{1}{2}\ln\frac{A+B}{A-B}\right) \tag{4.13}$$

where $A > |B|$ and

$$\ln(\alpha + \sqrt{\alpha^2 + 1}) = \sinh^{-1}\alpha \ ,$$

we obtain

$$\frac{1}{\nu'} = \frac{\Delta\tau}{N} = \frac{c}{Na}\left\{\sinh^{-1}\left(\frac{a\,\Delta T/c - \cos\theta}{|\sin\theta|}\right) + \sinh^{-1}\left(\frac{\cos\theta}{|\sin\theta|}\right)\right\} \ , \tag{4.14}$$

where ν' is the frequency as determined by O.

This formula is singular when $\theta = 0$ or π as the identity (4.13) does not hold when $|B| = A$. These special cases are obtained directly from (4.10), (4.11) and (4.12). When $\theta = 0$

$$\frac{1}{\nu'} = -\frac{c}{Na}\ln\left(1 - \frac{a\,\Delta T}{c}\right) \ , \tag{4.15}$$

which agrees with that previously derived by Moreau [104] if we set $N = 1$ and $\Delta T = 1/\nu$. When $\theta = \pi$

$$\frac{1}{\nu'} = \frac{c}{Na}\ln\left(1 + \frac{a\,\Delta T}{c}\right) \ . \tag{4.16}$$

If the acceleration of O is low and the duration of the pulse in I is short then the velocity obtained by O in I over the time required to measure frequency will be small. This non-relativistic approximation for the frequency measured by O is found by combining (4.14), (4.15) and (4.16) and expanding by order of $a\,\Delta T/c$,

$$\frac{\nu'}{\nu} = 1 - \frac{a}{c}\frac{\cos\theta}{2}\Delta T + O(\frac{a^2\,\Delta T^2}{c^2}) \ . \tag{4.17}$$

This Döppler shift relation differs, at first order, from that derived by applying the hypothesis of locality (which automatically yields $\nu' = \nu$) by $\nu\, c\,\Delta T/\mathcal{L}$, where $\mathcal{L} = c^2/a$ is the acceleration length scale for O. The assumption that an accelerating detector is physically equivalent to a momentarily comoving inertial detector yields an accurate prediction for the frequency observed by an accelerating detector in the limit $a\Delta T/c \ll 1$. One cannot demand, however, that $\Delta T \to 0$ and obtain $\nu = \nu'$. In such circumstances the uncertainties associated with the measurement of frequency become infinite. It is a simple consequence of Fourier analysis that a radiation pulse which approximates a delta function has virtually indeterminant frequency. Only in the unphysical ray limit $\lambda_S \to 0$, when the radiation behaves in a completely point like manner, may one allow $\Delta T \to 0$ and recover the locality hypothesis. The novel feature of this analysis is that our model has enabled an analytic expression for the Döppler effect for accelerating observers, including the transverse frequency shift, to be derived. A discrepancy arises between this result and that predicted through application of the hypothesis of locality because the measurement of frequency is not instantaneous. As with the example of the linearly accelerating clock, section 4.2, and the frequency spectra recorded for a Gaussian wavepacket when resolved by a linearly accelerating observer [87], it is the ratio of the intrinsic duration of the measurement with the time scale characteristic of the acceleration which gives the magnitude of the locality hypothesis violation.

The dependence of the Döppler shift relation, Eq (4.17), on the duration of the measurement is not reflected by the the standard frequency transformations calculated using the geometric formalism of general relativity [54, 28]. This implies a rigorous quantum mechanical treatment of frequency measurements by accelerated observers would expose a dependence of the Döppler effect on, for example, the coherence time of the emitted radiation. A quantum mechanical treatment of the measurement of frequency by non-inertial observers clearly falls outside the standard geometric formalism of general relativity and therefore remains to be formulated. Such a theory would almost

certainly provide a better understanding of the Unruh effect [149, 18], which predicts that an observer accelerating in vacuum appears to be immersed in a thermal bath. The close relation of the Unruh effect to Hawking radiation [57], a cornerstone of modern treatments of quantum gravitation, implies that a rigorous quantum mechanical theory of measurement for accelerating observers would also be of significance to quantum gravitation.

To illustrate the magnitude of the extra terms in Eq. (4.17) we suppose that our accelerating observer wishes to resolve a radio wave of AM broadcast frequency, $\nu \sim 10^5$, to within an accuracy of one part per million. Therefore we require $N \sim 10^6$ such that the pulse duration $\Delta T \sim 10$ s. If O has an acceleration of 10 m.s^{-2} then, with $\theta = 0$, the frequency correction from Eq. (4.17) is $-\nu \cos\theta \; a\Delta T/(2\,c) \sim -0.15$ Hz, which is significant within the desired level of accuracy. This discussion represents a more realistic assessment of the importance of these classical corrections to the Döppler effect than that presented earlier [108]. Previously we neglected to consider the importance of uncertainties within a classical context.

4.5 Frequency measurement by observers in Schwarzschild geometry

As in section 4.4 we derive the Döppler shift in frequency when the source is inertial and the observer is non-inertial. In Schwarzschild geometry an inertial source is one which is freely falling. For simplicity we assume our radiation source, Σ, is freely falling from infinity. In the following analysis we consider two observers, A and B, who are stationary in the spacetime manifold but are, respectively, above and below the source when the signal is emitted, illustrated in figure 4.2. In section 4.5.1 we calculate this frequency shift predicted by the geometric formalism of general relativity. In the section 4.5.2 we repeat the calculation but this time treating the radiation as a pulse of finite duration. This work reported the first derivation of the Doppler effect in a gravitational context which explicitly discussed the effect of frequency measurement being of finite duration [109]. As with all the results within this chapter, we find the resulting Döppler shift relations differ from the predictions of general relativity due to the finite duration of the measurement.

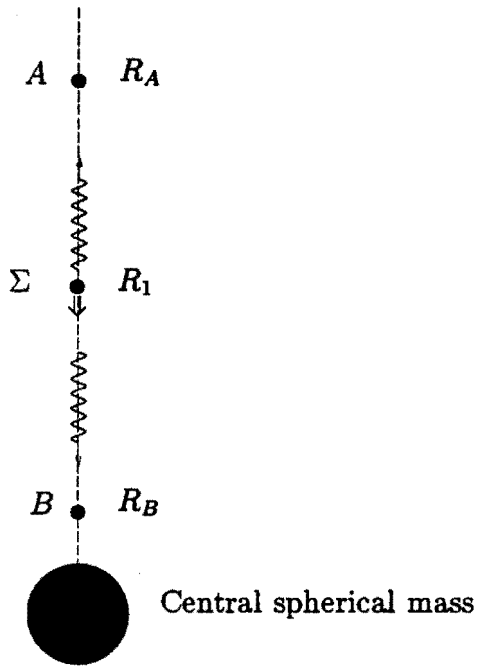

Figure 4.2: Location of the falling source relative to observers A and B in the Schwarzschild spacetime at the time of emission of two wavepackets

4.5.1 Frequency measurements in general relativity.

The Schwarzschild solution to Einstein's gravitational field equations describes the space-time geometry outside a non-rotating, spherically symmetric central body of mass M. The line element for Schwarzschild geometry is given by Eqs. (3.1),

$$ds^2 = -(1 - \frac{r_0}{r})\, c^2\, dt^2 + (1 - \frac{r_0}{r})^{-1} dr^2 + r^2(d\theta^2 + \sin^2\theta\, d\phi^2) \ , \qquad (4.18)$$

where $r_0 \equiv 2GM/c^2$ is the Schwarzschild radius and $\{t, r, \theta, \phi\}$ are the usual spherical spacetime coordinates.

Again we consider a radiation source, Σ, of frequency ν and mass m. As in section 4.4.1 we assume the effect of radiation back reaction on the worldline of Σ, and the effect of S on spacetime curvature, are negligible. The propagation of radiation emitted by Σ must be treated in accordance with Maxwell's equations. If, however, $\lambda = c/\nu$ is much less than the radius of curvature of the spacetime then the radiation may be considered to follow null geodesics [101, p.571-6].

Let Σ fall in Schwarzschild geometry from $r = \infty$ along $\theta = \pi/2$, $\phi = 0$.

The worldline of Σ is described by [101, p.667]

$$T = -\tfrac{2}{3} R^{3/2} - 2 R^{1/2} + \ln\left\{\tfrac{R^{1/2}+1}{R^{1/2}-1}\right\} \quad , \tag{4.19}$$

$$\mathcal{T} = -\tfrac{2}{3} R^{3/2} \quad , \tag{4.20}$$

where $R \equiv r/r_0 > 1$, $T \equiv ct/r_0$ and $\mathcal{T} \equiv c\tau/r_0$, τ being the proper time along the worldline of Σ. The use of uppercase letters to define dimensionless time and radial co-ordinates represents a change of convention, as we have used uppercase T to represent the coordinate time of an inertial frame of reference elsewhere in this thesis. However, we do not define a locally inertial frame freely falling with Σ in the following derivation and therefore this change of convention should not cause confusion.

When at $R = R_1 > 1$, Σ simultaneously emits two bursts of radiation, one radially away from the central mass and the other radially toward it. Denote the 4-wavevectors of the outwardly and inwardly propagating radiation as k_+ and k_- respectively. In the geometrical optics approximation we may use the following geometric (frame independent) identities to evaluate k_+ and k_- : (i) the wave vector is null, $k_\pm \cdot k_\pm = 0$, and (ii) the frequency of emission, $2\pi\nu = -k_\pm \cdot u_\Sigma|_{R_1}$ [152] where $u_\Sigma|_{R1}$ is the 4-velocity of Σ at R_1. From Eqs. (4.19) and (4.20), $dT/dR|_{R=R_1} = -R_1^{1/2}/(1 - R_1^{-1})$ and $dT/d\mathcal{T}|_{R_1} = 1/(1 - R_1^{-1})$ along the worldline of S. The 4-velocity of Σ at R_1 in the stationary Schwarzschild coordinates is thus

$$\{u_\Sigma\}^\mu|_{R_1} = c\left\{\frac{1}{1 - R_1^{-1}}, -R_1^{-\frac{1}{2}}, 0, 0\right\} \quad ,$$

such that

$$\{k_\pm\}_\mu = \frac{2\pi\nu}{c}\left\{-1 \pm R_1^{-\frac{1}{2}}, \frac{\pm 1}{1 \pm R_1^{-\frac{1}{2}}}, 0, 0\right\} \quad .$$

k_+ and k_- are tangent to the null geodesics along which the radiation propagates. If ξ^μ denotes the components of a Killing vector field, then the contraction $\xi_\mu k^\mu$ is constant along the the geodesic which the radiation propagates [152, p.442]. The two radiation pulses emitted by Σ are detected by two stationary observers, A located at $R_A \geqslant R_1$ and B located at R_B, where $1 < R_B \leqslant R_1$. In the stationary Schwarzschild frame A and B have 4-velocities $\{u_{\substack{A\\B}}\}^\mu = c\left\{(1 - R_{\substack{A\\B}}^{-1})^{-\frac{1}{2}}, 0, 0, 0\right\}$, which are both unit vectors pointing in the direction of the timelike Killing field $\xi^\mu = (1, 0, 0, 0)$ [152, p.137], such that

$$\{u_{\substack{A\\B}}\}^\mu = \left.\frac{\xi^\mu}{\sqrt{-\xi_\mu \xi^\mu}}\right|_{\substack{A\\B}} \quad .$$

It follows immediately that frequency of the radiation measured by A and B predicted by the geometric formalism of general relativity is [152]

$$\nu_A = -\frac{k_+ \cdot u_A}{2\pi} = \nu \frac{1 - R_1^{-\frac{1}{2}}}{(1 - R_A^{-1})^{\frac{1}{2}}} , \tag{4.21}$$

$$\nu_B = -\frac{k_- \cdot u_B}{2\pi} = \nu \frac{1 + R_1^{-\frac{1}{2}}}{(1 - R_B^{-1})^{\frac{1}{2}}} . \tag{4.22}$$

4.5.2 Non-instantaneous measurement of frequency

We now apply the classical definition of frequency presented in section 4.4 to determine the frequency measured by the observers A and B. The electromagnetic pulses emitted by Σ are no longer considered to be point-like particles but are regarded as wavetrains of duration $\Delta\tau$, measured along the world line of Σ, and containing N wave peaks. The uncertainty or spread in frequency associated with these wavetrains is $\Delta\nu \sim 1/\Delta\tau$, where our discussion of uncertainties concerns only orders of magnitude. In the following it is convenient to write the duration of the radiation pulse in dimensionless coordinates, $\Delta\mathcal{T} \equiv c\,\Delta\tau/r_0$.

From our construction, Σ was at R_1 when the emission of the two wavetrains began. This event occurred along the worldline of Σ at $\mathcal{T}_1 = \mathcal{T}(R_1)$. The wavetrain emitted by Σ ceased at $\mathcal{T}_2 = \mathcal{T}_1 + \Delta\mathcal{T}$, when Σ was at R_2. From Eq. (4.20)

$$R_2 = \left(R_1^{3/2} - \frac{3}{2}\Delta\mathcal{T}\right)^{2/3} . \tag{4.23}$$

We assume, as in the previous section, observers A and B are located at R_A and R_B respectively, now requiring R_1, R_B and $\Delta\mathcal{T}$ to be such that $1 < R_B \leqslant R_2$. Furthermore, as discussed in section 4.2, we assume that the clocks of A and B are sufficiently massive that we may neglect their uncertainty in measuring proper time intervals [126], yet not so massive that their effect on spacetime curvature is significant. Observers A and B measure the frequency of the radiation emitted by Σ by recording the duration of the radiation along their worldlines, $\Delta\tau_A$ and $\Delta\tau_B$, and counting the number of complete cycles of the radiation, which is N as the number of radiation cycles in any wavetrain is conserved. The frequency measured by A and B is thus $\nu_{\substack{A \\ B}} = N/\Delta\tau_{\substack{A \\ B}}$, with associated uncertainties $\Delta\nu_{\substack{A \\ B}} \sim 1/\Delta\tau_{\substack{A \\ B}}$.

The wavetrain duration measured by A and B is calculated by treating each end of the two electromagnetic pulses as separate null-rays, which prop-

agate radially from their points of emission to observers A and B. These null-geodesics are obtained by substituting $ds = d\phi = d\theta = 0$ into Eq. (4.18), producing a first order differential equation with solution

$$T_{\pm} = \pm R \pm \ln(R-1) + \text{const}_{\pm} \ , \tag{4.24}$$

where T_+ and T_- describe the outwardly and inwardly propagating geodesic paths respectively. The integration constants are found by demanding the worldlines representing the beginning of the two electromagnetic pulses intersect R_1 at $T(R_1)$, where $T(R_1)$ is defined by Eq. (4.19), and the worldlines representing the end of the two pulses intersect R_2 at $T(R_2)$. Combining Eqs. (4.19) and (4.24), the coordinate time interval between the detection of either ends of the respective wavetrains at A and B is

$$\begin{aligned} \Delta T_{\substack{A \\ B}} &= \Delta\mathcal{T} + 2\,R_1^{1/2} - 2\,R_2^{1/2} + \ln\left\{\frac{(R_2^{1/2}+1)(R_1^{1/2}-1)}{(R_2^{1/2}-1)(R_1^{1/2}+1)}\right\} \\ &\quad \pm R_1 \mp R_2 \pm \ln\left\{\frac{R_1-1}{R_2-1}\right\} \ . \end{aligned} \tag{4.25}$$

The proper time duration of the electromagnetic pulses measured by A and B is related to the coordinate time duration by Eq. (4.18), $\Delta\mathcal{T}_{\substack{A \\ B}} = (1-R_{\substack{A \\ B}}^{-1})^{\frac{1}{2}}\Delta T_{\substack{A \\ B}}$. Realising $\nu_A/\nu = \Delta\mathcal{T}/\Delta\mathcal{T}_A$ and $\nu_B/\nu = \Delta\mathcal{T}/\Delta\mathcal{T}_B$, and expanding Eqs. (4.23) and (4.25) by order of $\Delta\mathcal{T}$, we obtain

$$\frac{\nu_A}{\nu} = \frac{1-R_1^{-\frac{1}{2}}}{(1-R_A^{-1})^{\frac{1}{2}}} - \frac{\Delta\mathcal{T}}{4R_1^2(1-R_A^{-1})^{\frac{1}{2}}} + O(\Delta\mathcal{T}^2) \ , \tag{4.26}$$

$$\frac{\nu_B}{\nu} = \frac{1+R_1^{-\frac{1}{2}}}{(1-R_B^{-1})^{\frac{1}{2}}} + \frac{\Delta\mathcal{T}}{4R_1^2(1-R_B^{-1})^{\frac{1}{2}}} + O(\Delta\mathcal{T}^2) \ . \tag{4.27}$$

These expressions agree with those obtained by applying the 4-vector formalism of general relativity, Eqs. (4.21) and (4.22), to leading order in $\Delta\mathcal{T}$. However, as discussed in the case for an accelerated observer, one cannot demand that $\Delta\mathcal{T} \to 0$ and obtain agreement between the two derivations, as the uncertainties associated with the measurement of frequency would become infinite in such circumstances. Only in the unphysical ray limit $\lambda_S \to 0$ may one allow $\Delta\mathcal{T} \to 0$ and recover the previous geometric results.

Again, as in section 4.4, the Döppler shifts, Eqs (4.26) and (4.27), are dependent on the duration of the radiation, a dependence not predicted by the geometric formalism of general relativity. In this example the discrepancy between the results of our analysis and the predictions of general relativity is

proportional to $\pm\nu a\,\Delta\tau/[4\,c\sqrt{1-R_{\frac{A}{B}}}]$, where $a \equiv -MG/R_1^2$ is the apparent acceleration of Σ relative to observers A and B when the pulse is emitted. When comparing this discrepancy with the equivalent result of section 4.4.1 we find an extra factor of $2\sqrt{1-R_{\frac{A}{B}}}$ appear in the denominator. This arises because of the effect of time dilation in Schwarzschild geometry, and also because Σ is moving relative to A and B at the time the wavetrain was first emitted. However, the central conclusion remains, that the finite duration of the measurement causes the frequency transformation formulae of general relativity to be only approximate in a non-inertial context. Thus all conclusions drawn for linearly accelerating motion will apply to Schwarzschild geometry. Again this example highlights the need for a rigorous quantum mechanical treatment of frequency measurement when the observer is not moving inertially in Minkowski spacetime, as does all of the material presented within this chapter.

To observe the divergence of Eq. (4.26) from (4.21) one must accurately determine R_1. This, however, comes at a cost as a decrease in the uncertainty of the position of Σ will result in an increase the uncertainty of the momentum of Σ, increasing the uncertainty of the measured frequency. This effect is negligible in comparison with the uncertainty due to the wavetrain being of finite duration if, as we have assumed, $mc^2 \gg h/\Delta\tau$. We require that the discrepancy between Eqs. (4.21) and (4.26) is larger than their uncertainty. This condition is expressed as

$$\Delta\tau_S{}^2 \gtrsim \frac{r_1^2}{c\,\omega_S\,r_0}\left(1-\sqrt{\frac{r_0}{r_1}}\right)\ , \tag{4.28}$$

where numerical factors have been omitted. For example, at the surface of the earth using the Mössbauer effect in Fe^{57}, transition energy 14.4 keV [51, p.87], the condition (4.28) requires $\Delta\tau_S \gtrsim 10^{-6}$ s, which is an order of magnitude greater than the lifetime of this Mössbauer transition. Longer lived Mössbauer transitions, such as the Zn^{67} 93.3 keV transition with a half-life of 9.4 $\times 10^{-6}$ s [51, p.497], or the Ag^{107} 93.1 keV transition with a half-life of 43 s [51, p.504], would appear too experimentally problematic to enable a direct observation of any transition time dependence in gravitational frequency shifts. Nevertheless, by the principle of equivalence, large gravitational fields may be studied in the laboratory through acceleration. An obvious approach would be to modify earlier experiments which successfully detected the transverse Doppler effect using Mössbauer spectroscopy [58]. In these experiments both source and observer were mounted on a rotating disk. If, for example, the

Mössbauer source were fixed in the laboratory displaced from the absorber axis of rotation, it would introduce a time dependence in the relative velocities of the source and observer. This may allow a direct observation of any transition time dependence in the Doppler effect for accelerating systems.

Significantly, the resolution requirement (4.28) becomes less stringent as $r_1 \to r_0$. While the validity of our classical derivation may be questioned in the strong gravitational regime, this example illustrates that a measurement of the frequency of radiation from a source falling into a black hole will show effects stemming from the non-instantaneous nature of frequency measurement.

Finally, from Eqs. (4.26) and (4.27), the ratio

$$\frac{\nu_A}{\nu_B} = \left(\frac{1-R_B^{-1}}{1-R_A^{-1}}\right)^{\frac{1}{2}} \left\{\frac{1-R_1^{-\frac{1}{2}}}{1+R_1^{-\frac{1}{2}}} - \frac{\Delta\mathcal{T}}{2R_1\,(R_1^{\frac{1}{2}}+1)^2}\right\} + O(\Delta\mathcal{T}^2),$$

is dependent on $\Delta\mathcal{T}$. This indicates the 4-vector formalism of general relativity is only approximate when used to predict the ratio of frequency measurements performed by separated stationary observers. The dependence of ν_A/ν_B on $\Delta\mathcal{T}$ would cancel if both observers were directly above or both directly below the falling source. It is apparent, however, that the ratio of frequency measurements performed by separated observers will, in general, be dependent on the duration of the measurement. One obvious exception is when both source and observer are stationary in Schwarzschild geometry. In this instance the geometric formalism of general relativity predicts the correct expression, $\nu_A/\nu = \sqrt{1-R_1^{-1}}/\sqrt{1-R_A^{-1}}$, which was first observed using Mössbauer spectroscopy by Pound and Rebka [119], where R_1 represents the location of the Mössbauer source.

In all of the examples analysed within this chapter we obtained a discrepancy, proportional to $c\Delta\tau/\mathcal{L}$, between the predictions of general relativity and predictions derived assuming the hypothesis of locality. Throughout we found our non-instantaneous prescription used to describe a physical measurement ultimately led to a violation of the locality hypothesis. This central conclusion is in full agreement with that of Mashhoon and this work further motivates the search for a quantum mechanical formalism which will describe the measurement of frequency by non-inertial observers.

Chapter 5

Reanalysis of the light drag experiment of Sanders and Ezekiel

In this chapter we present a full relativistic reanalysis of the modified Laub drag experiment of Sanders and Ezekiel [128]. In their analysis they neglected a number of relativistic corrections which are potentially significant at the order of 100 ppm. Our calculation demonstrates an overall discrepancy between the experimental results of Sanders and Ezekiel and theory of 1300 ppm, which is substantially larger than their claimed overall agreement to 60 ppm. Furthermore, this discrepancy is 4.7 times larger than their stated experimental uncertainty.

5.1 Fresnel drag

Despite the popular mythology which surrounds the historical development of the special theory of relativity, Einstein repeatedly claimed the famous ether drag experiment of Michelson and Morley [99] had only an indirect influence on his thinking, through the writings of Lorentz, in the period leading up to his publication of the special theory of relativity [37]. Instead Einstein consistently stated [62] that the key results which led to his belief in the validity of the special theory were: (a) his conviction that the electromotive force induced in a body in motion in a magnetic field was nothing other than an electric field; and (b) the results of the Fizeau light drag experiment [45] and the phenomenon of angular aberration [19]. Thus, the observation of light drag in media moving relative to the frame of the laboratory had a profound influence on the scientific revolution at the turn of this century which was to radically alter our perception of the nature of space and time.

Within the special theory of relativity the concept of light drag is easily understood. Suppose a dielectric sample with refractive index $n(\omega)$ is moving with velocity v relative to a laboratory fixed in an inertial frame I. In the frame

of the dielectric I' the velocity at which a plane of constant phase propagates is $\omega'/|\boldsymbol{k}'| = c/n(\omega')$. Making an inverse first order Lorentz boost from I' to I we find

$$\omega = \omega' + \boldsymbol{v}\cdot\boldsymbol{k}' = \omega'\left\{1 + n(\omega')\,\frac{\boldsymbol{v}\cdot\hat{\boldsymbol{k}}'}{c}\right\} ,$$

$$|\boldsymbol{k}| = \left|\boldsymbol{k}' + \frac{\omega'\,\boldsymbol{v}}{c^2}\right| = |\boldsymbol{k}'|\left\{1 + \frac{\boldsymbol{v}\cdot\hat{\boldsymbol{k}}}{c\,n(\omega')}\right\} ,$$

such that, in I, the velocity of a plane of constant phase is

$$\frac{\omega}{|\boldsymbol{k}|} = \frac{c}{n(\omega')} + \boldsymbol{v}\cdot\hat{\boldsymbol{k}}'\left(1 - \frac{1}{[n(\omega')]^2}\right) . \tag{5.1}$$

This expression for the velocity of light dragged by media moving relative to an inertial observer was first proposed by Fresnel [48], for the special case of $\boldsymbol{v} \parallel \boldsymbol{k}$, on the basis of an elastic ether theory. For reasons of priority the dragging of light in moving media has become known as Fresnel drag.

In Eq. (5.1) ω' is related to ω by the Döppler effect, with the exact form of ω' being specific to the apparatus used in any light drag experiment [116]. If the boundary of the dragging medium is stationary in I and the medium's velocity parallel to the incident beam, assumed to be normal to the medium's surface, we find $\omega' = \omega\{1 - n(\omega')\,v/c\}$ such that $n(\omega') = n(\omega) - \omega\,n(\omega)\,dn/d\omega\;v/c$ and therefore, at first order in velocity,

$$\frac{\omega}{|\boldsymbol{k}|} = \frac{c}{n} + v\left(1 - \frac{1}{n^2} + \frac{\omega}{n}\frac{dn}{d\omega}\right) \equiv \frac{c}{n} + v\,\epsilon_{Lorentz} . \tag{5.2}$$

where $n \equiv n(\omega)$ and we have defined the Lorentz drag coefficient, $\epsilon_{Lorentz}$, originally derived by Lorentz [82]. However, if the surface of the moving medium is stationary in I' and the incident beam propagates through vacuum, we find $\omega' = \omega\{1 - v/c\}$ such that

$$\frac{\omega}{|\boldsymbol{k}|} = \frac{c}{n} + v\left(1 - \frac{1}{n^2} + \frac{\omega}{n^2}\frac{dn}{d\omega}\right) \equiv \frac{c}{n} + v\,\epsilon_{Laub} . \tag{5.3}$$

where the dragging coefficient in this context, ϵ_{Laub}, was first obtained by Laub [78].

The first quantitative measurement of Fresnel drag was performed in 1851 by Fizeau [45]. In this experiment water flowed through two pipes of 5.3 mm in diameter and 1.49 m in length with a mean velocity of 3.7, 5.5 and 7.1 m.s^{-1}. Because the air/water interface was stationary relative to the interferometer Lorentz's expression, Eq. (5.2), provided the correct formula for the velocity

of light through the dragging media. In this experiment Fizeau [45] was able to confirm the dragging coefficient to an accuracy of 16% [12]. This was an excellent result given that thirty years later Michelson [98], using wider flow tubes and a more reliable light source, was only able to reduce the overall experimental uncertainty to 5 % [12]. The principle experimental advantage in using a ring interferometer was that the opposite beams followed the same path around the interferometer and through the dragging medium. As such inhomogeneities in the refractive index of the sample and surrounding air affected both beams in a symmetrical manner, hence spurious phase shifts of one beam relative to the other did not arise.

In order to study the effect of Fresnel drag in glass, Harress [55] constructed a circular ring interferometer entirely from adjacent glass prisms, with a total beam path through the polygon of 1.22 m. For convenience Harress rotated his entire interferometer with angular velocity from 38 to 76 rad.s^{-1}, thus achieving motion of his glass interferometer relative to the laboratory through which the effects of Fresnel drag could be studied. Two wavelengths of light were used in this experiment, centred at $\lambda = 535$ nm and $\lambda = 625$ nm respectively. Harress's results, however, contained an inexplicable bias in the fringe shift, which was not correctly interpreted as arising from the Sagnac effect [125] until after Harress's early death. Subtracting the Sagnac bias, an overall uncertainty of 2% and 3% was obtained for the modified Lorentz drag coefficient at the respective wavelengths [12].

Zeeman [156, 157, 158] further refined the use of a passive optical interferometer as a tool for measuring light drag. With collaborators, Zeeman [156] not only repeated the experiment of Michelson, reducing the overall experimental error in the determination of the light drag coefficient for moving water by a factor of six [12], but also provided the first measurement of the Laub drag coefficient, defined by Eq. (5.3), using samples of quartz [157] and flint glass [158] with length from 1.0 m to 1.4 m and velocities exceeding 10 m.s^{-1}. In these experiments Zeeman achieved an experimental accuracy in the measurement of ϵ_{Laub} of 5% for quartz and 1.7% for flint glass [12], both of which were sufficiently accurate to demand the inclusion of the dispersion term in Eq. (5.3). Furthermore, the dispersion of the flint glass samples was such that this experiment provided the first clear experimental distinction between $\epsilon_{Lorentz}$ and ϵ_{Laub}, the latter being demonstrated to be the appropriate coefficient in these experiments.

With the advent of the ring laser and related optical instruments, high

precision measurement of Fresnel drag in moving media became greatly facilitated. By converting a non-reciprocal phase shift into an easily resolvable beat frequency between the opposite modes of the ring laser cavity, an active optical device can achieve a sensitivity several orders of magnitude greater than its associated passive device.

Bilger and Zavodny [16] and Bilger and Stowell [15] placed a rotating fused silica disk along one arm of a ring laser with wavelength 633 nm. Light entered the plane face of the disk off centre and at an oblique angle of incidence, set at the Brewster angle so as to minimise losses from reflection and to maximise the sensitivity of the experiment. Fresnel drag in the rotating dielectric induced a non-reciprocal change in the optical path of the laser beams which resulted in an observable beat between the opposite beams. From the measured beat frequency and the angular velocity of the dielectric the drag coefficient was determined to an accuracy of 0.5% [16] and 400 ppm [15] respectively. In the earlier analysis Bilger and Zavodny [16] assumed the dragging coefficient had a Lorentz rather than a Laub form as the air/medium interface remained stationary in the laboratory frame. This was confirmed by Parks and Dowell [116] who generalised the drag formula to include arbitrary angles between the velocity vector of the medium and the incident and refracted light beam. However, the more accurate measurement of Bilger and Stowell differed from their theoretical prediction by two standard deviations, which was considered too small to claim a discrepancy.

Sanders and Ezekiel [128] employed a passive ring resonator, also with wavelength 633 nm, and used a shuttle rod arrangement at the drag site, similar to that used by Zeeman, whereby their glass samples were oscillated along the optical path of their optical cavity. By using the Ezekiel-Balsamo passive resonator technique [129] they converted an asymmetrical phase shift into a frequency shift such that their observable was also the beat frequency between the counter-propagating beams. With the corresponding improvement in experimental sensitivity they measured the value of the Fresnel drag coefficient with an overall experimental uncertainty of 280 ppm, and claimed agreement with their theoretical calculation to 60 ppm. This experimental result of Sanders and Ezekiel therefore appears to be the most accurate verification of the Fresnel drag coefficient in moving media to date. However, this claim can only be justified on the basis of a much fuller analysis than attempted by Sanders and Ezekiel. At levels of 1000 ppm or less one may expect a wide variety of geometrical and relativistic complications to affect the observed frequency

difference.

Bilger and Stedman [13] have made an extensive attempt to include all of the corrections which will arise at this sensitivity. In this chapter we improve on this earlier work and concern ourselves entirely with theoretical corrections to the analysis of the experiment of Sanders and Ezekiel. Novel aspects of this analysis include the derivation of the phase shift for the experiment of Sanders and Ezekiel from first principles, rather than through the addition of a number of small corrections as different effects are analysed piecewise. We also include, throughout our derivation, geometric effects arising from the specific geometry of the optical cavity used by Sanders and Ezekiel. This chapter is unique in this thesis as it, alone, is not concerned with acceleration. While the glass samples in this experiment were oscillated, an analysis assuming the samples are moving with constant velocity is sufficient for our purposes.

Since the publication of the experiment of Sanders and Ezekiel the only significant light drag experiment to be reported in the literature is that of Kowalski et al. [76]. In this experiment a sample of fused silica and two mirrors were mounted on a platform which was linearly accelerated along the path of a ring laser. In their analysis Kowalski et al. presented their results as experimental verification of the, not unexpected, phenomenon that a plane of constant phase propagates at the phase velocity through their glass sample, which had a modest acceleration of ~ 0.053 m.s^{-2}. If this is reinterpreted as the measurement of the Laub drag coefficient we find the accuracy of their experiment was an order of magnitude below that claimed by Sanders and Ezekiel [75].

In recent years there have been several successful experiments using thermal neutrons which are analogous to the passive interferometer light drag experiments discussed above. As is the case with light drag experiments, the resulting phase shift is dependent on whether the boundary is moving with the dragging media or is stationary in the laboratory. However, this distinction for neutrons is considerably more pronounced than it is for light. Whereas only the coefficient of the dispersion term distinguishes the the two cases in optical interferometry, Horne et al. [63] have shown that when the boundary of the moving medium is stationary relative to the neutron interferometer *no phase shift results* if the neutron-nucleus potential of the material medium is independent of the velocity of the medium, which holds if the medium does not have a nuclear resonance at thermal energies.

The first successful neutron Fizeau effect experiment was that of Klein et al. [68] in 1981. In this experiment a square quartz rod was rotated along the path of both the separated neutron beams. The axis of rotation of this quartz rod, which was aligned parallel to the vector area of the interferometer, passed through the centre of the interferometer so that each beam encountered the rod moving in opposite directions. Through this arrangement Klein et al. were able to achieve an experimental verification of the expected drag coefficient to 9 %. Bonse and Rumpf [17], who used a rotating sample shaped like a four winged propeller, were able to improve upon the experiment of Klein et al. and achieve an overall accuracy of 1.5 %.

Arif et al. [8] confirmed the prediction of Horne et al. by observing a null phase shift for a neutron de Broglie wave when the boundary of the moving media was stationary relative to the interferometer. Arif et al. [6, 7] extended this result by performing a similar experiment, but this time with the moving media having a nuclear resonance at thermal energies. As such the neutron beams experienced an energy dependent potential inducing a phase shift analogous to the historic experiment of Fizeau. Upon measuring this velocity dependent phase shift for the neutron de Broglie waves the dragging coefficient was determined with an overall accuracy of 18 %.

5.2 The experiment of Sanders and Ezekiel

Sanders and Ezekiel [128] employed a passive ring resonator technique to measure the Fresnel drag coefficient for a variety of glass samples of different indices of refraction and dispersion. Their square optical cavity contained two plane mirrors and two concave mirrors with a mirror separation of 0.7 m. The concave mirrors were located at opposite corners of the cavity and each had a radius of curvature $R \approx 1.2$ m. The dimensions of their glass samples were from 0.6 cm to 1.9 cm, the indices of refraction ranged from 1.46 to 1.84 and dispersion from $-0.029\ \mu\text{m}^{-1}$ to $-0.14\ \mu\text{m}^{-1}$. In order to avoid experimental complications arising from multiple reflections within their glass samples, Sanders and Ezekiel inclined each sample's normal to an angle θ relative to the optical axis of the optical cavity, where θ varied from 5.15° to 15.65°. The glass sample was then moved sinusoidally along the optical axis of the passive cavity without changing its tilt. Because the boundary of the sample moved with the medium, this experiment was itself a modified Laub drag experiment. Light drag within the dielectric sample resulted in a non-reciprocal phase shift

which, in turn, led to an observable beat frequency between the opposite beams of the cavity. Sanders and Ezekiel claimed an overall agreement between their experimental results and theoretical predictions of 60 ppm.

A full reanalysis of the experiment of Sanders and Ezekiel, including all phenomena which may affect the observed beat frequency at this level of sensitivity, constitutes the focus of this chapter. However, before proceeding with this somewhat detailed theoretical analysis we outline some of the assumptions implicit in, and systematic errors arising from, the experiment of Sanders and Ezekiel. These have previously been discussed in detail by Bilger and Stedman [13]

5.2.1 Systematic errors

Bilger and Stedman noted that the technique used by Sanders and Ezekiel to cope with the non-uniformity of the motion of their glass samples, and with finite sampling time, is not clear from their account, despite its importance in achieving measurement accuracies at the level of 100 ppm. Each sample was moved sinusoidally with a frequency of 5 Hz and a peak velocity of 25.525 $\mathrm{cm.s^{-1}}$. The driver which oscillated the samples had to be carefully constructed so as to insure to constancy of the tilt of the glass samples relative to the optical axis of the interferometer. Since only about 100 counts can be accumulated during a half period (a typical beat frequency is 1 kHz) careful precautions have to be taken in order to maintain an overall accuracy of 100 ppm. Period counting with proper gating of the interferometric velocity readout would achieve the required accuracy.

The opposite faces of all glass samples were assumed to be parallel. Sanders and Ezekiel gave the thickness with a typical error of 0.5 μm, which implies a sufficiently small divergence of the opposite faces for this assumption to be accepted. All samples were anti-reflection coated, although the nature and thickness of the coatings was not reported. If we assume all anti-reflection coatings consist of a film of MgF_2 (refractive index $n = 1.38$) of thickness $633/(4\times1.38)$ nm $= 115$ nm we find corrections to the measured drag coefficient of between 3 and 24 ppm arise due to the presence of anti-reflection coatings. This correction, while contained within our final analysis for completeness, is practically negligible within the overall uncertainty of the experiment.

As did Sanders and Ezekiel, we assume the material is homogeneous with constant refractive index $n_s(\omega)$ and dispersion $dn_s(\omega)/d\omega$ *against vacuum*,

where the subscript s denotes the refractive index of the glass sample. In their manuscript [128] Sanders and Ezekiel quoted the refractive indices as supplied by the manufacturer. However, through his own experience, Bilger was aware that manufacturers always quote the refractive index of glass samples *relative to air not vacuum.* At 20 °C and 100 kPa the refractive index of air is $n_a = 1 + 2.7 \times 10^{-4}$. The leading term in the drag coefficient of Sanders and Ezekiel is proportional to the refractive index of their sample, so we may immediately expect a correction at the order of 270 ppm arising from this oversight.

A major obstacle to the ultimate precision of the experiment of Sanders and Ezekiel was their decision to allow their beams to propagate through an air filled cavity. The moving sample pushes the surrounding air back and forth causing additional drag. The induced turbulence makes the magnitude of this component of the drag difficult to evaluate. This problem is well known; the classic work of Zeeman[156] included very careful attention to end effects in cells containing the moving fluid. In experimental arrangements where the motion of the sample is traverse, such as that employed by Bilger and Zavodny [16] and Bilger and Stowell [15], the problem is greatly lessened. Fortunately, Sanders and Ezekiel noted the additional drag was independent of the lengths of the glass used and were able to determine it separately by linear extrapolation of the total observed drag to zero glass length. From this extrapolation a beat frequency offset of 9.9 ± 0.7 Hz was obtained, from which it is inferred that the thickness of the air moved is an order magnitude greater than the thickness of the glass itself. The uncertainty in their extrapolation in a typical measurement of 1 kHz amounts to a systematic error contribution of 700 ppm. This is a very substantial error in the quest to achieve an overall accuracy of 100 ppm.

An additional systematic error arises from the presence of air in their optical cavity which cannot be easily estimated. When a glass sample is moving relative to the optical interferometer, the relativistic form of Snell's law predicts that the opposite beams will suffer different refraction through the moving media. Therefore the counterclockwise (*ccw*) and clockwise (*cw*) beams become separated by the motion of the dielectric sample. Because the opposite beams do not follow identical paths around the optical cavity, but are separated by relativistic effects as a consequence of tilting the glass sample, it does not follow that inhomogeneities in the refractive index of the air around the paths of the opposite beams automatically cancel. This may lead to spurious non-

reciprocal phase shifts of the opposite beams relative to each other and hence additional systematic uncertainty in the measured drag coefficient. We shall, of necessity, follow Sanders and Ezekiel in ignoring these problem and assume that the air is homogeneous and dispersionless, with refractive index n_a, and is always at rest in the laboratory. However, within the stated aim of Sanders and Ezekiel to achieve an accuracy to 100 ppm, it is clear that this would have been better facilitate by evacuating the optical cavity through which the opposite beams propagate.

5.2.2 Relativistic effects

Within their manuscript Sanders and Ezekiel did not present their calculation of the modified Laub drag coefficient appropriate for their experiment. Surprisingly they simply quote the result, without explicit reference to Sander's PhD thesis [127] in which it is calculated. The calculation of the modified Laub drag coefficient is greatly complicated by the tilting of the glass sample. Sanders, in his analysis, provided a partial solution but neglected a number of effects which are potentially important at the order of 100 ppm. Below we outline the important relativistic corrections to this analysis, and discuss how these were incorporated into, or neglected by, the analysis of Sanders. The remainder of this chapter is then dedicated to incorporating all of the effects discussed below.

All of the glass samples used by Sanders and Ezekiel had significant dispersion. This dispersion was highly desirable within their experiment as a key aim of this work was to provide an irrefutable experimental distinction between the modified Laub drag coefficient and the Lorentz drag coefficient. However, the presence of dispersion complicates the theoretical analysis of this experiment. As discussed in section 5.1, the refractive index which appears in Fresnel's light drag formula, Eq. (5.1), must be evaluated at the frequency of the light, ω', as measured in the moving frame of the sample I'. Dispersion enters through $n_s(\omega') = n_s(\omega) + \{\omega' - \omega\}\, dn_s/d\omega$ and $\omega' \neq \omega$ because of the Döppler effect. Sanders used a transit time approach in his calculation and so the appropriate phase velocity of light through the moving media is an issue of central importance to his analysis. We note that, within this derivation of the modified Laub drag coefficient, Sanders [127] was careful to accurately distinguish between the different roles of $n_s(\omega')$ and $n_s(\omega)$ in Eq. (5.1).

In order to calculate the path taken by light through the moving dielectric,

the relativistic form of Snell's law has to be applied at the moving boundary. This calculation is best performed in the moving frame of the sample, I'. Again the refractive index of the sample which is used in the expression of Snell's law should be $n_s(\omega')$ and this was used by Sanders. However, Sanders assumed the glass was immersed in vacuum when applying Snell's law and the correction to angles arising from the refractive index of air was neglected. In the following analysis we include all effects arising from the sample being immersed in air when we apply the relativistic form of Snell's law, which we discuss in detail in section 5.3.1. A further error in Sander's analysis also arose because he neglected the influence of angular aberration when transforming all angles from I', the frame of the moving dielectric, back into I, the frame of the laboratory. This neglect of aberration is the primary cause for the eventual discrepancy between Sander's algebraic expression for the dragging coefficient and the result which we derive below. In our analysis we use a snapshot approach to calculate of the modified Laub drag coefficient. As a result we are able to utilise the invariance of $k_\mu dx^\mu$ in our expression for the phase shift through the glass sample, and thereby calculate this contraction in I'. This enables us to avoid complications arising from aberration, as we do not need to transform any angles from I' back to I.

We mention, in passing, an apparent ambiguity in the transit time analysis given by Sanders which relates to the different roles of group and phase velocity in optical systems with dispersion. Sanders correctly began with the assumption that a plane of constant phase will propagate in I' through the dielectric sample with velocity $c/n(\omega')$. However, when transforming the *magnitude* of this velocity into I (Sanders consistently neglected aberration) Sanders used the particle or *group* velocity transformation formula. It is well known that group and phase velocity transform differently under a Lorentz boost [138], and one would expect, at a first glance, that it would be the *phase* velocity transformation formula which should be used in this case. A correct interpretation of this starting point of Sanders is that he has treated the 'points' where planes of constant phase intercept the path taken by the laser beam through the dielectric as 'particles' in their own right. As such these 'particles' transform under the group velocity transformation law. While this is an acceptable perspective to take in a transit time calculation, Sanders made no attempt to explain or justify this surprising use of the transformation laws.

A potentially significant effect of tilting the dielectric sample relative to the optical axis of the cavity is that the laser beam is perturbed off the optical

axis. This perturbation was not included at all in the analysis of Sanders. Partial attempts to include this perturbation have been made by Bilger and Stedman [13], although these were never satisfactorily brought to a conclusion. In our analysis we give a full treatment of all geometric effects which arise from the tilt of the glass sample relative to the optical axis of the resonant cavity. Thus we provide the most comprehensive analysis of the modified Laub drag experiment of Sanders and Ezekiel to date.

Our results consistently differ from the theoretical predictions of Sanders and Ezekiel by 1200 ppm and an overall discrepancy between experiment and theory of 1300 ppm is found. This clearly demonstrates that Sanders and Ezekiel were unjustified in their claim of agreement between the observed Laub drag coefficient and theory to 60 ppm.

5.3 Phase shift through the moving glass sample

We introduce our calculation of the phase shift induced by the motion of the glass sample in the experiment of Sanders and Ezekiel by first considering the apparently trivial case of the dielectric stationary in I. We do this so as to lay the groundwork for what is to follow and to familiarise the reader with the definitions of several variables used in the remainder of this chapter.

In figure 5.1 we illustrate the path taken by a photon through the glass sample of thickness L when the dielectric is stationary in the laboratory frame I. An immediate consequence of tilting the normal of the glass sample by an angle θ relative to the optical axis of the cavity is that the incident beam is no longer parallel to the optical axis of the cavity but is skewed by an angle α. The algebraic form for this perturbation angle α is calculated explicitly in section 5.4. As we would expect, α is dependent on θ, L and the specific geometry of the optical cavity.

Using a snapshot calculation, with $\Delta T = 0$, we find the change phase of the laser beam upon a traverse of the glass sample is

$$\Phi_s = k_\mu \Delta X^\mu = \boldsymbol{k}_s \cdot \boldsymbol{P} = \frac{\omega n_s}{c} \frac{L}{\cos\phi} \ , \tag{5.4}$$

where ϕ is defined by Snell's law

$$n_a \sin(\theta - \alpha) = n_s \sin\phi \ , \tag{5.5}$$

ω is the frequency of the laser beam and we adopt the notation $n_s \equiv n_s(\omega)$ for convenience. In later sections we use the notation $n_s' \equiv n_s(\omega') = n_s + (\omega' -$

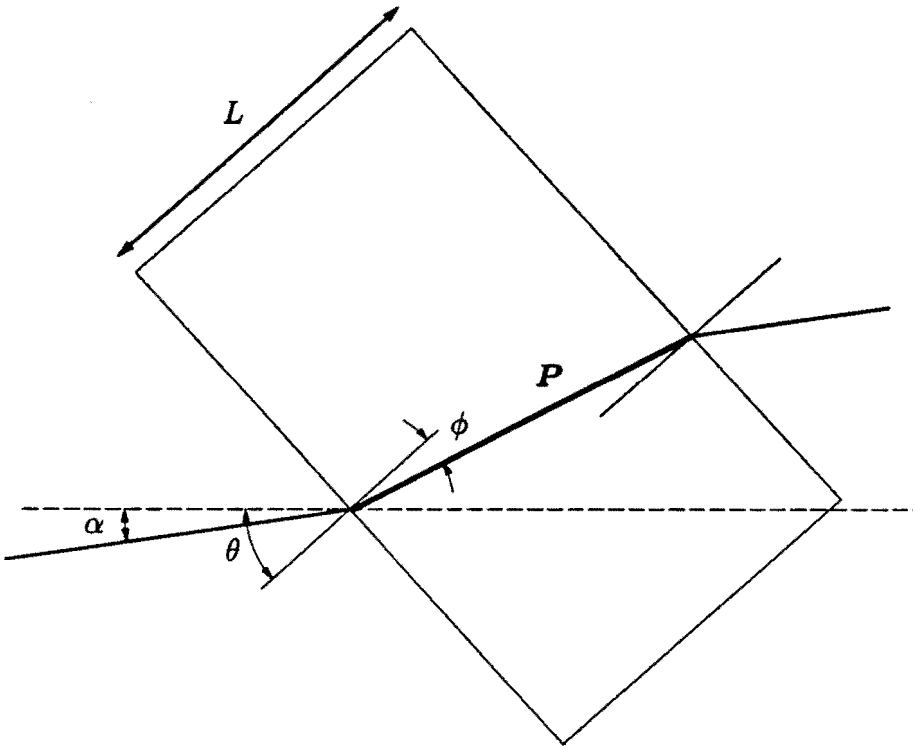

Figure 5.1: Schematic illustration of the path $\boldsymbol{P}$ (bold line) taken by a photon through a glass sample stationary in I. An immediate consequence of tilting the normal of the glass sample by an angle θ relative to the optical axis of the cavity (dashed line) is that the incident beam becomes perturbed off the optical axis by an angle α. The optical axis defines the X axis of I.

$\omega)dn_s/d\omega$ so as to distinguish these two different uses of the refractive index of our sample.

5.3.1 Relativistic form of Snell's law

We now allow our sample to move with velocity $\boldsymbol{v}$ parallel to the optical axis of our cavity. This models the experimental situation of Sanders and Ezekiel. We first derive the relativistic form of Snell's law as viewed in I', the frame of the glass sample in which the boundary is stationary.

Snell's law for plane waves can be derived by matching the phase at the boundary separating samples of different refractive index. We illustrate this matching condition in figure 5.2. The velocity at which the point where both planes of constant phase intercept the glass/air boundary moves along the surface of our sample is given by

$$u = \frac{u'_a}{\sin(\theta - \alpha')} = \frac{u'_s}{\sin\beta'} \ , \tag{5.6}$$

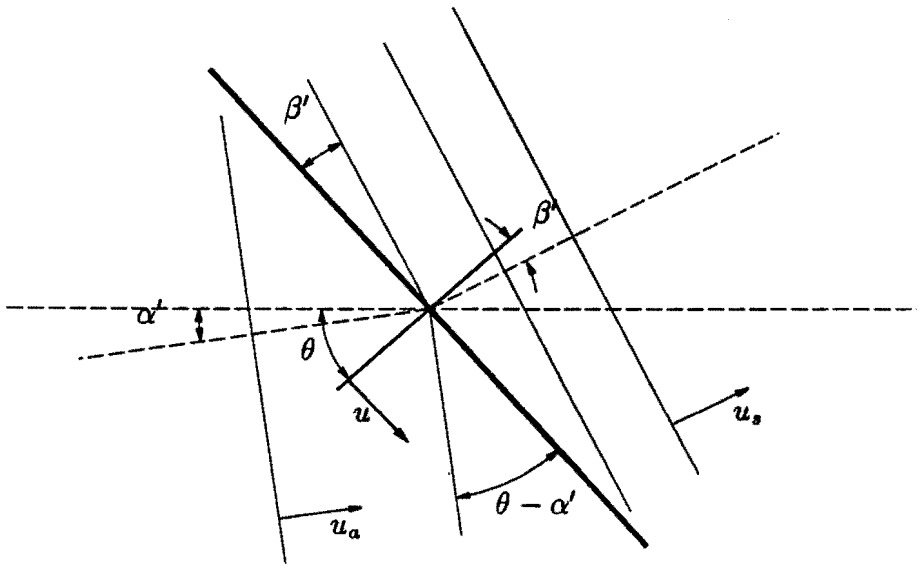

Figure 5.2: The velocity with which the point of intersection of planes of constant phase moves along the air/sample boundary must be equal on both sides of this boundary. From this requirement we are able to derive the relativistic form of Snell's law, Eq. (5.8).

where u'_a and u'_s represent the phase velocity in I' of the light through air and the glass sample respectively. If the dielectric is stationary in I then $u'_a = u_a = c/n_a$ and $u'_s = u_s = c/n_s$ and we recover Snell's law, Eq. (5.5), with $\alpha' = \alpha$ and $\beta' = \phi$. When the dielectric is moving relative to I we find $u'_s = c/n'_s$ and, from Eq. (5.1), $u'_a = c/n_a - \boldsymbol{v}\cdot\hat{\boldsymbol{k}}(1-1/n_a^2)$. The angle α' suffers aberration upon being boosted from I to I', given by [138]

$$\tan\alpha' = \frac{\sin\alpha}{\cos\alpha - v/(cn_a)} \ . \tag{5.7}$$

Substituting Eq. (5.7) into Eq. (5.6) we are led to the relativistic form of Snell's law when the dragging medium is moving relative to air

$$n'_s \sin\beta' = \frac{n_a \sin(\theta-\alpha')}{1-(n_a - 1/n_a)\,\boldsymbol{v}\cdot\hat{\boldsymbol{k}}/c} \ . \tag{5.8}$$

To the best of our knowledge this relativistic expression for Snell's law has not previously been reported. Sanders, within his analysis, used this equation in the limit $\alpha \to 0$ and $n_a \to 1$. In the otherwise highly relevant discussions of Bilger and Stowell [16], Bilger and Zavodny [15] and Parks and Dowell [116] the expression used for Snell's law is again Eq. (5.8) in the limit $n_a \to 1$. Our expression, however, contains a term arising from Fresnel drag in air which appears in the denominator of the RHS of Eq (5.8). Because β' is dependent upon the velocity of the glass sample and the corresponding expression for the

beam propagating in the opposite direction is recovered from Eq. (5.8) with the substitution $v \rightarrow -v$, we find $\beta'_{cw} \neq \beta'_{ccw}$ and hence the opposite beams follow different paths through the dielectric and around the optical cavity.

In I' the glass sample is stationary. Because our sample is homogeneous and isotropic the group velocity of a photon as it passes through the sample will be parallel to the phase velocity when viewed from I'. However, because group and phase velocities do not transform in the same manner under a Lorentz boost [138], they will not appear parallel in I. Similarly, the laser beam when propagating through air will have its group and phase velocities parallel in I, and therefore not parallel in I'. The different angular aberration laws for group and phase velocity can be regarded as yet another consequence of Fresnel's drag relation, Eq. (5.1). Saca [124] has shown how the different aberration laws for group and phase velocities can easily be derived from the definition $\boldsymbol{g} = d\omega/d\boldsymbol{k}$ and the Lorentz transformation laws relating the coordinates of I to I'. The different roles of group and phase aberration were entirely overlooked by Sanders [127] within his analysis, who failed to account for any aberration effects whatsoever. This is a significant error in his analysis as he chose to calculate the phase shift from I, whereas we use a geometric identity to enable us to calculate the phase shift entirely from I', which thus sidesteps aberration effects.

5.3.2 Snapshot of the glass sample in I'

Now that we have established the relativistic form of Snell's law we begin our calculation of the phase shift induced by the motion of the glass in earnest. Our approach to calculating phase shifts in this analysis is based upon the 'snapshot' approach, in which a moment in time is fixed and the phase shift is found by integrating $\boldsymbol{k}_s \cdot d\boldsymbol{r}$ along the path of the laser beam through the glass sample. If we set $\Delta T' = 0$ we observe a snapshot of the dielectric from I'. In this figurative snapshot we would see a wave pattern stretching across the dielectric sample along the path $\boldsymbol{P}'$, as illustrated in figure 5.3. The opposite ends of $\boldsymbol{P}'$ are separated by

$$\Delta X' = L \frac{\cos(\theta - \kappa')}{\cos \kappa'} \ , \tag{5.9}$$

$$\Delta Y' = L \frac{\sin(\theta - \kappa')}{\cos \kappa'} \ , \tag{5.10}$$

where $L/\cos\kappa'$ is the length of the beam through the dielectric.

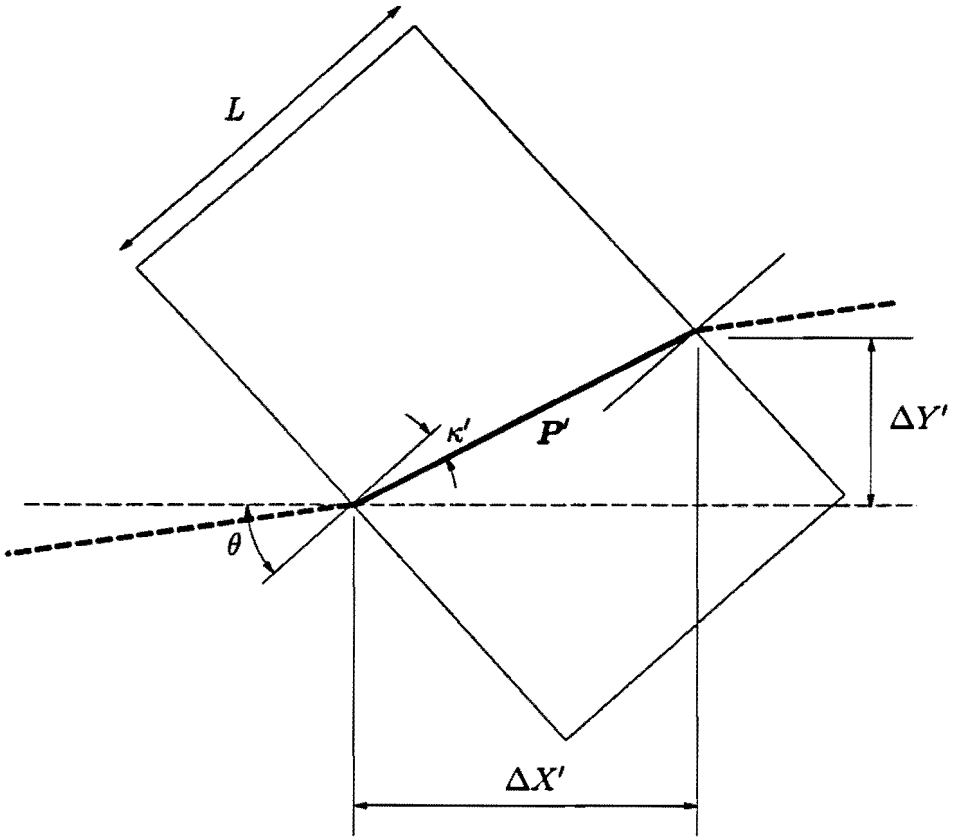

Figure 5.3: A snapshot of the dielectric taken from I'. The heavy unbroken line represents the path, $\boldsymbol{P}'$, along which the beam stretches at the instant when $\Delta T' = 0$. Algebraic expressions for $\Delta X'$ and $\Delta Y'$ are given by Eqs. (5.9) and (5.10). The light dashed line represents the optical axis of the cavity and defines the X' axis of I'.

As we have argued in the previous section, the group velocity of our light through the glass sample is parallel to the phase velocity when viewed from I'. Therefore, because the physical path taken by a photon is determined by its group velocity, we would initially expect that $\kappa' = \beta'$, where β' was defined by the relativistic form of Snell's law, Eq. (5.8), which gives the orientation of the phase velocity. However, as we show below, $\boldsymbol{P}'$ is not in fact parallel to the group velocity in I' because the incident beam moves across the surface of the glass sample in I'. It follows that $\boldsymbol{P}' \nparallel \boldsymbol{k}'_s$ such that $\kappa' \neq \beta'$.

In all of the experiments of Sanders and Ezekiel the opposite faces of their glass samples were parallel. This results in the beam emerging from the dielectric being parallel to the incident beam. We show in section 5.4 that the requirement that emerging and incident beams be parallel results in the laser beam selecting a well defined orientation within the optical cavity, with the beam always intersecting the plane mirror opposite the glass sample on the

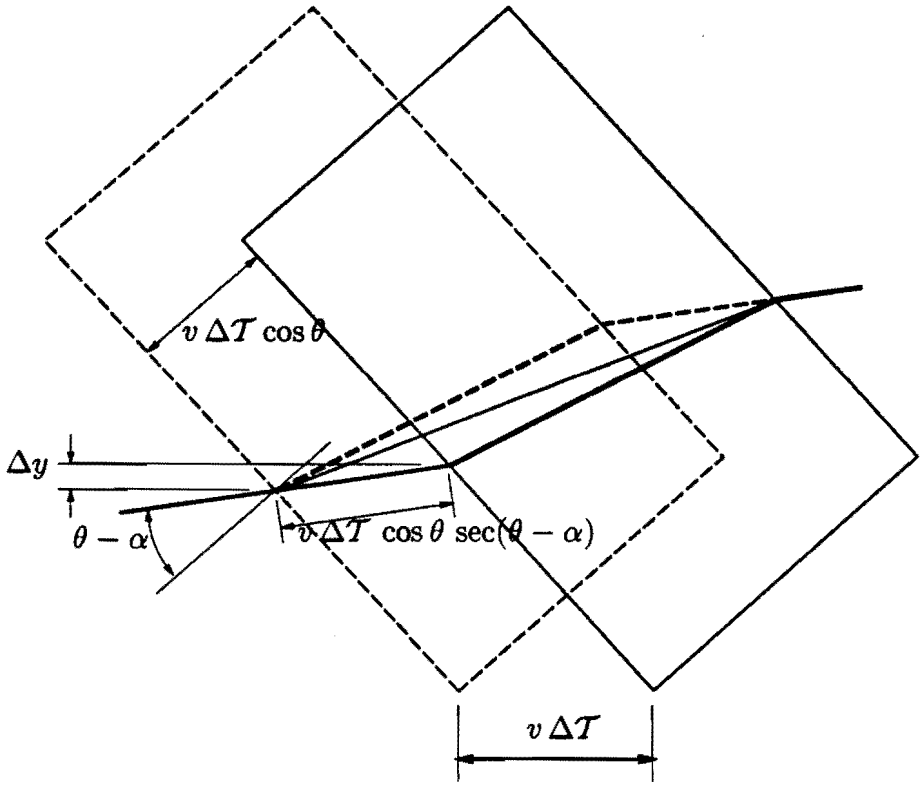

Figure 5.4: Two snapshots of the dielectric sample, taken from I, separated by a time interval $\Delta\mathcal{T}$, where $\Delta\mathcal{T}$ is the time required for a photon to complete a transit of the dielectric sample. The dashed image represents the earlier snapshot, taken at the time the incident photon enters the sample, and the unbroken image represents the later snapshot, taken when the photon emerges from the sample. The light unbroken line stretching from the opposite corners of the parallelogram represents the physical path of the photon through the moving glass sample. Because the incident beam is not parallel to the velocity of the dielectric the Y coordinate of where the beam is incident upon the boundary will change by an amount $\Delta Y_i = v\,\Delta\mathcal{T}\sin\alpha\cos\theta\sec(\theta-\alpha)$ in the interval $\Delta\mathcal{T}$. Therefore $dY_i/d\mathcal{T} = v\sin\alpha\cos\theta\sec(\theta-\alpha)$.

optical axis. This orientation of the laser beam is illustrated in Figure 5.6. As the velocity of the dielectric is not parallel to the laser beam the glass sample will pass through the laser beam as well as moving along it. Consequently, in the frame of the dielectric the incident beam appears to be moving along the dielectric's surface.

We now view the dielectric from I, as is illustrated in Figure 5.4. In I a photon will take a time interval $\Delta\mathcal{T}$ to propagate through the moving glass sample. In figure 5.4 the dotted image represents the snapshot of the dielectric and laser beam when a photon first enters the dielectric, and the unbroken image illustrates the snapshot when the photon emerges from the

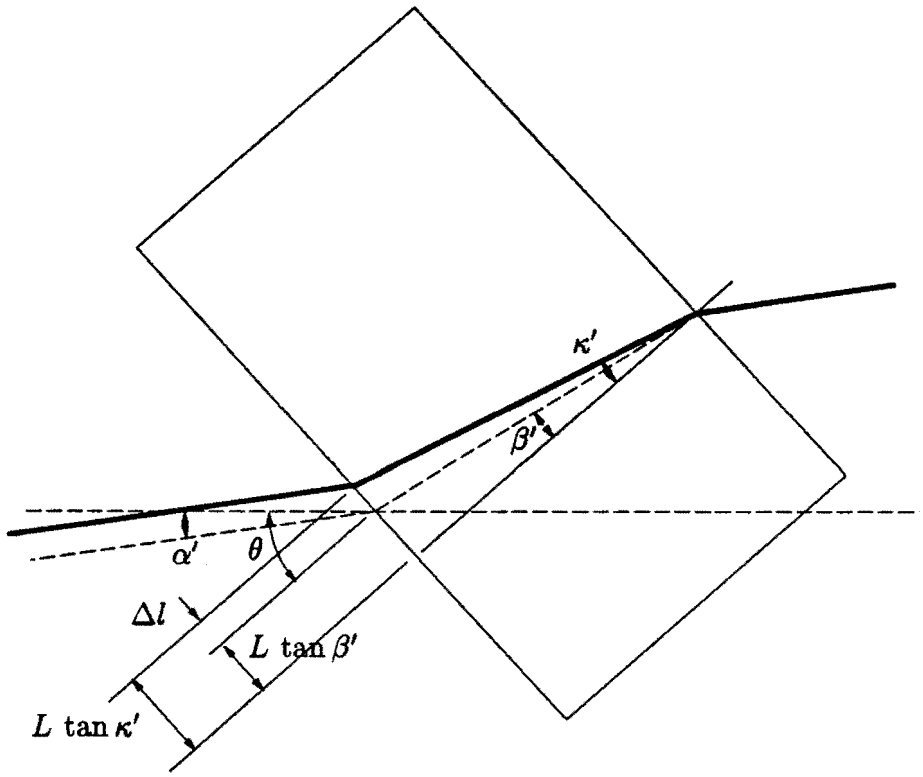

Figure 5.5: Because the incident beam moves across the surface of the dielectric in I' $\beta' \neq \kappa'$. The light dashed line represents the physical path of a photon which emerges from the RHS of the dielectric when this snapshot is taken in I'. The heavy unbroken line represents the laser beam at the time of the snapshot. In the time interval $\Delta T'$ required for this photon to propagate through the sample, the incident beam has moved a distance Δl along the surface to the dielectric. κ' and β' are related by $L \tan \kappa' = \Delta l + L \tan \beta'$. β' denotes the angle by which the incident beam is refracted when it enters the dielectric, determined by the relativistic form of Snell's law, Eq. (5.8).

dielectric sample, a time interval ΔT later. The physical path of this photon through the dielectric is represented by the lighter unbroken line. The angular displacement of this path can be found by transforming the angle β' from I' to I using the group aberration formula, but to the accuracy required in the following argument (leading order) we may assume the path followed by the photon is an angle ϕ from the optical axis of the cavity, defined by Eq. (5.5). A simple geometrical argument gives $dY_i/dT = v \sin\alpha \cos\theta / \cos(\theta - \alpha)$, where Y_i represents the Y coordinate of the point where the incident beam intersects the glass surface. A Lorentz boost into I' gives $dY_i'/dT' = dY_i/dT + O(v)$ such that the velocity with which the incident laser beam slides across the dielectric surface is $v_s = \sec\theta \; dY_i'/dT = v \sin\alpha \sec(\theta - \alpha)$.

Figure 5.5 views the same situation, but now from I'. Δl represents

the amount which the laser beam has moved across the dielectric surface during the time interval $\Delta T'$ for the dashed photon to traverse the dielectric. Explicitly $\Delta T' \approx L \sec\phi/|\boldsymbol{g}'| = L \sec\phi(n'_s + \omega\,\partial n'_s/\partial\omega)/c$, where it is the group velocity which determines the time required for the photon to complete a transit of the dielectric, and we use an approximate sign as we are only concerned with the leading order contribution. Therefore $\Delta l = v_s \Delta T' = v \sin\alpha \sec(\theta - \alpha) \sec\phi\, L\,(n'_s + \omega\,\partial n'_s/\partial\omega)/c$. From Figure 5.5 we obtain, through simple trigonometric arguments, at first order in velocity

$$\tan\kappa' = \tan\beta' + \frac{\Delta l}{L} = \tan\beta' + \frac{v \sin\alpha\,(n_s + \omega\,\partial n_s/\partial\omega)}{c\cos\phi\,\cos(\theta - \alpha)}\ , \tag{5.11}$$

and $\kappa' - \beta'$ is the angular separation of $\boldsymbol{P}'$ and $\boldsymbol{k}'_s$.

5.3.3 Phase shift through the moving sample

In the preceding sections we have viewed the dielectric sample using a snapshot in I'. This has enabled us, through straight forward but algebraically tedious arguments, to determine algebraic expressions for β' and κ'. With the physical basis and algebraic expressions for these angles established we may proceed to calculate the the shift in phase suffered by the laser beam as it passes through the glass sample.

We are interested in the phase shift induced by a motion of the dielectric when viewed from the laboratory frame I. In line with our previous discussion, we proceed by taking a snapshot of the moving sample, but now from I. Through this approach we find the change in phase of the laser beam as it passes through the dielectric is

$$\Phi_s\Big|_{\Delta T=0} = \boldsymbol{k}_s \cdot \boldsymbol{P} = k_\mu \Delta X^\mu\ , \tag{5.12}$$

where the final equality follows as $\Delta T = 0$. This expression is of the same form as that found when the sample is stationary in I, Eq. (5.4), but both $\boldsymbol{k}_s$ and $\boldsymbol{P}$ differ from that given earlier because the sample is now moving relative to I.

In Eq. (5.12) the contraction $k_\mu \Delta X^\mu$ is a geometric quantity and, as such, is independent of frame in which it is evaluated. In the case at hand it proves extremely convenient to evaluate this contraction in I' rather than in I. Through choosing to evaluate this contraction in I' we are able to avoid further algebraic complications which would arise because of the effects of angular aberration

when transforming β' and κ' from I' to I. Thus we are able to sidestep one of the most significant errors in the analysis of Sanders [127], who neglected angular aberration entirely.

With $\Delta T = 0$ a first order Lorentz transformation from I to I' gives $\Delta X = \Delta X'$, $\Delta Y = \Delta Y'$, $\Delta T' = -v/c^2\,\Delta X$, such that

$$\Phi_s\Big|_{\Delta T=0} = k'_\mu\,\Delta X'^\mu = \boldsymbol{k_s}' \cdot \boldsymbol{P}' - \omega'_s\,\Delta T' = \boldsymbol{k_s}' \cdot \boldsymbol{P}' + \frac{v}{c^2}\,\omega'_s\,\Delta X' \quad . \tag{5.13}$$

In I' the surface of the dielectric is stationary and therefore $\omega'_a = \omega'_s = \omega'$. A Lorentz boost from I to I' gives

$$\omega' = \omega_a - \boldsymbol{k}_a \cdot \boldsymbol{v} = \omega_a\,(1 - \frac{v}{c}\,n_a \cos\alpha) \quad . \tag{5.14}$$

From the vector product we have

$$\boldsymbol{k}'_s \cdot \boldsymbol{P}' = \frac{n'_s\,\omega'}{c}\,\frac{L}{\cos\kappa'}\,\cos(\kappa' - \beta') = \frac{n'_s\,\omega'}{c}\,\frac{L}{\cos\kappa'} \quad ,$$

as $|\boldsymbol{k}'_s| = n'_s\,\omega'/c$ and in the last step we have used Eq (5.11) giving $\kappa' - \beta' \sim \alpha v/c$ such that $\cos(\kappa' - \beta') = 1$ at first order in velocity. Substituting into Eq. (5.13) we find

$$\Phi_s\Big|_{\Delta t=0} = \frac{\omega'\,L}{c\,\cos\kappa'}\left\{n'_s + \frac{v}{c}\cos(\theta - \kappa')\right\} \quad , \tag{5.15}$$

where we have used Eq. (5.9) to substitute for ΔX. Eq. (5.15) is the expression at first order in velocity for the relative phase of the incident and emerging beams when viewed from I and is the central result of this section. We note that, in the limit as $v \to 0$, $\omega' \to \omega$, $n'_s \to n_s$ and $\kappa' \to \phi$ which recovers Eq. (5.4).

Before we evaluate the modified Laub drag coefficient for the experiment of Sanders and Ezekiel we must first pause to consider the effect of the motion of the glass sample on the phase shift in the light beam as it propagates around the optical interferometer through air. This we do in the following section, and we calculate the explicit form of the Laub drag coefficient in section 5.5.

5.4 Phase shift in air

Sanders and Ezekiel employed a square optical cavity with a mirror separation of $l \approx 0.7$ m in their Fresnel drag experiment. Their optical cavity contained two plane mirrors and two concave mirrors. The concave mirrors were located

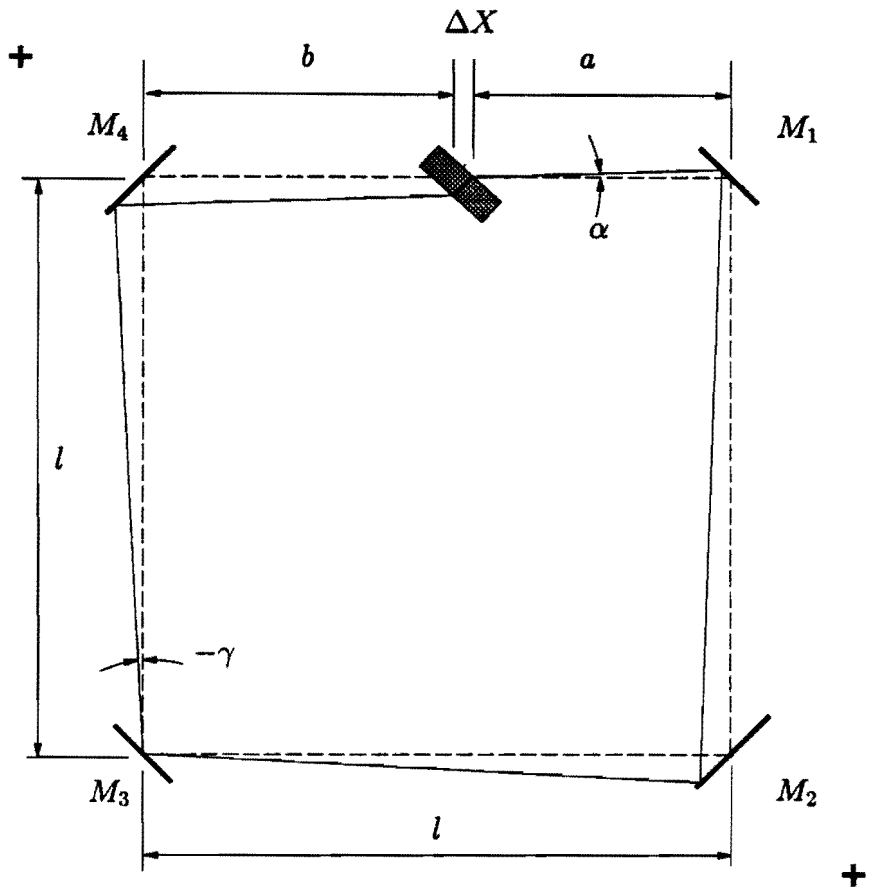

Figure 5.6: The geometry of the resonant cavity of Sanders and Ezekiel. The presence of the dielectric sample deflects the beam (unbroken line) off the optical axis of the resonant cavity (broken line). M_2 and M_4 are the two concave mirrors of the optical cavity, their centres of curvature being denoted by a cross diagonally opposite these mirrors.

at opposite corners of the cavity and each had a radius of curvature $R = 1.2 \pm 0.05$ m. This optical cavity is illustrated in figure 5.6. In this section we determine an expression for the perturbation angle α which arises because of the tilt of the normal of the dielectric sample at an angle θ relative to the optical axis of the cavity. We determine both the effect this has on the path of the laser beam, and the phase shift of the laser beam as it stretches around the cavity perimeter.

Again we begin by taking a snapshot of the interferometer from I. With $\Delta T = 0$ we first trace the path of the clockwise beam around the interferometer using a linear optics approximation for this calculation. It therefore proves convenient to define a new coordinate, ξ, which is at right angles to the optical axis of the cavity and denotes the distance of the beam from the optical axis. The ξ axis lies in the plane of the interferometer and the positive ξ direction is

chosen as that which points away from the centre of the cavity. At each mirror the optical axis of the cavity makes a 90° clockwise turn, such that the ξ axis is also rotated 90° clockwise. At the jth mirror, M_j, we denote the ξ coordinate of the incident beam ξ_j^i and the ξ coordinate of the reflected beam ξ_j^r, where $j = 1$ to 4. It is apparent that $\xi_j^r = -\xi_j^i$ due to the rotation of the ξ axis at M_j. The ξ coordinate where the clockwise beam emerges from the dielectric sample is denoted ξ_0. Similarly ξ_5 labels the ξ coordinate at the point where the clockwise beam is incident on the sample.

We also denote α_j as the angle of the laser beam relative to the optical axis of the cavity between the mirrors M_{j-1} and M_j. Because the faces of the dielectric sample are parallel the beams incident upon and emerging from the glass sample are also parallel. As in the previous section we denote α as the angle with which the laser beam is orientated relative to the optical axis of the cavity along the arm in which the glass sample is located. At the M_j, α_j^i and α_j^r respectively label the angles of the incident and reflected beams relative to the optical axis of the cavity.

A linear optics approximation predicts that ξ is altered by an amount

$$\begin{pmatrix} \xi_{j+1} \\ \alpha_{j+1} \end{pmatrix} = \begin{pmatrix} 1 & d \\ 0 & 1 \end{pmatrix} \begin{pmatrix} \xi_j \\ \alpha_j \end{pmatrix} , \tag{5.16}$$

when the beam propagates a distance d along the cavity perimeter from the point ξ_j to ξ_{j+1}. Similarly, the matrix operation representing each mirror is

$$\begin{pmatrix} \xi_j^r \\ \alpha_j^r \end{pmatrix} = \begin{pmatrix} -1 & 0 \\ +1/f_j & -1 \end{pmatrix} \begin{pmatrix} \xi_j^i \\ \alpha_j^i \end{pmatrix} , \tag{5.17}$$

where $f_j = R_j \cos 45°/2$ with $R = 1.2$ m for M_2 and M_4 and $R = \infty$ for M_1 and M_3. Because $1/f_1 = 1/f_3 = 0$ we define $f \equiv f_2 = f_4$, which is the focal length of the two concave mirrors.

We first note that the distance separating the points ξ_j^r and ξ_{j+i}^i is itself dependent on the coordinates ξ_j^r and ξ_{j+1}^i, the separation being $d_{j+1} = l - \xi_j^r - \xi_{j+1}^i$. Therefore

$$\xi_{j+1}^i = \xi_j^r + \alpha\,(l - \xi_{j+1}^i - \xi_j^r) \ .$$

However, as the beam suffers only a small perturbation off the optical axis we have $\xi_{j+1}^i + \xi_j^r \sim \alpha\, l$, such that $\alpha\,(\xi_{j+1}^i + \xi_j^r) \sim \alpha^2\, l$ which is negligible within our linear optics approximation. We may therefore assume the distance between the points ξ_j^r and ξ_{j+1}^r is l when calculating ξ coordinates. Furthermore, we denote the distance along the optical axis of the cavity from M_4 to ξ_5 as b and

from ξ_0 to M_1 as a, where M_4 and M_1 specify the location of the fourth and first mirrors along the optical axis in this context. Clearly $a + b = l - \Delta x$, where Δx is given by Eqn. (5.9).

Starting at the dielectric, Figure 5.6 shows M_2 is the first concave mirror which the clockwise beam intersects. From the above matrix operators we find $\alpha_2^i = -\alpha_0 \equiv -\alpha$. Upon reflection from M_2,

$$\alpha_2^r = \alpha + \xi_2^i/f \equiv \gamma \ , \tag{5.18}$$

which defines γ. Tracing the beam from M_2 to M_4 gives $\alpha_4^i = -\gamma$ such that

$$\alpha_4^r = \gamma + \frac{\xi_4^i}{f} = \alpha \ , \tag{5.19}$$

where, in the last step we note $\alpha_4^r \equiv \alpha$ by our earlier definition of α. Eqs. (5.18) and (5.19) give $\xi_4^i = -\xi_2^i$ such that $\xi_3^r = -\xi_3^r = 0$, independent of the dimensions of the dielectric sample. Therefore the laser beam *always intersects the plane mirror opposite the glass sample on the optical axis.* It should be appreciated that the only physical assumption made in deriving this result is that the opposite faces of the dielectric sample are parallel and therefore the incident and emerging beams are also parallel. This proves our claim in section 5.3.3 that the laser beam remains fixed relative to the optical cavity and the dielectric moves diagonally across the fixed beam.

With $\xi_3^r = 0$ we have $\xi_4^i = -\gamma\, l$ such that, from Eq. (5.19),

$$\gamma = \alpha \frac{f}{f - l} \ .$$

Tracing the beam around the perimeter of the interferometer gives

$$\xi_0 - \xi_5 = -\alpha\,(2\,l - \Delta x) - \gamma\, 2\, l$$

and hence

$$\alpha = -\frac{\xi_0 - \xi_5}{4\,l - \Delta x + 2\,l^2/(f - l)} \ .$$

In order for the laser beam to join at either edge of the dielectric we require $\xi_0 - \xi_5 = \Delta Y$ where ΔY is given by Eq. (5.10). Sanders and Ezekiel used dielectric samples with $L \leq 1.5$ cm, $\theta \leq 15°$ and $n_s \leq 1.9$. Therefore $\Delta y \leq 0.2$ cm such that $|\alpha| \leq 3 \times 10^{-3}$ rad. As α is so small it eventuates that both terms of $O(\alpha^2)$ and of $O(d\alpha/dv)$ lead to corrections to the modified Laub drag coefficient which are less than 10 ppm, which is negligible within this

experimental context. We therefore treat α as independent of velocity and keep only first order in α. Thus, at first order in α we have

$$\alpha = -\frac{L\sin(\theta-\phi)\sec\phi}{4l-\Delta x+2l^2/(f-l)} \ , \tag{5.20}$$

where ϕ was previously defined by $n_a\sin(\theta-\alpha) = n_s\sin\phi$, Eq. (5.5), and is the angle of the refracted beam relative to the normal of the dielectric when the sample is stationary. Values of α are given in table 5.1. An uncertainty of 30 % in α arises from an uncertainty in $R = 1.2 \pm 0.05$ m.

Again we calculate the phase shift of the laser beam due to its propagation around the ring perimeter by taking a snapshot of the interferometer in I. At first order in α the distance the laser beam stretches through air around the perimeter of the interferometer from the opposite edges of the dielectric is

$$\begin{aligned}\sum_{i=1}^{5} d_i &= (a-\xi_1^i)+(l-\xi_1^r-\xi_2^i)+(l-\xi_2^r-\xi_3^i)+(l-\xi_3^r-\xi_4^i)+(b-\xi_4^r) \\ &= 4l-\Delta X \ ,\end{aligned} \tag{5.21}$$

where we have noted $\xi_j^r = -\xi_j^i$. Within a linear optics approximation we find that, apart from ΔX being dependent on α, the path length of the beam is unchanged by the perturbation of the beam off the optical axis. It follows immediately that the phase shift in air of the clockwise beam upon traversing the interferometer perimeter is

$$\Phi_s\Big|_{\Delta t=0} = \frac{\omega_a n_a}{c}\{4l-\Delta x\} \ . \tag{5.22}$$

where we have noted $k_a = n_a\omega_a/c$.

5.5 Modified Laub Drag coefficient

Having calculated the shift in phase of the *ccw* laser beam as it propagates through the moving glass sample and around the perimeter of the optical interferometer, we are now in a position to determine the modified Laub drag coefficient for the experiment of Sanders and Ezekiel. By definition the Laub drag coefficient expresses the amount the total phase shift in the interferometer is altered by the velocity of the dielectric.

We proceed by differentiating the total phase $\Phi = \Phi_s + \Phi_a$ with respect to v and then set $v = 0$. This yields the first order correction for Φ in a Taylor series

expansion. Substituting in Eqs. (5.15) and (5.22) and then differentiating we obtain

$$\begin{aligned}\left.\frac{d}{dv}\Phi\right|_{v=0} &= \left.\frac{d}{dv}\Phi_s\right|_{v=0} + \left.\frac{d}{dv}\Phi_a\right|_{v=0} , \\ &= \left.\frac{d}{dv}\left\{\frac{\omega' L}{c\cos\kappa'}\left(n_s' + \frac{v}{c}\cos(\theta-\kappa')\right)\right\}\right|_{v=0} \\ &\quad + \left.\frac{d}{dv}\left\{\frac{\omega_a n_a}{c}\left(4l - L\frac{\cos(\theta-\kappa')}{\cos\kappa'}\right)\right\}\right|_{v=0} , \end{aligned} \tag{5.23}$$

From Eq. (5.14) we find

$$\frac{d\omega'}{dv} = -\frac{\omega_a n_a \cos\alpha}{c} ,$$

and hence

$$\left.\frac{dn_s'}{dv}\right|_{v=0} = \left.\frac{dn_s}{d\omega'}\frac{d\omega'}{dv}\right|_{v=0} = -\frac{\omega n_a \cos\alpha}{c}\frac{dn_s}{d\omega} .$$

When differentiating $\sec\kappa'$ we use the identity

$$\left.\frac{d}{dv}\sec\kappa'\right|_{v=0} = \left\{\sin\kappa'\frac{d}{dv}\tan\kappa'\right\}\Big|_{v=0} = \sin\phi\left.\frac{d}{dv}\tan\kappa'\right|_{v=0} , \tag{5.24}$$

which follows from $\sec\kappa' = \sqrt{1+\tan^2\kappa'}$. Setting $v = 0$ after differentiation causes $\kappa' \to \phi$, where ϕ is the angle of refraction when the sample is stationary.

Substituting $\cos(\theta-\kappa') = \cos\theta\cos\kappa' + \sin\theta\sin\kappa'$ into Eq. (5.22) we find

$$\begin{aligned}\frac{d}{dv}\Phi_a &= -\frac{L\omega_a n_a}{c}\sin\theta\frac{d}{dv}\tan\kappa' , \\ &= -\frac{L\omega_a}{c}\{n_s\sin\phi\cos\alpha + n_a\cos(\theta-\alpha)\sin\alpha\}\frac{d}{dv}\tan\kappa' , \end{aligned} \tag{5.25}$$

where, in the last step, we have written $\sin\theta = \sin(\theta-\alpha)\cos\alpha + \cos(\theta-\alpha)\sin\alpha$ and have identified $n_a\sin(\theta-\alpha) = n_s\sin\phi$, Eq. (5.5), which defined ϕ.

Using the above results to perform the differentiation in Eq. (5.23) we obtain

$$\begin{aligned}\left.\frac{d}{dv}\Phi\right|_{v=0} &= \frac{L\omega_a\sec\phi}{c^2}\left\{-n_a n_s\cos\alpha + \cos(\theta-\phi) - n_a\cos\alpha\,\omega_a\frac{dn_s}{d\omega}\right\} \\ &\quad + \frac{L\omega_a}{c}\{n_s\sin\phi(1-\cos\alpha) - n_a\cos(\theta-\alpha)\sin\alpha\}\left.\frac{d}{dv}\tan\kappa'\right|_{v=0} \end{aligned} \tag{5.26}$$

The final term, which remains to be differentiated, explicitly gives the change in the phase shift of the clockwise beam due to the velocity dependence of κ'. As κ' describes the orientation of the beam through the dielectric, this term

predicts a measurable phase shift at first order in velocity due to the path the beam follows through the sample being velocity dependent. Differentiating Eq. (5.11) gives

$$\frac{d}{dv}\tan\kappa'\Big|_{v=0} = \frac{d}{dv}\tan\beta'\ \Big|_{v=0} + \frac{(n_s+\omega\partial n_s/\partial\omega)\,\sin\alpha}{c\,\cos\phi\,\cos(\theta-\alpha)}\ ,$$

where the effect of the incident laser beam moving across the surface of the glass sample has appeared explicitly as the final term. Differentiation of $\tan\beta'$ is aided by the identity

$$\frac{d}{dv}\tan\beta' = \frac{1}{\cos^3\beta'}\,\frac{d}{dv}\sin\beta'\ .$$

which follows from $\tan\beta' = \sin\beta'/\sqrt{1-\sin^2\beta'}$. From Eq (5.8),

$$\begin{aligned}\frac{d}{dv}\sin\beta'\Big|_{v=0} &= n_a\frac{d}{dv}\left\{\frac{\sin(\theta-\alpha')}{n_s'\,[1-v\,\cos\alpha\,(n_a-1/n_a)/c]}\right\}\Big|_{v=0}\\ &= \frac{n_a}{n_s}\,\sin\phi\,\cos\alpha\,\frac{\omega}{c}\,\frac{dn_s}{d\omega} - \cos(\theta-\alpha)\,\frac{\sin\alpha}{n_s\,c}\\ &\quad + \left(n_a-\frac{1}{n_a}\right)\frac{\sin\phi\,\cos\alpha}{c}\ ,\end{aligned} \tag{5.27}$$

where we have differentiated both sides of Eq (5.7) to obtain $d\alpha'/dv\,|_{v=0} = \sin\alpha/(c\,n_a)$. Upon setting $v=0$ we find $n_s'\to n_s$, $\alpha'\to\alpha$, $\beta'\to\phi$ and $\kappa'\to\phi$. It is helpful to consider the physical origins of Eq (5.27): the first term arises from dispersion causing $n_s'\neq n_s$ because $\omega'\neq\omega$ due to the Döppler effect; the second term stems from the angular aberration suffer by the incident beam when boosted from I to I'; the final term arises from Fresnel drag in air as the incident beam does not propagate with phase velocity c/n_a when viewed from I'.

In the experiment of Sanders and Ezekiel α ranged from 3×10^{-4} radians to 12×10^{-4} radians such that $\alpha^2 < 1.4\times10^{-6}$, which is negligible. The dominant term in the correction of Eq. (5.26) stemming from the differentiation of $\tan\kappa'$ is the term which is proportional to dispersion. However, this leads only to corrections ranging from 0.6 ppm to 4.2 ppm in all of the experimental runs of Sanders and Ezekiel, which is negligible in this experimental context. It follows that all terms in Eq. (5.26) which stem from the application of the relativistic from of Snell's law, Eq. (5.8), as opposed to the non-relativistic form, Eq. (5.5), and the term which arose from the motion of the glass sample diagonally through the incident laser beam, are experimentally insignificant.

Nevertheless, it would not be difficult to construct an experiment for which relativistic terms in the expression for Snell's law would produce an appreciable phase shift. Consider, for example, an experimental arrangement where the velocity of the dielectric is inclined relative to the axis of the optical cavity so that $\alpha = \pi/4$. In such an experiment terms arising from the relativistic application of Snell's law, and the motion of the sample through the laser beam, would be of the same order of magnitude as the leading order terms in Eq. (5.26). Therefore we are led to the conclusion that while the experiment of Sanders and Ezekiel was (quite deliberately) not designed, nor sensitive enough, to test the relativistic form of Snell's law, such an experiment could easily be constructed. It would be of interest to apply the fully relativistic formalism developed within this chapter to the experiment of Bilger and Stowell [15], who inclined their rotating sample such that the laser beam was incident at the Brewster angle. Such an analysis has not been performed to date.

If we neglect all terms which contribute less than 10 ppm then Eq. (5.26) reduces to

$$\begin{aligned} \left.\frac{d\Phi_s}{dv}\right|_{v=0} &= \frac{L\omega_a}{c^2}\sec\phi\left\{\cos(\theta-\phi) - n_s\, n_a\ - \omega_a\, n_a \frac{dn_s}{d\omega}\right\}\ , \\ &= \frac{L\omega_a}{c^2}\,\epsilon_N\ , \end{aligned} \tag{5.28}$$

which defines the modified Laub drag coefficient ϵ_N which results from our calculation. It should be noted that our definition of the drag coefficient differs from that of Sanders and Ezekiel in so far as we have incorporated the factor $\sec\phi$ into ϵ_N. This expression has previously been obtained by Bilger and Stedman [13] on the basis of a first order calculation. Their analysis did not successfully incorporate all geometric effects arising from tilting the glass sample relative to the optical axis of the cavity and, as such, our analysis provides a significant improvement on this earlier work. This comparison shows, however, that our calculation, while approached from a different perspective to earlier work (our calculation has proceeded entirely from first principles), is in full agreement with that of Bilger and Stedman in the appropriate limit.

5.5.1 Comparison with the analysis of Sanders

In his thesis Sanders obtained [127] the expression

$$\left.\frac{d\Phi_s}{dv}\right|_{v=0} = \frac{L\omega_a}{c^2}\sec\phi_0\left\{\cos(\theta-\phi_0) - \bar{n}_s\, n_a\ - \frac{\omega_a}{n_a}\frac{d\bar{n}_s}{d\omega}(1-\tan^2\phi_0)\right\}\ ,$$

$$= \frac{L\omega_a}{c^2}\epsilon_{SE} \ , \tag{5.29}$$

where we have noted that

$$\omega_a \frac{dn_s}{d\omega} = \omega_a \frac{dn_s}{d\lambda}\frac{d\lambda}{d\omega} = -\frac{c}{\omega_a}\frac{dn_s}{d\lambda} = -\lambda_0 \frac{dn_s}{d\lambda} \ ,$$

where $\lambda = c/\omega$ is the wavelength in vacuum and $\lambda_0 \equiv c/\omega_a$. In this expression we use the notation ϕ_0 to represent the fact that this angle is calculated assuming $\alpha = 0$, and $\bar{n}_s$ is used to represent the *refractive index of the sample relative to air*, which is quoted by manufacturers and was (incorrectly) used by Sanders and Ezekiel in their numerical analysis, whereas their derivation assumed n_s represented the absolute refractive index of their sample.

All terms which define ϵ_N and ϵ_{SE} in Eqs. (5.28) and (5.29) differ. We consider, in turn, the physical origin of each of these terms and the magnitude of the discrepancy between our result and that of Sanders and Ezekiel.

Physically, the term proportional to $\cos(\theta - \phi)$ in ϵ_N arises in our analysis because simultaneous events in I (the frame in which we took our snapshot) are not simultaneous in I' (the frame in which we calculated κ'). This term differs from that calculated by Sanders and Ezekiel because $\phi \neq \phi_0$. These angles are not equal because the laser beam is perturbed off the optical axis of the cavity by an angle α and because the absolute (n_s) rather than that relative ($\bar{n}_s$) value of the refractive index must be used in the numerical application of Snell's law. However the later correction is typically an order of magnitude down on that due to $\alpha \neq 0$. In the experiment of interest the term proportional to $\cos(\theta - \phi)$ in ϵ_N contributes corrections to the analysis of Sanders and Ezekiel from 15 ppm to 89 ppm, with a mean correction of 36 ppm. Corrections to the numerical value of the factor $\sec\phi$ in ϵ_N because $\phi \neq \phi_0$ are also in the range from 15 to 90 ppm. While these represent the smallest of our numerical corrections to the analysis of Sanders and Ezekiel, they are significant given that Sanders and Ezekiel claimed an overall agreement of 60 ppm between theory and experiment. Furthermore, because these corrections arise out of an effect completely neglected in the analysis of Sanders they are important for reasons of completeness.

Our second term in our modified Laub drag coefficient is proportional to $n_s n_a$. This term has its physical origin in the Döppler effect, with $\omega' - \omega$ proportional to $v n_a$. Because it is the magnitude of the wave vector, $|\boldsymbol{k}'_s| = n'_s \omega'/c$, which is used to calculate the phase shift through the sample we find, upon differentiating the total phase with respect to velocity, the term proportional to $n_s n_a$ appears in our expression for ϵ_N. In this instance our expression

differs from that obtained by Sanders and Ezekiel because $n_s\, n_a \neq \bar{n}_s\, n_a$. As mentioned earlier, Sanders and Ezekiel incorrectly believed that manufacturers quoted the absolute rather than the relative refractive index of their glass samples. This numerical error in their analysis was first detected by Bilger who, from his own experience, was aware of this misleading convention adopted by manufacturers. Corrections to the modified Laub drag coefficient arising from this term range from 535 ppm to 826 ppm, which clearly constitutes a very significant analytical error in the quest to achieve an overall accuracy of 100 ppm. The mean discrepancy arising from this term over all experimental runs reported by Sanders and Ezekiel is 700 ppm.

Again our final term, which is proportional to dispersion, is significantly different to that reported by Sanders and Ezekiel. This term also arises because of the Döppler effect. Because $\omega' \neq \omega$ we find $n'_s \neq n_s$ and their difference $(\omega' - \omega)\, dn/d\omega$ is velocity dependent, which leads to a dispersion term in the drag coefficient ϵ_N. Factors of n_a by which our expression differs from that of Sanders and Ezekiel arise because of Sanders' decision to neglect corrections in the dispersion term due to the fact that the experiment was performed in air [127, p.178]. The spurious term $\tan^2\phi_0$ in Eq. (5.29) is an algebraic error in Sanders' work which derives from his failure to include angular aberration throughout his analysis. As previously mentioned, we sidestepped algebraic complications arising from aberration by using the invariance of our expression for phase. The magnitude of our correction to Sander's prediction arising from this term ranges from 174 ppm to 1394 ppm, with a mean discrepancy of 523 ppm. Again this constitutes a very significant error in the analysis of Sanders and Ezekiel in their aim to achieve experimental verification of Fresnels' light dragging law to 100 ppm.

A final correction in the analysis of this experiment arises because all samples were anti-reflection coated. We account for the presence of two thin films on each glass sample by regarding each sample as the sum of two slabs of different refractive index. Assuming all anti-reflection coatings are a film of MgF_2 (refractive index $n = 1.38$) with thickness $633/(4 \times 1.38)$ nm $= 115$ nm we obtain corrections to the measured drag coefficient between 3 ppm and 24 ppm in our numerical analysis. This small effect is negligible within the overall uncertainty of the experiment.

Numerical results from the analysis of each run are given in Table 1. Our discrepancy with the calculation of Sanders and Ezekiel ranges from 860 ppm to 2190 ppm, with a mean of 1200 ppm and standard deviation 360 ppm.

We therefore conclude, as stated in the introduction of this chapter, that the analysis of Sanders and Ezekiel contained a number of errors and did not accurately account for all relativistic effects. From the results presented above it is apparent that their claim of experimental agreement with theory to 60 ppm was unjustified.

5.5.2 Comparison with the experimental results

Sanders and Ezekiel compared their predictions for the modified Laub drag coefficient with their measured, and corrected, beat frequency when the velocity of each sample was 225.525 (235 ppm) cm.s^{-1}. Below we provide an analysis which enables us to experimentally determine the modified Laub drag coefficient ϵ_{expt} from the measured beat frequency $\Delta\nu$.

From Eqs. (5.15) and (5.22), when the dielectric is stationary the total optical path-length of the ring cavity is

$$P = P_0 + \{n_s - n_a \cos(\theta - \phi)\} \frac{L}{\cos\phi} \ ,$$

where $P_0 = 4\, n_a\, l$ is the optical path length of the cavity in the absence of the glass sample. This expression corrects that given by Sanders and Ezekiel [128, p667] who found

$$P_{SE} = P_0 + \{\bar{n}_s - n_a\} \frac{L}{\cos\phi_0} \ .$$

Our correction to the optical path length, however, results in a correction to ϵ_{expt} which is less than 10 ppm and is regarded as insignificant.

For optical resonance to occur we require the total change in phase of the laser beam upon a transit of the ring perimeter to be an integer multiple of 2π radians. If the glass sample has velocity v_0 the resonant condition is

$$\frac{\omega_a\, P}{c} + v_0 \left.\frac{d\Phi}{dv}\right|_{v=0} = 2\,\pi\, m \ , \tag{5.30}$$

where m is an integer. Substituting Eq. (5.28) into Eq. (5.30) and solving for ω_a we obtain

$$\omega_a \ = \ \omega_0 \left\{1 - \frac{v_0}{c}\frac{L}{P}\epsilon_N\right\} \ , \tag{5.31}$$

where $\omega_0 \equiv 2\pi\, m\, c/P$ is the resonant frequency when the dielectric is stationary. At this point we remind the reader that Eq. (5.31) gives the resonant frequency for the beam propagating parallel to the velocity of the dielectric,

this being the *cw* beam when defined by figure 5.6. As we would expect, the dragging of the wavefronts of the beam propagating with the glass sample has caused the optical path length to decrease (as ϵ_N, defined by Eq. (5.28), is negative) and hence the resonant frequency to increase. Our prediction for the *ccw* beam is recovered from Eq. (5.31) with the substitution $v_0 \rightarrow -v_0$.

Upon combining the opposite beams at optical resonance a beat frequency, in hertz, is predicted with

$$\Delta\nu = \frac{(\omega_a)_{cw} - (\omega_a)_{ccw}}{2\pi} = -\omega_0 \frac{v_0}{\pi c} \frac{L}{P} \epsilon_N \ . \tag{5.32}$$

As such we find the experimentally observed modified Laub drag coefficient is

$$\epsilon_{expt} = \frac{P\lambda_0}{2Lv_0} \Delta\nu \ , \tag{5.33}$$

where $\lambda_0 \equiv c/\omega_0 = 632.99$ nm in the experiment of Sanders and Ezekiel.

By accurately measuring the free spectral range of the cavity in the absence of any dielectric sample Sanders and Ezekiel determined $P_0 = 294.3496$ (2 ppm) cm. They took the refractive index of air to be 1.00027 (10 ppm) at λ_0. To distinguish the drag effect from various sources of drift and noise Sanders and Ezekiel oscillated their glass sample at a frequency of 5 Hz. The velocity of the glass sample was determined interferometrically using a stabilised He-Ne laser source and a mirror attached to the same mount as the glass sample. All reported data was recorded for $v_0 = 25.525 \pm 0.006$ cm.s^{-1}.

In table 1 we provide a full numerical comparison between ϵ_{expt}, ϵ_{SE} and ϵ_N. Conclusions drawn from the comparison of the two predicted drag coefficients have been discussed in section 5.5.1. When comparing the experimental results of Sanders and Ezekiel with our predicted drag coefficient we find our predictions for the modified Laub drag coefficient are consistently larger than that observed by between 450 ppm and 2860 ppm, with an overall mean discrepancy of 1300 ppm and standard deviation 590 ppm.

In figure 5.7 we plot the distribution of the discrepancies between Sanders and Ezekiels' experimental results and theoretical predictions. It is apparent that every measurement of the drag coefficient is significantly below that predicted by the above analysis. This clearly demonstrates Sanders and Ezekiel's claim of an overall agreement between theory and experiment to 60 ppm was false. If we accept Sanders and Ezekiel's estimate of their experimental uncertainty to be 280 ppm we find our theoretical and experimental analyses differ by 4.6 standard deviations. This is an extremely large discrepancy and would

warrant the rejection of the theoretical foundations of this analysis if one had a high degree of confidence in this experimental result. However, in light of the discussion presented in section 5.2.1, it is apparent that the accuracy of this experiment would have been greatly improved if the opposite beams propagated through an evacuated chamber. This author takes the opinion that not all systematic errors arising within this experiment were accurately accounted for by Sanders and Ezekiel, and this neglect degrades the quality of their work. Regardless, this result, with a mean discrepancy of 1300 ppm, is 30 % less accurate than that of Bilger and Stowell [15], who achieved agreement between experiment and theory to 1000 ppm. Unlike Sanders and Ezekiel, Bilger and Stowell found their experimental results gave a slightly larger drag coefficient than expected. Therefore, Sanders and Ezekiel's claim that their experiment provided the most accurate verification of the Fresnel drag relation to date was unjustified.

Within this chapter we have provided a thorough and definitive analysis of the light drag experiment of Sanders and Ezekiel. This analysis has built upon, and corrected, previous attempts at a complete analysis by Sanders [127] and Bilger and Stedman [13]. Our most novel contribution is to provide a comprehensive treatment of how the modified Laub drag coefficient is affected by tilting each glass sample relative to the optical axis of the cavity. We have also given a fully relativistic treatment of Snell's law in this context, although the relativistic corrections thus uncovered are not significant experimentally. Our calculated discrepancy of 1300 ppm between theory and experiment illustrate that Sanders and Ezekiel did not improve on the accuracy of Bilger and Stowell (1000 ppm) in this experiment.

n_s	$\partial n_s/\partial\lambda$ (μm^{-1})	L (cm)	θ (deg)	α (deg) (30%)	$\Delta\nu$ (Hz)	ϵ_{expt}	ϵ_{SE}	ϵ_N	$\frac{\epsilon_{SE}-\epsilon_N}{\epsilon_N}$ (ppm)	$\frac{\epsilon_{expt}-\epsilon_N}{\epsilon_N}$ (ppm)
BK-7										
1.51537 (66)	-0.03422	0.64050 (70)	5.15 (4.9%)	0.021	944.4 (1100)	0.5388 (1100)	0.53877 (200)	0.53927	-920	-960
1.51537 (66)	-0.03422	0.64050 (70)	6.45 (3.9 %)	0.026	945.1 (1100)	0.5392 (1100)	0.53954 (200)	0.54008	-1000	-1710
1.51537 (66)	-0.03422	0.64050 (70)	10.00 (2.7%)	0.041	950.5 (1300)	0.5422 (1300)	0.54250 (240)	0.54322	-1310	-1800
1.51537 (66)	-0.03422	0.64050 (70)	12.70 (2.3%)	0.052	956.5 (1600)	0.5457 (1670)	0.54563 (280)	0.54653	-1640	-1580
1.51537 (66)	-0.03422	1.28100 (70)	5.15 (4.9%)	0.041	1885.3 (1200)	0.5384 (1100)	0.53877 (200)	0.53928	-930	-1700
SF-1										
1.71275 (58)	- 0.09625	0.62378 (80)	5.15 (4.9 %)	0.025	1323.5 (760)	0.7756 (775)	0.77572 (155)	0.77640	- 860	- 1070
1.71275 (58)	- 0.09625	0.62378 (80)	6.60 (3.7 %)	0.032	1325.8 (750)	0.7769 (775)	0.77675 (155)	0.77754	-1000	-790
1.71275 (58)	- 0.09625	0.62378 (80)	10.15 (2.6 %)	0.049	1332.3 (980)	0.7807 (1030)	0.78035 (120)	0.78151	-1480	-1000
SF-57										
1.83980 (54)	-0.13829	0.59854 (84)	6.60 (3.8%)	0.034	1523.9 (850)	0.9308 (860)	0.93067 (140)	0.93156	-960	-780
1.83980 (54)	-0.13829	0.59854 (84)	10.00 (2.7 %)	0.051	1530.0 (1180)	0.9346 (1180)	0.93439 (170)	0.93573	-1430	-1240
1.83980 (54)	-0.13829	1.19708 (84)	6.65 (3.7 %)	0.067	3042.0 (690)	0.9307 (750)	0.93072 (140)	0.93162	-970	-1040
F.S.										
1.45704 (41)	-0.02904	0.19910 (251)	15.65 (1.9 %)	0.019	265.6 (3770)	0.4870 (3760)	0.48736 (270)	0.48843	-2190	-2860
1.45704 (41)	-0.02904	0.49520 (101)	10.20 (2.8 %)	0.030	6521.1 (1700)	0.4810 (1680)	0.48068 (170)	0.48136	-1420	-770
1.45704 (41)	-0.02904	1.04290 (50)	5.15 (4.8 %)	0.031	1359.9 (1030)	0.4767 (1050)	0.47705 (125)	0.47752	-1000	-1750
1.45704 (41)	-0.02904	1.49370 (35)	5.15 (4.8 %)	0.044	1948.9 (1080)	0.47731 (1050)	0.47705 (125)	0.47752	-1000	-450

Table 5.1: Numerical comparisons between the theoretical and experimental results of Sanders and Ezekiel with the analysis presented within this chapter. The modified Laub drag coefficients are labelled respectively ϵ_{expt} (experimental), ϵ_{SE} (Sanders and Ezekiels' theoretical prediction) and ϵ_N (our theoretical prediction). A mean discrepancy of 1300 ppm arises between the experimental results of Sanders and Ezekiel and the theoretical analysis presented in this chapter.

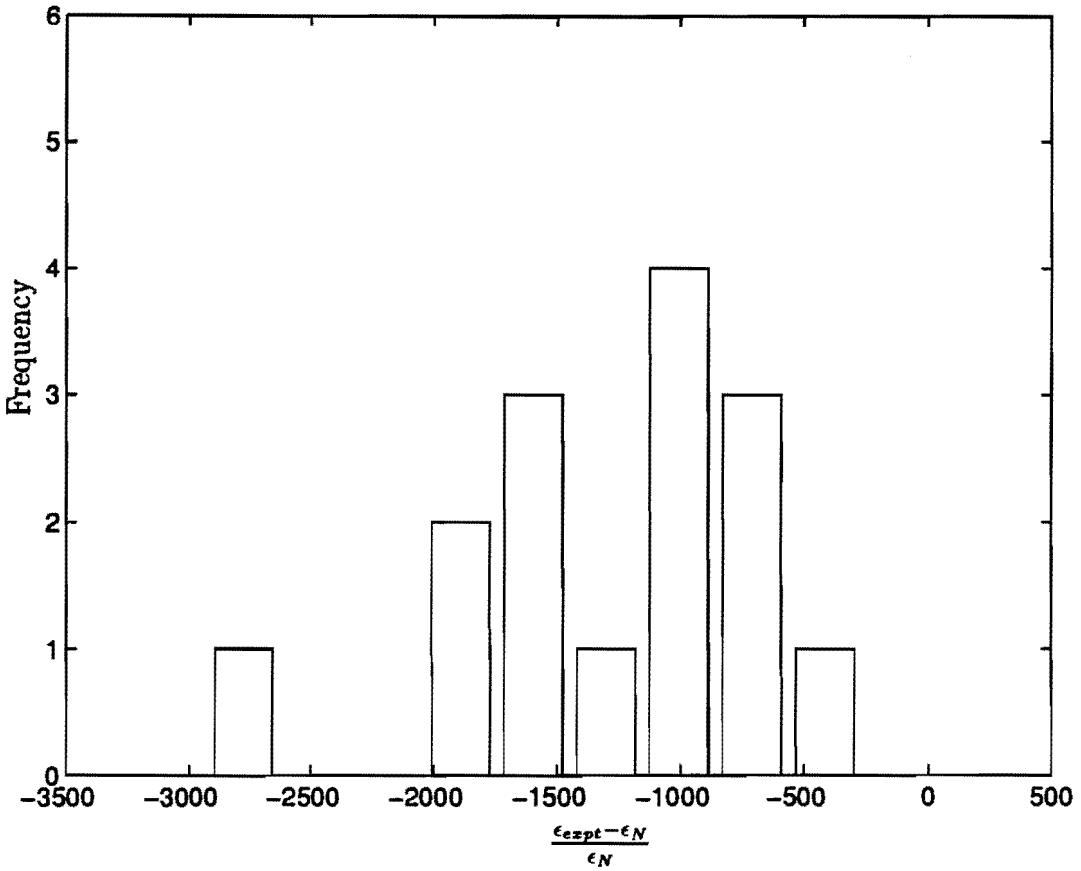

Figure 5.7: Comparison between experimental results and theoretical predictions for the light drag experiment of Sanders and Ezekiel. It is apparent that every measurement of the drag coefficient is significantly below that predicted by the analysis presented within this chapter. Each bar has thickness $\sigma/2 = 295$ ppm and the mean discrepancy is 1300 ppm.

Chapter 6

Fresnel drag in a linearly accelerating dielectric

In this chapter we apply the covariant formulation of Maxwell's equations to the problem of light propagation through an accelerating dielectric. As predicted by Tanaka [146], we find light which propagates through accelerating media suffers a shift in frequency. We investigate three potential experiments which are, in principle, sensitive to this frequency shift. All proposals involve a glass sample being accelerated, or freely falling, along one arm of a ring interferometer. We show the response profile of a resonant cavity is asymmetric when a glass sample is accelerating relative to the optical interferometer, and we predict sideband structure will be observed when the sample is oscillated along one arm of a passive optical interferometer and the resulting beat between opposite arms Fourier analysed.

6.1 Optical tests of Maxwell's covariant equations

Light propagation through moving media is one of the basic and interesting problems in electrodynamics. When the media through which light is propagating is moving inertially in flat spacetime, the original formulation of Maxwell's equations [96] will fully describe this phenomenon. This is a direct consequence of the form invariance of Maxwell's equations under a Lorentz boost. When the media is moving non-inertially, however, the problem cannot be analysed within Maxwell's theory, as Maxwell's equations do not maintain their standard form under arbitrary coordinate transformations. For the description of light propagating through accelerating media a covariant formulation of Maxwell's equations must be employed.

There have been several high precision light drag experiments in which dielectric samples are moved non-inertially. Bilger and Zavodny [16] and Bilger and Stowell [15] placed a rotating fused silica disk along one arm of a ring laser.

Fresnel drag in the rotating dielectric induced a non-reciprocal change in the optical path of the laser beams which, in turn, produced a beat frequency between the opposite beams. From comparing this observed beat frequency with the velocity of the dielectric the light drag coefficient was obtained. In these experiments the drag coefficient was measured to an accuracy of 0.5% [16] and 0.04% [15] respectively. However, their more accurate measurement differs from their theoretical predictions by two standard deviations, which was considered too small to claim a discrepancy. In their modified Laub drag experiments Sanders and Ezekiel [128] oscillated their glass samples along the path of their optical cavity. As discussed in detail in chapter 5, their analysis contained a number of errors which invalidate their claimed agreement between experiment and theory of 0.02%. Kowalski et al. [76] mounted a dielectric and two mirrors on a platform which was linearly accelerated along the path of a ring laser. If the results of Kowalski et al. are reinterpreted as the measurement of the Laub drag coefficient then their results were accurate to 0.2% [75].

All of these experiments were performed using dielectrics moving non-inertially. One may therefore expect a satisfactory understanding of these experimental results to require a description in terms of the covariant form of Maxwell's equations. Because of the modest accelerations involved, however, all authors assumed the effect of acceleration on the measured phase shift was negligible, and provided analyses concerned only with Fresnel drag at the instantaneous velocity of of the glass sample. Sanders and Ezekiel recorded their beat frequency when the glass sample had maximum velocity and no acceleration. Kowalski et al. used samples with a typical acceleration ~ 0.053 $\mathrm{m.s^{-2}}$. Bilger et al. [15] rotated their glass sample with a range of angular velocities from 8 Hz to 17 Hz with the laser beam passing through the dielectric sample up to 2cm off the axis of rotation, such that the maximum centripetal acceleration was ~ 5 $\mathrm{m.s^{-2}}$. Even if the dielectrics used in these experiments had sufficiently large acceleration for the acceleration induced phase shift to be experimentally significant, it would be almost impossible to resolve as it would manifest itself as a small correction to the dominant velocity induced phase shift. From these reflections one is led to conclude that these highly accurate, non-reciprocal light drag experiments were not sensitive to acceleration induced light drag. While they all provided excellent optical tests of the effect of light drag in media with constant velocity, which is accurately explained in terms of Maxwell's original formulation of electrodynamics, these experiments

have not provided an optical test of the covariant formulation of Maxwell's equations.

There have, however, been several optical tests for light propagating in a gravitational field which cannot be explained in terms of the original formulation of Maxwell's equations. Dyson, Eddington and Davidson [36] first observed the bending of light as it passed near the sun in the solar eclipse of May 29, 1919. This experiment, with an accuracy of $\sim$ 10% (although a modern estimate is $\sim$ 50 %), provided early verification of one of the novel predictions of the general theory of relativity, and was a milestone in the acceptance of general relativity within the scientific community. Using radio waves emitted from a quasar as it was eclipsed by the sun, Fomalont and Sramek [46] were able to improve the accuracy of light bending experiments to $\sim$ 1%. A closely related experiment is the measurement of the time interval required for a light signal emitted from Earth to propagate to a known target and return. Reasenberg et al. [120], by tracking a spacecraft which was emitting an electromagnetic signal, were able to confirm the predictions of Schwarzschild geometry to 0.2%. However, all of these experiments were performed with light propagating in vacuum. While they provide excellent verification of the covariant formulation of Maxwell's vacuum equations in Schwarzschild geometry, they do not provide any information on the propagation of light through non-inertial media.

Similarly, Pound and Rebka's [119] experimental verification, using Mössbauer spectroscopy, of the frequency shift induced by the Earth's gravitational field, and the closely related experiment of Hay et al. [58], using a Mössbauer source and receiver mounted upon a rotating disk, do not provide tests of the the effect of matter on optics in a gravitational context. Even if these experiments were not performed in vacuum the observed frequency shifts would be independent of whether material medium or vacuum separated the Mössbauer source and detector as gravitational redshift observations may be explained purely in terms of time dilation effects between separated clocks.

Experimental support for the covariant formulation of Maxwell's equations in non-inertial media has been provided by the observation of the Sagnac effect [125]. Using a covariant formulation of Maxwell's equations, Post [118] demonstrated that the fringe shift observed in a rotating optical interferometer is dependent on whether the light source and the medium through which the light propagates are stationary in the laboratory or rotating with the interferometer. The development of high precision, rotation sensitive ring lasers [26]

has provided further support for the theory of non-inertial optics in material media. Nevertheless, to date the Sagnac effect has only been verified to first order in the rotation rate, Ω. An observer at rest in a rotating frame has a centripetal acceleration which is second order in Ω. Therefore, even the numerous [5] high precision rotation experiments to date have not provided a test of the propagation of light through material media at the order at which centripetal acceleration effects can be expected to be observed.

It is therefore of fundamental interest to consider if it is possible to design an experiment which is *intrinsically sensitive to the effect of acceleration induced light drag by accelerating media.* In this chapter we answer this question by providing three, closely related, experimental proposals which are sensitive to light drag in an accelerating dielectric. Crucial to the following analysis and any feasible experiment is that our acceleration induced effects are not swamped by dominant velocity induced effects.

In section 6.2 we sketch the standard formulation of Maxwell's equations in a spacetime with arbitrary metric. We highlight the physical basis for the definition of the standard constitutive relations, which relate the components of the suitably defined electric displacement $\boldsymbol{D}$ and magnetic intensity $\boldsymbol{H}$ to the components of the electric field $\boldsymbol{E}$ and magnetic field $\boldsymbol{B}$. Having established a covariant formulation of Maxwell's equations with suitable constitutive relations, we then apply these to the problem of an electromagnetic wave propagating through an accelerating dielectric. We perform this analysis from an accelerating frame, S, using French's coordinates, introduced in section 3.3. From the result of chapter 3 we can relate this accelerating coordinate system to a local frame of reference stationary in Schwarzschild geometry. We are therefore able to treat the analogous problems of light propagation in an accelerating frame and light propagating in Schwarzschild geometry within one unified framework.

We derive the wave equation for light propagating in S in section 6.3. In the section immediately following we solve the wave equation when an accelerating dielectric is stationary in S. We then consider the example of a monochromatic light source, stationary in an inertial frame I, being incident upon this accelerating dielectric. Upon propagating through the dielectric it is observed that the light suffers a change in frequency proportional to the acceleration of the dielectric, its thickness and the difference of its refractive index from unity, but this frequency shift is independent of the velocity of the dielectric. This effect was first predicted by Tanaka [146]. However, we

go beyond the work of Tanaka and analyse two experiments which would, in principle, be sensitive to the light drag in the accelerating dielectric.

In the first proposal we examine the Fourier spectra which would result from an experiment in which light from a highly stable source is split, one of the two beams transmitted through an oscillating dielectric, and then the beams are recombined with their beat frequency being recorded. Because of the frequency shift induced by the acceleration of the dielectric we would expect to observe sideband structure in the spectra thus obtained, with the spacing between each line proportional to the frequency at which the sample was oscillated. This experiment appears to be on the borderline of current technology. In the second experimental proposal we consider the effect of a linearly accelerating dielectric on the optical response of a resonant cavity. This calculation predicts asymmetry in the temporal response profile arising from Fresnel drag in the accelerating glass sample. Experimental verification of this effect would appear outside of current technology, as the quality of the optical cavity is significantly decreased by the presence of the dielectric sample.

In the final section of this chapter we examine an experiment analogous to that above. In this instance we allow our glass sample to freely fall within a resonant cavity stationary on the surface of the Earth. Again we find the frequency of light incident upon this glass sample is shifted because of the acceleration of the sample relative to the source, now stationary with respect to the Earth's surface. As in the previous example, this frequency shift results in an asymmetric response profile for the resonant cavity. However, the physical interpretation of the propagation of light through the moving media differs in principle from the previous experimental proposal. This difference in interpretation arises from the fact that the frame of the media is an accelerating frame in the first proposal, whereas the dielectric itself defines a locally inertial frame of reference when falling in a gravitational field, the situation discussed in the second proposal.

6.2 Covariant formulation of Maxwell's equations

In an inertial frame of reference we define the antisymmetric covariant Faraday tensor [33, Eq. 18.24]

$$F_{\mu\nu} = \partial_\mu A_\nu - \partial_\nu A_\mu \equiv A_{\mu,\nu} - A_{\nu,\mu} \ , \tag{6.1}$$

where A^μ are the components of the electromagnetic 4-vector potential and $A_\mu = g_{\mu\nu}A^\nu$. In terms of the components of the electric field $\boldsymbol{E}$ and magnetic field $\boldsymbol{B}$ we have,

$$F_{\mu\nu} = \begin{pmatrix} 0 & -E_x & -E_y & -E_z \\ E_x & 0 & cB_z & -cB_y \\ E_y & -cB_z & 0 & cB_x \\ E_z & cB_y & -cB_x & 0 \end{pmatrix} . \tag{6.2}$$

Maxwell's equations in an inertial frame of reference are

$$F_{\mu\nu,\rho} + F_{\nu\rho,\mu} + F_{\rho\mu,\nu} = 0 \ , \tag{6.3}$$

$$F^{\mu\nu}{}_{,\nu} = -\mu_0 J^\mu \ , \tag{6.4}$$

where μ_0 is the vacuum permeability, J^μ is the 4-vector current density and $F^{\mu\nu} \equiv \eta^{\alpha\mu}\eta^{\beta\nu}F_{\alpha\beta}$ is the contravariant Faraday tensor.

These field equations maintain their form under a Lorentz boost. To obtain Maxwell's equations under an arbitrary coordinate transformation we apply the prescription given by Misner et al. [101] and replace all partial derivatives in Eqs. (6.1) to (6.4) with covariant derivatives, and we also let $\eta_{\mu\nu} \rightarrow g_{\mu\nu}$, the metric tensor of an arbitrary spacetime. In the form of an exercise with the solution given, Schleich and Scully [130] have shown that this prescription leads to the covariant form of Maxwell's equations being written

$$F_{\mu\nu} = A_{\mu,\nu} - A_{\nu,\mu} \ , \tag{6.5}$$

$$F_{\mu\nu,\rho} + F_{\nu\rho,\mu} + F_{\rho\mu,\nu} = 0 \ , \tag{6.6}$$

$$\tfrac{1}{\sqrt{-g}}\left(\sqrt{-g}F^{\mu\nu}\right)_{,\nu} = -\mu_0 J^\mu \ , \tag{6.7}$$

where $g \equiv \det g_{\mu\nu}$ and only the contravariant field equation has been affected by the change to arbitrary coordinates.

When there are no free charges but material media is present the current densities described by J^μ arise from electric and magnetic displacement currents within the media. For this situation it proves convenient to incorporate the components of J^μ into the LHS of Eq. (6.7) by defining the contravariant electromagnetic tensor density [4] $G^{\mu\nu}$, such that Eq. (6.7) is simplified to become

$$G^{\mu\nu}{}_{,\nu} = 0 \ , \tag{6.8}$$

and the components of $G^{\mu\nu}$ are

$$G^{\mu\nu} = \begin{pmatrix} 0 & cD_x & cD_y & cD_z \\ -cD_z & 0 & H_z & -H_y \\ -cD_y & -H_z & 0 & H_x \\ -cD_z & H_y & -H_x & 0 \end{pmatrix} . \tag{6.9}$$

Eqs. (6.6) and (6.8) may therefore be written in the familiar vector form as

$$\nabla \times \boldsymbol{E} = -\frac{\partial \boldsymbol{B}}{\partial t} , \tag{6.10}$$

$$\nabla \cdot \boldsymbol{B} = 0 , \tag{6.11}$$

$$\nabla \times \boldsymbol{H} = \frac{\partial \boldsymbol{D}}{\partial t} , \tag{6.12}$$

$$\nabla \cdot \boldsymbol{D} = 0 . \tag{6.13}$$

These equations, valid in an arbitrary spacetime geometry, have an identical form to Maxwell's equations in an inertial frame of reference, but this similarity is misleading. This is because the vectors $\boldsymbol{E}$ and $\boldsymbol{D}$, and $\boldsymbol{B}$ and $\boldsymbol{H}$, are no longer directly proportional to each other, as is the case for a linear dielectric in an inertial frame, but are dependent on both the dispersive properties of the medium *and the spacetime metric.*

Up until this point the generalisation of Maxwell's equations into an arbitrary frame of reference has followed a straightforward mathematical prescription. However, when we relate the components of the generalised electric displacement $\boldsymbol{D}$ and magnetic intensity $\boldsymbol{H}$ to the components of the electric field $\boldsymbol{E}$ and magnetic field $\boldsymbol{B}$ we must choose a particular prescription, motivated by physical considerations. As Eqs. (6.10) to (6.13) are valid in any frame of reference it is clear that in an inertial frame I with stationary, linear and homogeneous media

$$\boldsymbol{D} = \epsilon\epsilon_0 \boldsymbol{E} , \tag{6.14}$$

$$\boldsymbol{B} = \mu\mu_0 \boldsymbol{H} , \tag{6.15}$$

such that Maxwell's equations take their familiar form in I, where ϵ_0 and μ_0 are respectively the permittivity and permeability of the vacuum and ϵ and μ are the dielectric and magnetic constants of the medium.

In generalising this result to include media with arbitrary acceleration, Heer [59] imposed the physical assumption that the above constitutive relations hold in the inertial frame of reference instantaneously comoving with the accelerating media. This assumption is tantamount to assuming that the optical properties of accelerating media are unaffected by its acceleration. While

this would clearly be only approximate in conditions of extreme acceleration, we accept this prescription throughout this thesis. Following Heer, but adopting the notation of Tanaka [145], we obtain the constitutive relations in an accelerating frame in which the material media is stationary by making use of the transformation properties of $F_{\mu\nu}$ and $G^{\mu\nu}$. Under arbitrary coordinate transformations $x^\mu \rightarrow x^\mu(x^{\nu'})$ the Faraday tensor and tensor density transform according to

$$F_{\mu'\nu'} = \frac{\partial x^\alpha}{\partial x^{\mu'}} \frac{\partial x^\beta}{\partial x^{\nu'}} F_{\alpha\beta} \ ,$$

$$\left| \det \left(\frac{\partial x^\beta}{\partial x^{\nu'}} \right) \right| G^{\mu'\nu'} = \frac{\partial x^{\mu'}}{\partial x^\alpha} \frac{\partial x^{\nu'}}{\partial x^\beta} G^{\alpha\beta} \ .$$

The determinant in the transformation formula for $G^{\mu'\nu'}$ arises because this transforms as a tensor density [103, Eq. 9.70] rather than a tensor. If our unprimed coordinate system is inertial then it has the metric $\eta_{\alpha\beta}$ such that $\sqrt{-\det(\eta_{\alpha\beta})} \equiv \sqrt{-\eta} = 1$. Therefore, from the transformation properties of the second rank tensor $g_{\mu\nu}$, if we transform from an inertial coordinate system I to an accelerating coordinate system S then $\left|\det\left(\partial X^\beta/\partial x^\nu\right)\right| = \sqrt{-\det(g_{\mu\nu})} = \sqrt{-g}$ [103, Eq. 9.46]. By transforming $F_{\mu\nu}$ and $G^{\mu\nu}$ from the an inertial frame instantaneously comoving with the accelerating dielectric, into the accelerating frame of the dielectric, we obtain the constitutive relations [145]

$$G_{0k} = \sqrt{\frac{-g\,\epsilon_0}{\mu_0}}\, \epsilon\, F_{0k} \ , \tag{6.16}$$

$$\mu\, G^{kl} = \sqrt{\frac{-g\,\epsilon_0}{\mu_0}}\, F^{kl} \ , \tag{6.17}$$

where the indices k, l run from 1 to 3, $F^{\mu\nu} = g^{\mu\alpha} g^{\nu\beta} F_{\alpha\beta}$ and $G_{\mu\nu} = g_{\mu\alpha} g_{\nu\beta} G^{\alpha\beta}$. In vacuum $\epsilon = \mu = 1$ such that

$$G_{\mu\nu} = \sqrt{\frac{-g\,\epsilon_0}{\mu_0}}\, F_{\mu\nu} \ ,$$

and Eq. (6.7) in the vacuum limit is recovered from Eq. (6.8)

Several authors have studied the propagation of electromagnetic waves in a linearly accelerating medium using the above formulation of Maxwell's equations. Anderson and Ryon [4, 123] and Mo [102] both derived a wave equation for the propagation of light through a dispersionless dielectric with constant acceleration, and obtained an approximate solutions to this wave equation. Tanaka [145] was the first to find an analytic solution for the propagation of electromagnetic waves through a dielectric stationary within an accelerating

frame using Fermi coordinates. In this work Tanaka demonstrated that the relativistic energy and phase velocity addition laws for an arbitrary wave propagating within accelerating media are equivalent to the well known Einstein velocity addition laws for media moving at the instantaneous velocity of the accelerating media. Similarly, for normal incident light, Tanaka proved that the amplitude and frequency for an electromagnetic wave reflected from an accelerating dielectric surface is given by the standard Döppler relations for reflection from an identical dielectric boundary moving inertially at the instantaneous velocity of the accelerating surface. In a later publication, Tanaka [146] showed that light propagating through an accelerating dielectric is shifted in frequency by an amount proportional to the acceleration of the glass sample, its thickness and the difference of its refractive index from unity. Significantly this frequency shift is independent of the velocity of the dielectric.

6.3 Wave equation in a linearly accelerating frame

In this section we derive the wave equation for light propagating through media stationary in an accelerating frame of reference. Our first task is to choose an accelerating coordinate system convenient for our purposes. In section 3.3 we presented the line elements for two linearly accelerating coordinate systems, Fermi coordinates and French's coordinates. Because of the analogy between the French coordinate system and Schwarzschild geometry, it is convenient to analyse all the experimental proposals using the French coordinate system for an accelerating frame. This choice of coordinate system enables the problem of light propagating in an accelerating frame of reference and in Schwarzschild geometry to be approached within the same framework.

The line element for a linearly accelerating frame of reference S in French's coordinates is

$$ds^2 = -\left(\kappa + \frac{2\,a\,z}{c^2}\right) c^2\,dt^2 + dx^2 + dy^2 + \left(\kappa + \frac{2\,a\,z}{c^2}\right)^{-1} dz^2 \ . \qquad (6.18)$$

The close analogy of this line element with the Schwarzschild line element was discussed in detail in chapter 3. We note $\det(g_{\mu\nu}) = -1$ and, as the metric is diagonal, $g^{\mu\nu} = 1/g_{\mu\nu}$. A coordinate transformation from an inertial frame I to our accelerating frame S is defined by

$$\begin{aligned} T &= \frac{c}{a}\sqrt{\kappa + \frac{2\,a\,z}{c^2}}\,\sinh\left(\frac{a\,t}{c}\right) \ , \\ X &= x \ , \end{aligned}$$

$$\begin{aligned} Y &= y \ , \\ Z &= \frac{c^2}{a}\sqrt{\kappa + \frac{2\,a\,z}{c^2}}\,\cosh\left(\frac{a\,t}{c}\right) - \frac{c^2}{a}\sqrt{\kappa} \ . \end{aligned} \tag{6.19}$$

In section 6.4 we assume our interferometer is stationary in I and S is the frame of the accelerating glass sample. In the final section of this chapter we reverse these roles and assume that our interferometer is stationary on the surface of the Earth and the glass sample freely falls within this spacetime. We can model the spacetime of Schwarzschild geometry with sufficient accuracy using our accelerating frame S, and the freely falling sample defines a locally inertial frame I.

For simplicity we assume, in both cases, our wave is propagating parallel to the acceleration of the dielectric such that $\boldsymbol{k}$ is parallel to the z axis. It follows immediately that $E_z = 0$ and we orientate our x and y axes so that the electric field is polarised in the x direction. If our dielectric sample is stationary in S then the covariant constitutive relations, Eqs. (6.16) and (6.17), and the a metric components of Eq. (6.18), enable us to find the non-zero components of the vectors $\boldsymbol{D}$ and $\boldsymbol{H}$:

$$D_x = \epsilon^* \epsilon_0 \ E_x \left(\kappa + \frac{2\,a\,z}{c^2}\right)^{-1} \ ,$$

$$H_y = \frac{1}{\mu * \mu_0} B_y \left(\kappa + \frac{2\,a\,z}{c^2}\right) \ .$$

By taking the curl of Eq. (6.10) and using Eqs. (6.10) to (6.13) and the expressions above to substitute E_x in favour of D_x, H_y, B_y, we obtain the wave equation for an x-polarised light wave propagating parallel to the acceleration of the dielectric. In French's coordinates the wave equation is

$$\left(\kappa + \frac{2\,a\,z}{c^2}\right)^2 \frac{\partial^2 E_x}{\partial z^2} + \frac{2\,a}{c^2}\left(\kappa + \frac{2\,a\,z}{c^2}\right)\frac{\partial E_x}{\partial z} - \frac{n^2}{c^2}\frac{\partial^2 E_x}{\partial t^2} = 0 \ , \tag{6.20}$$

where we have used $\epsilon_0\,\mu_0 = 1/c^2$ and $\epsilon\mu = n^2$ where n is the refractive index of the medium. It is interesting to note that this wave equation has a very similar form to that derived by Tanaka [145] for the propagation of waves in an accelerating dielectric stationary in a Fermi coordinate system. However, as we have chosen to use the French coordinate system, the coefficients of the partial derivatives with respect to z are powers of g_{00} of the French metric, whereas Tanaka obtained similar coefficients but with powers of $\sqrt{g_{00}}$ of the Fermi metric. Furthermore, and closely related, the wave equation derived by Tanaka does not have the factor of 2 in the second term.

6.4 Accelerating dielectric within a stationary cavity

Consider an experiment in which a dielectric is accelerated within an evacuated optical cavity, illustrated in figure 6.1. Our glass sample is assumed to be stationary in the accelerating frame, S, has parallel faces and is of proper thickness h. We align this sample with its surface normal parallel to the z axis. From Eq. (6.18) if one boundary of our sample is at $z = 0$ then the second boundary is at $z = h\sqrt{\kappa}$. Because κ is a parameter which specifies the location of the coordinate time in S, we are free to choose any convenient value for κ. It is advantageous to let coordinate time be kept by a clock located at the first boundary of the dielectric. This choice leads to $\kappa = 1$. From Eq. (6.19) with $\kappa = 1$ we observe the spatial coordinates of S are equal to those of I in a small region about the origin when $t = 0$. Furthermore, upon a Lorentz boost into an inertial frame I' instantaneously comoving with S, Eq. (6.19) gives that these spatial coordinates are also equal in a small region about the origin. This provides the physical interpretation of the coordinate system of French.

In the laboratory frame, I, in which the resonant cavity is stationary, an X polarised arbitrary electromagnetic signal which propagates along the Z axis is injected into the cavity. This radiation is incident upon the accelerating dielectric and is described by

$$E_X = f\left(\Phi_{vac}\right) \quad ,$$

$$B_Y = \frac{1}{c} f\left(\Phi_{vac}\right) \quad ,$$

where

$$\Phi_{vac} = -\omega_0 T + k Z \quad ,$$

$\omega_0 = ck$ as the light is propagating in vacuum and $f(\Phi_a)$ is an arbitrary complex wave function which satisfies Maxwell's vacuum wave equation in I. Using the covariant transformation properties of the Faraday tensor, $F_{\mu\nu}$, we can express this electromagnetic wave in the lowercase coordinates of S,

$$E_x = \sqrt{1 + \frac{2\,a\,z}{c^2}}\, \exp\left(-\frac{a\,t}{c}\right)\, f(\phi_{vac}) \quad , \tag{6.21}$$

where

$$\phi_{vac} = \frac{\omega_0\, c}{a}\left\{\sqrt{1 + \frac{2\,a\,z}{c^2}}\exp\left(-\frac{a\,t}{c}\right) - 1\right\} \quad , \tag{6.22}$$

and we have modified the convention that lowercase coordinates represent those measured in S to include the lowercase ϕ_a to represent the phase of

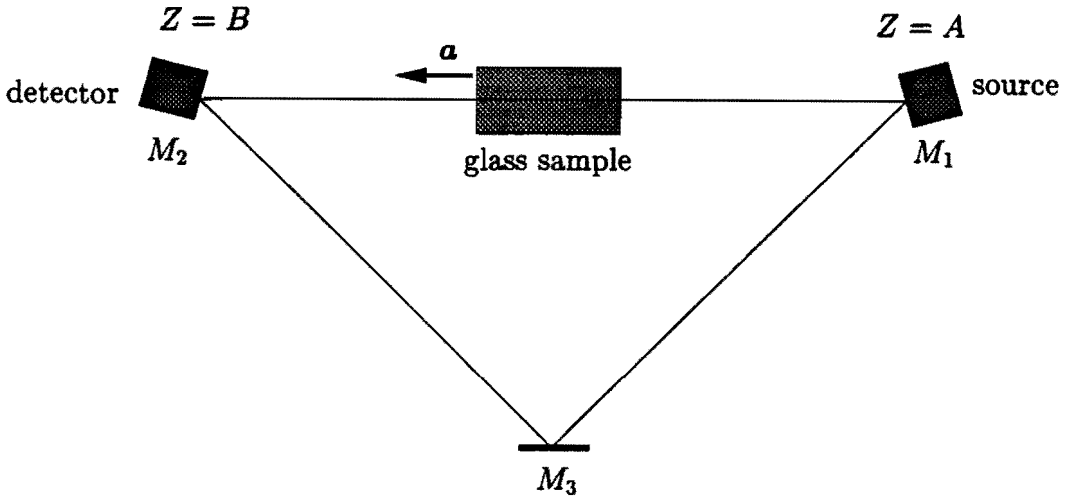

Figure 6.1: Resonant cavity containing an accelerating dielectric.

the arbitrary wave-function as measured in S. This electromagnetic wave is propagating in vacuum and, as such, will satisfy the vacuum wave equation in S, Eq. (6.20), in the limit $n \to 1$. When $n \neq 1$ the wave equation can be solved by noting that n appears only as a factor scaling the partial derivative of E_x with respect to t. Therefore, if we replace t by t/n in Eqs. (6.21) and (6.22) our solution will now satisfy the wave equation in S, derived assuming the dielectric is stationary in S. Thus we find

$$E_x = \sqrt{1 + \frac{2\,a\,z}{c^2}}\, \exp\left(-\frac{a\,t}{n\,c}\right)\, f(\phi_d)\ , \tag{6.23}$$

satisfies the wave equation Eq. (6.20), where ϕ_d is the phase within the dielectric and is given by

$$\phi_d = \frac{\omega_0\, c}{a}\left\{\sqrt{1 + \frac{2\,a\,z}{c^2}}\, \exp\left(-\frac{a\,t}{n\,c}\right) - 1\right\}\ . \tag{6.24}$$

At the boundaries of the dielectric we must match the amplitude and phase of the incoming and outgoing waves. We assume that the dielectric sample has been coated with multi-layered thin films to enhance its transmission of the incident light. For simplicity we neglect the phase contribution of the thin film in the remaining analysis. This simplification assumes the only effect of the boundary is to decrease the amplitude of the electric field by a factor of r, where $r < 1$. We also ignore internal reflections within the dielectric in this analysis. One could, for example, tilt the dielectric to the Brewster angle [110] to remove experimental complications arising from multiple reflections. This is

similar to the method used by Sanders and Ezekiel [128] to avoid experimental complications induced by multiple reflections within their dielectric samples. This tilting of the dielectric sample would, of course, further complicate the theoretical analysis. We assume the simplest possible case in this analysis in order to avoid the central result being obscured by detail. For the analysis of a specific experiment one would, of course, be required to include all complications arising from the surface coatings of the dielectric and internal reflections.

The phase of the incident light at the boundary of the dielectric is given by Eq. (6.22) with $z = 0$. We also note, at $z = 0$,

$$\phi_{vac} = \left(\frac{\omega_0 c}{a}\right)^{1-n} \left(\phi_d + \frac{\omega_0 c}{a}\right)^n - \frac{\omega_0 c}{a} \quad . \tag{6.25}$$

If $z \neq 0$ but $0 \leq z \leq h$ then the RHS of Eq. (6.25) gives the phase of the light within the dielectric in S. Similarly, if we raise the amplitude modulation term in Eq. (6.23) by a power of n we can match this to the amplitude modulation in Eq. (6.21) at the boundary of the dielectric.

We now assume the input signal in I is harmonic and monochromatic, with frequency ω_0 and complex amplitude $E_0 \exp i\psi$, such that

$$E_x^{in} = E_0 \exp i\left\{\omega_0 (T - z/c) + \psi\right\} \quad .$$

At the boundary of the dielectric we match the phase of the incident and transmitted light, and reduce the electric field amplitude by a factor of r, for all values of t. These boundary conditions give the value of the electric field within the dielectric sample as

$$\begin{aligned} E_x^d &= r E_0 \left(1 + \frac{2 a z}{c^2}\right)^{n/2} \exp\left(-\frac{a t}{c}\right) \\ &\quad \times \exp i \left\{\frac{\omega_0 c}{a}\left(1 + \frac{2 a z}{c^2}\right)^{n/2} \exp\left(-\frac{a t}{c}\right) - \frac{\omega_o c}{a} + \psi\right\} \quad . \end{aligned} \tag{6.26}$$

That this solution satisfies the wave equation, Eq. (6.20), follows immediately from the fact that it has the same form as the general solution, Eq. (6.23). If we chose $f(\Phi_{vac}) = \exp i\Phi_{vac}$ and take the nth power of the RHS of Eq. (6.23) we recover Eq. (6.26) to within a complex amplitude.

At $z = h$ this signal emerges from the dielectric. Again we match the phase and amplitude at the boundary, with the electric field amplitude decreasing by a factor of r. Repeat of the matching procedure above at the second dielec-

tric/vacuum interface leads to

$$E_x^{out} = r^2 E_0 \left(1+\frac{2ah}{c^2}\right)^{(n-1)/2} \sqrt{1+\frac{2az}{c^2}} \exp\left(\frac{at}{c}\right) \times \exp i\left\{\frac{\omega_0 c}{a}\left(1+\frac{2ah}{c^2}\right)^{(n-1)/2} \sqrt{1+\frac{2az}{c^2}} \exp i\left(-\frac{at}{c}\right) - \frac{\omega_0 c}{a} + \psi\right\}$$

which, when transformed back into I, gives

$$E_x^{out}(T,X) = E_0 s^2 \left(1+\frac{2ah}{c^2}\right)^{(n-1)/2} \exp i\left\{-\omega_1 (T - Z/c) + \psi + \Delta\psi\right\} \quad , \tag{6.27}$$

where the frequency of the emerging beam is

$$\omega_1 = \omega_0 \left(1+\frac{2ah}{c^2}\right)^{(n-1)/2} \quad , \tag{6.28}$$

and the phase has changed by

$$\Delta\psi = \frac{c}{a}(\omega_1 - \omega_0) \quad . \tag{6.29}$$

Equation (6.28) predicts that light which has propagated through the accelerating dielectric has suffered a shift in frequency by an amount dependent on the acceleration but independent of the velocity of the dielectric. This frequency shift was first predicted by Tanaka [146], who derived this result assuming the glass sample was stationary in a Fermi coordinate system. Our result agrees with that of Tanaka at first order, which is the order to which the Fermi and French coordinates have the same physical interpretation. This shift in frequency can be understood by considering the transit of a single photon through the dielectric. Suppose when measured at the first boundary in S this photon has a frequency ω_S (assuming, of course, that within this classical system the act of measurement does not destroy or affect the photon). When it propagates to the second boundary it will have suffered a gravitational redshift in S, but this gravitational redshift is independent of whether the photon has propagated through a medium or vacuum. Therefore, in S, the frequency of our hypothetical photon at the second boundary is independent of the presence of the dielectric sample. However, the presence of the dielectric does cause an extra delay of $h(n-1)/c$ in the photon's transit from the first to the second boundary. In I this extra delay enables the second boundary to accelerate to a velocity ahn/c relative to the first boundary, rather than

the velocity difference being $a\,h/c$ as is the case when our photon propagates through vacuum. This extra velocity of the second boundary relative to the first results in the frequency shift given by $\omega_0\,a\,h\,(n-1)/c$, which is the first order expansion of Eq. (6.28).

It is interesting to note that the covariant form of Maxwell's equations predict the electric field amplitude is increased by a factor of $(1+2\,a\,h/c^2)^{(n-1)/2}$ upon propagating through our glass sample. However, this increase is several orders of magnitude less than the losses in amplitude at the dielectric surfaces. We therefore neglect this contribution to the electric field amplitude in the remainder of this analysis, as this would be impossible to resolve experimentally with current technology.

6.4.1 Passive interferometer containing an oscillating glass sample

First consider a passive interferometer for which the change in phase of the light for a single pass of the dielectric is measured. This interferometer is illustrated in Figure 6.1, where the detector records the relative phase of the opposite beams. Expanding Eq. (6.28) in a Taylor series and keeping only first order in $a\,h/c^2$ we obtain the extra phase shift due to the presence of an accelerating glass sample measured by a detector located at $Z = B > h$ at time T as

$$\Delta\Phi = \frac{\omega_0}{c}\,h\,(n-1)\left\{1-\frac{a\,T}{c}+\frac{a\,B}{c^2}\right\}\ . \tag{6.30}$$

The first term is precisely the change in phase due to the presence of a stationary dielectric. By noting $aT = v$ is the instantaneous velocity of dielectric sample, the second term can be interpreted as the phase shift induced by Laub drag in the medium due to its instantaneous velocity. The final term is new and arises from the frequency shift suffered by the light which has passed through the dielectric. Despite the existence of a new term in the above phase, we could not expect to experimentally resolve this effect as it is swamped by the much larger Laub drag term.

Suppose that instead of recording a phase shift, our detector records the beat frequency induced by the acceleration of the dielectric between the opposite beams of this interferometer. In an experiment one would oscillate the dielectric sample along one arm of the passive optical interferometer and use a high precision laser as a frequency source. Because the frequency shift induced in the light from its propagation through the glass sample is proportional to the sample's acceleration, then oscillating the dielectric will cause frequency

modulation of one beam. Upon recombining the two beams we will observe a time dependent beat frequency at the detector. Fourier transformation of this signal will unveil sideband structure in the resulting frequency spectrum. Side band analysis in a precision ring laser has been discussed in detail by Stedman et al. [139]. If our sample is oscillated at an angular frequency Ω we find the photo-multiplier tube would record a signal

$$\begin{aligned} V(t) &= \mathcal{R}\{V_c \exp i[\gamma \sin(\beta t)]\} \quad , \\ &= \mathcal{R}\left\{V_c \omega_c t \left[J_0(\gamma) + 2\sum_{n=1}^{\infty}\left(i\, J_{2n-1}(\gamma)\, \sin([2n-1]\beta t)\right.\right.\right. \\ &\qquad \left.\left.\left. + J_{2n}(\gamma)\, \sin(2n\beta t)\right)\right]\right\} \quad . \end{aligned}$$

where

$$\gamma \equiv (\omega_1 - \omega_0)/\Omega$$

and is the ratio of the maximum frequency shift suffered by the light divided by the angular frequency of oscillation. If γ is small then the height of the first and largest sideband relative to the carrier peak is given by [31]

$$\mathrm{R} = \frac{J_1(\gamma)}{J_0(\gamma)} \approx \frac{\gamma}{2} = \omega_0 \frac{h\, A_0\, \Omega}{2\, c^2}(n-1) \quad ,$$

where A_0 is the amplitude of the oscillation of the dielectric. To date the Canterbury ring laser has achieved a noise floor 60 dB below the carrier. Therefore if $R > 10^{-3}$ the first sideband should be resolvable. With $A_0 = h \sim 10$ cm and $n \sim 2$ we require $\Omega > 6.2$ Hz. This corresponds to a minimum acceleration of ~ 4 m.s^{-2}, which is easily attained within the laboratory. From Eq. (6.28), with the wavelength of the incident beam 633 nm, we find a shift in frequency of 2 mHz would result from one pass of the dielectric sample. The Canterbury ring laser has achieved a frequency resolution of 0.16μHz. If we were to use the output of the Canterbury ring laser as a stable light source then a frequency shift of 2 mHz should be, in principle, experimentally resolvable. If this frequency shift were less than the resolution of the frequency source then any structure in the predicted spectra would be unresolvable, as sidebands would be broadened and reduced in amplitude to the point where they are indistinguishable from noise.

An important feature of this experimental proposal is that the central phenomenon under investigation, a shift in frequency induced by the acceleration of the glass sample, is independent of the velocity of the glass sample. Therefore the effect we wish to investigate is not obscured by a dominant contribution from the velocity of the glass sample, but manifests itself as the central

experimental feature. However, in an experiment care would have to be taken to isolate the frequency source and the detector from optical feedback due to light scattered off the accelerating dielectric, and mechanical feedback from the vibration of the sample. Both of these effects would result in spurious structure in the Fourier resolved spectra, also with a line spacing of Ω. Optical feedback would cause spurious structure because the light reflected off our accelerating dielectric would be Döppler shifted by the velocity of the glass sample, which is also varying sinusoidally. If this reflected light were to reach the photo-multiplier tube then this would superpose its own structure on the final spectra. Tilting the glass sample relative to the incident beam will prevent the reflected beam feeding back into the optical interferometer, but light scattered off the glass surface will be a significant experimental obstacle. Another important and possibly fatal experimental limitation of this proposal is the influence of amplitude modulation on the resolved spectra. Because of dispersion (neglected in this analysis) and the presence of anti-reflection coatings on our glass sample, the transmission properties of the dielectric will be velocity dependent. As such a time dependent transmission amplitude will result with its Fourier transform also showing sideband structure which could mask the central experimental feature of interest. Nevertheless, the apparent accessibility of this experiment within current technology clearly warrants further investigation.

6.4.2 Resonant cavity containing a linearly accelerating glass sample

We now turn our attention to another, closely related, experimental proposal. We are motivated by previous investigations of optical systems when the optical path length is time dependent. Optical systems in which the frequency of an external laser and the resonant frequency of an optical device cross over in time display the phenomenon of optical ringing. Ioannidis et al. [64, 65] observed ringing in an optical fibre ring resonator, a variable optical path length being obtained through wrapping a length of optical fibre around a piezoelectric cylinder. Upon exciting a high finesse ring cavity with a frequency modulated external laser, Li et al. [79] were able to determine the finesse of this cavity through the observed ringing profile. An asymmetric response profile was also observed by Li et al. [80] when the scanning rate of a scanning Fabry-Pérot interferometer multiplied by the decay time of the interferometer squared was the order of unity. Neutze [107] has predicted that optical ringing will be

observed when a ring optical interferometer with angular acceleration is excited by an external monochromatic signal.

In our previous discussion of a passive optical interferometer we placed an accelerating dielectric along one arm of the interferometer. If instead of measuring a phase or frequency shift we allowed the counter clockwise beam to continuously propagate around the optical interferometer then our interferometer will behave as a resonant cavity. As the velocity of this sample changes the effect of Laub drag within the sample will alter the optical path length of the cavity. Therefore the optical path length of the optical cavity will be time dependent, suggesting that optical ringing will occur as the resonance of the cavity moves through the frequency of the external light source.

Suppose our interferometer consists of three mirrors which form a closed optical path, as illustrated in figure 6.1. At $Z = A$ we locate our radiation source which injects the monochromatic signal through the first mirror, M_1. At $Z = B > h$ we locate our second mirror, M_2, and our detector now records the intensity of light which is transmitted through M_2. The third mirror, M_3, merely closes the optical path of the light and it is located anywhere convenient, causing the total optical path length of the evacuated interferometer to be its perimeter P in the absence of the glass sample. Because our interferometer is planar we may assume its resonant modes are linearly polarised [14]. Along the interferometer arm which contains the accelerating dielectric sample we align the x axis parallel to the electric field polarisation.

At the detector the electric field will consist of an infinite sum of partial contributions, $E_l(T, B)$, which have traversed the ring perimeter l times and have therefore passed through the accelerating glass sample $l+1$ times. Upon each pass through the dielectric the electric field suffers a drop in amplitude of r^2. Each transit of the ring perimeter also causes the amplitude to decrease by a factor of s^3 due to three reflections from the mirrors of the interferometer. Finally, transmission through M_1 and M_2 cause a further decrease in amplitude of a factor of $(1 - s^2)$. Therefore

$$\begin{aligned} E_l(T,B) &= E_0\,(1-s^2)\,r^2\,\left(s^3r^2\right)^l \exp i\left\{\omega_0\left[-cT+B\right.\right. \\ &\qquad \left.\left.-h\,(n-1)\left(1-\frac{aT}{c}+\frac{aZ}{c^2}\right)\right]+\Phi_l+\psi\right\}\ . \end{aligned} \tag{6.31}$$

where Φ_l is the phase contribution due to the electric field component $E_l(T, B)$ having traversed the ring perimeter l times. This phase is calculated directly from the Taylor series expansion of the phase in Eq. (6.27). If we take a

snapshot at time T and match the phase upon each transit of the interferometer we find

$$\Phi_l = \frac{\omega_0}{c}\left\{l\left(P+h\,(n-1)+\frac{a\,h}{c^2}\,(n-1)\,(-cT+B)\right)\right.$$
$$\left.+l^2\,\frac{a\,h}{c^2}\,(n-1)\,P\right\}\ , \tag{6.32}$$

Thus the electric field at the detector is

$$E_{out}(T,B) = \left(1-s^2\right)\,r^2\;E_0$$
$$\times\exp i\omega_0\left\{-cT+B-h\,(n-1)\left(1-\frac{aT}{c}+\frac{aZ}{c^2}\right)+\psi\right\}$$
$$\times\sum_{l=0}^{\infty}\left(s^3\,r^2\right)^l\exp\left\{i\,\Phi_l\right\}\ . \tag{6.33}$$

The summation within Eq. (6.33) is of the same form as that which arises in the analysis of the optical response of a scanning Fabry-Pérot interferometer [80]. Li et al. derived the temporal variation of the output intensity of a scanning Fabry-Pérot interferometer by utilising its equivalence with the intensity profile of a Fabry-Pérot interferometer with a frequency modulated input signal. In Appendix A we present the calculation which enabled the summation in Eq. (6.33) to be completed. Applying the solution, Eq. (A.6), to the problem at hand, and identifying the variables through the analogy of Eq. (6.30) with Eq. (A.4), we obtain the output intensity of a resonant cavity with angular acceleration. If we assume optical resonance occurs when the dielectric is stationary, such that τ of Eq. (A.4) corresponds to $P/c+h(n-1)/c$, we observe

$$\frac{I_{out}}{I_0}=\frac{|A_{out}|^2}{|A_0|^2}=\left(\frac{1-s^2}{1-s^3\,r^2}\right)^2\,\frac{\pi}{8\eta}\,|w(\zeta)|^2\ , \tag{6.34}$$

where [1]

$$w(\zeta)=\frac{i}{\pi}\int_{-\infty}^{\infty}d\nu\frac{\exp(-\nu^2)}{\zeta-\nu}=\exp(-\zeta^2)\,\mathrm{erfc}(-i\zeta)\qquad(\mathrm{Im}\;\zeta>0)\ ,$$

$\mathrm{erfc}(-i\zeta)$ being the complex error function. The asymmetry parameter $\eta\equiv\beta/\Gamma^2$, where $\beta\equiv-2\,\omega_0\,(n-1)\,a\,h\,P/(c\,[P+h(n-1)]^2)$ and $-\beta$ is almost exactly twice the change in frequency from each traverse of the ring perimeter divided by the duration of each traverse, and $\Gamma=2c\,(1-s^3r^2)/(Ps^3r^3)$ is the power rate of decay of the cavity. The variable $\zeta\equiv\pm\exp(-i\pi/4)\{-i\Gamma+\beta(T-B/c)/(1+[n-1]h/P)\}/\sqrt{8\beta}$, the sign being positive when $\beta(T-Z_0/c)>2\,\Gamma\,(1+[n-1]h/P)$ and was chosen to keep the imaginary part of ζ positive. The

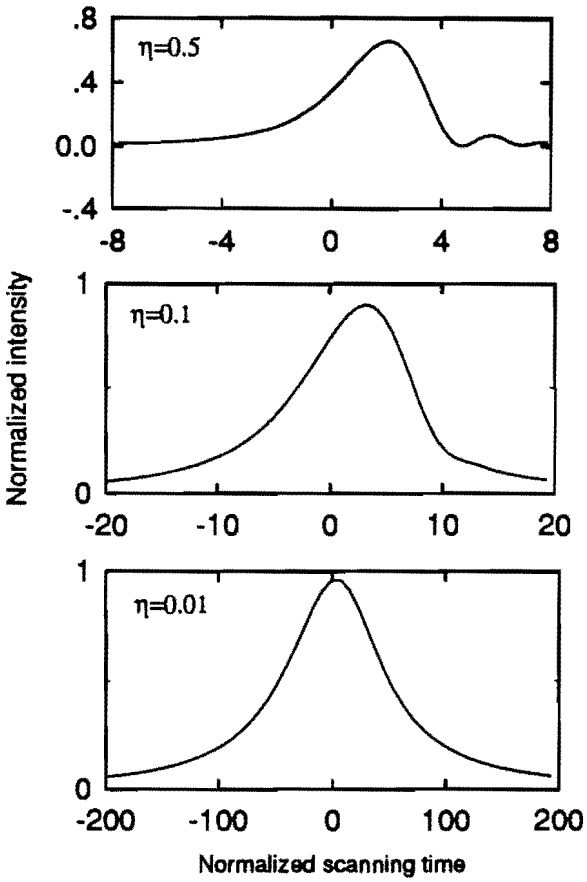

Figure 6.2: Intensity profiles for a resonant cavity containing a linearly accelerating dielectric sample, from numerical evaluation of Eq. (6.34) at various values of the asymmetry parameter η: (a) $\eta = 0.5$, (b) $\eta = 0.1$ and (c) $\eta = 0.01$. The normalised time is related to real time by $\tau = \Gamma T$.

factor $(1 - s^2)^2/(1 - s^3r^2)^2 \approx [2(1 - s)/\{3(1 - s) + 2(1 - r)\}]^2$ in Eq. (7.13) expresses the fact that this cavity has transmission losses from 3 mirrors and two surfaces of the dielectric, whereas a Fabry-Pérot interferometer [80] suffers losses from only two mirrors.

Plots of I_{out}/I_0 versus the normalised time $\tau = \Gamma T/(1 + [n - 1]h/P)$ for $P \gg h$ and $\eta = 0.01$, 0.10 and 0.50 are given in Figure 6.2. With $\eta \sim 0.10$ the asymmetry is easily resolved experimentally. Consider a state of the art

ring cavity with a perimeter of three metres containing commercially available mirrors with $1 - s \sim 10$ ppm. This cavity has $\Gamma \sim 6000$ Hz. Inclusion of a dielectric within the cavity, however, dramatically decreases the ring-down time of the cavity, $\tau_c = 1/\Gamma$. If we assume that the multiple thin layer coatings on the dielectric achieve an optical transmission such that $1 - r \sim 10^{-4}$, which is approximately the current limit of optical technology, then we obtain $\Gamma \sim 46,000$. With a dielectric of 10 cm in length and refractive index $n = 2$ we would require an acceleration of $a \sim 2000$ m.s^{-2} for our asymmetry parameter $\eta \sim 0.1$. Furthermore, for the dielectric to have sufficiently changed its velocity so that the cavity has scanned through the full optical resonance we require $\Gamma \Delta T \sim 40$. Thus, if the dielectric were to be mechanically oscillated, or oscillated by a piezoelectric crystal, the period of oscillation must be greater than 10^{-3} s. While it may be possible to achieve the necessary acceleration by oscillating the dielectric with an amplitude $\sim 50\,\mu$m at 1000 Hz, one would expect insurmountable experimental problems to arise upon attempting to impart such large acceleration to a macroscopic sample.

Nevertheless, the minimum acceleration is proportional to $[3(1-s)+2(1-r)]^2$ and P^{-1}. An improvement of an order of magnitude in the transmission losses of the electromagnetic field at the dielectric boundary, and a similar improvement in the reflection of the mirrors, could result in this proposed experiment falling within the achievable technological sphere, now requiring $a \sim 20$ m.s^{-2}. However, in the above analysis we have neglected amplitude losses within the dielectric itself, which would also lower the quality factor of the cavity. From these considerations it would appear that the above experimental proposal falls outside of current experimental realms.

Despite the experimental problems it should be appreciated that this proposal is sensitive to *light drag induced by the acceleration of the glass sample.* In the above derivation of an asymmetric output spectra for our resonant cavity, our central result again stems from the frequency shift suffered by a photon which has propagated through a linearly accelerating dielectric, Eq. (6.28). Our asymmetry parameter η is proportional to the dielectric's acceleration, thickness and $n - 1$, but is independent of the velocity of the dielectric. Therefore, the effect of primary interest will not be not be swamped by a dominant velocity induced contribution. Furthermore, unlike the previous proposal where amplitude modulation effects arising from dispersion in the sample (neglected in this analysis) and the presence of anti-reflection coatings masked the experimental feature of interest, this proposal is not affected by the velocity dependence of

the transmission properties of the sample. This is because we are searching experimentally for a distortion of the response profile when the sample has high acceleration relative to the low acceleration case. Any distortion of the output spectra due to a velocity dependence of the transmission properties of the sample will appear in the low acceleration limit and can be subtracted out from the spectra obtained when the sample has high acceleration.

Having established the optical output of a resonant cavity containing an accelerating glass sample is distorted by the acceleration of this sample, it is interesting to relate this result to the discussion of chapter 4 concerned with the hypothesis of locality. Our asymmetry parameter η represents the extent to which the output intensity of our resonant cavity would deviate from an equivalent cavity containing an identical glass sample, but moving inertially with its velocity instantaneously that of the accelerating sample. We found $\eta \equiv \beta/\Gamma^2 \approx -2\omega_0 \tau_c \times \tau_c \, a \, h \, (n-1)/Pc$, where $\tau_c = 1/\Gamma_c$ is the 'ring-down time' or radiation lifetime of the cavity. As discussed in chapter 4, it is the ratio of the intrinsic time scales of the phenomenon under observation with the time scale characteristic of the acceleration, $\mathcal{L}/c$, which determines the magnitude of any violations of the locality hypothesis. In this example the acceleration time scale is $a\,h/c^2$, and the characteristic time of the measurement is τ_c. Thus the asymmetry parameter η is proportional to $c\tau_c/L$, scaled by a phase factor $\omega_0 \tau_c(n-1)$ due to the presence of the accelerating media, specific to the experimental arrangement. This result supports our contention that it is the desired frequency resolution which determines the time scale characteristic of the measurement when considering the magnitude of deviations from the locality hypothesis. This follows from the fact that $1/\tau_c$ provides a fundamental limit to the frequency resolution of the cavity, which is also further limited by other factors such as frequency drift and backscatter.

6.5 Freely falling dielectric within a cavity stationary in Schwarzschild geometry

In the previous section we have demonstrated that a glass sample accelerating within a ring interferometer stationary in an inertial frame I will cause the optical response profile of a resonant cavity to become distorted. For the sake of symmetry it is interesting to consider the opposite case, in which the interferometer is fixed in a gravitational field and the dielectric sample is allowed to freely fall along one arm of the interferometer.

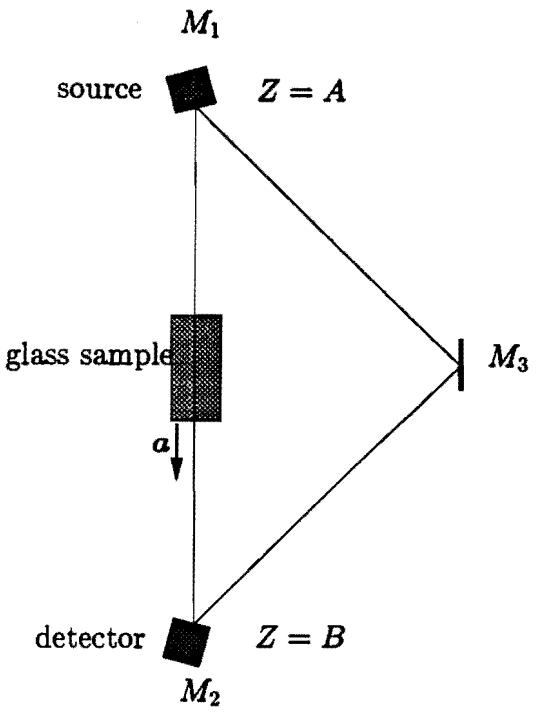

Figure 6.3: Resonant cavity containing an accelerating dielectric.

We align our interferometer in a laboratory on the surface of the earth with the arm containing the glass sample vertical. This arrangement is illustrated in figure 6.3. We allow our glass sample to freely fall so that, from the point of view of an observer stationary in Schwarzschild geometry, the dielectric sample accelerates downwards towards the centre of the Earth. Thus the experimental situation is analogous to that studied in section 6.4. There are, however, some important distinctions of principle which make the two cases independently interesting. In the previous example the acceleration of the dielectric caused a photon to deviate from a geodesic path as it passed through the glass sample. That is, from the point of view of an observer in I, Laub drag causes the photon itself to accelerate. When the dielectric sample is freely falling within a gravitational field, however, it defines a locally inertial set of comoving geodesic coordinates. In this geodesic frame, I, a photon will propagate through a comoving dielectric sample at constant velocity. Thus the photon will follow a geodesic path as it propagates through a freely falling glass sample, albeit a non-null geodesic. Within the experimental context discussed below, which could not hope to achieve an accuracy beyond first order in $a\,h/c^2$, this distinction does not cause any potentially resolvable differences.

The spacetime manifold at the surface of the Earth is described by the

exterior Schwarzschild solution [101]

$$ds^2 = -(1 - \frac{2m}{r})c^2\,dt^2 + (1 - \frac{2m}{r})^{-1}dr^2 + r^2(d\theta^2 + \sin^2\theta d\phi^2) \quad .$$

We locate the frame of our laboratory, S', on the surface of the earth with its origin at $r = R$. In the following analysis we neglect the effects of tidal forces. We use the result of chapter 3 and approximate S' in a small region about its origin by an accelerating frame, S, in French's coordinates. The lower case coordinates of S are related to those of the geodesic coordinates of our dielectric sample, I, by Eq. (6.19) with $\kappa = 1 - 2GM/Rc^2$ and $a \equiv GM/R^2$. An economy arising from our choice of French's coordinates is now apparent. In section 6.3 we derived the wave equation describing the propagation of electromagnetic radiation parallel to the z axis of S. Because of the close analogy between French's coordinates and the Schwarzschild solution, Eq. (6.20) also describes the propagation of electromagnetic radiation along an axis perpendicular to the surface of the earth. This equation does not, however, contain any information on the influence of spacetime curvature on the propagation of electromagnetic radiation. Nevertheless, this approximation is quite satisfactory within the following experimental context.

At $z = A > 0$ we locate a harmonic and monochromatic radiation source. In S our freely falling dielectric accelerates in the negative z direction. We are interested in the problem directly analogous to the analysis of the previous section in which the acceleration of the dielectric was parallel to the direction of the propagation of the radiation. We therefore search for a solution to the wave equation which describes an electromagnetic wave propagating in the negative z direction. Light from our stationary harmonic source which is incident upon our freely falling sample is assumed to propagate through vacuum. As such we require that $d\phi_{vac}/dt|_{z=A} = \omega_0$ and is independent of time. Assuming also that the amplitude does not change with time we are led immediately to the vacuum solution

$$E_x = E_0 \exp -i\left\{\omega_0\left(t + \frac{c}{2\,a}\ln\left[\kappa + \frac{2\,a\,z}{c^2}\right]\right) - \psi\right\} \quad . \tag{6.35}$$

From Eq. (6.10) we find the non-zero magnetic field component,

$$B_y = -\frac{E_x}{c}\left(\kappa + \frac{2\,a\,z}{c^2}\right)^{-1} \quad . \tag{6.36}$$

This solution, valid throughout the accelerating frame S, is only valid at first order in az/c^2 within the Schwarzschild spacetime as this is the order to which

the accelerating frame's metric and the Schwarzschild metric match. Transforming Eq. (6.35) into I we find that the non-zero electric field component is

$$\begin{aligned} E_X &= \frac{1}{\sqrt{\kappa - 2\,a\,z/c^2}} \left\{ E_x \cosh\frac{a\,t}{c} + B_y \sinh\frac{a\,t}{c} \right\} , \\ &= \frac{E_0}{Z + \xi_0 + cT} \exp -i \left\{ \omega_0 \frac{c}{a} \ln\left[\frac{a}{c^2}(Z + \xi_0 + cT) \right] - \psi \right\} , \end{aligned} \tag{6.37}$$

where we have defined the constant $\xi_0 \equiv \sqrt{\kappa}c^2/a$ for notational convenience.

At the first dielectric surface, located at $Z = 0$, the electric field suffers a reduction in amplitude by a factor of r. Eq. (6.37) with $Z = 0$ gives the incident amplitude and phase at this boundary. In the geodesic frame I, the covariant constitutive relations give $D_X = \epsilon\epsilon_0 E_X$ and $B_Y = \mu\mu_0 H_Y$ such that Maxwell's equations produce the usual wave equation for an inertial frame of reference:

$$\frac{\partial^2 E_X}{\partial z^2} - \frac{n^2}{c^2}\frac{\partial^2 E_X}{\partial t^2} = 0 ,$$

with solution $E_X = f(\Phi_d)$, where $\Phi_d = \omega T + k X$, $n\omega = ck$ and $f(\Phi)$ is an arbitrary wave-function. Thus, within the dielectric

$$E_X^d(Z,T) = \frac{r\,E_0}{n\,Z + \xi_0 + cT} \exp -i \left\{ \omega_0 \frac{c}{a} \ln\left[\frac{a}{c^2}(n\,Z + \xi_0 + cT) \right] - \psi \right\} , \tag{6.38}$$

which clearly matches Eq. (6.37) at $Z = 0$ and the amplitude decreases by a factor of r upon transmission through the boundary. As previously our dielectric sample has thickness h. In I the spatial coordinates label proper distances such that the second boundary is located at $Z = -h$, negative as the wave is propagating in the negative z direction. We match the electric field at this second dielectric surface with the beam emerging from the dielectric into vacuum by comparing Eq. (6.38) with Eq. (6.37) at $Z = h$, after substituting $E_0 \to E_1$, $\omega_0 \to \omega_1$ and $\psi \to \psi + \Delta\psi$. As we are only interested in first order in ah/c^2, we assume that $a^2\,h\,T/c^4 \ll 1$ and is negligible. From this assumption we are led to

$$\begin{aligned} E_x^{out}(z,t) &= r^2\,E_0 \left(1 + \frac{a\,h}{c^2\sqrt{\kappa}}(n-1) \right) \\ &\quad \times \exp -i \left\{ \omega_1 \left(t + \frac{z}{c\kappa} \right) + \omega_0 \frac{c}{a} \ln\sqrt{\kappa} + \psi + \Delta\psi \right\} . \end{aligned} \tag{6.39}$$

ω_1 is found by matching the time derivatives of both phases at the boundary surface when $T = 0$. This yields

$$\omega_1 = \omega_0 \left(1 + \frac{a\,h}{\sqrt{\kappa}\,c^2}(n-1) \right) . \tag{6.40}$$

This frequency shift is almost exactly that predicted by Eq. (6.28) at first order in $a\,h/c^2$. It does, however, contain an extra factor of $\sqrt{\kappa}$ in the denominator. On the surface of the Earth $\kappa - 1 = -2GM/Rc^2 = 2aR/c^2 \sim 1.4 \times 10^{-9}$ and we may neglect this divergence from unity in an experimental context. While Tanaka [145] has previously predicted a frequency shift for an electromagnetic wave propagating through an accelerating dielectric sample, the above prediction constitutes the first derivation of a frequency shift for light having propagated through a dielectric medium freely falling in a gravitational field. From Eqs. (6.39) and (6.40) it follows that the change in phase,

$$\Delta\psi = -\omega_0 \frac{h}{c\sqrt{\kappa}}(n-1) \ . \tag{6.41}$$

Equations (6.39) to (6.41) with $\kappa = 1$ are directly analogous to the first order expansions of Eqs. (6.27) to (6.29), apart from differences in signs arising from the fact that, in this second example, the wave is propagating in the negative z direction. If we were to proceed to calculate the optical response of a resonance cavity in a gravitational field with a glass sample freely falling in one arm, we would recover the result of section 6.4. In particular, this cavity would display optical ringing. However, the experimental constraints for observation of this phenomenon are even more rigorous than in the previous section as we are limited by the gravitational acceleration on the surface of the Earth of 10 $\mathrm{m.s}^{-2}$. It follows that a successful experimental observation of this asymmetric response profile is well outside the experimental sphere accessible with current technology and would require better than an order of magnitude improvement in the reflection/transmission losses at each mirror/dielectric boundary for this experiment to be viable.

Chapter 7

Optical interferometer with angular acceleration

In this chapter we analyse the optical behaviour of a ring interferometer with angular acceleration. A transit time technique is used to calculate the observable phase and frequency shift when the optical cavity is evacuated. When material media separates the mirrors we apply the covariant form of Maxwell's equations and solve the wave equation for this system. Both approaches agree in the appropriate limits. Our analysis predicts an asymmetric response profile will be observed for a resonant cavity with angular acceleration. We also show the beat frequency for a ring laser with angular acceleration is precisely that given by the instantaneous Sagnac effect.

7.1 Sagnac effect

In 1893 Sir Oliver Lodge [81] first proposed the detection of rotation by an optical interferometer. Within the context of an ether theory, Lodge derived an expression for the phase shift induced by rotation which yields the correct expression for the Sagnac phase shift when transformed into relativity theory. On the basis of this calculation Lodge suggested that the rotation of the Earth could be detected with an interferometer with an area of a square kilometre. This speculative idea was later borne out, in 1925, by the superb experimentalist Michelson [97] who, along with Gale and Pearson, constructed a 2010 ft by 1113 ft (and so 0.21 km^2) optical interferometer which successfully measured the phase shift induced by the rotation of the Earth.

The enduring significance of Sagnac's celebrated paper [125] is that it was the first to report an experimental observation and correctly interpret the optical phase shift induced by rotation. For an optical interferometer with

area $\boldsymbol{A}$ and rotation $\boldsymbol{\Omega}$ Sagnac predicted and observed a shift in phase

$$\Delta\Phi = 4\,\omega\,\frac{\boldsymbol{A}\cdot\boldsymbol{\Omega}}{c^2}\ , \tag{7.1}$$

of the counterclockwise (*ccw*) beam relative to the clockwise (*cw*) beam, when both had completed a full circuit of the interferometer before being recombined at the detector.

A few years previously, Harress [55] had performed a very similar experiment. Studying the effects of light drag in glass, Harress constructed a circular ring interferometer in which the opposite beams propagated entirely through adjacent glass prisms. For convenience Harress rotated the entire interferometer, thus achieving motion of his glass interferometer relative to the laboratory, enabling the effects of light drag to be studied. His results, however, contained an inexplicable bias in the fringe shift, which was not correctly interpreted as arising from the Sagnac effect until after Harress's early death. In hindsight Harress's experiment provided a more accurate observation of the Sagnac effect than Sagnac's own later experiment. Moreover, it demonstrated that the observed fringe shift is unaffected by dispersion [118].

With the invention of the laser the sensitivity of optical devices to rotation was dramatically improved. Ring lasers [84] and fibre optic gyroscopes [150] are now commonplace and are used in inertial navigation systems [26] and as a novel seismic instrument [139]. A rotationally induced phase shift has also been observed for super-conducting Cooper pairs [159], in neutron interferometry [153], in atom interferometry with ^{40}Ca beams [121] and in interferometry with bare electrons [56]. It has also been proposed that rotation should induce a detectable phase transition in superfluid Helium gyroscopes [115].

Excellent reviews of the history and development of the Sagnac effect have been given by Post [118], Heer [60], Hasselbach and Nicklaus [56] and Anderson et al. [5]. There exists an exhaustive experimental and theoretical literature concerned with the effect of constant rotation on various types of interferometers. While an interferometer with constant angular velocity has received a comprehensive treatment in the literature, the extension to include angular acceleration [10, 143, 43, 44] is considerably less extensive. This omission is surprising as technological applications of ring laser gyroscopes are not restricted to instances of constant rotation. Highly developed for inertial guidance systems, they often operate under relatively high angular accelerations [26]. Dither [26], when a ring laser is rapidly oscillated by a piezoelectric crystal so as to unlock the opposing beams, contributes significant angular

acceleration to the ring laser. Furthermore, the theory of ring laser seismographs, which detect variations in the rotation rate of the Earth and motion of the Earth's surface, requires the inclusion of angular acceleration [139].

Belenov and Markin [10] considered a circular ring laser with angular acceleration about its axis of symmetry. Appealing to the equivalence principle they assumed a photon spends its life climbing through the gravitational field associated with the acceleration of the interferometer and thus obtained a frequency shift, in addition to the usual Sagnac effect, between the oppositely propagating beams. This conclusion, however, is invalid as they neglected the change in angular velocity of the ring during the photon's transit.

More satisfactory analyses of an angularly accelerating ring laser have been given by Takahashi and Baierlein [143] and Fateev [43, 44]. Both worked from the time-dependent spacetime geometry of an angularly accelerating frame of reference. Maxwell's equations within this geometry were solved by postulating the spatial dependence of the electromagnetic wave. Examining a circular ring laser with acceleration about its axis of symmetry, Takahashi and Baierlein concluded that the beat frequency at any instant of time is that of an equivalent comoving ring laser without angular acceleration, so giving an 'instantaneous Sagnac effect'. Fateev gave a more general treatment of wave propagation in a fibre optic interferometer with angular acceleration, concluding that the beat frequency of a ring laser differs from the instantaneous Sagnac beat frequency by an amount proportional to the vector product of the angular acceleration and area of the ring.

In light of these contradictory positions it is desirable to approach the problem of a ring interferometer with angular acceleration from an alternative viewpoint. In sections 7.2-7.4 we work entirely from an inertial frame of reference, which sidesteps the problems associated with interpreting Maxwell's equations in a frame of reference with a time dependent metric. Using the transit time approach, with the assumption that the mirrors are separated by vacuum, we derive the phase difference between oppositely propagating beams in a Sagnac interferometer in section 7.2. The frequency shift induced by the angular acceleration of the interferometer is obtained from the time derivative of the phase upon completion of a transit of the ring perimeter. A novel application to the optical response of a resonant cavity with angular acceleration is presented in section 7.3, the output intensity as a function of time being asymmetric due to ringing in the optical cavity. This may provide a direct experimental test of the response of an optical device to angular acceleration.

In section 7.4 a ring laser with angular acceleration is analysed. This analysis generalises the result of Takahashi and Baierlein [143] to a ring laser with arbitrary geometry accelerating about an arbitrary axis. An error in the work of Fateev [43] is also corrected.

Our assumption that vacuum separates the mirrors of the ring interferometer enables us to work entirely from a reference inertial frame I, providing a simple and intuitive presentation of the problem of an interferometer with angular acceleration. However, a physical ring laser must contain a gas within the lasing cavity with population inversion along at least a portion of it. Therefore, in section 7.5 we re-examine the problem of a ring laser assuming a dielectric of constant refractive index separates the mirrors. We approach this problem by formulating and solving Maxwell's equations in an angularly accelerating frame of reference. For mathematical convenience we make the additional assumption that both the angular velocity and angular acceleration are parallel to the vector area of the ring laser. Our results are in full agreement with those of Takahashi and Baierlein in the appropriate limit. We also recover all of the results of sections 7.2-7.4 in the limit that the mirrors are separated by vacuum. That our solution to the covariant form of Maxwell's equations produces the same results as the, much simpler, transit time approach illustrates the power of this transit time technique when applied correctly in the appropriate context.

7.2 Sagnac interferometer with angular acceleration

In the experiment of Sagnac the oppositely propagating beams of an optical interferometer complete a circuit of the interferometer before being recombined at the source. We first examine the effect of angular acceleration on the phase shift which is observed in this experiment. We also include the rotation of the Earth in our analysis, assuming that our interferometer is held within a laboratory which is itself rotating with the Earth.

Let the centre of the earth, following a geodesic about the sun, define the origin of two coordinate systems. The geodesic coordinates, I, are locally inertial so that Maxwell's equations take their familiar form in I. S, however, is defined to be stationary with respect to the Earth's surface, rotating relative to I with angular velocity Ω, its period being the sidereal day. At first order

in velocity $t = T$ and [49]

$$\frac{d\boldsymbol{R}(T)}{dT} = \frac{d\boldsymbol{r}(t)}{dt} + \boldsymbol{\Omega} \times \boldsymbol{R}(T) \ ,$$

where we have maintained our convention that inertial coordinates are represented by uppercase letters and non-inertial coordinates are lowercase. Let $\boldsymbol{R}_i(T)$ and $\boldsymbol{r}_i(t)$ specify, in I and S respectively, the location of N mirrors, separated by vacuum, which form an arbitrary closed optical path. The 'counterclockwise' path (ccw), as opposed to the clockwise path (cw), is defined as that for which i increases.

In S at $t = 0$ our optical interferometer is assumed to have angular velocity $\boldsymbol{\omega}$ and angular acceleration $\boldsymbol{\alpha}$ about an axis which passes through $\boldsymbol{\rho}$. We construct a Taylor series for $\boldsymbol{R}_i(T)$ about $T = 0$ and keep only first order in Ω, ω and α; this neglects terms of the order of centripetal acceleration. We assume coincidence of the axes when $T = 0$ and define $\boldsymbol{R}_i(0) = \boldsymbol{r}_i(0) \equiv \boldsymbol{r}_i$. For small T

$$\boldsymbol{R}_i(T) = \boldsymbol{r}_i + \{\boldsymbol{\Omega} \times \boldsymbol{r}_i + \boldsymbol{\omega} \times (\boldsymbol{r}_i - \boldsymbol{\rho})\}\ T + \boldsymbol{\alpha} \times (\boldsymbol{r}_i - \boldsymbol{\rho})\frac{T^2}{2} \ . \quad (7.2)$$

Having made the identification $\boldsymbol{R}_i(0) = \boldsymbol{r}_i(0) \equiv \boldsymbol{r}_i$ we could have used the notation $\boldsymbol{R}_i$ in favour of $\boldsymbol{r}_i$ on the right side of Eq. (7.2). The use of lowercase $\boldsymbol{r}_i$ may possibly cause confusion as it would appear that we have mixed the coordinates of I with those of S in Eq. (7.2). We prefer to use lowercase $\boldsymbol{r}_i$ as these have a more intuitive interpretation, being the location of the ring laser in the laboratory frame at $T = 0$. If one keeps in mind that $\boldsymbol{r}_i$ are constant vectors then no confusion should arise.

At $\boldsymbol{R}_0(T)$ we locate a harmonic source which is moving with the interferometer and has wavenumber k, and therefore time dependence $A_0 \exp -ick\tau$ when measured by a comoving observer, where τ is the proper-time along the worldline of our source. In a Sagnac interferometer the oppositely propagating beams complete a circuit of the interferometer before being recombined at the source, where their phase difference is measured. We calculate this difference in phase by determining the difference in the time for the opposite beams to complete a circuit of the interferometer. When considering accelerated motion this transit time approach in the vacuum limit has significant calculational advantages over the widely used 'snapshot' technique [34]. In the snapshot technique $\oint \boldsymbol{k} \cdot d\boldsymbol{r}$, integrated around the geometry of the interferometer at a given instant of time, determines the phase at the detector relative to the source. If no allowance is made for the anharmonic nature of the light due

to the acceleration of the source and mirrors then the effect of angular acceleration is lost and the Sagnac effect with the instantaneous angular velocity will be recovered. The transit time approach, however, explicitly includes the angular acceleration throughout.

Restricting attention to the *ccw* path, the time interval for a plane of constant phase to propagate from the $(i-1)$th mirror to the ith mirror is determined by

$$\begin{aligned} c(T_i - T_{i-1}) &= |\boldsymbol{R}_i(T_i) - \boldsymbol{R}_{i-1}(T_{i-1})| \ , \\ &= \left\{\Delta r_i^2 + 4\,\boldsymbol{\Omega}\cdot\boldsymbol{A}_i\,(T_i - T_{i-1}) + 4\,\boldsymbol{\omega}\cdot\boldsymbol{a}_i\,(T_i - T_{i-1})\right. \\ &\quad \left. +2\,\boldsymbol{\alpha}\cdot\boldsymbol{a}_i\,(T_i^2 - T_{i-1}^2)\right\}^{1/2} \ , \end{aligned} \tag{7.3}$$

where c is the speed of light in vacuum, $\Delta\boldsymbol{r}_i \equiv \boldsymbol{r}_i - \boldsymbol{r}_{i-1}$, $\boldsymbol{A}_i \equiv \boldsymbol{r}_i \times \Delta\boldsymbol{r}_i/2 = \boldsymbol{r}_{i-1}\times\Delta\boldsymbol{r}_i/2$ is the vector area of the triangle formed by the origin, $\boldsymbol{r}_i$ and $\boldsymbol{r}_{i-1}$, and $\boldsymbol{a}_i \equiv (\boldsymbol{r}_i-\boldsymbol{\rho})\times\Delta\boldsymbol{r}_i/2 = (\boldsymbol{r}_{i-1}-\boldsymbol{\rho})\times\Delta\boldsymbol{r}_i/2$ is the vector area of the triangle formed by $\boldsymbol{\rho}$, $\boldsymbol{r}_i$ and $\boldsymbol{r}_{i-1}$. The physical basis for Eq. (7.3) is the fact that in vacuum the phase velocity and group velocity for a photon are always parallel. Thus a point of constant phase propagates along a null geodesic, which is a straight line in the locally inertial frame I, from $\boldsymbol{R}_{i-1}(T_{i-1})$, the spacetime point where it intersected the $(i-1)$th mirror, to $\boldsymbol{R}_i(T_i)$, the spacetime point where it intersects the ith mirror.

Solving Eq. (7.3) for $T_i - T_{i-1}$ we obtain

$$\begin{aligned} (T_i - T_{i-1})_{ccw} &= \frac{\Delta r_i}{c} + 2\,\frac{\boldsymbol{\Omega}\cdot\boldsymbol{A}_i}{c^2} + 2\,\frac{\boldsymbol{\omega}\cdot\boldsymbol{a}_i}{c^2} \\ &\quad +2\,\frac{\boldsymbol{\alpha}\cdot\boldsymbol{a}_i}{c^2}\left\{(T_{i-1})_{ccw} + \frac{\Delta r_i}{2\,c}\right\} \ . \end{aligned} \tag{7.4}$$

A reversal of sign on the left side of Eq. (7.3) describes the propagation of the *cw* beam from the ith mirror to the $(i-1)$th mirror. An almost identical calculation to that above produces

$$\begin{aligned} (T_{i-1} - T_i)_{cw} &= \frac{\Delta r_i}{c} - 2\,\frac{\boldsymbol{\Omega}\cdot\boldsymbol{A}_i}{c^2} - 2\,\frac{\boldsymbol{\omega}\cdot\boldsymbol{a}_i}{c^2} \\ &\quad -2\,\frac{\boldsymbol{\alpha}\cdot\boldsymbol{a}_i}{c^2}\left\{(T_{i-1})_{cw} - \frac{\Delta r_i}{2\,c}\right\} \ . \end{aligned} \tag{7.5}$$

Eqs. (7.4) and (7.5) are both dependent on the time when their respective phase planes intersect the $(i-1)$th mirror. Choosing both phase planes to return to the source at T we obtain, at leading order,

$$(T_{i-1})_{ccw} \approx T - \sum_{j=i}^{N}\frac{\Delta r_j}{c} \ ,$$

$$(T_{i-1})_{cw} \approx T - \sum_{j=1}^{i-1} \frac{\Delta r_j}{c} \approx 2\,T - \frac{P}{c} - (T_{i-1})_{ccw} \ , \qquad (7.6)$$

where $P \equiv \sum \Delta r_i$ is the perimeter of the ring. The summation of Eq. (7.4) or Eq. (7.5) is dependent on the geometry of the interferometer. However, by subtracting Eq. (7.5) from Eq. (7.4), using Eq. (7.6) to substitute for $(T_{i-1})_{cw}$ and summing from $i = 1$ to N, we obtain the difference of their sums. This difference determines the time by which the two phase planes, which intersect the detector at T, were separated when they left the world line of the source at $(T_0)_{ccw}$ and $(T_0)_{cw}$ respectively. Along the world line of the source the radiation has wavenumber k such that the phase difference observed at T is

$$\Delta\Phi = c\,k\ \{(\tau_0)_{ccw} - (\tau_0)_{cw}\} = \frac{4\,k}{c}\,\boldsymbol{A}\cdot\left\{\boldsymbol{\Omega} + \boldsymbol{\omega} + \boldsymbol{\alpha}\left(T - \frac{P}{2\,c}\right)\right\} \ , \qquad (7.7)$$

where τ denotes the proper time along the worldline of $\boldsymbol{R}_0(T)$. At first order $(\tau_0)_{ccw} = (T_0)_{ccw}$ and $(\tau_0)_{cw} = (T_0)_{cw}$, which produces the final term in Eq. (7.7).

When $\alpha = 0$ we recover the usual Sagnac effect for a ring of arbitrary geometry with rotation $\boldsymbol{\omega}$ on the surface of the Earth, Eq. (7.1). This simple construction has demonstrated the linearity of the Sagnac effect under the addition of angular velocities about separated and non parallel axes of rotation. When $\alpha \neq 0$ however, this phase difference is not equivalent to the Sagnac effect for an identical, instantaneously comoving ring without angular acceleration. Eq. (7.7) is of the same form as the Sagnac effect but has, for the angular velocity of the interferometer, its average over the time of flight of the phase plane around the ring. This phase shift agrees with that obtained by Fateev [43, Eq.(22)] when a difference in convention is noted: Fateev chose $T = 0$ when the signal left the source.

Upon reflection off each mirror moving relative to I the beam suffers a change in wavenumber. It is crucial to our understanding of the resonance cavity and ring laser to obtain the cumulative effect of these Doppler shifts. While this can be derived from the Doppler effect due to the motion of the source and each mirror, and this calculation has been performed as a test of consistency, a more direct derivation is given below. In this derivation we obtain the frequency shift of the wave having completed a circuit of the interferometer from the time derivative of the phase measured by a comoving observer.

In the following work we neglect the phase changes upon reflection off each of the N mirrors as these only change the phase by a constant factor. This

assumed, consider the phase $\Phi_{ccw}(T)$ of the *ccw* phase plane which intersects an observer O comoving with $\boldsymbol{R}_0(T)$ at T. This phase will be precisely the phase it was when it left the source at $(\tau_0)_{ccw}$, explicitly $\Phi_{ccw}((\tau_0)_{ccw}) = -c\,k \times (\tau_0)_{ccw}$, where τ, as defined earlier, is the proper-time along the worldline of O and, at first order, $\tau = T$. Substituting Eq. (7.6) into Eq. (7.4), differentiating with respect to T and performing the summation from $i = 1$ to N we obtain $d(T_0)_{ccw}/dT = 1 - 2\boldsymbol{\alpha} \cdot \boldsymbol{A}/c^2$. The frequency as measured by O will be $d\,\Phi_{ccw}(\tau)/d\tau$, such that

$$c\,k_{ccw} = -\frac{d\,\Phi_{ccw}(T)}{dT} = c\,k\,[1 - 2\frac{\boldsymbol{\alpha} \cdot \boldsymbol{A}}{c^2}] \ , \tag{7.8}$$

Repetition of this calculation for the *cw* beam gives a frequency shift of the same magnitude but with opposite sign. If one were to recombine the beams at $\boldsymbol{R}_0(T)$ then O would observe a beat, that is a time dependent phase shift, between the opposite modes in a passive Sagnac cavity of frequency

$$|\omega_{ccw} - \omega_{cw}| = 4\,k\,\frac{\boldsymbol{\alpha} \cdot \boldsymbol{A}}{c} \ .$$

With a ring interferometer of area 1 m^2 and an angular acceleration of 10 $rad.s^{-2}$ we would require a frequency resolution of one part in 10^{18} for this beat to be experimentally resolvable. The Canterbury ring laser has achieved a frequency resolution of one part in 3×10^{21} [139], and thus an experimental observation of an angular acceleration induced beat in a passive Sagnac interferometer should be attainable within current technology. An obvious approach would be to oscillate the ring interferometer and record the output beat frequency with time. Upon Fourier transformation of the optical output we would expect to observe sideband structure in the output spectra. However, because a passive cavity is several orders of magnitude less sensitive to phase shifts than its corresponding active ring laser device, it is considerably more straightforward to detect this time dependent phase shift using a ring laser, as is discussed in sections 7.4 and 7.5.

It is a simple extension of Eq. (7.8) to show that an observer comoving with the interferometer at $\boldsymbol{r}_i$ will register a shift in wavenumber of $-2\,k/c^2 \sum_{j=1}^{i} \boldsymbol{a}_j \cdot \boldsymbol{\alpha}$ in the *ccw* beam. In particular, if there is no angular acceleration then all observers located along the beam and comoving with the ring interferometer will measure the same frequency.

7.3 Resonant Cavity with angular acceleration

Optical ringing has been investigated in a variety of systems in which the frequency of an external laser and the resonant frequency of the optical device cross over in time. Ioannidis et al. [64, 65] observed ringing in an optical fibre ring resonator, a variable optical path length being obtained through wrapping a length of optical fibre around a piezoelectric cylinder. Upon exciting a high finesse ring cavity with a frequency modulated external laser, Li et al. [79] were able to determine the finesse of this cavity through the observed ringing profile. An asymmetric response profile was also observed by Li et al. [80] when the scanning rate of a scanning Fabry-Pérot interferometer multiplied by the decay time of the interferometer squared was the order of unity. In section 6.4.2 we showed a dielectric sample linearly accelerating within an optical cavity causes the cavity to display a ringing profile.

When a ring interferometer has angular acceleration the optical path length around its perimeter is changing with time. We therefore expect ringing to be observed as the resonance frequency of the cavity passes through the frequency of an external monochromatic signal. In the following we present a novel analysis of a resonance cavity with angular acceleration, obtaining an asymmetric response profile.

Comoving with the mirror at $\boldsymbol{R}_0(T)$ we place a monochromatic source which injects an electromagnetic signal with time dependence $A_0 \exp\{-i\,ck\,\tau\}$ into the cavity, where A_0 is a complex constant. Also at $\boldsymbol{R}_0(T)$ we locate a detector which records the intensity of the radiation which is transmitted out of the cavity through this mirror. The electromagnetic field at the detector will consist of an infinite sum of waves $A_l(T, \boldsymbol{R}_0(T))$ which have traversed the ring perimeter l times. To evaluate $A_l(T, \boldsymbol{R}_0(T))$ we first determine the time for a *ccw* phase plane to complete l circuits of the ring perimeter by summing Eq. (7.4) from $i = 1$ to Nl. As this summation has no general solution we consider an optical cavity which forms a planar N-sided regular polyhedron.

Define $\boldsymbol{C}$ as the centre of symmetry of this optical cavity when $T = 0$, thus

$$\boldsymbol{\alpha} \cdot \boldsymbol{a}_i = \frac{\boldsymbol{\alpha} \cdot \boldsymbol{A}}{N} + \frac{1}{2}\,\boldsymbol{\alpha} \times (\boldsymbol{C} - \boldsymbol{\rho}) \cdot \Delta \boldsymbol{r}_i \ . \tag{7.9}$$

We define $\mathcal{T}_l$ as the time the *ccw* phase plane leaves the source before traversing the ring perimeter l times and intersecting $\boldsymbol{R}_0(T)$ at $T = 0$. Summing Eq. (7.4)

from $i = 1$ to Nl with $(T_{Nl})_{ccw} = 0$ gives

$$\mathcal{T}_l = -l\left\{\frac{P}{c}\left(1+\frac{\boldsymbol{g}\cdot\boldsymbol{h}}{c^2}\right)+2\frac{\boldsymbol{A}\cdot(\boldsymbol{\Omega}+\boldsymbol{\omega})}{c^2}\right\}+l^2\frac{P}{c^3}\,\boldsymbol{\alpha}\cdot\boldsymbol{A}\ , \qquad (7.10)$$

where $\boldsymbol{g} \equiv \boldsymbol{\alpha}\times(\boldsymbol{C}-\boldsymbol{\rho})$ and is the linear acceleration of the centre of symmetry of the ring, $\sum_{j=1}^{N} j\,\Delta\boldsymbol{r}_j = N(\boldsymbol{r}_0 - \boldsymbol{C}) \equiv N\,\boldsymbol{h}$ and we have used $\sum_{j=1}^{q} j = (q^2+q)/2$.

Again neglecting the phase changes upon reflection off each mirror we find the phase of each component wave at the detector is the phase of the source at the time this wave left the source. Therefore $A_l(0) = (1-s^2)\,s^{lN}$ $\times A_0\,\exp\{-i\,ck\,\mathcal{T}_l\}$, where s^2 is the reflectance of all N mirrors, the first factor giving the reduction in amplitude due to two transmissions through the mirror at $\boldsymbol{r}_0(t)$ and the second factor is due to losses from $l\,N$ reflections. Furthermore $A_l(T) = A_l(0)\,\exp\{-i\,c\,k\,T\,[1-2\,l\,\boldsymbol{\alpha}\cdot\boldsymbol{A}/c^2]\}$ as each transit of the ring perimeter results in a frequency shift given by Eq. (7.8). Thus the field at the detector is

$$A_{out}(T, \boldsymbol{R}_0(T)) = \left(1-s^2\right)\ A_0\,\exp\{-i\,ck\,T\}\sum_{l=0}^{\infty} s^{lN}\,\exp\{i\,\Phi_l\}\ , \qquad (7.11)$$

where

$$\Phi_l = -c\,k\left\{\mathcal{T}_l - 2\,l\,\frac{\boldsymbol{\alpha}\cdot\boldsymbol{A}}{c^2}\,T\right\}\ . \qquad (7.12)$$

The summation of Eq. (7.11) is identical in form to that obtained for the optical response of a scanning Fabry-Pérot interferometer [80], and that derived in section 6.4.2 for a resonant cavity containing an accelerating dielectric sample. As previously discussed, Li et al. obtained the output intensity of a scanning Fabry-Pérot interferometer as a function of time by utilising its equivalence with the intensity profile of a Fabry-Pérot interferometer with a frequency modulated input signal. In Appendix A we summarise this mathematical result. Applying the solution, Eq. (A.6), to the problem at hand, and identifying the variables through the analogy of Eq. (7.12) with Eq. (A.4), we obtain the output intensity of a resonant cavity with angular acceleration. If we assume that optical resonance occurs when the interferometer is stationary, such that τ of Eq. (A.4) corresponds to P/c, we observe

$$\frac{I_{out}}{I_0} = \frac{|A_{out}|^2}{|A_0|^2} = \left(\frac{1-s^2}{1-s^N}\right)^2\frac{\pi}{8\eta}|w(\zeta)|^2\ , \qquad (7.13)$$

where [1]

$$w(\zeta) = \frac{i}{\pi}\int_{-\infty}^{\infty} d\nu\frac{\exp(-\nu^2)}{\zeta-\nu} = \exp(-\zeta^2)\,\mathrm{erfc}(-i\zeta) \qquad (\mathrm{Im}\,\zeta > 0)\ ,$$

erfc$(-i\zeta)$ being the complex error function. The asymmetry parameter $\eta \equiv \beta/\Gamma^2$, where $\beta \equiv 2k\,\boldsymbol{\alpha}\cdot\boldsymbol{A}/P$ and corresponds to the change in frequency from each traverse of the ring perimeter divided by the duration of each traverse, and $\Gamma = 2c\,(1-s^N)/Ps^N$ is the power rate of decay of the cavity. The variable $\zeta \equiv \pm\exp(-i\pi/4)\,\{-i\Gamma + 2\,\beta(t - z_0/c)\}\,/\sqrt{8\beta}$, the sign being positive when $\beta(T - z_0/c) > \Gamma$ and was chosen to keep the imaginary part of ζ positive, and $z_0 = -[P\boldsymbol{g}\cdot\boldsymbol{h} + 2\boldsymbol{A}\cdot(\boldsymbol{\Omega}+\boldsymbol{\omega})/c]/2\boldsymbol{\alpha}\cdot\boldsymbol{A}$ merely shifts the origin of time. The factor $(1-s^2)^2/(1-s^N)^2 \approx (2/N)^2$ in Eq. (7.13) expresses the fact that this cavity has transmission losses from N mirrors, whereas a Fabry-Pérot interferometer [80] suffers losses from only two.

Plots of I_{out}/I_0 versus the normalised time $\tau = \Gamma t$ for $\eta = 0.01$, 0.10 and 0.50 are given in Figure 7.1. With $\eta \sim 0.10$ the asymmetry is easily resolved experimentally. Consider a state of the art square ring cavity with a perimeter of four metres [79]. Commercially available mirrors with $1 - s \sim 10$ ppm give $\Gamma \sim 6000$ Hz for this cavity. If this cavity is excited with radiation of wavelength 633 nm then we require $\alpha \sim 5$ rad.s^{-2} to obtain $\eta \sim 0.10$. This surprisingly low acceleration is certainly within the realms of experimentation and could be achieved by oscillating the platform on which the interferometer rests at a frequency of 70 Hz with an amplitude of 10^{-3} radians. The minimum acceleration does, however, vary with P^{-3} and $(1-s)^2$. Improving the reflectance of the mirrors will lower the minimum angular acceleration required to observe ringing, but the perimeter of the ring interferometer must be kept relatively large. Furthermore, acceleration induced distortions to the interferometer and frequency drift in the external laser would lead to spurious asymmetries in the output intensity as a function of time.

It is important to appreciate that the monochromatic source, the detector and the interferometer are all stationary when viewed from the angularly accelerating frame of reference. *In this frame the asymmetry in the optical output must be interpreted as a direct consequence of the time dependence of the spacetime metric*, Eq. (7.17). Therefore an observation of optical ringing in an optical cavity with angular acceleration would provide a significant experimental test of general relativity, as the experiment of Hay et al. [58], Champeney et al. [24, 25] and Kundig [77], who all mounted a Mössbauer source and receiver on a rotating disk, verified the general relativistic 'gravitational' redshift in a uniformly rotating frame of reference. Unlike a ring laser with angular acceleration, for which the beat frequency is exactly that of an identical instantaneously co-rotating ring laser (derived in sections 7.4

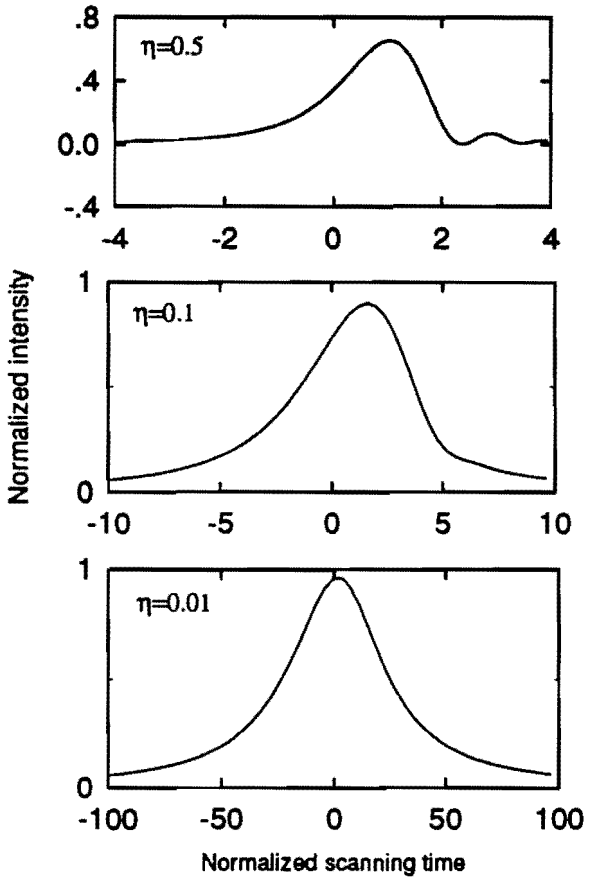

Figure 7.1: Intensity profiles for a resonant cavity with angular acceleration, obtained from numerical evaluation of Eq. (7.13) at various values of the asymmetry parameter η: (a) $\eta = 0.5$, (b) $\eta = 0.1$ and (c) $\eta = 0.01$. The normalised time is related to real time by $\tau = \Gamma t$.

and 7.5), this optical output differs from that of an instantaneously co-rotating passive interferometer with constant angular velocity. In predicting an asymmetric optical response profile the angular acceleration plays an important and transparent role. In this sense an observation of an asymmetric optical output for a resonant cavity with angular acceleration would provide a direct verification of the influence of angular acceleration on optics, as it is not obscured by an otherwise dominant rotation induced effect.

This result is closely related to the debate concerning the locality hypothesis, discussed in chapter 4. In this instance we are concerned with the influence of angular acceleration on a rotating (non-inertial) interferometer, but the underlying principle is the same. Deviation of the output from that of an instantaneously comoving ring interferometer with constant angular velocity is characterised by the parameter $\eta \equiv \beta/\Gamma^2 = 2ck\tau_c \times \tau_c \boldsymbol{\alpha} \cdot \boldsymbol{A}/Pc$, where $\tau_c = 1/\Gamma_c$ is the 'ring-down time' or radiation lifetime of the cavity. In chapter 4 we found, for a variety of non-inertial systems, that it is the ratio of the intrinsic time scales of the phenomena under observation with the time scale characteristic of the acceleration, $\mathcal{L}/c$, which determines the magnitude of any violations of the locality hypothesis. In this case the acceleration time scale is $\mathcal{L}/c = Pc/(\boldsymbol{\alpha} \cdot \boldsymbol{A})$ and the characteristic time of the measurement is τ_c. In this context the asymmetry parameter η is proportional to $c\tau_c/L$, scaled by a phase factor $ck\tau_c$ specific to the experimental arrangement. This result, as did the result of section 6.4.2, again supports our contention that it is the desired frequency resolution which determines the time scale associated with the measurement when considering the significance of deviations from the locality hypothesis. This follows from that fact that $1/\tau_c$ provides a fundamental limit to the frequency resolution of the cavity.

Finally, should this experiment be performed it could provide limits on the extent to which electrodynamics in angularly accelerating frames of reference differs from the covariant formalism of general relativity. One would expect, for example, that the non-local theory of electrodynamics suggested by Mashhoon [93] would lead to small differences in the output spectra for this experimental arrangement. This calculation, however, has not been pursued within the framework of this thesis but would provide an interesting avenue for further research.

7.4 Ring laser with angular acceleration

A ring laser enables one to measure angular velocities because the Sagnac effect results in the counter-propagating beams being separated in frequency by an amount proportional to the angular velocity of the ring. This feature has found application in ring laser gyrometers, used in inertial guidance systems [26], and as a novel seismic detector [139]. In both of these applications, however, the ring laser often has angular acceleration about an unknown axis of rotation. It is therefore important to gain an understanding of the operation of a ring

laser in these conditions.

A ring laser will resonate provided the phase of the source and a phase plane upon its return to the source differ only by an integer multiple of 2π radians. If the optical path length of the lasing cavity is constant with time then one need only match the phase of the source and returning phase plane to obtain the eigenmodes of the cavity. When a ring laser has angular acceleration, however, the optical path length is not constant but is changing linearly with time. Therefore, both the phase of the source and its first time derivative must be matched to the returning phase plane in order to determine the lasing frequency.

As in section (7.3) we first consider a ring laser which forms a planar N-sided regular polyhedron. If we define $k_{ccw}(T)$ as the wavenumber of the laser as measured by an observer O comoving with $\boldsymbol{R}_0(T)$, then the reference phase plane, which intersects O at $T = 0$, had wavenumber $k_{ccw}(\mathcal{T}_1)$ when it previously intersected O at $\mathcal{T}_1$, given by Eq. (7.10). From Eq. (7.8), this reference phase plane has wavenumber $k_{ccw}(\mathcal{T}_1)\,[1 - 2\boldsymbol{\alpha}\cdot\boldsymbol{A}/c^2]$ when it again intersects O at $T = 0$. Because of the necessity of matching the first time derivatives of the phase of the laser and the returning wavefront at $\boldsymbol{R}_0(T)$ we require $k_{ccw}(0) = k_{ccw}(\mathcal{T}_1)\,[1 - 2\boldsymbol{\alpha}\cdot\boldsymbol{A}/c^2]$. We also require the phase of the laser at $\boldsymbol{R}_0(T)$ to have evolved an integer multiple of 2π radians over the time of flight of the reference phase plane around the ring laser, thus

$$2\,\pi\,m = \int_{\mathcal{T}_1}^{0} c\,k_{ccw}(T)\,dT \quad .$$

As the optical path of the lasing cavity is changing linearly with time we assume a linear variation of $k_{ccw}(T)$, giving $k_{ccw}(T) = k(0)\,\{1 - 2\,\boldsymbol{A}\cdot\boldsymbol{\alpha}\,T/cP\}$, which leads to, upon integration,

$$k_{ccw}(T) = K\,\left\{1 - \frac{\boldsymbol{g}\cdot\boldsymbol{h}}{c^2} - \frac{2}{c\,P}\,\boldsymbol{A}\cdot(\boldsymbol{\Omega} + \boldsymbol{\omega} + \boldsymbol{\alpha}\,T)\right\} \quad , \tag{7.14}$$

where $K \equiv 2m\,\pi/P$ is the lasing frequency of the unperturbed laser. Repeat of this calculation for $k_{cw}(T)$ produces a similar expression, recovered from Eq. (7.14) with the substitution $\boldsymbol{A} \rightarrow -\boldsymbol{A}$.

When the oppositely propagating beams are recombined a beat will be observed with wave number

$$|k_{ccw} - k_{cw}| = 4\,\frac{K}{c\,P}\;|\;\boldsymbol{A}\cdot(\boldsymbol{\Omega} + \boldsymbol{\omega} + \boldsymbol{\alpha}\,T)\;| \quad . \tag{7.15}$$

Thus the beat frequency is that predicted by the Sagnac effect for an identical ring with an angular velocity equal to this ring's angular velocity at the instant

of measurement. Eq. (7.15) is also the correct expression for the beat frequency of a ring laser with arbitrary geometry. This follows from Eq. (7.7), valid for any ring geometry, giving the difference between $(T_1)_{ccw}$ and $(T_1)_{cw}$ as $-4/c^2\, \boldsymbol{A} \cdot \{\boldsymbol{\Omega} + \boldsymbol{\omega} - P\boldsymbol{\alpha}/2c\}$. Upon determining the lasing frequency for the opposite modes and taking the difference to obtain the beat frequency, one finds that all other terms of order α cancel and the correct expression for the beat frequency for a ring laser of arbitrary geometry is given by Eq. (7.15).

This provides a significant generalisation of the result of Takahashi and Baierlein [143] and now encompasses arbitrary ring geometry with both angular acceleration and velocity about separated and arbitrary axes. Takahashi and Baierlein found the beat frequency of a ring laser in the special case of a circular ring laser with angular acceleration about its centre of symmetry and parallel to the vector area of the interferometer. Furthermore, this analysis demonstrates the linearity of the Sagnac effect for an active ring laser device under the addition of non-parallel angular velocities. An error in the analysis of Fateev [43, Eq.(29)] has also become apparent. Fateev matched the phases of the opposite beams upon a transit of the ring perimeter, but failed to account for the changing frequency of the laser and thus incorrectly obtained an extra contribution of $-2\,K\,\boldsymbol{\alpha} \cdot \boldsymbol{A}\,/c$ to the beat frequency. In section 7.5 we derive the optical response of a ring laser by solving Maxwell's equations. From this approach we again obtain Eq. 7.15 and the error of Fateev is transparent.

An unexpected consequence of Eq. (7.14) is that, through the presence of the term $-K\,\boldsymbol{g} \cdot \boldsymbol{h}/c^2$, a ring laser is, in principle, sensitive to the location of the axis of acceleration at first order in $\boldsymbol{\alpha}$. If clocks of arbitrary accuracy were to measure the frequency of the *ccw* laser beam at three mirrors, then the value and direction of $\boldsymbol{g} = \boldsymbol{\alpha} \times (\boldsymbol{C} - \boldsymbol{R})$ relative to the plane of the ring laser could be deduced. From the time derivative of the beat frequency $\boldsymbol{\alpha} \cdot \boldsymbol{A}$ is also known. Combining these four measurements one is able to determine where the axis of acceleration intersects the plane of the ring laser. This novel prediction is in contrast with the Sagnac effect for a ring laser with constant angular velocity, for which the lasing frequency is independent of the location of the axis of rotation at first order in angular velocity. However, this prediction is not expected to be observable within current technology, but it does provide an interesting feature as a matter of principle.

7.5 Solution of Maxwell's equations for a ring laser with angular acceleration

In the previous three sections we have provided a comprehensive treatment of an accelerating interferometer which has its mirrors separated by vacuum. This vacuum assumption enabled us to work entirely from a reference inertial frame I, providing a straightforward and intuitive analysis. The analysis given for a ring laser with angular acceleration demonstrated that its beat frequency is exactly that of an instantaneously comoving ring laser with constant angular velocity, irrespective of the relative orientations of the ring laser and angular acceleration.

In assuming the mirrors were separated by vacuum we have, however, failed to accurately model a ring laser, which requires a low pressure gas with population inversion along a portion of the beam for lasing to occur. Therefore, in this section we treat the ring laser as containing a gas with constant refractive index, n. We formulate and solve the covariant form of Maxwell's equations in the angularly accelerating frame of our ring laser. The solution thus obtained immediately determines the lasing frequency and output beat frequency and these results are in complete agreement with the results of sections 7.4 in the vacuum limit. While this provides a better model for an active ring laser device with angular acceleration than that given in the previous section, there are several obvious shortcomings in this model. For example, an effect of angular acceleration is to compress the gas, causing a gradient in the refractive index throughout the ring laser. Furthermore, because a portion of the beam is excited by a radio frequency power supply, we cannot regard the gas as homogeneous and dispersionless. Nevertheless, the effects of inhomogeneity in the refractive index of the gas cancel if the beams follow identical paths but in opposite directions. This simplification results in the assumption of constant refractive index providing a sufficiently good model for the predominant features of the optical output to be predicted.

In formulating Maxwell's equations we make the additional assumption, for calculational simplicity, that the angular acceleration vector is parallel to the vector area of the ring laser. This assumption is not unreasonable within the experimental sphere of the Canterbury Ring Laser Group. Interest in a ring laser with angular acceleration stems from the use of the Canterbury Ring Laser to monitor torsional modes in an earthquake [139]. In so far as we may approximate the angular acceleration felt by the ring laser during an earth-

quake by a time dependent vector perpendicular to the Earth's surface, this analysis provides a satisfactory model. From the Sagnac effect for a ring laser with constant angular velocity and the results of the previous section, we would not expect predictions obtained using this approximation to be unrealistic. We would expect, however, upon considering a more general case, the predicted beat frequency would have to be multiplied by the cosine of the angle between the vector area of the ring laser and its angular acceleration. If that were the only experimentally significant effect of such a generalisation, then the measured beat frequency of the ring laser could not, in itself, resolve the relative orientation of $\boldsymbol{\alpha}$ to $\boldsymbol{A}$, being indistinguishable from a reduced magnitude of the angular acceleration. The solution of this more realistic model of a ring laser with angular acceleration provides the theoretical foundation for the Fourier analysis methods used when analysing the output spectra of the Canterbury Ring Laser recorded during an earthquake.

7.5.1 Maxwell's equations in a angularly accelerating frame of reference

A coordinate system, S, with both angular velocity Ω and angular acceleration α about the z axis of an inertial frame I may be defined by a Galilean transformation to rotating coordinates,

$$\begin{aligned} T &= t \ , \\ X &= x\cos\left(\Omega t+\alpha t^2/2\right)-y\sin\left(\Omega t+\alpha t^2/2\right) \ , \\ Y &= y\cos\left(\Omega t+\alpha t^2/2\right)+x\sin\left(\Omega t+\alpha t^2/2\right) \ , \\ Z &= z \ , \end{aligned} \tag{7.16}$$

which is valid on a restricted region of the spacetime manifold $\sqrt{x^2+y^2} < c/(\omega+\alpha t)$, and again we adopt the convention that uppercase letters represent inertial coordinates and lowercase letters represent non-inertial coordinates. If an arbitrary point (x,y,z) in S is fixed then Eqs. (7.16) predict that this point will follow a circular trajectory in I with angular acceleration α about the origin, such that S defines a frame of reference with angular acceleration relative to I. The line element for S is

$$\begin{aligned} ds^2 &= -\left(1-\frac{(\Omega+\alpha t)^2(x^2+y^2)}{c^2}\right)c^2\,dt^2+dx^2+dy^2+dz^2 \\ &\quad +(\Omega+\alpha t)\,(x\,dy-y\,dx)\,dt \ . \end{aligned} \tag{7.17}$$

At first order in Ω and α this coordinate system has $\det(g_{\mu\nu}) = -1$ and $g_{\mu\nu} = g^{\mu\nu}$.

There has been considerable debate within the literature concerned with the correct physical interpretation of coordinates used to describe a rotating frame of reference [147, 103, 52, 23]. Our perspective is that S merely provides a convenient choice for labelling the points of the flat spacetime manifold. In so far as we may neglect the effects of length contraction in our ring laser, which arises at second order in Ω and α, then our ring laser appears stationary when viewed from S. Through this perspective we avoid the debate concerned with the physical interpretation of our rotating coordinate system. It is noted, in passing, that the Galilean transformation has been universally accepted as an appropriate description of a rotating frame of reference at first order in angular velocity, which is the order to which we are interested. Furthermore, the coordinate transformations Eq. (7.16) are equivalent to those used by both Takahashi and Baierlein [143] and Fateev [43, 44] when considering the behaviour of a ring laser with angular acceleration.

For mathematical simplicity we assume the vector area of our ring laser $\boldsymbol{A}$ is parallel to its angular acceleration $\boldsymbol{\alpha}$, which automatically aligns $\boldsymbol{A}$ parallel to the z axis. In the Canterbury Ring Laser the electric field is polarised parallel to $\boldsymbol{A}$ and therefore the only nonzero component of $\boldsymbol{E}$ is E_z, which is itself independent of z. The covariant formulation of Maxwell's equations in a non-Minkowskian spacetime has been presented in section 6.2. Equation (6.10) leads immediately to the conclusion that B_z is also zero. From the covariant constitutive relations, Eqs. (6.16) and (6.17), and using the a metric components of Eq. (7.17), we obtain the non-zero components of the vectors $\boldsymbol{D}$ and $\boldsymbol{H}$ as

$$D_z = \epsilon\epsilon_0 E_z + \frac{\epsilon_0}{\mu}(\Omega + \alpha t)(x B_x + y B_y) \ ,$$

$$H_x = \frac{1}{\mu\mu_0} B_x - \frac{\epsilon_0}{\mu}(\Omega + \alpha t)\, x E_z \ ,$$

$$H_y = \frac{1}{\mu\mu_0} B_y - \frac{\epsilon_0}{\mu}(\Omega + \alpha t)\, y E_z \ ,$$

where we have used $\epsilon_0 \mu_0 = 1/c^2$. By taking the curl of Eq. (6.10) and using Eqs. (6.10) to (6.13) and the expressions above to substitute E_z in favour of D_z, H_x, H_y, B_x, B_y, we obtain the wave equation for the electric field with z polarisation in a frame of reference with angular acceleration about the z axis,

$$\frac{\partial^2 E_z}{\partial x^2} + \frac{\partial^2 E_z}{\partial y^2} - \frac{n^2}{c^2}\frac{\partial^2 E_z}{\partial x^2} = -2\frac{(\Omega + \alpha t)}{c^2}\left\{x\frac{\partial E_z}{\partial y} - y\frac{\partial E_z}{\partial x}\right\}\frac{\partial E_z}{\partial t}$$

$$-3\frac{\alpha}{c^2}\left\{x\frac{\partial E_z}{\partial y}-y\frac{\partial E_z}{\partial x}\right\} \quad . \tag{7.18}$$

This wave equation, derived assuming the gas of refractive index n through which the light is propagating is angularly accelerating with the ring laser, forms the basis of the following analysis.

7.5.2 Solution of Maxwell's equations for a ring laser with angular acceleration

Schleich and Scully [130, pp.1068-1071] have given the solution to the wave equation when a ring laser has constant angular velocity in vacuum, which Eq. (7.18) reduces to in the limit $\alpha \to 0$ and $n \to 1$. If again we locate N mirrors at $\boldsymbol{r}_l$ respectively and define the counterclockwise (ccw) path to be that for which l increase, then the solution of Schleich and Scully for the electric field along the perimeter of the ring joining the mirrors at $\boldsymbol{r}_l$ and $\boldsymbol{r}_{l-1}$ is

$$\begin{aligned} E_z \;=\; E_0 \exp i\Bigg\{\left(1-2\frac{\boldsymbol{A}\cdot\boldsymbol{\Omega}}{cP}\right)(-\omega_0 t+\boldsymbol{k}_l\cdot(\boldsymbol{r}-\boldsymbol{r}_{l-1})) \\ +\boldsymbol{r}_{l-1}\times\hat{\boldsymbol{k}}_l\cdot\boldsymbol{\Omega}\,\frac{\boldsymbol{k}_l\cdot(\boldsymbol{r}-\boldsymbol{r}_{l-1})}{c}+\phi_l\Bigg\} \quad , \end{aligned} \tag{7.19}$$

where $k_l \equiv |\boldsymbol{k}_l| = \omega_0/c$ in vacuum and $\boldsymbol{k}_l/k \equiv \hat{\boldsymbol{k}}_l = (\boldsymbol{r}_l-\boldsymbol{r}_{l-1})/|\boldsymbol{r}_l-\boldsymbol{r}_{l-1}|$ is the unit normal in the direction of the ccw laser beam, and ϕ_l is a constant phase. This solution is valid only along the path the beam follows. If one wished to obtain the solution in a small region surrounding the optical axis of the cavity then a numerical Gaussian beam optics approach would have to be used. For our current interests an analytic solution along the perimeter of the ring laser is sufficient. It should be appreciated that while we have adopted the vector notation, this solution and the remainder of this work has $\boldsymbol{A} \parallel \boldsymbol{\Omega} \parallel \boldsymbol{\alpha}$. This vector notation is adopted as it is more succinct than writing these equations in their component form.

In searching for a solution to Eq. (7.18) we modify Eq. (7.19) to include angular acceleration and we also require that $n \neq 1$. The most immediately obvious changes are to let $\boldsymbol{\Omega} \to \boldsymbol{\Omega}+\boldsymbol{\alpha}t$, $\boldsymbol{\Omega}t \to \boldsymbol{\Omega}t+\boldsymbol{\alpha}t^2/2$ and $\omega_0 = ck \to \omega_0 = ck/n$. However, if we now substitute these modifications to Eq. (7.19) into Eq. (7.18) we find that the wave equation is not satisfied. By introducing quadratic terms in $\hat{\boldsymbol{k}}_l\cdot(\boldsymbol{r}-\boldsymbol{r}_{l-1})$ in the phase and damping the electric field amplitude we are able to cancel any additional terms which arise. Through

this approach we are led to the solution

$$E_z = E_0 \left\{ 1 - \boldsymbol{r}_{l-1} \times \hat{\boldsymbol{k}}_l \cdot \boldsymbol{\alpha} \frac{\hat{\boldsymbol{k}}_l \cdot (\boldsymbol{r} - \boldsymbol{r}_{l-1})}{c^2} + 2 \frac{\boldsymbol{A} \cdot \boldsymbol{\alpha}}{c P} \left(\hat{\boldsymbol{k}}_l \cdot (\boldsymbol{r} - \boldsymbol{r}_{l-1}) - \frac{c t}{n} \right) \right\} \exp i\Phi_l \ , \qquad (7.20)$$

where

$$\begin{aligned} \Phi_l = & - \left(1 - 2 \frac{\boldsymbol{A} \cdot (\boldsymbol{\Omega} + \boldsymbol{\alpha} t/2)}{n c P} \right) \omega_0 t + \left(1 - 2 \frac{\boldsymbol{A} \cdot (\boldsymbol{\Omega} + \boldsymbol{\alpha} t)}{n c P} \right) \boldsymbol{k}_l \cdot (\boldsymbol{r} - \boldsymbol{r}_{l-1}) \\ & + \boldsymbol{r}_{l-1} \times \boldsymbol{k}_l \cdot (\boldsymbol{\Omega} + \boldsymbol{\alpha} t) \frac{\hat{\boldsymbol{k}}_l \cdot (\boldsymbol{r} - \boldsymbol{r}_{l-1})}{n c} - \boldsymbol{r}_{l-1} \times \boldsymbol{k}_l \cdot \boldsymbol{\alpha} \frac{(\hat{\boldsymbol{k}}_l \cdot (\boldsymbol{r} - \boldsymbol{r}_{l-1}))^2}{2 c^2} \\ & + \boldsymbol{A} \cdot \boldsymbol{\alpha} \frac{k \, (\hat{\boldsymbol{k}}_l \cdot (\boldsymbol{r} - \boldsymbol{r}_{l-1}))^2}{c^2 P} + \phi_l \ , \end{aligned} \qquad (7.21)$$

The first term in Φ_l quadratic in $\hat{\boldsymbol{k}}_l \cdot (\boldsymbol{r} - \boldsymbol{r}_{l-1})$ was introduced to compensate for the time dependence of the term immediately before it, as the second term quadratic in $\hat{\boldsymbol{k}} \cdot (\boldsymbol{r} - \boldsymbol{r}_i)$ compensates for the time dependence of the coefficient of $\boldsymbol{k}_l \cdot (\boldsymbol{r} - \boldsymbol{r}_{l-1})$. With the addition of these quadratic terms in the phase we find

$$- \left(\frac{d\Phi}{dx} \right)^2 - \left(\frac{d\Phi}{dy} \right)^2 + \frac{n^2}{c^2} \left(\frac{d\Phi}{dt} \right)^2 = - \frac{\omega_0}{c^2} (\boldsymbol{\Omega} + \boldsymbol{\alpha} t) \cdot \boldsymbol{r}_{l-1} \times \boldsymbol{k} \ ,$$

where we have used $\omega_0 \equiv c\,k/n$. Along the perimeter of the ring laser this result leads to the real portion of the LHS of Eq. (7.18) being equal to the first, and real, term which arises from the substitution of Eq. (7.20) into the RHS of Eq. (7.18). In drawing this equality we note $\boldsymbol{r}_{l-1} \times \boldsymbol{k} = \boldsymbol{r} \times \boldsymbol{k}$ if $\boldsymbol{r}$ lies along the line joining $\boldsymbol{r}_{l-1}$ and $\boldsymbol{r}_l$.

Imaginary terms on the LHS of Eq. (7.18) arise from both the second order derivatives of Φ_l and damping terms in the electric field amplitude. When we substitute Eqs. (7.20) into the wave equation we find that the imaginary terms arising from the second order derivative of Φ_l with respect to t are cancelled by the terms arising from the second order derivatives with respect to x and y of final term in Eq. (7.21). However, the second order derivatives of the first term quadratic in $\hat{\boldsymbol{k}}_l \cdot (\boldsymbol{r} - \boldsymbol{r}_{l-1})$ in Eq. (7.21) produce an imaginary term $-i\,\boldsymbol{\alpha} \cdot \boldsymbol{r}_{l-1} \times \boldsymbol{k}\ E_z/c^2$ on the LHS of Eq. (7.18). Along the ray perimeter, $\boldsymbol{r}_{l-1} \times \boldsymbol{k} = \boldsymbol{r} \times \boldsymbol{k}$ and therefore this term is exactly a third of the imaginary term which arises from the substitution of Eq. (7.20) into the final term on the RHS of Eq. (7.18). By damping the electric field amplitude by the term proportional to $\boldsymbol{r}_{l-1} \times \hat{\boldsymbol{k}}_l \cdot \boldsymbol{\alpha}$, as was done in Eq. (7.20), we are able to equate

the imaginary terms arising on both sides of Eq. (7.18) and thus fully satisfy the wave equation.

However, without the term proportional to $2\,\boldsymbol{A}\cdot\boldsymbol{\alpha}\,\hat{\boldsymbol{k}}_l\cdot(\boldsymbol{r}-\boldsymbol{r}_{l-1})$ in Eq. (7.20), the tracing of a snapshot in S around the ring perimeter would show the electric field amplitude is decreased by $2\,E_0\,\boldsymbol{A}\cdot\boldsymbol{\alpha}/c^2$. If E_z is to represent the electric field amplitude of a ring laser then it must return to its starting value when traced around the ring perimeter, otherwise the field would be multivalued. We are therefore forced to add the term $2\,E_0\,\boldsymbol{A}\cdot\boldsymbol{\alpha}\,\hat{\boldsymbol{k}}_l\cdot(\boldsymbol{r}-\boldsymbol{r}_{l-1})/(P\,c^2)$ to the electric field amplitude, which guarantees the electric field amplitude is unchanged when traced around a full transit of the ring perimeter. Addition of this term in turn requires the addition of $2\,E_0\,\boldsymbol{A}\cdot\boldsymbol{\alpha}t/(P\,n\,c)$ to the electric field amplitude for Maxwell's equations to be satisfied. This provides the physical motivation for all of the damping terms in Eq. (7.20). In tracing the electric field around the ring perimeter we have, of course, neglected the losses at each mirror and the subsequent gain in in the electric field amplitude at the radio frequency source.

In section 7.4, within the context of a transit time calculation, we found the lasing frequency of the ring laser by requiring the phase of the source to have evolved an integer number of 2π radians over the time of flight of a point of constant phase around the ring perimeter, and the frequency of the light having traversed the perimeter of the laser cavity was required to match the frequency of the source upon its return. In this section we show our solution does in fact describe a ring laser by applying very similar arguments, now within the context of a snapshot calculation.

At time t an observer O located at a point $\boldsymbol{r}$ between the mirrors at $\boldsymbol{r}_{l+1}$ and $\boldsymbol{r}_l$ will record a frequency

$$\begin{aligned}\omega(\boldsymbol{r},t) &= \frac{d\Phi_l}{d\tau}(\boldsymbol{r},t)\\ &= \omega_0\left\{1-2\,\frac{\boldsymbol{A}\cdot(\boldsymbol{\Omega}+\boldsymbol{\alpha}t/2)}{n\,c\,P}\right.\\ &\qquad\left.+\left(2\,\frac{\boldsymbol{A}}{P}-\boldsymbol{r}_{l-1}\times\hat{\boldsymbol{k}}_l\right)\cdot\boldsymbol{\alpha}\,\frac{\hat{\boldsymbol{k}}_l\cdot(\boldsymbol{r}-\boldsymbol{r}_{l-1})}{c^2}\right\}\ , \qquad (7.22)\end{aligned}$$

where τ is the proper time along the worldline of O, equal to t at first order. In S all of the mirrors are stationary and therefore the frequency of the incident and reflected light are equal at each mirror. Matching Eq. (7.22) at each mirror

gives the frequency of the light at $\boldsymbol{r}_l$ at t,

$$\omega(\boldsymbol{r}_l,t)=\omega(\boldsymbol{r}_0,t)+\frac{2}{c^2}\,\boldsymbol{\alpha}\cdot\left\{\frac{\boldsymbol{A}}{P}\sum_{j=1}^{l}\Delta r_j-\sum_{j=1}^{l}\boldsymbol{A}_j\right\}\ , \tag{7.23}$$

where $\Delta r_j\equiv|\boldsymbol{r}_j-\boldsymbol{r}_{j-1}|=\hat{\boldsymbol{k}}_j\cdot(\boldsymbol{r}_j-\boldsymbol{r}_{j-1})$ and we have noted $\boldsymbol{r}_{l-1}\times\hat{\boldsymbol{k}}_l\,\Delta r_l=\boldsymbol{r}_{l-1}\times\boldsymbol{r}_l=2\,\boldsymbol{A}_l$ along the path of the laser beam. The frequency of our laser beam at $\boldsymbol{r}_N$ at any instant t is found by summing Eq. (7.23) from $j=1$ to N. Both summations add to $\boldsymbol{A}$ and cancel, predicting that the frequency of our laser beam at $\boldsymbol{r}_N\equiv\boldsymbol{r}_0$ is $\omega(\boldsymbol{r}_N,t)=\omega(\boldsymbol{r}_0,t)$ so that the frequency at $\boldsymbol{r}_0$ is single valued, which is required for our solution to describe a ring laser. An almost identical argument to that above demonstrates that the amplitude of E_z returns to its initial value when traced around the ring perimeter.

For our solution to describe a ring laser operating at its resonant frequency we require, at any moment t, that the phase change upon a transit of the ring perimeter is an integer number of 2π radians. Fixing t, Eq. (7.21) gives the phase change upon a transit of the ring perimeter as

$$\begin{aligned}\Delta\Phi &= \sum_{j=1}^{N}\{\Phi_j(\boldsymbol{r}_j,t)-\Phi_j(\boldsymbol{r}_{j-1},t)\}\\ &= k\left\{P+\frac{2}{n\,c}\sum_{j=1}^{N}\left(\frac{\boldsymbol{A}}{P}\Delta r_j-\boldsymbol{A}_j\right)\cdot(\boldsymbol{\Omega}+\boldsymbol{\alpha}t)\right.\\ &\qquad\left.+\frac{1}{c^2}\sum_{j=1}^{N}\left(\boldsymbol{A}_j\,\Delta r_j-\frac{\boldsymbol{A}(\Delta r_j)^2}{P}\right)\cdot\boldsymbol{\alpha}\right\}\ .\end{aligned} \tag{7.24}$$

The first summation vanishes automatically, which demonstrates that k is independent of time for arbitrary ring geometry. This is an important issue of consistency, as Maxwell's equations would not hold if k was time dependent. The second summation is more difficult. If, however, each arm of the ring laser cavity is of equal length, as is the case for the Canterbury ring laser, then $\Delta r_j=P/N$ and this summation equals $P/N\,\{\boldsymbol{A}-\boldsymbol{A}\}$ which also vanishes. Setting $\Delta\Phi=2\pi m$ we obtain $k=2\pi\,m/P$ such that $\omega_0=2\pi\,m\,c/(nP)$.

The solution for the clockwise (cw) beam is found by by letting $\boldsymbol{k}_l\rightarrow-\boldsymbol{k}_l$. In order to satisfy the wave equation we must change the sign of all terms proportional to $\boldsymbol{\Omega}$ and $\boldsymbol{\alpha}$ in Eq. (7.20) and Eq. (7.21). Upon recombining the beams, Eq. (7.22) predicts a beat frequency

$$\Delta\omega(t)=|\omega_{ccw}(t)-\omega_{cw}(t)|=4\,\omega_0\,\frac{\boldsymbol{A}\cdot(\boldsymbol{\Omega}+\boldsymbol{\alpha}t)}{n\,c\,P}\ , \tag{7.25}$$

which, again, is the beat frequency for a uniformly rotating ring laser instantaneously co-rotating with our angular accelerating ring laser. In the vacuum limit we recover Eq. (7.15), the key result of section 7.4, but calculated from an entirely different perspective. We remind the reader that throughout this derivation we have assumed $\boldsymbol{A} \parallel \boldsymbol{\Omega} \parallel \boldsymbol{\alpha}$, but the shape of our planar ring laser, and the location of the centre of rotation relative to the ring laser, are arbitrary. This provides a significant generalisation of result of Takahashi and Baierlein [143] who also solved Maxwell's covariant equations but considered only the simpler problem of a circular ring laser with angular acceleration about its centre of symmetry.

In order to complete the comparison with the results of section 7.4 we return to the case of a ring laser which forms a regular N sided polyhedron with its centre of symmetry located at $\boldsymbol{r} = \boldsymbol{C}$. As in section 7.3, we can now replace $\boldsymbol{\alpha} \cdot \boldsymbol{A}_j$ in the summation of Eq. (7.23) with $\boldsymbol{\alpha} \cdot \boldsymbol{A}/N + 1/2\ \boldsymbol{\alpha} \times \boldsymbol{C} \cdot \Delta \boldsymbol{r}_j$. The summation then produces

$$\omega(\boldsymbol{r}_l, t) = \omega_0 \left\{ 1 - \frac{\boldsymbol{g} \cdot \boldsymbol{h}}{c^2} \right\} \quad , \tag{7.26}$$

where, in this instance, $\boldsymbol{h} \equiv \boldsymbol{r}_l - \boldsymbol{r}_0$ and again $\boldsymbol{g} \equiv \boldsymbol{\alpha} \times \boldsymbol{C}$. This reproduces exactly the gravitational redshift effect predicted by Eq. (7.14), and is independent of the refractive index of the medium. Thus our solution for a ring laser with angular acceleration is in full agreement with our previous results derived using a transit time approach. Our solution to Maxwell's equations, however, also contains information on the time and spatial dependence of the electric field amplitude. This information could also have been derived from the transit time approach if we had chosen to calculate changes in the electric field amplitude when the light was reflected from mirrors moving relative to I.

An intuitive picture for the beat frequency measured by a ring laser with constant angular velocity was given by Schulz-DuBois [131]. At any instant of time, in the inertial frame I' with which $\boldsymbol{C}$ is comoving, Schulz-DuBois envisioned a standing electromagnetic wave pattern which stretches from one mirror to the next, rather like pearls on a necklace. In I' the detector has an angular velocity Ω, and it samples the antinodes of the standing wave pattern as it moves. In this model of Schulz-DuBois it is the sampling of the antinodes, or the pearls of the necklace, which is the observed beat frequency. If we now extend this model to the case of a ring laser with angular acceleration we observe that at any instant of time the centre of the ring laser cavity has an acceleration $\boldsymbol{g}$. Therefore the frame with which Schulz-DuBois' standing wave

pattern is comoving, S', is now a frame with linear acceleration $\boldsymbol{g}$. Schulz-DuBois' standing wave pattern must now satisfy Maxwell's equations in S'. In an accelerating frame gravitational redshift is a familiar concept and the term $-\omega_0\ \boldsymbol{g}\cdot\boldsymbol{h}/c^2$ in Eq. (7.26) is naturally interpreted as arising from this gravitational frequency shift. In S' the detector has an angular velocity $\Omega+\alpha t$ relative to Schulz-DuBois' standing wave pattern such that the observed beat frequency is that predicted by Eq. (7.25).

7.5.3 Sagnac interferometer with angular acceleration: a comparison

Having established the consistency of our solution to Maxwell's equations for a ring laser with our vacuum transit time approach of section 7.4, we return to the example of a Sagnac interferometer with angular acceleration. This both demonstrates that our solution to Maxwell's equations in this context is consistent with our earlier calculation given in section 7.2 and, through this analysis, the error made by Fateev when calculating the beat frequency for an angularly accelerating ring laser becomes transparent.

If we locate a harmonic source with frequency ω_0 and constant electric field amplitude E_0 at $\boldsymbol{r}_0$, then the wave equation, Eq. (7.18) with these boundary conditions has the solution

$$E_z \;=\; E_0\left\{1-\boldsymbol{r}_{l-1}\times\hat{\boldsymbol{k}}_l\cdot\boldsymbol{\alpha}\,\frac{\hat{\boldsymbol{k}}_l\cdot(\boldsymbol{r}-\boldsymbol{r}_{l-1})}{c^2}\right\}\exp i\Phi_l\ , \qquad (7.27)$$

where now

$$\begin{aligned}\Phi_l \;=\;& -\omega_0 t+\boldsymbol{k}_l\cdot(\boldsymbol{r}-\boldsymbol{r}_{l-1})+\boldsymbol{r}_{l-1}\times\boldsymbol{k}_l\cdot(\boldsymbol{\Omega}+\boldsymbol{\alpha}t)\,\frac{\hat{\boldsymbol{k}}_l\cdot(\boldsymbol{r}-\boldsymbol{r}_{l-1})}{n\,c}\\ &-\boldsymbol{r}_{l-1}\times\boldsymbol{k}_l\cdot\boldsymbol{\alpha}\,\frac{(\hat{\boldsymbol{k}}_l\cdot(\boldsymbol{r}-\boldsymbol{r}_{l-1}))^2}{2\,c^2}+\phi_l\ . \qquad (7.28)\end{aligned}$$

By matching the frequency of the light at each mirror we find that light which has propagated once around the ring perimeter has changed in frequency and become

$$\omega(\boldsymbol{r}_N)=\omega_0\left\{1-2\,\frac{\boldsymbol{\alpha}\cdot\boldsymbol{A}}{c^2}\right\}\ ,$$

which is independent of time as our source is harmonic and stationary in S. This frequency shift, which is also independent of the refractive index of the material through which the light propagates, is exactly that predicted previously for vacuum using a transit time calculation, Eq. (7.8).

Calculation of the phase shift observed in a Sagnac interferometer with angular acceleration is complicated by the fact that $|\boldsymbol{k}_l| = n\,\omega_l/c$ for the *ccw* beam is no longer constant around the ring interferometer but is given by

$$k_{ccw}(\boldsymbol{r}) = k_0 \left\{ 1 - \frac{2}{c^2} \sum_{j=1}^{l-1} \boldsymbol{\alpha} \cdot \boldsymbol{A}_j \right\} \quad , \tag{7.29}$$

which follows from matching ω_l at each mirror. The terms quadratic in $\hat{\boldsymbol{k}} \cdot (\boldsymbol{r} - \boldsymbol{r}_l)$ in Eq. (7.28) cancel upon taking the difference between the phase of the *ccw* and *cw* path. The terms linear in $\hat{\boldsymbol{k}} \cdot (\boldsymbol{r} - \boldsymbol{r}_l)$ produce a phase difference of $4\,\omega_o\,\boldsymbol{A} \cdot (\boldsymbol{\Omega} + \boldsymbol{\alpha} t)/c^2$ between the opposite beams, which is the instantaneous Sagnac phase shift. The contribution to the phase shift due to the variation of k around the beam perimeter can be calculated by noting that, at any point $\boldsymbol{r}$ along the ring perimeter, $k_{ccw} - k_{cw} = -2\,k\,\boldsymbol{\alpha} \cdot \boldsymbol{A}/c$, which follows from Eq. (7.29) and its *cw* equivalent. Upon summing around the ring perimeter this effect contributes a phase shift $-2\,n\,\omega_0\,\boldsymbol{\alpha} \cdot \boldsymbol{A}\,P/c^3$. Thus the total phase change due to the motion of the interferometer is

$$\Delta\Phi = 4\,\frac{\omega_0}{c^2} \left\{ \boldsymbol{A} \cdot \left(\boldsymbol{\Omega} + \boldsymbol{\alpha} \left(t - \frac{n\,P}{2\,c} \right) \right) \right\} \quad , \tag{7.30}$$

which is of the same form of the Sagnac effect, but has the angular velocity of the interferometer averaged over the time of flight of a photon around the ring in place of the usual angular velocity. This result agrees with Eq. (7.7) in the limit as $n \rightarrow 1$, which demonstrates the consistency of the two approaches.

Fateev's solution of Maxwell's equations [43] reduces to Eq. (7.27) in the appropriate limit. This solution is only valid if the source has constant frequency. Fateev then applied this solution to the case of a ring laser by demanding the total change in phase upon a circuit of the interferometer be 2π radians. This requirement led to the conclusion that ω_0 was a function of time. However, as Eq. (7.27) explicitly requires ω_0 to be constant for Maxwell's equations to hold, the solution which Fateev claimed described a ring laser with angular acceleration *is not itself a solution of Maxwell's equations.* Fateev failed to add the additional terms quadratic in $\hat{\boldsymbol{k}}_l \cdot (\boldsymbol{r} - \boldsymbol{r}_{l-1})$ to the phase, which appear in Eq. (7.21), and the terms linear in $\boldsymbol{\alpha} \cdot \boldsymbol{A}$ in the amplitude, given in Eq. (7.20), which are required for the wave equation and boundary conditions to be satisfied. Furthermore, as the frequency and amplitude of Eq. (7.27) change upon a transit of the ring perimeter, Fateev's description of the electric field within a ring laser with angular acceleration is not even single valued. This error led Fateev to the incorrect conclusion that the beat frequency measured when

a ring laser has angular acceleration differs from that of the instantaneous Sagnac effect by an amount $-2\omega_0\,\boldsymbol{\alpha}\cdot\boldsymbol{A}/c^2$.

In this chapter we have given the most complete analysis of a ring interferometer with angular acceleration yet reported. Our results complement and correct previous attempts at this problem. We have analysed the problem of light propagating in an interferometer with angular acceleration using two distinct calculational methods: a vacuum transit time approach was used in sections 7.2-7.4; and we formulated and solved the covariant form of Maxwell's equations in a frame of reference with angular acceleration in section 7.5.

Our results have shown the phase shift which would be observed in a Sagnac interferometer with angular acceleration is given by an expression of the same form as the usual Sagnac effect but has, for the angular velocity of the interferometer, its average over the time of flight of a photon around the ring perimeter. Furthermore, light propagating around an interferometer with angular acceleration is shifted in frequency by

$$\Delta\omega = -2\,\omega_0\,\frac{\boldsymbol{A}\cdot\boldsymbol{\alpha}}{c^2}$$

for each transit of the ring perimeter. We have demonstrated that a resonant cavity with angular acceleration will display optical ringing, having an asymmetric temporal response profile, the degree of asymmetry being proportional to the angular acceleration of the interferometer. Finally, the beat frequency for a ring laser with angular acceleration is given by the Sagnac beat frequency for an identical ring laser instantaneously co-rotating with our angularly accelerating ring laser.

Chapter 8

Oscillating mirror within a rotating ring laser

In this chapter we derive the optical response of a rotating ring laser with one mirror oscillating. For this analysis we develop a novel formalism, based upon geometric quantities, which enables phase shifts in non-Minkowskian frames of reference with time dependent boundary conditions to be calculated. We predict sideband structure will be observed when the counter-rotating beams, and when adjacent lasing modes, are combined and the output signal Fourier transformed.

8.1 Ring laser locking

In a provisional experiment of February 1993, a single mirror of the Canterbury Ring Laser was mounted on a piezo-electric crystal and oscillated with an amplitude of 0.05 μm and a frequency between 10 Hz and 1 MHz. At the adjacent mirror the clockwise and counterclockwise beams were combined, as illustrated in figure 8.1. Upon Fourier analysis of this signal no sideband structure was observed, nor was a reduction in the effect of mode pulling recorded for high frequency oscillations. Throughout this chapter this experiment will be referred to as the 'February 1993 oscillation of a piezo mounted mirror'. This provisional experiment was motivated by the suggestion of Kowalski [73] that oscillating a mirror parallel to its normal should lead to a reduction of coupling between the opposite beams of the ring laser, which is the physical cause of mode locking.

Mode pulling, which arises from coupling between the counter-propagating beams of a ring laser, is the source of one of the major experimental limitations associated with the performance of any ring laser. Dust and imperfections on the surface of the mirrors within a ring laser cause light from the *ccw* beam to be 'back-scattered' into the *cw* beam. If the opposite beams are of similar frequency then backscatter causes the frequency of the *ccw* beam to feedback

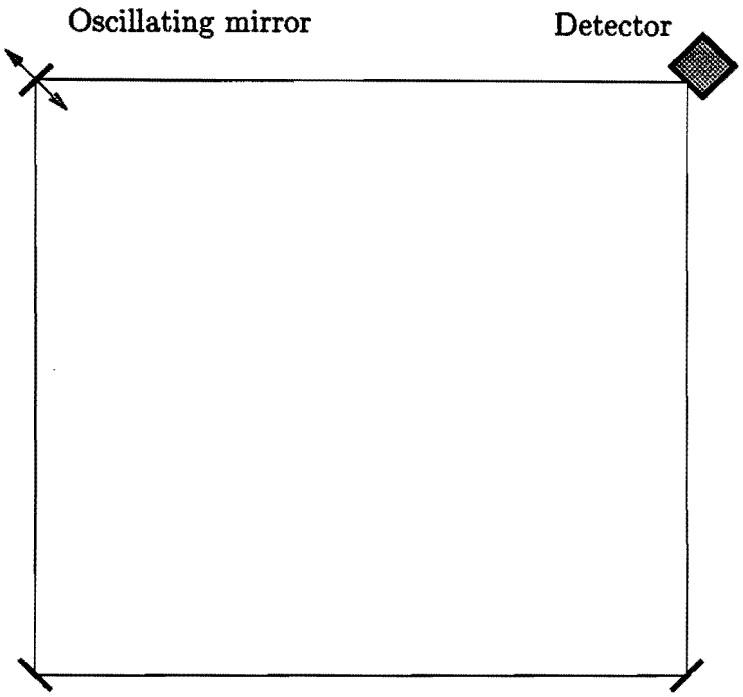

Figure 8.1: Schematic representation of the location of the oscillating mirror relative to the detector in the February 1993 oscillation of piezo mounted mirror experiment.

into the *cw* beam, and vice versa, and this optical feedback 'pulls' the frequencies of the opposite beams together [140]. If the contribution of backscatter becomes too large the opposite beams become locked, thus lasing at the same frequency and no beat between the opposite beams is observed. If we consider a ring laser which is sensitive to rotation through the Sagnac effect, then mode pulling may be understood through a simple intuitive model. While lasing the opposite beams of a ring laser form an electromagnetic standing wave pattern around the ring perimeter, rather like the beads of a pearl necklace [131]. As the ring laser rotates the detector moves past the beads of the necklace, the detection of the antinodes being the observed Sagnac beat frequency. In the absence of dirt and imperfections on the surface of the mirrors the beads are unaffected by the motion of the mirrors. When there is dirt, however, the beads tend to stick to the mirrors, causing a partial dragging of the necklace by the rotation of the ring laser. Because the necklace is now partially rotating with the laser itself, the rate of sampling of the antinodes, and thus the beat frequency, is reduced. If backscatter is so large that the entire necklace is held rigidly to the laser then no beat frequency is detected and the ring laser is 'locked', with the opposite beams lasing at the same frequency [140].

A common method for unlocking the opposite beams is to rapidly oscillate,

or dither, the entire ring laser [26]. This results in the opposite beams being frequency modulated in a non-reciprocal manner. A second method is to oscillate the cavity mirrors in a direction parallel to the plane of the mirror [27]. This generates a Döppler shift in the back-scattered light which reduces the coupling between the counter-propagating beams but does not modulate the lasing frequency. In both of these mechanisms the key idea is that the frequency of the light back-scattered from the *ccw* beam into the *cw* beam is substantially different from the lasing frequency of the *cw* beam. Because this frequency difference is significantly increased from when the laser is uniformly rotating with all mirrors stationary, the coupling between the opposite modes is reduced and the beams become unlocked.

In 1993 Kowalski suggested that oscillating a mirror parallel to its surface normal should also unlock the opposite beams of the ring laser [73]. This oscillation causes both beams of the laser to become frequency modulated. Central to Kowalski's proposal is that the frequency modulations of the *ccw* and *cw* beams are not simultaneous at all points along the perimeter of the laser. Therefore, the counter-propagating beams have an enhanced separation in frequency at each point around the perimeter of the ring. Because of this difference in frequency, calculated in detail in the following sections, Kowalski concluded that the back-scatter induced coupling between the opposite beams should be reduced, leading to a reduction in the effects of mode pulling.

In the following work we provide a full analysis of the effect of oscillating a mirror within a ring laser rotating with constant angular velocity Ω. Apart from the partial solution of Kowalski [73], the Canterbury ring laser collaboration has been unable to uncover any literature concerned with this problem. This is in spite of the many years of development of servo mechanisms of this sort, in which a mirror is mounted upon a piezo-electric crystal and is moved to compensate for drift in the lasing frequency arising from fluctuations in the ring perimeter due to thermal and pressure effects. Our work generalises that of Kowalski [73] in three significant aspects. Unlike Kowalski we assume a dispersive medium separates the mirrors of the ring laser. This provides a better physical model than that given by Kowalski, who assumed the light signals propagated at the speed of light in vacuum. Furthermore, Kowalski only considered the requirement that the optical path of the ring laser be $2\pi n$ radians when calculating the lasing frequency. In his analysis he neglected the Döppler effect off the moving mirrors entirely. As shown in section 7.5.3, neglect of the Döppler effect led to errors in the work of Fateev when analysing the behaviour

of a ring laser with angular acceleration. One of the features of our analysis is that we are very careful to incorporate the influence the Döppler effect due to the motion of the mirror. Finally, by working from the rotating frame of reference of the ring laser we include the effect of rotation within the calculational framework, whereas Kowalski added the Sagnac effect as a constant beat frequency at the conclusion of his calculation. Nevertheless, within this generalised framework, the central conclusions of Kowalski are recovered.

We do not derive the extent to which oscillating a mirror may unlock the opposite beams, as this work is outside the expertise of the author and beyond the scope of this thesis. Instead, we predict the Fourier transformed frequency spectra which would be recorded when a mirror is oscillated within the Canterbury Ring Laser. We obtain both the spectra recorded when the *ccw* and *cw* beams are mixed at the detector, and calculate the resulting spectra when two *ccw* beams are combined when the laser has several longitudinal modes operating simultaneously. From this perspective we regard oscillating a mirror within a ring laser cavity as simply an experiment in ring laser spectroscopy, and the predictions of this chapter contribute directly to the current experimental interests of the Canterbury Ring Laser Group.

Before proceeding with the analysis of this optical system it is intuitive to reflect upon the likely physical effects of moving a mirror within a lasing cavity. There are two obvious mechanisms which will both lead to the lasing frequency of the cavity being time dependent. Firstly, the motion of the mirror decreases (or increases) the perimeter of the lasing cavity. Because the lasing frequency is proportional to the inverse of the cavity perimeter, the changing optical path length of the cavity due to the motion of the mirror leads to the resonant frequency of the cavity becoming time dependent. A second mechanism for changing the lasing frequency arises from the Döppler effect. The rate at which the Döppler shift changes the frequency of the light within the lasing cavity is equal to the change in frequency upon each reflection divided by the time required for a point of constant frequency to propagate around the ring perimeter. An important conclusion of our analysis is that we show the rate at which the moving mirror causes the resonant frequency of the cavity to change is *exactly* the rate at which the Döppler effect changes the frequency of the light within the lasing cavity. Thus, any photon which is at the resonance frequency of the cavity at any time whatsoever will remain at the, now time dependent, resonant frequency of the cavity because of the influence of the Döppler effect.

We could begin our analysis by deriving the wave equation in a rotating frame, S, and proceed to search for a solution which satisfies the boundary condition that one mirror is moving. This approach would be similar to that followed in chapter 6 and section 7.5, where we derived and solved the wave equation for light propagating through linearly accelerating and angular accelerating dielectrics respectively. However, it is more economical to derive the lasing frequency using a snapshot approach. Our snapshot approach is based upon an invariant (frame independent) expression for the phase at one spacetime point relative to another. From this result it is straightforward to calculate the beat frequency between the counter-propagating beams, and the beat frequency between two counterclockwise beams when the laser has multi-mode operation.

The motion of the mirror causes the frequency of the laser beam to be Döppler shifted upon each reflection. Because we wish to determine the rate at which the Döppler effect changes the frequency of the light within the cavity we must determine the time required for a shift in frequency to propagate around the ring perimeter. We therefore calculate the velocity of a frequency modulated signal using standard Fourier methods. Again we base our Fourier analysis on an invariant expression for the phase. A bonus of this calculation is that it provides a transparent interpretation of the transit time technique, often used to calculate phase shifts in optical interferometry. This clarification is highly desirable as confusion over the interpretation and application of the transit time technique has resulted in some bizarre experimental predictions being reported in the literature [144, 70, 72, 74]

8.2 Invariant phase in a rotating frame of reference

We locate a ring laser of arbitrary geometry in a frame S with angular velocity Ω about the origin of an inertial frame I. This laser has N mirrors located in S at $\boldsymbol{r}_i(t)$ respectively. The time dependence in $\boldsymbol{r}_i(t)$ arises because these mirrors may have motion in S. We let $x_{i-1} \equiv x^{\mu}_{i-1} e_{\mu}$ and $x_i \equiv x^{\mu}_i e_{\mu}$ represent two separated spacetime points which lie along a spacetime curve C contained within the world sheet of our laser beam. Within a ray optics approximation the phase at x_i relative to x_{i-1} is

$$\Phi(x_i) - \Phi(x_{i-1}) = \int_{x_{i-1}}^{x_i} k_{\mu} dx^{\mu} \ , \tag{8.1}$$

where dx^μ follows the curve C. We note that this expression is based upon the coordinate-invariance of the phase and excludes the influence of helicity-rotation coupling, which was discussed in section 4.3. This neglect of helicity-rotation coupling can be justified on the basis that the magnitude of any such coupling would be down on the influence of the Sagnac effect by the ratio of the wavelength of light to the perimeter of the ring and would therefore be experimentally insignificant. Our expression for the difference in phase between two spacetime events is closely related to that given by Opat [114]. Opat began his analysis by defining the action functional

$$S\{x(\lambda), x_i, x_{i-1}\} = \int_{x_{i-1}}^{x_i} \mathcal{L}\,(x(\lambda), dx(\lambda)/d\lambda)\; d\lambda \;\; .$$

where the integration is along the curve C. Noting, for arbitrary endpoint variations $\delta S = \hbar k_\mu \delta x^\mu = \hbar \delta \Phi$, Opat obtained an expression for the phase

$$\Phi(x_i) - \Phi(x_{i-1}) = \frac{1}{\hbar} \int_{x_{i-1}}^{x_i} \mathcal{L}\, d\lambda \;\; .$$

From this argument it is clear that Eq. (8.1) can be recovered directly in the limit $\delta x \rightarrow dx$, which provides the link between the two approaches. Furthermore, the approach outlined below for the specific example of a rotating ring laser with an oscillating mirror is as flexible as the formalism of Opat and can be applied to the problems of wave propagation through media, in an arbitrary spacetime, and with time dependent boundary conditions.

Because the contraction $k_\mu dx^\mu$ is an invariant it follows that Eq. (8.1) is independent of the frame in which it is evaluated. We are therefore free to evaluate this geometric expression in which ever coordinate system proves convenient. In the current analysis we work within the spacetime of the rotating frame S in which our ring laser is stationary.

Our rotating frame S, at first order in Ω, has the spacetime metric given by Eq (7.17) with $\alpha = 0$,

$$ds^2 = -c^2\, dt^2 + d\boldsymbol{r}^2 + \boldsymbol{\Omega} \cdot \boldsymbol{r} \times d\boldsymbol{r}\; dt \;\; .$$

It follows that the difference in phase between two points along C is

$$\Phi(x_i) - \Phi(x_{i-1}) = \int_{x_{i-1}^\mu}^{x_i^\mu} \left\{ -c\, k^0\; dt + \boldsymbol{k} \cdot d\boldsymbol{r} + \boldsymbol{\Omega} \cdot \boldsymbol{r} \times \boldsymbol{k}\; dt + \frac{k^0}{c}\; \boldsymbol{\Omega} \cdot \boldsymbol{r} \times d\boldsymbol{r} \right\} \;\; , \tag{8.2}$$

where $\boldsymbol{k} \equiv (k^x, k^y, k^z)$ and $d\boldsymbol{r} \equiv (dx, dy, dx)$ and these variables are evaluated in S. The variables k^μ are not required to be constants in the above analysis, but may be functions of the spacetime coordinates, $k^\mu(x)$.

In general relativity the frequency measured by any observer O who has a 4-velocity u^μ is given by $\omega = -k_\mu u^\mu$ [152, p.137] , which is independent of the frame in which it is measured. All observers stationary in S have a 4-velocity $u^\mu = (c, 0, 0, 0)$ at first order in Ω, such that

$$-\omega = g_{\mu\nu}\, k^\mu\, u^\nu = -c\, k^0 + \boldsymbol{\Omega}\cdot\boldsymbol{r}\times\boldsymbol{k} \ , \tag{8.3}$$

where ω represents the frequency of the laser beam as measured by an observer stationary in S. A second useful geometric invariant arises from the contraction of the wave vector with itself. An inertial observer, O', instantaneously comoving with an observer in S would also determine the light to have frequency ω. Furthermore, because the dielectric is stationary with respect to O' at the instant of measurement, the light would have a wavenumber $|\boldsymbol{k}'| = n(\omega)\,\omega/c$ according to O'. The spacetime of O has a Minkowski metric such that $k'_\mu k'^\mu = -\omega^2\,(1 - [n(\omega)]^2)/c^2$. As this is a geometric quantity it immediately follows that it also holds in S such that

$$\begin{aligned} -\frac{\omega^2}{c^2}\left(1-[n(\omega)]^2\right) &= k_\mu k^\mu \\ &= -(k^0)^2 + \boldsymbol{k}\cdot\boldsymbol{k} + \frac{2}{c}k^0\,\boldsymbol{\Omega}\cdot\boldsymbol{r}\times\boldsymbol{k} \ . \\ &= -\frac{\omega^2}{c^2} + \boldsymbol{k}\cdot\boldsymbol{k} \ , \end{aligned}$$

where we have taken the square of Eq. (8.3) and substituted this into the RHS of Eq. (8.4) in the final step. Therefore, in S, $|\boldsymbol{k}| = n\ \omega/c$, where we set $n(\omega) \equiv n$ for notational convenience.

If the medium through which the light is propagating is homogeneous and isotropic it follows that the group velocity, $\boldsymbol{g}$ and phase velocity, $\boldsymbol{p}$, are parallel. If we integrate along the path of the beam in S such that $d\boldsymbol{r} \parallel \boldsymbol{g}$ we also find $d\boldsymbol{r} \parallel \boldsymbol{k}$. Substituting of Eqs. (8.3) and $|\boldsymbol{k}| = n\ \omega/c$, into Eq. (8.2) we find

$$\Phi(x_i) - \Phi(x_{i-1}) = \int_{x_{i-1}}^{x_i} \left\{-\omega\ dt + \frac{n\,\omega}{c}\ d\boldsymbol{r} + \frac{\omega}{c^2}\,\boldsymbol{\Omega}\cdot\boldsymbol{r}\times d\boldsymbol{r}\right\} \ . \tag{8.4}$$

It is important to appreciate that the only physical assumption made in deriving Eq. (8.4), valid at first order in Ω, is that the medium at rest in S is homogeneous. This medium may be dispersive. Because Eq. (8.4) was derived from general principles we do not require that ω is constant along the path of integration, but may be a function of the spacetime coordinates x^μ. In section 8.4 we find ω, which describes the frequency of the laser beam in S when a mirror is moving, is both a function of time and the spatial coordinates.

Therefore, the flexibility within our formalism above is utilised in our calculation the lasing frequency for a ring laser with both rotation and one mirror oscillating.

It is useful, however, to consider the form of Eq. (8.4) if the wave at x_{1-i} has constant frequency. In section 7.2 we demonstrated, at first order in Ω, that the frequency of light propagating from one observer stationary in a rotating frame of reference to another is unchanged if the frame does not have angular acceleration. Using a simple geometric argument, Misner et al. [101, pp.63-4] also showed that light does not suffer a gravitational redshift at first order in Ω in a rotating system. Experimental support for this null redshift result at first order in Ω has been provided by several experiments performed using Mössbauer spectroscopy [58, 24, 25, 77] in which both source and receiver were mounted on a rotating disk. All of these experiments provided experimental verification of the transverse Döppler effect, which gives a frequency shift at second order in $|\boldsymbol{\Omega} \times \boldsymbol{r}|/c$. Equivalently, one can regard this frequency shift as a gravitational red shift induced by the effective gravitational field of the rotating frame of reference. Therefore, if the source is harmonic in S at x_{i-1} then ω in Eq. (8.4) is independent of x and is identical to the frequency of the radiation as measured at x_{i-1}. This result is particularly useful when we develop our transit time approach based on Fourier methods, as a harmonic basis wave-function at the source will be harmonic throughout S.

8.3 Sagnac effect

We first illustrate the consequences of Eq. (8.4) by considering the example of a Sagnac interferometer. Such an interferometer has all of its mirrors stationary in S and we locate a harmonic source with frequency ω_0 at $\boldsymbol{r}_0$. Taking a snapshot of the interferometer, such that $dt = 0$, and integrating Eq. (8.4) around the perimeter of the interferometer, we find that the beam has undergone a change in phase of

$$\Phi_{ccw} = \frac{\omega_0}{c}\left\{n\,P + 2\,\frac{\boldsymbol{\Omega}\cdot\boldsymbol{A}}{c}\right\} \quad . \tag{8.5}$$

The phase shift for the *cw* beam has an identical form but with $\boldsymbol{A} \rightarrow -\boldsymbol{A}$. Taking the difference between the *ccw* and *cw* beams we find

$$\Delta\Phi = 4\,\omega_0\,\frac{\boldsymbol{\Omega}\cdot\boldsymbol{A}}{c^2} \quad , \tag{8.6}$$

which is precisely the Sagnac phase shift. This calculation is closely related to that of Dresden et al. [34], who determined the phase shift by taking a snapshot

in the inertial frame I and then calculated the influence of the Döppler effect on the wave vector upon each reflection off the mirrors moving relative to I. In this approach we have worked entirely from the rotating frame. Therefore our mirrors are stationary and as such we need not concern ourselves with the Döppler effect.

Again we use the example of a Sagnac interferometer to illustrate how Eq. (8.4) can be incorporated into a transit time approach based upon Fourier analysis. A bonus of this analysis is that we derive an expression for the rate at which a frequency modulation of an input signal will propagate around the perimeter of the interferometer. In our analysis of a ring laser with an oscillating mirror it is necessary to determine the time interval required for a frequency modulation, induced by reflection from the moving mirror, to propagate around the perimeter of the ring. From this information we can determine the influence of the Döppler effect on light within the lasing cavity.

Assume a source at $\boldsymbol{r}_0$ injects an electromagnetic signal with time dependence $I(t)$ into the cavity. Decomposing this signal into its Fourier components at $\boldsymbol{r}_0$ we find

$$I(\omega) = \frac{1}{\sqrt{2\pi}} \int_{-\infty}^{\infty} I(t) \exp\{-i\omega t\}\, dt \ . \tag{8.7}$$

If we now take a snapshot of the ring interferometer then Eq. (8.4) tells us that the phase of each component wave at $\boldsymbol{r}_1$ is related to that at $\boldsymbol{r}_0$ by $\Phi(\boldsymbol{r}_1, t) = \Phi(\boldsymbol{r}_0, t) + \omega\{n\,\Delta r_1/c + 2\boldsymbol{\Omega}\cdot\boldsymbol{A}_1/c^2\}$, where $\Delta\boldsymbol{r}_1 \equiv \boldsymbol{r}_1 - \boldsymbol{r}_0$ and $\boldsymbol{A}_1 \equiv \frac{1}{2}\boldsymbol{r}_0 \times \boldsymbol{r}_1$. Thus the frequency components of the signal at $\boldsymbol{r}_1$, $O(\omega)$, are related to the frequency components of the wave at $\boldsymbol{r}_0$, $I(\omega)$, by

$$O(\omega) = I(\omega) \times \exp i\left\{\omega\left(\frac{n\,\Delta r_1}{c} + 2\frac{\boldsymbol{\Omega}\cdot\boldsymbol{A}_1}{c^2}\right)\right\} \ .$$

An inverse Fourier transform of $O(\omega)$ gives the time dependence of the field at $\boldsymbol{r}_1$:

$$\begin{aligned} O(t) &= \frac{1}{\sqrt{2\pi}} \int_{-\infty}^{\infty} O(\omega) \exp\{i\omega t\}\, d\omega \\ &= \frac{1}{\sqrt{2\pi}} \int_{-\infty}^{\infty} I(\omega) \times \exp i\left\{\omega\left(\frac{n\,\Delta r_1}{c} + 2\frac{\boldsymbol{\Omega}\cdot\boldsymbol{A}_1}{c^2}\right)\right\} \exp\{i\omega t\}\, d\omega \ , \\ &= I(t) \otimes \zeta(t) \ , \end{aligned} \tag{8.8}$$

where $\otimes$ represents the Fourier convolution, and

$$\zeta(t) = \frac{1}{\sqrt{2\pi}} \int_{-\infty}^{\infty} \exp i\left\{\omega\left(\frac{n\,\Delta r_1}{c} + 2\frac{\boldsymbol{\Omega}\cdot\boldsymbol{A}_1}{c^2}\right)\right\} \exp\{i\omega t\}\, d\omega \ ,$$

$$= \frac{1}{\sqrt{2\pi}} \exp\left(-i\,\omega_0^2\,\frac{\Delta r_1}{c}\,\frac{\partial n}{\partial \omega}\bigg|_{\omega_0}\right)$$
$$\times\delta\left\{t + \frac{n_0\,\Delta r_1}{c} + \frac{\omega_0\,\Delta r_1}{c}\,\frac{\partial n}{\partial \omega}\bigg|_{\omega_0} + 2\,\frac{\boldsymbol{\Omega}\cdot\boldsymbol{A}_1}{c^2}\right\}\ , \qquad (8.9)$$

where $\delta(t-t_0)$ represents the Dirac delta function and we have expanded the refractive index n about a carrier frequency ω_0 such that

$$n\,\omega = n_0\,\omega_0 + \frac{d}{d\omega}\{n\,\omega\}\bigg|_{\omega_0}(\omega-\omega_0) = n_0\,\omega + \omega_0\,\frac{\partial n}{\partial \omega}\bigg|_{\omega_0}(\omega-\omega_0)\ ,$$

and $n_0 \equiv n(\omega_0)$. Combining Eqs. (8.8) and (8.9) we find

$$O(t) = I\left(t - \frac{n_g\,\Delta r_1}{c} - 2\,\frac{\boldsymbol{\Omega}\cdot\boldsymbol{A}_1}{c^2}\right)\exp\left\{-i\,\omega_0^2\,\frac{\Delta r_1}{c}\,\frac{\partial n}{\partial \omega}\bigg|_{\omega_0}\right\}\ , \qquad (8.10)$$

where the group velocity refractive index

$$n_g \equiv n_0 + \omega_0\,\frac{\partial n}{\partial \omega}\bigg|_{\omega_0}\ .$$

This derivation of $O(t)$, derived using Fourier methods, provides an extension to a rotating frame of reference of earlier work of Stedman, who was concerned with the use of transit time techniques for phase calculations in an inertial frame [137].

If we apply Eq. (8.10) to a full transit of the ring perimeter in the *ccw* direction we find the value of the wave-function at the output is

$$O_{ccw}(t) = I\left(t - \frac{n_g\,P}{c} - 2\,\frac{\boldsymbol{\Omega}\cdot\boldsymbol{A}}{c^2}\right)\exp\left\{-i\,\omega_0^2\,\frac{P}{c}\,\frac{\partial n}{\partial \omega}\bigg|_{\omega_0}\right\}\ . \qquad (8.11)$$

Similarly, the wave function for the output of the *cw* beam is given by the same expression but with $\boldsymbol{A} \rightarrow -\boldsymbol{A}$. Thus we find, apart from dispersion causing a phase shift as the beams propagate around the ring perimeter, the temporal variation of the wave-function is unchanged by this transit. It is, however, retarded by a time interval $n_g\,P/c \pm 2\,\boldsymbol{\Omega}\cdot\boldsymbol{A}/c^2$, with positive and negative signs corresponding to the *ccw* and *cw* beams respectively. It is this difference in the degree of retardation which is the origin of the Sagnac effect. If we assume the input signal is harmonic, $I(t) = I_0\,\exp\{-i\,\omega_0\,t\}$, then this analysis again predicts that the phase of the beam having completed a transit of the interferometer relative to the phase of the source is

$$\Phi_{ccw} = \frac{\omega_0}{c}\left\{n\,P + 2\,\frac{\boldsymbol{\Omega}\cdot\boldsymbol{A}}{c}\right\}\ ,$$

and the *ccw* and *cw* beams differ in phase by

$$\Delta\Phi = 4\,\omega_0 \frac{\boldsymbol{\Omega}\cdot\boldsymbol{A}}{c^2}\ .$$

Thus we recover Eqs. (8.5) and (8.6) but derived from a substantially different point of view.

An important consequence of Eq. (8.11) occurs when we assume that $I(t)$ is not harmonic but is frequency modulated. In this instance an observer located at $\boldsymbol{r}_0$ who measures the frequency of *ccw* beam when it has completed one circuit of the interferometer will observe that a frequency modulation of the source has taken a time interval

$$\Delta t_{ccw} = n_g\, P/c + 2\,\Omega\cdot\boldsymbol{A}/c^2 \tag{8.12}$$

to propagate once around the perimeter of the interferometer.

It is worthwhile to consider how Eq. (8.11) should be interpreted in the context of a transit time calculation in an inertial frame of reference. If we let $\Omega \to 0$ then S becomes an inertial frame of reference. Equation (8.11) therefore proves that *the phase of the output signal is equal to the phase of the input signal retarded by a time interval equal to the distance separating these two observations divided by the group velocity of the signal.* In interpreting this proof it is tempting to assume that it is a point of constant phase which has propagated at the group velocity from the source to the receiver. Such an interpretation, however, is quite clearly incorrect. The temporal variation of the phase of $I(t)$ may be any function, but an observer at $\boldsymbol{r}_0$ would conclude that the points of constant phase are propagating at the phase velocity, $c/n \neq c/n_g$ if the medium is dispersive. Eq. (8.4) tells us that the output, $O(t)$, has an identical temporal variation as $I(t)$, and the amount by which the output lags the input depends on the group velocity. This *does not imply* that it is a point of constant phase which has propagated between each observation at the group velocity.

Nevertheless, several authors have derived the phase shift induced by rotation and Fresnel drag using a transit time approach through tracing points of constant phase around the perimeter of an optical interferometer. In most instances, when the source is harmonic and the boundary conditions are independent of time, such a technique will yield accurate predictions when one uses the phase velocity to extrapolate phase shifts. However, Takahashi [144] used a transit time approach to calculate the Sagnac effect when viewed from an inertial frame of reference. A misinterpretation of the roles of phase and

group velocity led Takahashi to claim that the relevant velocity when calculating the Sagnac phase shift was the group velocity when the dimensions of the interferometer were greater than the neutron or photon wavepacket, but one should use the phase velocity if the interferometer is smaller than the wavepacket. In a series of articles [70, 72, 74], Kowalski has calculated the phase shift within an optical and neutron interferometer containing accelerating media. In formulating these problems, Kowalski used a transit time approach and, for calculational simplicity, assumed the samples were moving with constant velocity, this velocity being the average velocity over the time required for a phase plane to propagate around the interferometer. While this approach may provide a correct first order result, Kowalski claimed a violation of the equivalence principle at higher orders. This apparent violation of the equivalence principle arises from the use of the transit time approach outside its scope of validity. If Kowalski had formulated and solved the covariant form of the appropriate wave equation in the experimental context discussed, as we did in chapter 6, then no violation of the equivalence principle would have been predicted. This may also be seen from the central result of chapter 3, where an accelerating frame and Schwarzschild geometry are equivalent if we neglect the influence of curvature.

In section 7.2 we used a transit time technique to calculate the phase shift induced by a ring interferometer with angular acceleration. In this calculation we assumed the mirrors were separated by vacuum. Therefore $n_g = n \equiv 1$ and, as such, no confusion arose because of differences between group and phase velocity. In this context the transit time approach has a natural interpretation as the tracing of a point of constant phase around the ring interferometer.

8.4 Rotating ring laser with a moving mirror

Having established the mathematical structure required in the following calculation, and demonstrated its consistency with respect to the Sagnac effect, we consider the case of a ring laser with a mirror at $\boldsymbol{r}_0$ moving with velocity

$$\frac{d\boldsymbol{r}_0(t)}{dt} = \boldsymbol{v}$$

in S. To establish the Döppler shift in frequency suffered by a photon reflected from this moving mirror we first consider a similar situation, but viewed from an inertial frame I. Suppose a photon with wavevector $\boldsymbol{k}_i$ and frequency ω_i is incident upon a mirror with constant velocity $\boldsymbol{v}$ in I. The rest frame of the

mirror is denoted I'. In I' the incident wave has frequency $\omega_i' = \omega_i - \boldsymbol{v}\cdot\boldsymbol{k}_i$ at first order in v/c. As the mirror is stationary in I' the frequency of the reflected beam $\omega_{i+1}' = \omega_i'$ with wave vector $\boldsymbol{k}_{i+1}' = \boldsymbol{k}_{i+1} - \boldsymbol{v}\,\omega_{i+1}/c^2$. Transforming back into I we find, at first order in velocity,

$$\omega_{i+1} = \omega_i \left\{1 + \frac{n}{c}\boldsymbol{v}\cdot(\hat{\boldsymbol{k}}_{i+1} - \hat{\boldsymbol{k}}_i)\right\} \quad , \tag{8.13}$$

where $\hat{\boldsymbol{k}}_{i+1} \equiv (\boldsymbol{r}_{i+1} - \boldsymbol{r}_i)/|\boldsymbol{r}_{i+1} - \boldsymbol{r}_i|$ and is the unit normal in the direction of the reflected beam, and $\hat{\boldsymbol{k}}_i$ is similarly defined. This calculation is similar to that of Dresden et al. [34]. However, Dresden et al. found, upon transforming in to the moving frame of their dielectric,

$$k_{i+1} = k_i \left\{1 + \frac{1}{nc}\boldsymbol{v}\cdot(\hat{\boldsymbol{k}}_{i+1} - \hat{\boldsymbol{k}}_i)\right\} \quad .$$

If we were to assume $k = n\omega/c$ in I then this result appears in conflict with Eq. (8.13). The cause of this discrepancy uncovers an important and subtle feature of special relativity. In their calculation Dresden et al. assumed the medium was comoving with the mirror, the mirror being attached to a rigid interferometer rotating about an arbitrary axis. Therefore, in I' we have $k' = n\omega'/c$ such that $k = n\,\omega/c\,\{1 - \boldsymbol{v}\cdot\hat{\boldsymbol{k}}(n - 1/n)\}$ in I. In deriving Eqs. (8.13), however, we assumed the mirror was moving relative to a dielectric of refractive index n which was stationary in I. Therefore $k = n\omega/c$ in I and $k' = n\,\omega'/c\,\{1 + \boldsymbol{v}\cdot\hat{\boldsymbol{k}}(n - 1/n)\}$ in I'. Our result differs from that of Dresden et al. because we matched the frequency of the incident and reflected beam in a frame in which the dielectric was not stationary,

In the current problem of interest the frame of reference in which the dielectric is stationary, S, is a rotating frame. As such it does not necessarily follow that the Döppler shift arising from reflection off the moving mirror is given by Eq. (8.13). To calculate this Döppler shift in S we first use the coordinate transformation relations, Eqs. (7.16) with $\alpha = 0$, to transform our incident 4-wavevector from S to I. We then note that if a mirror at $\boldsymbol{r}_i$ in S has velocity $\boldsymbol{v}_i$ in S, then its velocity in I is $\boldsymbol{v}_i + \boldsymbol{\Omega}\times\boldsymbol{R}_i$, where again we adopt the notation that spatial coordinates in an inertial frame are uppercase. Using Eq. (8.13) to determine the frequency of the reflected beam in I and transforming our 4-wavevector back into S we find Eq. (8.13) does, in fact, give the correct expression for the frequency of the reflected beam, to first order in velocity and angular velocity.

Because a ring laser contains at least two concave mirrors a modest misalignment in the orientation of the mirrors will be automatically compensated.

In such circumstances the laser beam is perturbed off the optical axis of the cavity and establishes a new orientation for which optical resonance can be maintained. When we oscillate a mirror in the ring laser cavity the ability of the ring laser to compensate for the perturbation of the cavity geometry is crucial for lasing to be maintained.

In figure 8.2 we illustrate the effect of the motion of the mirror on the optical beam path. In the following analysis we neglect path length and phase shift effects arising from the fact that the orientation of the incident and reflected beams, $\hat{\boldsymbol{k}}_0$ and $\hat{\boldsymbol{k}}_1$, are not constant with time. If the amplitude of the oscillations of the mirror at $\boldsymbol{r}_0$ is a_0, then this assumption is accurate to $(a_0/\Delta r_i)^2$. In the February 1993 oscillation of a piezo mounted mirror experiment, discussed in section 8.1, the amplitude of oscillation was $\sim 5 \times 10^{-8}$ m and the separation between each mirror was ~ 1 m, such that $(a_0/\Delta r)^2 \sim 2.5 \times 10^{-15}$, which justifies this approximation within the current experimental context. From figure 8.2 the change in path length of the optical beam in a time interval Δt is

$$\Delta P = -v\,\Delta t \left\{ \frac{\cos(\theta - \delta)}{\cos\delta} + \frac{\cos(\theta + \delta)}{\cos\delta} \right\} = 2\,v\,\Delta t\,\cos\theta \ , \tag{8.14}$$

where θ is the angle between the incident beam and the normal of the mirror, equal to half the angle between each arm of the interferometer. Figure 8.2 also illustrates

$$\boldsymbol{v} \cdot \left(\hat{\boldsymbol{k}}_{i+1} - \hat{\boldsymbol{k}}_i \right) = 2\,v\,\cos\theta \ ,$$

such that

$$\omega_{i+1} = \omega_i \left\{ 1 + 2\,n\,\cos\theta\,\frac{v}{c} \right\} \ . \tag{8.15}$$

For our laser with a moving mirror to operate we require that the change in phase upon a full transit of the ring perimeter is an integer number of 2π radians, with the boundary condition that the lasing frequency increases in magnitude by $2\,\omega_{ccw}\,n\,\cos\theta\,v/c$ per transit of the interferometer. This boundary condition is a direct consequence of Eq. (8.15), which states that this is the change in frequency for each reflection off the moving mirror.

In section 8.3 we established that a frequency modulation of the *ccw* beam will take a time interval Δt_{ccw}, given by Eq. (8.12), to propagate around the perimeter of the ring interferometer. For the frequency of the reflected beam at $\boldsymbol{r}_0(t)$, which we define $\omega_{ccw}(t)$, to match the frequency of the light which has completed a circuit of the interferometer in a time interval Δt_{ccw} and again been reflected, we require that the source has evolved in frequency

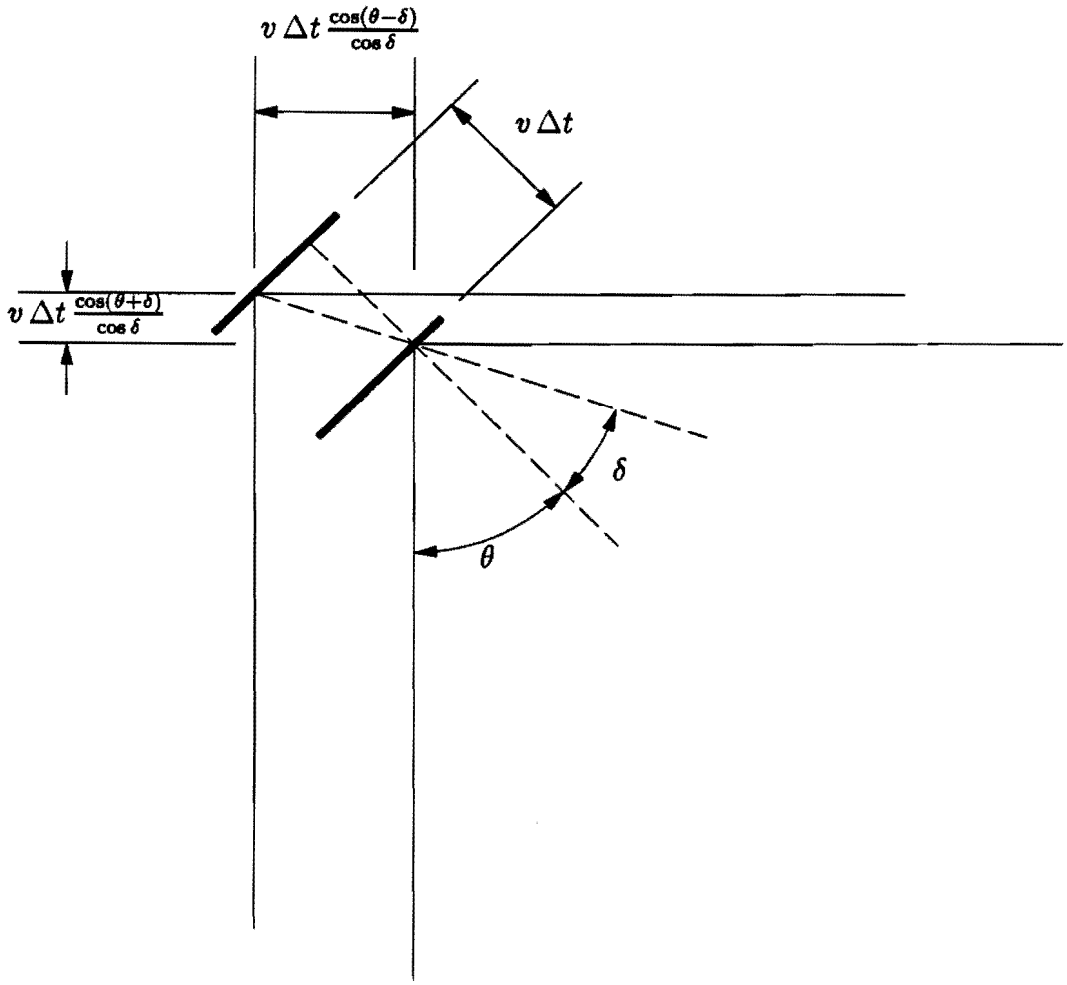

Figure 8.2: Change of the optical path length due to the motion of the mirror. This change of optical path is the sum of two terms, given by Eq. (8.14)

by $2\,\omega_{ccw}\,n\,\cos\theta\,v/c$ in this time interval. It immediately follows that $\omega_{ccw}(t)$ has the temporal variation

$$\frac{d\omega_{ccw}(t)}{dt} = 2\,\omega_{ccw}\,\cos\theta\,\frac{n}{n_g}\,\frac{v}{P}\ . \tag{8.16}$$

To calculate the change in phase upon a transit of the ring perimeter we take a snapshot of the laser at $t = 0$. Because the frequency modulation induced by the moving mirror at $\boldsymbol{r}_0(t)$ will propagate around the ring laser at the group velocity, it follows that there is a linear variation of $\omega(\boldsymbol{r})$ around the ring perimeter at the time of the snapshot. Defining λ as the distance around the ring perimeter in the *ccw* direction from $\boldsymbol{r}_0$ at $t = 0$ we find the frequency at λ is the frequency at $\boldsymbol{r}_0$ retarded by $\lambda\,n_g/c$. Integrating Eq. (8.16)

and substituting $t = \lambda n_g/c$ we obtain

$$\omega_{ccw}(\lambda) = \omega_{ccw}\left\{1 - 2n\,\cos\theta\,\frac{v}{c}\,\frac{\lambda}{P}\right\}\ ,$$

and hence

$$k(\lambda) = \frac{n\,\omega_{ccw}}{c}\left\{1 - 2n\,\cos\theta\,\frac{v}{c}\,\frac{\lambda}{P}\right\} - 2\,\frac{\omega_{ccw}^2}{c}\,\frac{\partial n}{\partial\omega}\bigg|_{\omega_{ccw}} n\,\cos\theta\,\frac{v}{c}\,\frac{\lambda}{P}\ ,$$

where ω_{ccw} is the frequency of the reflected beam at $\boldsymbol{r}_0$ at t=0, and we have expanded the refractive index in a Taylors series of first order in frequency. Substituting into Eq. (8.4) we find

$$\begin{aligned}
\Phi_{ccw} &= \oint\left\{k(\boldsymbol{r})\,d\boldsymbol{r} + \frac{\omega_{ccw}}{c^2}\,\boldsymbol{\Omega}\cdot\boldsymbol{r}\times d\boldsymbol{r}\right\}\ , \\
&= \int_0^P k(\lambda)\,d\lambda + 2\,\frac{\omega_{ccw}}{c^2}\,\boldsymbol{\Omega}\cdot\boldsymbol{A}\ , \\
&= \frac{n\,\omega_{ccw}\,P}{c}\left\{1 - n_g\,\cos\theta\,\frac{v}{c}\right\} + 2\,\frac{\omega_{ccw}}{c^2}\,\boldsymbol{\Omega}\cdot\boldsymbol{A}\ , \\
&= 2\,\pi\,m\ ,
\end{aligned} \tag{8.17}$$

and we have used $n_g = n + \omega_{ccw}\ \partial n/\partial\omega$. It immediately follows that the frequency at $t = 0$ is given by

$$\omega_{ccw} = \omega_{nat}\left\{1 + n_g\,\cos\theta\,\frac{v}{c} - 2\,\frac{\boldsymbol{\Omega}\cdot\boldsymbol{A}}{n\,P\,c}\right\}\ , \tag{8.18}$$

where $\omega_{nat} \equiv 2\pi mc/(nP)$ and is the frequency at which the laser would operate at if $\Omega = 0$ and all mirrors were stationary.

For an arbitrary time t the integration of Eq. (8.16) yields,

$$\omega_{ccw}(t) = \omega_{ccw} + 2\,\omega_{nat}\,\cos\theta\,\frac{n}{n_g}\,\frac{v\,t}{P}\ . \tag{8.19}$$

The reader should appreciate that this expression for the time dependence of the frequency at $\boldsymbol{r}_0(t)$ was derived from consideration of the Döppler effect. Given that the frequency at the source at $t = 0$ was defined by Eq. (8.18), such that the laser was at resonance at $t = 0$, then the requirement that the frequency of the light at $\boldsymbol{r}_0(t)$ always equals the frequency of the Döppler shifted light as it returns to $\boldsymbol{r}_0(t)$ led directly to Eq. (8.19).

However, it is not obvious that the influence of the Döppler effect constrains the frequency of the light within the lasing cavity to always be at the resonant frequency of the optical cavity. The requirement for optical resonance

at an arbitrary time follows from Eq. (8.14) which gives $P(t) = P - 2\cos\theta\, v\, t$. Substituting this time dependent optical perimeter into Eq. (8.18) and differentiating with respect to time tells us that the time dependence of $\omega_{ccw}(t)$ for optical resonance to be maintained is

$$\begin{aligned}\frac{d}{dt}\omega_{ccw}(t) &= 2\pi\, m\, c \frac{d}{dt}\left(\frac{1}{n\,P}\right) \ , \\ &= \omega_{nat}\left\{-\frac{1}{P}\frac{dP}{dt} - \frac{1}{n}\frac{dn}{dt}\right\} \\ &= \omega_{nat}\left\{2\cos\theta\frac{v}{P} - \frac{1}{n}\frac{dn}{d\omega}\bigg|_{\omega_{ccw}} \frac{d}{dt}\omega_{ccw}(t)\right\} \ .\end{aligned}$$

Moving the final term onto the LHS, dividing both sides by the coefficient of $d\omega_{ccw}(t)/dt$ and integrating we find

$$\omega_{ccw}(t) = \omega_{ccw} + 2\,\omega_{nat}\ \cos\theta\,\frac{n}{n_g}\frac{v\,t}{P} \ ,$$

which is identical to Eq. (8.19). Thus we have demonstrated that the influence of the Döppler effect and the influence of the time dependence of the optical path-length of the cavity perimeter lead to identical expressions for the temporal evolution of the lasing frequency. This proves that the two mechanisms by which a moving mirror alters the frequency of the light within the lasing cavity are not competing but require exactly the same temporal evolution of the frequency. Our analysis, therefore, provides justification for Kowalski's neglect of the influence of the Döppler effect [73].

It is, of course, possible to use the transit time technique derived in section 8.3 to calculate the phase shift upon a transit of the interferometer, as we did for the phase shift induced by rotation in a Sagnac interferometer. If one in careful to note that the path length of the ring laser perimeter is time dependent then Eq. (8.17) is recovered.

8.5 Output spectra of a rotating ring laser with one mirror oscillating

In the February 1993 oscillation of a piezo mounted mirror experiment performed at Canterbury, discussed in section 8.1, the mirror did not move with constant velocity but was oscillated. Our results of the previous section may be generalised to this situation by letting $v \rightarrow -a_0\,\beta\,\sin(\beta t)$, where a_0 is the amplitude of the oscillation, and β is the angular frequency of the oscillation.

If follows that $v(t)|_{t=0}$ vanishes in Eq. (8.18) and $vt \rightarrow \int_0^t v(t')dt' = a_0 \cos\beta t$ in Eq. (8.19). Similar expressions are found for the frequency of the *cw* beam with the additional change that $\boldsymbol{A} \rightarrow -\boldsymbol{A}$ in Eq. (8.18).

A second alteration to the the previous analysis arises from our definition of $\omega_{ccw}(t)$ as the the frequency of the laser beam in S when reflected off the oscillating mirror at t. In an experiment one would not attempt to mix the two beams at the moving mirror, but would combine these beams at a stationary mirror located at $\boldsymbol{r}_d$. In section 8.3 we demonstrated that the frequency at $\boldsymbol{r}_d$ is merely $\omega_{ccw}(t)$ delayed by the *ccw* distance around the ring perimeter from $\boldsymbol{r}_0(t)$ divided the group velocity of the light. Therefore, as our detector at $\boldsymbol{r}_d$ is a distance D from the oscillating mirror at $\boldsymbol{r}_0$, where $D \equiv \sum_{i=1}^{d} \Delta r_i$, the frequency at this mirror will be $\omega_{ccw}(t - D\,n_g/c)$. Similarly the frequency for the *cw* beam at $\boldsymbol{r}_d$ will be $\omega_{cw}(t - [P - D]\,n_g/c)$ where P is the perimeter of the ring laser.

8.5.1 Beat frequency between opposite beams

We first consider an experiment in which the *ccw* and *cw* beams are combined at the detector and the intensity recorded as a function of time. Eq. (8.19) with $v\,t \rightarrow a_0 \cos(\beta\{t - D\,n_g/c\})$ gives the time dependence of the lasing frequency for the *ccw* beam at $\boldsymbol{r}_d$. Similarly, with $v\,t \rightarrow a_0 \cos(\beta\{t - [P - D]\,n_g/c\})$ we obtain the time dependence for the *cw* beam. Combining the two beams at $\boldsymbol{r}_d$ we predict, from Eqs. (8.18) and (8.19), a beat frequency

$$\omega_{ccw}(t) - \omega_{cw}(t) = \omega_{nat}\left\{-4\,\frac{\boldsymbol{\Omega}\cdot\boldsymbol{A}}{n\,P\,c} - 2n\,\cos\theta\,\frac{a_0}{P}\,\frac{\beta\,[P-2D]}{c}\,\sin\left(\beta\left[t - \frac{P\,n_g}{2\,c}\right]\right)\right\} \quad (8.20)$$

where we have expanded $\sin(\beta[P - 2D]n_g/2c)$ to first order, which arises from the algebraic identity $\cos A - \cos B = 2\sin\{(A+B)/2\}\sin\{(B-A)/2\}$.

When comparing this result with that obtained by Kowalski [73, Eq. 6], who assumed the mirrors were separated by vacuum, we find full agreement when $n \rightarrow 1$. Kowalski obtained both of the terms in Eq. (8.20), although his derivation was considerably simplified by the vacuum assumption. Furthermore, Kowalski added the Sagnac beat frequency as a bias at the completion of his calculation, whereas we have deliberately included the influence of rotation within our formalism. Of crucial importance for Kowalski's suggestion that oscillating a mirror should unlock the opposite modes of the ring laser is that

the frequency separation between the opposite beams arising from the motion of the mirror will be larger than the Sagnac effect if $a_0\,\beta\,(P-2D) > \boldsymbol{\Omega}\cdot\boldsymbol{A}/n$. A large amplitude of oscillation at high frequency should have a significant impact on mode pulling if $L-2D$ is not zero for all mirrors. We note that for a square (or rectangular) ring laser, which includes that possessed by Canterbury, the frequency modulating term vanishes at the mirror opposite the oscillating mirror. Thus, this geometry will significantly suppress any mode coupling improvements achieved by oscillating a mirror parallel to its normal. It is interesting to note that, despite the inclusion of dispersion throughout this analysis, the only influence of dispersion on this beat frequency is through the dependence on n_g of the phase of the sine function, which would be unresolvable experimentally.

We now compare this prediction with the result of the provisional February 1993 oscillation of a piezo mounted mirror experiment. In this experiment the *ccw* and *cw* beams were combined at the mirror adjacent to the oscillating mirror. The Canterbury Ring Laser is rectangular with sides 0.838 m and 0.900 m, such that $D = 0.900$ m and $P = 3.476$ m. Sideband analysis in a precision ring laser has been discussed in detail by Stedman et al. [139]. A signal with the beat frequency given by Eq. (8.20) will produce an output potential at the photo-multiplier tube given by

$$\begin{aligned} V(t) &= \mathcal{R}\left\{V_c \exp i[\omega_c t + \gamma \sin(\beta t)]\right\} \ , \\ &= \mathcal{R}\left\{V_c \exp i\omega_c t \left[J_0(\gamma) + 2\sum_{n=1}^{\infty}\Big(i\,J_{2n-1}(\gamma)\,\sin([2n-1]\beta t)\right.\right. \\ &\qquad \left.\left. + J_{2n}(\gamma)\,\sin(2n\beta t)\Big)\right]\right\} \ . \end{aligned} \tag{8.21}$$

where $J_n(x)$ is an nth order Bessel function and

$$\gamma \equiv 2\,\omega_{nat}\,n\,a_0\,\cos\theta\,\frac{P-2D}{cP}$$

and is the ratio of the maximum frequency shift suffered by the light divided by the angular frequency of the mirror oscillation. We note that all factors of β have cancelled in this definition of γ, which causes the amplitude of any sidebands to be independent of the frequency at which the mirror is oscillated.

In the experiment of interest the mirror was oscillated from 10 Hz to 1 MHz with a maximum amplitude of 0.05 μm. This amplitude, with $\omega_0 = 3\times10^{15}$ and $\theta = \pi/4$ as Canterbury ring laser forms a right angled rectangle, yields $\gamma \approx 0.33$, which results in the height of the first, and largest, sideband relative to the carrier peak being [31] R $= J_1(\gamma)/J_0(\gamma) \approx 0.17$. In February 1993

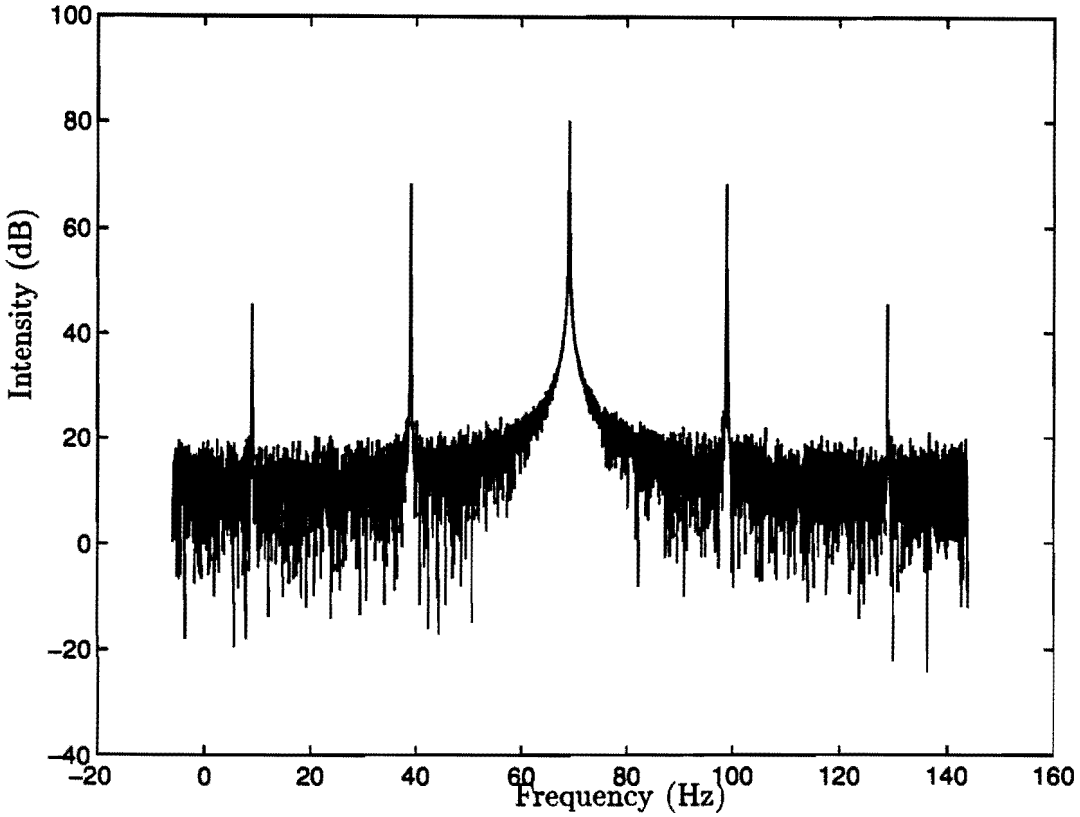

Figure 8.3: Numerical generation of the predicted spectra with $\gamma = 0.33$ and the noise floor 60 dB below the signal. In this example we assume $\beta = 30$ Hz, although the relative amplitudes of the sidebands is independent of β. The central peak is at 68.95 Hz, which corresponds to the beat between the opposite beams due to the rotation of the Earth.

the Canterbury ring laser had achieved a noise floor 60 dB below the carrier. Therefore any sideband with $R > 10^{-3}$ should have been resolvable. If the amplitude of the oscillation was accurately estimated to be 0.05 μm then the amplitude of the predicted sideband is two orders of magnitude larger than this noise floor, and should have been clearly visible. A numerical generation of the spectra expected in this experiment is given in figure 8.3. As stated in the introduction to this chapter, only a constant beat frequency of 68.95 Hz was observed, which arises from the Sagnac beat induced by the rotation of the Earth, and appeared unaffected by the oscillation of the mirror. Fourier analysis of the recorded output did not uncover any sideband structure.

In light of the analysis presented above there is strong motivation to repeat this experiment, being very careful to accurately gauge the amplitude at which the mirror is oscillated and also perform a thorough analysis of the resulting data. At low frequency it is possible to achieve $a_0 \sim 0.2$ μm, which would

provide a very large amplitude range, more than ample for a full investigation of the predictions of this section. A new ring laser, $C-II$, made entirely from one block of zerodur is currently under construction and is expected to significantly improve on the current optical performance of the Canterbury Ring Laser. $C-II$ will be installed at Canterbury in the first months of 1996 and will have one mirror permanently mounted upon a piezo-electric crystal, which will be used as a servo mechanism. As such a repeat of the experiment described above will be easy and we therefore expect that this experiment will be performed in the foreseeable future.

8.5.2 Beat frequency between adjacent modes

When the gain of the radio frequency source which drives the Canterbury Ring Laser is increased it is possible to excite more than one longitudinal mode of the ring laser cavity. In the Canterbury Ring Laser the difference in frequency between successive longitudinal modes is $c/(Pn) = 86.39$ MHz. If we beat two adjacent longitudinal modes together then a signal of 86.387 MHz will be detected at the output photo-multiplier tube. This may, in turn, be combined with a suitably tuned stabilised radio frequency source, producing a resolvable beat of the order of a few tens of Hz. This experimental technique, in which an output signal is combined with an external stable frequency source before recording the data for analysis, is commonplace and is known as heterodyne detection. Because heterodyne detection enables the carrier frequency to be moved to any convenient frequency for Fourier analysis, this method is particularly convenient when the output signal is of radio frequency. It is important to appreciate that this technique simply shifts the origin of the resulting Fourier spectrum to a frequency more convenient for analysis, and does not affect any structure within the spectrum itself.

If the gas through which the laser beams propagate is dispersionless then the spacing in frequency between successive longitudinal modes is constant. When measuring the beat between several adjacent longitudinal modes we would find, in such circumstances, all signals superpose and only one peak at 86.39 MHz would be observed. When the gas has dispersion, however, the spacings between adjacent longitudinal modes differ. Therefore, spectra recorded with several longitudinal modes operating simultaneously find several peaks at 86.387 MHz, but all evenly spaced by a few tens of Hertz.

To date, several frequency spectra have been recorded for the Canterbury

Ring Laser using heterodyne detection for multimode analysis. Considerable structure has been observed in the recorded output spectra. Spacing between peaks has typically been in the range from 100 to 200 Hz and is a function of the pressure within the cavity and gain of the lasing medium. These experimental parameters significantly change the optical properties of the gas through which the laser beam propagates and it is no surprise that the output spectra is affected. It is clear, however, that this multi-peak structure does not arise purely from dispersion within the gas. Backscatter from the *cw* beam into the *ccw* beam also causes structure in the resulting spectra as the Sagnac beat frequency is superposed onto the multimode observation. Furthermore, frequency pulling caused by hole burning in the laser gain curve and by optical feedback from the *cw* beam into the *ccw* beam, again an artifact of backscatter, may cause the spacing between adjacent longitudinal modes to shift, resembling the effect of dispersion. Because of these experimental complications it has not yet been possible to distinguish the effect of dispersion within the gas and other competing effects when analysing the structure in spectra obtained through heterodyne detection for multimode analysis. A thorough analysis of the behaviour of a laser with multimode operation has been given by Bennett [11]. However a detailed account of the behaviour of the Canterbury Ring Laser with multimode operation falls outside of the scope of this thesis and the reader is referred to Bennett's book for a more detailed analysis.

Bearing the limitations of our model in mind, in the following analysis we predict the spectra observed when two adjacent *ccw* longitudinal modes are combined at the output of a ring laser containing an oscillating mirror. Our model, which forms a preliminary analysis for the experimental situation, assumes (incorrectly) that all sideband structure observed in the heterodyne resolved spectra to date stems from the influence of dispersion. Unfortunately, the method of heterodyne detection for multimode analysis had not been utilised at Canterbury when experimental data was recorded from the February 1993 oscillation of a piezo mounted mirror. Therefore, as yet, there does not exist experimental data with which to compare the following predictions. Nevertheless, as stated above, we anticipate a careful repeat of this experiment will be performed at Canterbury in the foreseeable future. As we found in the previous section when analysing the beat between the opposite beams of the ring laser, sideband structure is predicted for the resulting output spectra. Unlike the previous example the amplitude of the sidebands relative to the carrier signal is dependent on the dispersive properties of the medium

and the frequency at which the mirror is oscillated. However, as the analysis of spectra arising from the multimode operation of the ring laser is not as well understood as the Sagnac spectra arising from beating the *ccw* and *cw* beams, the analysis presented in this section must be regarded as a preliminary theoretical study.

Because we are only interested in the *ccw* beams we may, without any loss of generality, redefine the origin of our time coordinate such that $\omega_{ccw}(t)$ now describes the frequency of the laser beam recorded at the detector at time t. Again we assume a single mirror is oscillating sinusoidally within a ring laser with amplitude $a_0 \cos(\beta t)$. Equation (8.19) with $vt \rightarrow a_0 \cos(\beta t)$ gives the temporal variation of the counterclockwise beam. If we mix the frequency of modes m and l together we find

$$\begin{aligned} \Delta\omega_{[l,m]}(t) &\equiv \omega_l(t) - \omega_m(t) \ , \\ &= (l-m)\,\frac{2\pi c}{n(\omega_m)\,P}\left(1 + 2\cos\theta\,\frac{a_0}{P}\,\frac{n}{n_g^2}\cos(\beta t)\right) \\ &\quad \times \left\{1 - 2\frac{\boldsymbol{\Omega}\cdot\boldsymbol{A}}{n\,c\,P}\right\} \ . \end{aligned} \tag{8.22}$$

Comparing this result with Eq. (8.19) with $vt \rightarrow a_0 \cos(\beta t)$ we find Eq. (8.22) has an extra factor of $1/n_g$ in the coefficient of $\cos(\beta t)$. This factor stems from the requirement that we must evaluate the ratio n/n_g in Eq. (8.19) at ω_l and ω_m respectively before we evaluate $\omega_l(t) - \omega_m(t)$, and $n/n_g|_{\omega_l} \neq n/n_g|_{\omega_m}$ because of dispersion. Once the difference has been taken the distinction between $n/n_g|_{\omega_l}$ and $n/n_g|_{\omega_m}$ becomes negligible, and as such n/n_g^2 in Eq. (8.22) may be evaluated at ω_m. As the rotation of the ring laser only re-scales Eq. (8.22) by an experimentally negligible amount, we drop this final factor in the remaining analysis.

We first consider an experiment in which three longitudinal modes are operating and all mirrors stationary. With three modes operating we would expect to see three peaks in frequency, $\Delta\omega_{[m+1,m]}$, $\Delta\omega_{[m+2,m+1]}$ and $\Delta\omega_{[m+2,m]}$, but the final frequency difference would fall outside of the frequency domain of the resulting Fourier spectrum. From Eq. (8.22), the separation between the two peaks in our spectrum would be

$$\Delta\omega_{[m+2,m+1]} - \Delta\omega_{[m+1,m]} = -\frac{1}{n(\omega_m)}\left(\frac{2\pi c}{n(\omega_m)\,P}\right)^2 \left.\frac{\partial n}{\partial \omega}\right|_{\omega_m} \ . \tag{8.23}$$

If the signal is dispersionless then this separation vanishes and only a single peak is observed.

To date, as discussed above, the multimode experiments performed using the Canterbury Ring Laser have shown a typical spacing of 100 to 200 Hz between each 86.4 MHz signal from adjacent longitudinal modes. If we assume, for the sake of argument, that a typical separation between peaks $\sim \pm 100$ Hz is entirely due to dispersion then Eq. (8.23) with $c/(n\,P) = 86.4$ MHz gives $\partial n/\partial\omega \sim 2.1 \times 10^{-15}$ such that $n_g/n = 1 + (\omega/n)\,\partial n/\partial\omega \sim 1 \pm 6.3$. This value for n_g is unreasonably large and shows that the observed structure cannot be entirely due to dispersion within the gas.

Brillouin [21] has demonstrated that the group velocity of light may diverge substantially from the phase velocity near an optical resonance. In such circumstances one must take care when interpreting the velocity at which light signals propagate. Within any lasing cavity the beam propagates through a gas with an atomic resonance at the lasing frequency. This atomic resonance is unavoidable as population inversion along a portion of the laser beam is required for lasing to occur. In our analysis presented above we have neglected second and higher order derivatives of n with respect to ω. This implicitly assumes $\partial^2 n/\partial\omega^2 = 0$. While this is certainly not true at the resonance frequency of the lasing gas, allowing higher order partial derivative to be non-vanishing does not provide a more satisfactory model for the above observations.

To explain the observation of an unexpectedly large spacing between the peaks in heterodyne resolved multimode spectra, one would be required to model the dispersion curve within the lasing cavity and include all effects such as the Sagnac frequency splitting between *ccw* and *cw* beams being superimposed on the resulting spectra through backscatter, and pulling effects between *ccw* and *cw* beams within the cavity causing a shift in the lasing frequency of each longitudinal mode, exaggerating the dispersion induced spacing. A rigorous approach to such a problem, although highly desirable within the interests of the Canterbury Ring Laser Group, falls outside of the research undertaken within this thesis. The work of Bennett [11], if modified so as to be applicable to the situation described above, would provide a valuable starting point for such an analysis. Nevertheless, in the following we assume that n_g differs from n by a modest, but potentially significant amount and predict the simplified Fourier spectra which would result in such circumstances. Support for this pragmatic approach is supplied by the numerous experiments using a ring lasers with time dependent boundary conditions which have been performed and analysed without theoretical complications arising from extremely large dispersion. This analysis, while clearly incomplete, motivates a repetition

of the February 1993 oscillation of a piezo mounted mirror experiment, this time recording multimode spectra as well as the usual Sagnac beat frequency. Furthermore, this work provides a useful preliminary analysis from which to interpret these spectra once recorded.

We now assume only two adjacent *ccw* longitudinal modes are operating. From Eq. (8.22) the signal incident upon the detector will be frequency modulated by the oscillation of the mirror. This frequency modulation will result in sidebands being observed within the final Fourier transformed spectra. Again we ask the reader to refer to the article of Stedman et al. [139] for the details of sideband analysis in a precision ring laser. If we again make the expansion of the signal recorded at the photo-multiplier tube in terms of Bessel functions, Eq. (8.21), we find

$$\begin{aligned} V(t) &= \mathcal{R}\{V_c \exp i[\omega_c t + \gamma \sin(\beta t)]\} \ , \\ &= \mathcal{R}\left\{V_c \exp i\omega_c t \left[J_0(\gamma) + 2\sum_{n=1}^{\infty}\Big(i\, J_{2n-1}(\gamma)\, \sin([2n-1]\beta t) \right.\right. \\ &\qquad \left.\left. + J_{2n}(\gamma)\, \sin(2n\beta t)\Big)\right]\right\} \ . \end{aligned} \tag{8.24}$$

where ω_c is the difference in frequency between the radio frequency source used in heterodyne analysis and $2\pi c/(nP)$ and, in this instance,

$$\gamma \equiv -\cos\theta \frac{a_0}{P}\frac{n}{n_g^2}\frac{2\pi\, c}{\beta\, n\, P} \ ,$$

where the only effect of heterodyne mixing, apart from shifting the origin to a convenient frequency, is to reduce γ by a factor of 2 from its value without heterodyne mixing. If we assume the mirror is oscillated with an amplitude $a_0 \sim 0.05$ μm, which is the estimated amplitude in the previous experiment, we find with $\theta = \pi/4$ that $\gamma \sim -5\, n/(n_g\, \beta)$, which is the order of unity for low oscillation frequency. Fourier analysis of Eq. (8.24) predicts the resulting spectra will show considerable sideband structure with a spacing of β Hz between each peak. The ratio of the sidebands relative to central carrier is given by $J_n(\gamma)/J_0(\gamma)$.

Sample spectra with $\beta = 20$ and 200 Hz, assuming $n/n_g = 1$, are generated in figure 8.4. These illustrate the relative heights of the sidebands depend on β. Unlike the case where *ccw* and *cw* beams are combined, in this instance γ is dependent on β and n_g. Through accurately measuring the amplitude of the sidebands in experimentally obtained spectra the parameter γ can be recovered. If the uncertainty in β and, with more difficulty, a_0 is low then

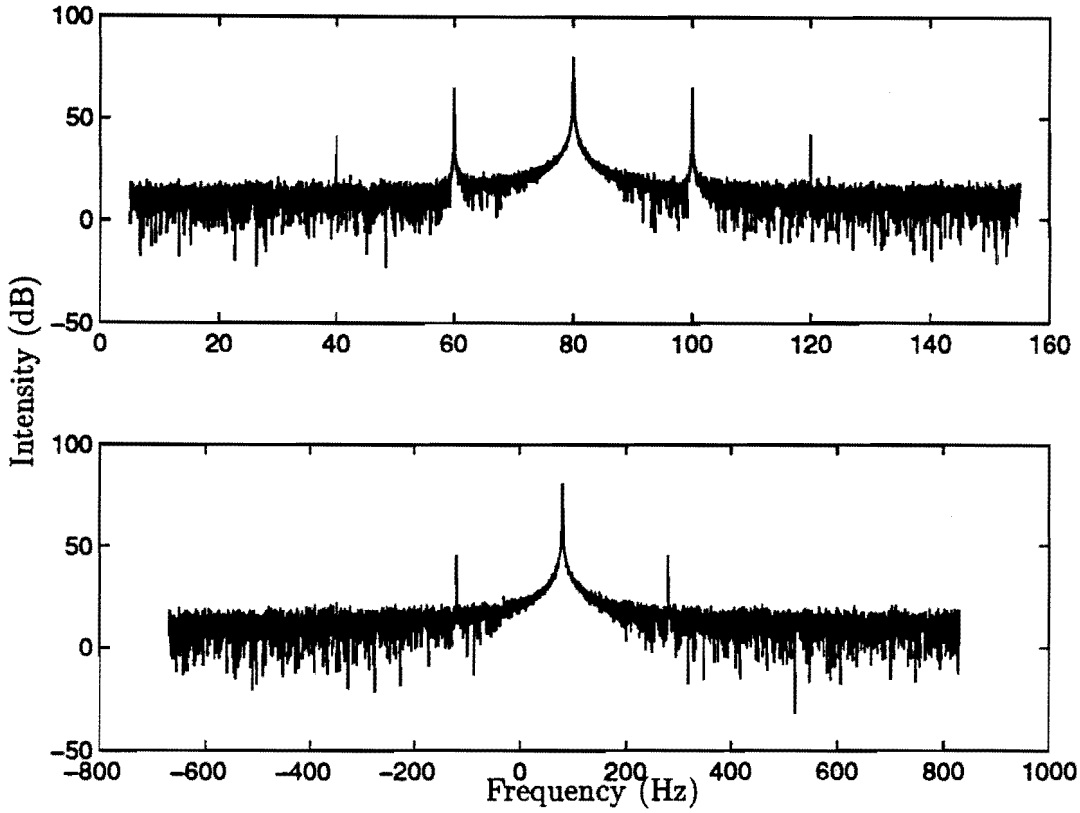

Figure 8.4: Numerically generated spectra assuming two adjacent *ccw* modes are operating simultaneously. These spectra correspond to an oscillation amplitude $a_0 = 0.05$ μm and frequency 20 Hz and 200 Hz respectively. We have, arbitrarily, set the carrier frequency to be 80 Hz. In an experiment using heterodyne techniques one is free to choose a convenient frequency for the carrier.

it may be possible to use this technique to measure n_g and thus determine the dispersion within the lasing gas. However, given that the model analysed here is considerably simpler than that which would generate experimentally observed spectra, these predictions are more likely to find a qualitative rather than a quantitative application in the first instance. Nevertheless, such an experiment in ring laser spectroscopy would uncover valuable information on the behaviour of a ring laser when the mirrors are oscillated, which may, in turn, improve our understanding of the subtleties of beam coupling and mode pulling.

Within this chapter we have given a rigorous description of the behaviour of a rotating ring laser with one mirror oscillating. We have, however, quite deliberately neglected the influence of backscatter, mode pulling and hole burning on the spectra predicted in this section. Therefore this analysis opens the way for further theoretical and experimental analyses of direct relevance to the

current interests of the Canterbury Ring Laser Group. In deriving these result we have developed a new and flexible method for calculating phase shifts in an interferometer in a non-inertial spacetime with dispersion and time dependent boundary conditions. This calculational technique was based upon purely geometric quantities and, as such, will find application in a number of other experimental contexts.

Chapter 9

Conclusion

All work presented within this thesis has been concerned with two topics within the theory of relativity: the influence of acceleration on physical systems and optical ring interferometry. In each chapter we discussed a problem of physical interest and presented a full solution in a self contained manner. In this sense each chapter is independent of the others. However, all chapters share a common thread, consisting of studies of acceleration, optical interferometry or both.

In chapter 2 we presented a full derivation of the motion of a relativistic particle attached to an idealised spring, of interest because of the wide variety of physical applications in which the basic classical model features. Chapter 3 provided a pedagogical demonstration of the local equivalence of Schwarzschild geometry with an appropriately chosen accelerating frame of reference. This local equivalence provides insight into the manner in which the equivalence principle has been incorporated into the general theory of relativity. In chapter 4 we discussed the assumption of locality, implicit within the general theory of relativity. Using the examples of a simple quantum mechanical clock with linear acceleration and the measurement of frequency by non inertial observers, we showed the locality hypothesis only approximates the physical behaviour of these systems. Chapter 5 was dedicated to a full relativistic reanalysis of the modified Laub drag experiment of Sanders and Ezekiel. This analysis corrected a number of errors in their work and completed earlier partial treatments of this problem by Bilger and Stedman. Our result demonstrated an overall discrepancy between experiment and theory of 1300 ppm, considerably worse than 60 ppm which was claimed by Sanders and Ezekiel. The following chapter extended our discussion of light drag into the context of linearly accelerating media. Using the covariant formulation of Maxwell's equations we predicted sideband structure would be observed if a glass sample was oscillated along one arm of a passive optical interferometer and the resulting signal Fourier analysed. We also showed a resonant cavity containing a linearly accelerating glass

sample will display optical ringing. These predictions pave the way for novel experimental tests of the covariant form of Maxwell's equations in the future. Chapter 7 contains the most complete analysis of a ring optical interferometer with angular acceleration reported to date. This work predicted a resonant cavity with angular acceleration will also have an asymmetric response profile due to the phenomenon of optical ringing. Our analysis also demonstrated the beat frequency in a ring laser with angular acceleration is given by an instantaneous Sagnac effect. Our final research chapter was concerned directly with an experiment of interest to the Canterbury Ring Laser Group. In this chapter we analysed a rotating ring laser with one mirror oscillating. We predicted sideband structure will appear in spectra obtained from Fourier analysis of the beat between the opposite beams of the same mode order, and Fourier analysis of the beat between adjacent modes when the laser has multimode operation. These results provide strong motivation for a repetition of the earlier preliminary experiment performed at Canterbury.

Throughout this thesis I was motivated by the desire to link my theoretical work to experiment. This link is transparent in chapters 5 to 8. In particular I have received a good deal of satisfaction from the conclusions of the final three chapters, in which I demonstrated an extension of the theory of optical interferometry into an accelerating context leads to a number of interesting and potentially observable experimental consequences.

Appendix A

Temporal response of a Fabry-Pérot interferometer to a frequency modulated signal

Using a scanning Fabry-Perót interferometer, Li et al. [80] observed an asymmetric response profile when the input signal was monochromatic. In their analysis of this observation, Li et al. utilised its formal equivalence with a Fabry-Pérot interferometer with a frequency modulated input signal and thus derive an analytic expression for the temporal response of the scanning Fabry Perót interferometer. Because the complex summation which arises within this analysis is of the same form as those obtained in sections 6.4.2 and 7.3 we reproduce their argument below.

The amplitude transfer function of a Fabry Perót interferometer with mirror separation d excited by a monochromatic signal $A_0 \exp i(k_0 Z - \omega_0 T)$ has the form

$$H(\omega) = \frac{1 - s^2}{1 - s^2 \exp i(\omega - \omega_0)\tau} = (1 - s^2) \sum_l s^{2l} \exp i\omega\tau l \ , \qquad \text{(A.1)}$$

where s is the amplitude reflectance of each mirror, $\tau = 2\,d/c$ is twice the time of flight of a photon between mirrors and $\omega_0 = 2\pi\, m/\tau$ is frequency for exact resonance. This may be approximated by $H(\omega) = [1 - 2i(\omega - \omega_0)/\Gamma]^{-1}$, where the power rate of decay of the cavity $\Gamma = 2\,c\,(1 - s^2)/Ps^2$. Eq. (A.1) has as its Fourier transform

$$h(t) = (1 - s^2) \sum_l s^{2l}\, \delta(T - l\,\tau) \ ,$$

where $\delta(T - l\,\tau)$ is the Dirac delta function.

Consider an input field which is ramped in frequency:

$$A_{in} = A_0 \exp\left\{-i \left[\omega_0 + \frac{1}{2}\beta(T - Z/c)\right] (T - Z/c)\right\} \ , \qquad \text{(A.2)}$$

where β is the frequency scanning rate. The instantaneous frequency is $\omega = \omega_0 + \beta\,(T - Z/c)$, which follows immediately from the time derivative of the phase. With $k = \omega/c$ this input satisfies the vacuum wave equation.

The output of the Fabry Perót interferometer is given by the convolution of the input field with the impulse response of the cavity:

$$\begin{aligned} A_{out}(T,Z) &= (1-s^2)\sum_l s^{2l} A_{in}(t-n\tau) \ , \\ &= (1-s^2)\, A_0 \exp i\left\{k_0 Z - \omega_0 T + \beta T\, Z/c - \frac{1}{2}\beta T^2 - \beta Z^2/2c^2\right\} \\ &\quad \times \sum_l s^{2l} \exp i\Phi_l \ , \end{aligned} \tag{A.3}$$

where

$$\Phi_l = \omega_0 \left\{ l\left[\tau + \frac{\beta\tau}{2\omega_0}(2T - 2Z/c)\right] - l^2 \frac{\beta\tau}{2\omega_0}\tau \right\} \ . \tag{A.4}$$

Because this summation is of the form $\sum_l a^l b^{l^2}$ it is difficult to perform directly. Instead this summation was evaluated by Li et al., to within a phase factor, by using Fourier methods to directly determine the output spectra of the interferometer with a frequency ramped input signal. From the equality of the two approaches the infinite sum could be evaluated.

The input signal, Eq. (A.2), has the Fourier Transform

$$\begin{aligned} A_{in}(\omega, Z) &= A_0 \exp i\left\{k_0 Z - \frac{\beta Z^2}{2c^2}\right\} \\ &\quad \times \int_{-\infty}^{\infty} dT \exp i\left\{(\omega - \omega_0 + \beta Z/c)T - \frac{1}{2}\beta T^2\right\} \ . \end{aligned}$$

By multiplying this input function by the response of the Fabry Perót interferometer, Eq. (A.1), and performing the inverse Fourier transformation using standard integration methods, Li et al. [80] we able to derive the temporal response of a Fabry-Perót interferometer with a ramped frequency input. The temporal response for such a system is given by

$$A_{out}(T,Z) = \mp \exp i\frac{\pi}{4}\sqrt{\frac{\pi}{8\eta}}\, A_0 \exp i\left\{k_0 Z - \omega_0 T - \frac{1}{2}\beta(Z/c - T)^2\right\} w(\zeta) \ , \tag{A.5}$$

where [1]

$$w(\zeta) = \frac{i}{\pi}\int_{-\infty}^{\infty} d\nu \frac{\exp(-\nu^2)}{\zeta - \nu} = \exp(-\zeta^2)\,\mathrm{erfc}(-i\zeta) \qquad (\mathrm{Im}\,\zeta > 0) \ ,$$

$\mathrm{erfc}(-i\zeta)$ being the complex error function. The asymmetry parameter $\eta \equiv \beta/\Gamma^2$, where $\Gamma = 2c(1-s^2)/Ps^2$ is the power rate of decay of the cavity. The variable $\zeta \equiv \pm\exp(-i\pi/4)\{-i\Gamma + 2\beta(T - Z/c)\}/\sqrt{8\beta}$, the sign being positive when $\beta(T - Z/c) > \Gamma$ and was chosen to keep the imaginary part of ζ positive. This definition of ζ corrects an algebraic error in the definition of

ζ in Appendix C of Li et al [80]: z and t variables should be primed in Eq. (C.6) and the coefficient of the primed variables in the definition of G and ζ should be 2η. Furthermore, z and t should be unprimed in Eq. (C.5).

Taking the modulus of Eqs. (A.3) and (A.5) we find

$$(1-s^2)\left|\sum_l s^{2l}\exp i\Phi_l\right| = \frac{\pi}{8\eta}\,|w(\zeta)| \quad . \tag{A.6}$$

Our analyses of the optical response profile of a resonant cavity containing an accelerating dielectric, section 6.4.2, and a resonance cavity with a angular acceleration, section 7.3, both produced summations of the same form as the LHS of Eq. (A.6). This result provides the mathematical foundation for the conclusions drawn in these sections.

Appendix B

Published papers

An analysis of a relativistic particle undergoing oscillatory motion, similar to that presented in chapter 2 but approached from a Lagrangian formulation of the problem, has been published in the article:

W. Moreau, R. Easther and R. Neutze,
Relativistic (an)harmonic oscillator,
Am. J. Phys, **62** (6) 531-535, June 1994 [106].

Our demonstration in chapter 3 of the first order equivalence of Schwarzschild geometry with a linearly accelerating frame of reference was also published in the American Journal of Physics:

W. Moreau, R. Neutze and D.K. Ross,
The equivalence principle in the Schwarzschild geometry,
Am. J. Phys, **62** (11) 1037-1040, November 1994 [105].

Both of our derivations in chapter 4 of the Döppler shift relations for a linearly accelerating observer and an observer stationary in Schwarzschild geometry have been published in Physics Letters A:

R. Neutze and W. Moreau,
Frequency measurements by uniformly accelerating observers,
Phys. Lett. A, **179** (6) 389-390, August 1993 [108],

R. Neutze and W. Moreau,
Quantum implications for frequency measurements in Schwarzschild geometry,
Phys. Lett. A, **183** (2,3) 141-144, December 1993 [109],

Of the analyses presented within this thesis concerned directly with optical

interferometry, only the derivation in chapter 7 of the optical response of a ring interferometer with angular acceleration has been published to date:

R. Neutze,
Ring interferometer with angular acceleration,
Phys. Rev. A, **51** (6) 5039-5042, June 1995 [107].

We intend to submit three further manuscripts concerned with optical interferometry for publication in the near future. These manuscripts will be based upon material presented in chapters 5, 6 and 8. We also consider the discussion of the rate of a linearly accelerating quantum mechanical clock, presented in section 4.2, may be appropriate as a letter.

References

[1] M. A. Abramowitz and I. A. Stegun, editors. *Handbook of Mathematical Functions.* Dover, New York, 1965.

[2] E. G. Adelberger. Modern tests of the universality of free fall. *Class. Quantum Grav.*, 11:A9–A21, 1994.

[3] C. G. Adler and R. W. Brehme. Relativistic solutions to the falling body in a uniform gravitation field. *Am. J. Phys.*, 59:209–213, 1991.

[4] J. L. Anderson and J. W. Ryon. Electromagnetic radiation in accelerated systems. *Phys. Rev.*, 181:1765–1775, 1969.

[5] R. Anderson, H. R. Bilger, and G. E. Stedman. "Sagnac" effect: a century of Earth-rotated interferometers. *Am. J. Phys*, 62:975–985, 1994.

[6] M. Arif, H. Kaiser, R. Clothier, S. A. Werner, R. Berliner, W. A. Hamilton, A. Cimmino, and A. G. Klein. Null Fizeau effect for thermal neutrons in moving matter. *Physica B*, 151:63–67, 1988.

[7] M. Arif, H. Kaiser, R. Clothier, S. A. Werner, W. A. Hamilton, , A. Cimmino, and A. G. Klein. Observation of a motion-induced phase shift of neutron de Broglie waves passing through matter near a nuclear resonance. *Phys. Rev. A*, 39:931–937, 1989.

[8] M. Arif, H. Kaiser, S. A. Werner, A. Cimmino, W. A. Hamilton, A. G. Klein, and G. I. Opat. Null Fizeau effect for thermal neutrons in moving matter. *Phys. Rev. A*, 31:1203–1205, 1985.

[9] J. Audretsch and C. Lämmerzahl. New inertial and gravitational effects made measurable by atomic beam interferometry. *Appl. Phys. B*, 54:351–354, 1992.

[10] E. M. Belenov and E. P. Markin. Shift of light frequency in an accelerated rotating ring laser. *JETP Lett.*, 7:381–382, 1968.

[11] W. R. Bennett. *The Physics of Gas Lasers.* Gordon and Breach, New York, 1977.

[12] H. R. Bilger. Longitudinal light drag in moving media: status of experimental results. Unpublished, 1979.

[13] H. R. Bilger and G. E. Stedman. Light drag: reanalysis of the Sanders-Ezekiel experiment. Unpublished, 1989.

[14] H. R. Bilger, G. E. Stedman, and P. V. Wells. Geometrical dependence of polarisation in near-planar ring laser. *Optics Comm.*, 80:133–137, 1990.

[15] H. R. Bilger and W. K. Stowell. Light drag in a ring laser: an improved determination of the drag coeffecients. *Phys. Rev. A*, 16:313–319, 1977.

[16] H. R. Bilger and A. T. Zavodny. Fresnel drag in a ring laser: measurement of the dispersive term. *Phys. Rev. A*, 5:591–599, 1972.

[17] U. Bonse and A. Rumpf. Interferometric measurement of neutron Fizeau effect. *Phys. Rev. Lett*, 56:2441–2444, 1986.

[18] T. H. Boyer. Thermal effects of acceleration through random classical radiation. *Phys. Rev. D*, 21:2137–2148, 1980.

[19] J. Bradley. *Phil. Trans. R. Soc.*, 35:637, 1728.

[20] V. B. Braginski and V. I. Panov. Verification of the equivalence of inertial and gravitational mass. *Zh. Eksp. & Teor. Fiz.*, 61:873–879, 1971.

[21] L. Brillouin. *Wave propagation and group velocity.* Academic Press, New York, 1960.

[22] R. Broucke. Linearization of Schwarzschild's line element: Application to the clock paradox. *Am. J. Phys.*, 39:1461–1465, 1971.

[23] B. Chakarborty and S. Sarkar. Physics in rotating frames: On uniform rotation about a fixed axis in some holonomic and anholonomic frames. *Ann. Phys.*, 163:167–198, 1985.

[24] D. C. Champeney, G. R. Isaak, and A. M. Khan. An 'aether drift' experiment based on the Mössbauer effect. *Phys. Lett.*, 7:241–243, 1963.

[25] D. C. Champeney, G. R. Isaak, and A. M. Khan. A time dilation experiment based on the Mössbauer effect. *Proc. Phys. Soc.*, 85:583–593, 1965.

[26] W. W. Chow, J. Gea-Banacloche, L. M. Pedrotti, V. E. Sanders, W. Schleich, and M. O. Scully. The ring laser gyro. *Rev. Mod. Phys.*, 57:61–104, 1985.

[27] J. D. Coccoli and J. R. Lawson. U.S. Patent 3,533,014, 1970.

[28] W. Cochran. Some results on the relativistic Doppler effect for accelerated motion. *Am. J. Phys*, 57:1039–1041, 1989.

[29] R. Colella, A. W. Overhauser, and S. A. Werner. Observation of gravitationally induced quantum interference. *Phys. Rev. Lett.*, 34:1472–1474, 1975.

[30] L. F. Cook. Einstein and $\Delta t\ \Delta E$. *Am. J. Phys.*, 48:142–145, 1980.

[31] L. Cooper and G. E. Stedman. Axion detection by ring lasers. Submitted to *Phys. Lett. B*, 1995.

[32] E. A. Desloge. Nonequivalence of a uniformly accelerating reference frame and a frame at rest in a uniform gravitational field. *Am. J. Phys.*, 57:1121–1125, 1989.

[33] N. A. Doughty. *Lagrangian Interaction.* Addison Wesley, 1990.

[34] M. Dresden and C. N. Yang. Phase shift in a rotating neutron or optical interferometer. *Phys. Rev. D.*, 20:1846–1848, 1979.

[35] J. Droste. Het veld van een enkle centrun in einstein's theorie der zwaartekracht en de beweging van een stoffelijk punt in dat veld. *Verslagen van de Gewone Vergaderingen der wis- en Natuurkundige Afdeeling, Koninklijke Akedemie van Wetenschappen te Amsterdam*, 25:163–180, 1916.

[36] F. W. Dyson, A. S. E. Eddington, and C. R. Davidson. A determination of the deflection of light by the Sun's gravitational field from observations made at the total eclipse of May 29, 1919. *Phil. Trans. Roy. Soc. A*, 220:291–333, 1920.

[37] A. Einstein. Zur Elektrodynamik bewegter Körper (On the electrodynamics of moving bodies). *Ann. d. Phys. (Germany)*, 17:891–921, 1905.

[38] A. Einstein. Über das Relativitätsprinzip und die aus demselben gezogenen Folgerungen (On the relativity principle and conclusions drawn from it). *Jahrbuch d. Radioakt. und Elektronik.*, 4:411–462, 1907.

[39] A. Einstein. Die Grundlage der allgemeinen Relativitätstheorie (The foundation of the general theory of relativity). *Ann.d.Phys. (Germany)*, 49:769–882, 1916.

[40] A. Einstein. Prinzipielles zur allgemeinen Relativitätstheorie. *Ann. d. Phys. (Germany)*, 55:241–244, 1918.

[41] A. Einstein and M. Grossmann. Entwerf einer verallgemeinerten Relativätstheorie und einer Theorie der Gravitation (A proposed general relativity theory and theory of gravitation). *Zeit. Math. Phys.*, 632:225–261, 1913.

[42] R. V. Eötvös, V. Pekár, and E. Fekete. Beiträge zum Gesetze der Proportionalität von Trägheit und Gravität (Contributions to the law of proportionality of inertia and gravity). *Ann. d. Phys.*, 68:11–66, 1922.

[43] V. F. Fateev. Accelerated rotation of a ring interferometer in a gravitational field. *Opt. Spectrosc.(USSR)*, 50:14–18, 1981.

[44] V. F. Fateev. Effect of light guide dispersion on the wave phase in a ring interferometer with rotational acceleration. *Opt. Spectrosc.(USSR)*, 54:412–413, 1983.

[45] A. H. L. Fizeau. Sur les hypothèses relatives à l'éther lumineaux, et sur une expérience qui parait démontrer que le mouvement des corps change la vitesse avec laquelle le luminère se propage dans leur intérieur. *Compt. Rend.*, 33:349–355, 1851.

[46] E. B. Fomalont and R. A. Sramek. Measurement of the solar gravitational deflection of radio waves in agreement with general relativity. *Phys. Rev. Lett.*, 36:1475–1478, 1976.

[47] J. D. French. Pedagogical trick for general relativity. *Am. J. Phys.*, 45:580–581, 1977.

[48] A. J. Fresnel. *Annls Chim. Phys.*, 9:57, 1818.

[49] H. Goldstein. *Classical Mechanics.* Addison-Wesley, 2nd edition, 1980.

[50] I. Gradshteyn and I. Ryzhik. *Table of Integrals, Series and Products, Corrected and Enlarged Edition.* Academic, San Diego, 1980.

[51] N. N. Greenwood and T. C. Gibb. *Mössbauer Spectroscopy.* Chapman and Hall, London, 1971.

[52] O. Gron. Relativistic description of a rotating disk with angular acceleration. *Found. Phys.*, 9:353–369, 1979.

[53] J. C. Hafele and R. E. Keating. Around the world atomic clocks: observed relativistic time gains. *Science*, 177:168–170, 1972.

[54] J. D. Hamilton. The uniformly accelerating reference frame. *Am. J. Phys.*, 60:561–564, 1992.

[55] F. Harress. Thesis; Jena. Unpublished, 1911.

[56] F. Hasselbach and M. Nicklaus. Sagnac experiment with electrons: Observation of the rotational phase shift of electron waves in vacuum. *Phys. Rev. A*, 48:143–151, 1993.

[57] S. W. Hawking. Particle creation by black holes. *Commun. Math. Phys.*, 43:199–220, 1975.

[58] H. J. Hay, J. P. Schiffer, T. E. Cranshaw, and P. A. Egelstaff. Measurement of the red shift in an accelerated system using the Mössbauer effect in Fe^{57}. *Phys. Rev. Lett.*, 4:165, 1960.

[59] C. V. Heer. Resonant frequencies of an electromagnetic cavity in an accelerated system of reference. *Phys. Rev. A*, 134:A799–A804, 1964.

[60] C. V. Heer. History of the laser gyro. *Proc. SPIE*, 487:2–12, 1984.

[61] F. W. Hehl and Wei-Tou Ni. Inertial effects of a Dirac particle. *Phys. Rev. D*, 42:2045–2048, 1990. gravitation, geometry.

[62] G. Holton. Einstein, Michelson, and the "crucial" experiment. *Isis*, 60:133–197, 1969.

[63] M. A. Horne, A. Zeilinger, A. G. Klein, and G. I. Opat. Neutron phase shift in moving matter. *Phys. Rev. A*, 28:1–6, 1983.

[64] Z. K. Ioannidis and I. P. Giles. Nonlinear phase modulation in optical fiber ring resonators. *Appl. Optics*, 27:3058–3059, 1988.

[65] Z. K. Ioannidis, P. M. Radmore, and I. P. Giles. Dynamic response of an all-fiber ring resonator. *Optics Lett.*, 13:422–424, 1988.

[66] I. Khan. The principles of reciprocity and equivalence of monads and their implications. *Nuovo Cimento*, LVII B:321–329, 1968.

[67] I. Khan. The principle of reciprocity. *IJTP*, 6:383–397, 1971.

[68] A. G. Klein, G. I. Opat, A. Cimmino, A. Zeilinger, W. Treimer, and R. Gähler. Neutron propagation in moving matter: The Fizeau experiment with massive particles. *Phys. Rev. Lett.*, 46:1551–1554, 1981.

[69] L. Koester. Verification of the equivalence of gravitational and inertial mass for the neutron. *Phys. Rev. D.*, 14:907–909, 1976.

[70] F. V. Kowalski. Gravitational effect on light propagating through a dielectric. *Phys. Lett. A.*, 170:11–15, 1992.

[71] F. V. Kowalski. Phase-invariant clock hypothesis for accelerating systems. *Phys. Rev. A*, 46:2261–2264, 1992.

[72] F. V. Kowalski. Interaction of neutrons with accelerating matter: test of the equivalence principle. *Phys. Lett. A*, 182:335–340, 1993.

[73] F. V. Kowalski. National science foundation grant application, 1993.

[74] F. V. Kowalski. Phase of neutrons propagating through an accelerating interferometer: test of the equivalence principle. *Phys. Rev. A*, 51:120–, 1995.

[75] F. V. Kowalski. Private communication, 1995.

[76] F. V. Kowlaski, J. Murray, and A. C. Head. Interaction of light with an accelerating dielectric. *Phys. Rev. A.*, 48:1082–1088, 1993.

[77] W. Kündig. Measurement of the transverse Döppler effect in an accelerated system. *Phys. Rev.*, 129:2371–2375, 1963.

[78] J. Laub. Zur Optik der bewegten Körper. *Ann.d. Phys. (Germany)*, 25:175–184, 1908.

[79] Z. Li, R. G. T. Bennett, and G. E. Stedman. Swept-frequency induced optical cavity ringing. *Optics Comm.*, 86:51–57, 1991.

[80] Z. Li and G. E. Stedman. Asymmetric response profile of a scanning Fabry-Pérot interferometer. *Optics Comm.*, 100:240–246, 1993.

[81] O. J. Lodge. Aberration problems-a discussion concerning the motion of the ether near the earth, and concerning the connection between ether and gross matter; with some new experiments. *Philos. Trans. R. Soc.*, 184:727–807, 1893.

[82] H. A. Lorentz. *Versuch einer Theorie der elektrischen und optischen Erscheinungen in bewgeten Körpern (Proposed theory for electrical and optical phenomena in moving bodies)*. Brill, Leiden, 1895.

[83] R. Loudon. *The Quantum Theory of Light : 2nd edn.* Claredon Press, Oxford, 1983.

[84] W. M. Macek and Jr. D. T. M. Davis. Rotation rate sensing with travelling-wave ring lasers. *Appl. Phys. Lett.*, 2:67–68, 1963.

[85] S. R. Mainwaring and G. E. Stedman. Accelerated clock principles in special relativity. *Phys. Rev. A*, 47:3611–3620, 1993.

[86] B. Mashhoon. General covariance and quantum theory. *Found. Phys.*, 16:619–635, 1986.

[87] B. Mashhoon. Electrodynamics in a linearly accelerated system. *Phys. Lett. A.*, 122:67–72, 1987.

[88] B. Mashhoon. Complementarity of absolute and relative motion. *Phys. Lett. A.*, 126:393–399, 1988.

[89] B. Mashhoon. Neutron interferometry in a rotating frame of reference. *Phys. Rev. Lett*, 61:2639–2642, 1988.

[90] B. Mashhoon. Electrodynamics in a rotating frame of reference. *Phys. Lett. A.*, 139:103–108, 1989.

[91] B. Mashhoon. The hypothesis of locality in relativistic physics. *Phys. Lett. A.*, 145:147–153, 1990.

[92] B. Mashhoon. Accelerated observers and conformal invariance. In F. Mansouri and J. Scanio, editors, *Topics on Quantum Gravity and Beyond*, pages 257–271. World Scientific, Singapore, 1993.

[93] B. Mashhoon. Nonlocal theory of accelerated observers. *Phys. Rev. A*, 47:4498–4501, 1993.

[94] B. Mashhoon. On the relativity of rotation. In B. L. Hu and T. A. Jacobson, editors, *Directions in General Relativity: Proceedings of the 1993 International Symposium, Maryland*, volume 2, pages 182–194. Cambridge University Press, Cambridge, 1993.

[95] B. Mashhoon. On the coupling of intrinsic spin with the rotation of the earth. *Phys. Lett. A*, 198:9–13, 1995.

[96] J. C. Maxwell. A dynamic theory of the electromagnetic field. *Phil. Trans. Roy. Soc.(London)*, 155:459–512, 1865.

[97] A. A. Michelson, H. G. Gale, and F. Pearson. The effect of the earth's rotation on the velocity of light. *Astrophys. J.*, 61:137–145, 1925.

[98] A. A. Michelson and E. W. Morley. Influence of motion of the medium on the velocity of light. *Am. J. Sci.*, 31:377–386, 1886.

[99] A. A. Michelson and E. W. Morley. On the relative motion of the earth and the lumniferous ether. *Am. J. Sci.*, 34:333–345, 1887.

[100] H. Minkowski. Das Relativitätsprinzip (The relativity principle). *Ann. d. Phys. (Germany)*, 47:927–938, 1907.

[101] C. W. Missner, K. S. Thorne, and J. A. Wheeler. *Gravitation.* Freeman, San Francisco, 1973.

[102] T. C. Mo. Theory of electrodynamics in media in noninertial frames and applications. *J. Math. Phys.*, 11:2589–2610, 1970.

[103] C. Moller. *The theory of relativity, 2nd edition.* Oxford University Press, New Delhi, 1972.

[104] W. Moreau. Nonlocality in frequency measurements of uniformly accelerating observers. *Am. J. Phys*, 60:561–564, 1992.

[105] W. Moreau, R. Easther, and R. Neutze. Relativistic (an)harmonic oscillator. *Am. J. Phys*, 62:531–535, 1994.

[106] W. Moreau, R. Neutze, and D.K. Ross. The equivalence principle in the Schwarzschild geometry. *Am. J. Phys.*, 62:1037–1040, 1994.

[107] R. Neutze. Ring interferometer with angular acceleration. *Phys. Rev. A*, 51:5039–5042, 1995.

[108] R. Neutze and W. Moreau. Frequency measurements by uniformly accelerating observers. *Phys. Lett. A*, 179:389,390, 1993.

[109] R. Neutze and W. Moreau. Quantum implications for frequency measurements in Schwarzschild geometry. *Phys. Lett. A*, 183:141–144, 1993.

[110] R. G. Newburgh and Jr T. E. Phipps. Brewster angle and the Einstein velocity addition theorem. *Am. J. Phys.*, 39:1079–1084, 1971.

[111] I. Newton. *Philosophiae Naturalis Principa Mathematica (Mathematical principles of Natural Philosophy).* Streater, London, 1st edition, 1687.

[112] J. Norton. What was Einstein's principle of equivalence? In D. Howard and J. Stachel, editors, *Einstein and the history of general relativity*, pages 5–47. Birkhäuser, Boston, 1989.

[113] H. C. Ohanian. What is this principle of equivalence? *Am. J. Phys.*, 45:903–909, 1977.

[114] G. I. Opat. Interferometry with particles of non-zero rest mass. Unpublished, 1992.

[115] R. E. Packard and S. Vitale. Principles of superfluid-helium gyroscopes. *Phys. Rev. B*, 46:3540–3549, 1992.

[116] W. F. Parks and J. T. Dowell. Fresnel drag in uniformly moving media. *Phys. Rev. A*, 9:565–567, 1974.

[117] W. Pauli. *Relativititätstheorie.* Teubner, Leipzig, 1921. Translation: *Theory of Relativity.* Pergamon, London, 1958.

[118] E. J. Post. Sagnac effect. *Rev. Mod. Phys*, 39:475–493, 1967.

[119] R. V. Pound and G. A. Rebka. Apparent weight of photons. *Phys. Rev. Lett.*, 4:337–341, 1960.

[120] R. D. Reasenberg, I. I. Shapiro, P. E. MacNeil, R. B. Goldstein, J. C. Breidenthal, J. P. Brenkle, D. L. Cain, T. M. Kaufman, T. A. Kormarek, and A. I. Zygielbaum. Viking relativity experiment: verification of signal retardation by solar gravity. *Astrophys. J. Lett.*, 234:219–221, 1979.

[121] F. Riehle, T. Kisters, A. Witte, J. Helmcke, and C. J. Borde. Optical ramsey spectroscopy in a rotating frame: Sagnac effect in a matter wave interferometer. *Phys. Rev. Lett.*, 67:177–180, 1991.

[122] P. G. Roll, R. Krotkov, and R. H. Dicke. The equivalence of inertial and passive gravitational mass. *Ann. Phys. (USA)*, 26:442–517, 1964.

[123] J. W. Ryon and J. L. Anderson. Electromagnetic wave propagation in a linearly accelerating relativistic dielectric. *Phys. Rev. D*, 2:2745–2755, 1970.

[124] J. M. Saca. Addition of group velocities. *Am. J. Phys*, 53:173,174, 1985.

[125] G. Sagnac. L'éther lumineux démontrè par l'effet du vent relatif d'éther dans un interféromètre en rotation uniforme (The luminiferous ether demonstrated by the effect of the relative motion of the ether in an interferometer in uniform rotation). *C. R. Acid. Sci.(Paris)*, 157:708–710, 1913.

[126] H. Salecker and E. P. Wigner. Quantum limitations of the measurement of space-time distances. *Phys. Rev.*, 109:571–577, 1958.

[127] G. A. Sanders. *Measurement of Fresnel drag using a passive ring resonator technique.* PhD thesis, Massachusetts Institute of Technology, Cambridge, Massachusetts, USA, 1983.

[128] G. A. Sanders and S. Ezekiel. Measurement of Fresnel drag in moving media using a ring-resonator technique. *J. Opt. Soc. Am. B*, 5:674–678, 1988.

[129] G. A. Sanders, M. G. Prentiss, and S. Ezekiel. Passive ring resonator method for sensitive inertial rotation measurements in geophysics and relativity. *Opt. Lett.*, 6:569, 1981.

[130] W. Schleich and M. O. Scully. General relativity and modern optics. In G. Grynberg and R. Stora, editors, *Tendances actuelles en physique atomique (New trends in atomic physics)*, chapter 10, pages 995–1124. Elsevier Science Publishers B. V., 1984.

[131] E. O. Schulz-DuBois. Alternative interpretation of rotation rate sensing by ring laser. *IEEE Journal of Quantum Electronics*, QE-2:299–305, 1966.

[132] K. Schwarzschild. Über das Gravitationfeld eines Massenpunktes nach der Einsteinschen Theorie. *Sitzber. Deut. Akad. Wiss. Berlin, Kl. Math.-Phys. Tech.*, pages 189–196, 1916.

[133] M. O. Scully, M. S. Zubairy, and M. P. Haugan. Proposed optical test of metric gravitation theories. *Phys. Rev. A.*, 24:2009–2016, 1981.

[134] M. P. Silverman. Measurement of hydrogen hyperfine splittings as a test of quantum mechanics in a noninertial reference frame. *Phys. Lett. A*, 152:133–136, 1991.

[135] R. Skinner. *Relativity.* Blaisdell, 1969.

[136] G. E. Stedman. Ring interferometric tests of classical and quantum gravity. *Contemp. Phys.*, 26:311–332, 1985.

[137] G. E. Stedman. Private communication, 1992.

[138] G. E. Stedman. Relativistic transformation of group velocity via spatial filtering. *Am. J. Phys*, 60:1117–1122, 1992.

[139] G. E. Stedman, Z. Li, and H. R. Bilger. Sideband analysis and seismic detection in a precision ring laser. *Appl. Optics*, 1995. In print.

[140] G. E. Stedman, Z. Li, C. H. Rowe, A. D. McGregor, and H. R. Bilger. Harmonic analysis in a large ring laser with backscatter-induced pulling. *Phys. Rev. A*, 51, 1995.

[141] J. L. Synge. Classical dynamics. In S. Flügge, editor, *Handbuch der Physik (Encyclopedia of Physics)*, volume III/I, chapter 8 and 9. Springer, Berlin, 1960.

[142] J. L. Synge. *Relativity: the general theory.* North-Holland, Amsterdam, 1960.

[143] T. Takahashi and R. Baierlein. Accelerated ring laser. *Phys. Rev. A*, 15:731–734, 1977.

[144] Y. Takahashi. The Sagnac effect on the wavefunction. *Phys. Lett.A*, 113:5–7, 1985.

[145] K. Tanaka. Relativistic study of electromagnetic waves in the accelerated dielectric medium. *J. Appl. Phys.*, 49:4311–4319, 1978.

[146] K. Tanaka. Reflection and transmission of electromagnetic waves by a linearly accelerated dielectric slab. *Phys. Rev. A*, 25:385–390, 1982.

[147] M. G. Trocheris. Electrodynamics in a rotating frame of reference. *Phil. Mag.*, 40:1143–1154, 1949.

[148] K. C. Turner and H. A. Hill. New experimental limit on velocity-dependent interactions of clocks and distant matter. *Phys. Rev.*, 134:B252–256, 1964.

[149] W. G. Unruh. Notes on black hole evaporation. *Phys. Rev. D*, 14:870–892, 1976.

[150] V. Vali and R. W. Shorthill. Fiber ring interferometer. *Appl. Opt.*, 15:1099–1100, 1976.

[151] B. J. Venema, P. K. Majumder, S. K. Lamoreaux, B. R. Heckel, and E. N. Fortson. Search for a coupling of the earth's gravitational field to nuclear spins in atomic mercury. *Phys. Rev. Lett*, 68:135, 1992.

[152] R. M. Wald. *General relativity*. University of Chicago Press, Chicago, 1984.

[153] S. A. Werner, J. L. Staudenmann, and R. Colella. Effect of earth's rotation on the quantum mechanical phase of the neutron. *Phys. Rev. Lett*, 42:1103–1106, 1979.

[154] E. P. Wigner. Relativistic invariance of quantum-mechanical equations. In A. Mercier and M. Kervaire, editors, *Jubilee of Relativity Theory*, pages 210–226. Birkhaüser, Basel, 1956.

[155] C. M. Will. The confrontation between gravitational theory and experiment. In S. W. Hawking and W. Israel, editors, *An Einstein centenary survey*, pages 24–89. Cambridge University Press, Cambridge, 1979.

[156] P. Zeeman. *Proc. R. Acad. Sci. Amsterdam*, 18:398–408, 1916.

[157] P. Zeeman. *Proc. R. Acad. Sci. Amsterdam*, 22:512–522, 1920.

[158] P. Zeeman, W. De Groot, A. Snethlage, and G. C. Dibbetz. *Proc. R. Acad. Sci. Amsterdam*, 23:1402–1411, 1922.

[159] J. E. Zimmermann and J. E. Mercereau. Compton wavelength of superconducting electrons. *Phys. Rev. Lett.*, 14:887–888, 1965.